A Systematic Study of Acene Derivatives: Synthesis, Crystal Structures, Optical and Electrochemical Characterizations

A DISSERTATION

SUBMITTED TO THE FACULTY OF THE

UNIVERSITY OF MINNESOTA

BY

Zhuoran Zhang

IN PARTIAL FULFILLMENT OF THE REQUIREMENTS

FOR THE DEGREE OF

DOCTOR OF PHILOSOPHY

Advisor: Christopher J. Douglas

August 2018

Acknowledgements

Pursuing a Ph.D. degree in the U.S. has been the most unimaginable life experience for me. Being the first person to do so in my family, I feel lucky, honored, and of course, stressed. These complicated feelings probably came from my parents, who raised me up around for more than twenty years, and finally decided to push me up to the other side of the world where I could chase something higher. It must be hard for them, because they have no idea what life is like in the U.S., they probably don't understand what a chemistry Ph.D. is. But they always respect and support my pursuit. They know it's time to let their son take care of himself and he will be fine. Suffice to say, it is the strength that comes from their trust and hope that keeps me strong. I guess this is the unique kind of love from parents, the love that nothing could ever compare. I am deeply grateful to the selfless love, the endless support, and the sacrifice they have to make. So, thank you, Mom and Dad!

I'd like to give my greatest gratitude to my advisor Prof. Chris Douglas, who has provided me with a wonderful opportunity to be a synthetic organic chemistry researcher at University of Minnesota. Chris is an excellent organic chemist to work with. He is very knowledgeable in organic chemistry and I have learnt so much from him. His enthusiasm in research triggers every group member to work hard on the research projects. Chris is not only a chemistry professor, but more importantly, an outstanding individual. He has demonstrated a high moral standard in terms of treating people equally and with respect, evaluating experimental results scientifically and with a serious academic attitude. He is a kind, patient and considerable person who is willing to think from others' perspective. I remember the 2015 summer, when my grandma was sick and eventually passed away,

Chris showed great care to me and my family. He kindly allowed me to travel back to China and be there with my family for the hard time. I feel really lucky to have an advisor like him, not only in academics, but also in life.

I want to thank all my lab mates, who have been so friendly and helpful throughout the past five years. It's been a lot of fun being with all of you, both in and out of lab. We work together as a team, keeping each other positive, focused, and most importantly, safe. There is no other place than the 5th floor of Kolthoff that makes me feel as comfortable as home. Though five years is not a long time in one's life, the time we spent together, the memory that we share is forever. I sincerely wish you all with a bright future. Same thanks are given to friends and staffs that works in the chemistry department. You all have made life easier for me.

Last but not the least, I met with the person in my life here at the U. My wife, my soul mate, my lifelong partner, the human being that I could give my entire love and life to. You are the first person I see every morning and the last person I see every night. And I know we will be with each other forever and ever. Thank you for all the love, understanding and support. You and science make my life real and beautiful. Of course, I will not forget the kittens, Tuantuan (Sparkle) and Yuanyuan (Sprinkle), who tried their best to add on to this dissertation by weird typos. Thank you both for the distractions when I am down, and for the natural meow alarms every morning. Good girls, papa love you both.

Dedication

To my beloved wife and parents

致我挚爱的妻子与父母

Abstract

This Thesis describes a systematic study towards a series of polycyclic aromatic hydrocarbons (PAHs). The objectives are to develop convenient and efficient synthetic approaches to unique aromatic frameworks in order to probe their optical and electronic properties. The ultimate goal for these studies is to establish structure−property relationships in organic electronic materials.

Chapter 1 of this Thesis briefly reviewed the history and current challenge in organic electronic materials. In Chapter 2, the study of a benchmark p-type organic semiconductive material – rubrene is described. Fluorination, a strategy often used to tune the crystallographic and opto-electronic properties, is involved. Synthetic routes to partially and fully fluorinated rubrene derivatives are developed. The effect of fluorination is examined by optical and electrochemical measurements, and more importantly, by the influence on the crystal packing motifs. Fluorine-based intermolecular interactions are found to play an important role in the assembly of rubrene crystals. Chapter 3 elaborates on the work in developing a new type of PAH – dibenzo[*g*,*s*]rubicene, the structure of which contains five-membered rings that are embedded in a large conjugated core structure. The synthesis takes advantage of dehydro-Diels−Alder reactions as a powerful and highly efficient method to access the polycyclic conjugated system. The functionalized rubicene derivatives are then characterized by optical, electrochemical and computational methods. This work contributes to discovery of potential candidates for innovative n-type organic semiconductors. In chapter 4, synthetic studies toward a carbon nanobelt – [12]cyclacene are performed. Though previous reports have made significant achievements in the

construction of a macrocyclic framework, however, late-stage modification to install the fully conjugated structure is proved to be challenging. In this work, a new strategy involving a thermally-driven cheletropic rearrangement is proposed to address the late-stage modification issue. In the effort towards the macrocycle synthesis, an advanced intermediate has been successfully obtained in a stereoselective manner *via* multiple stereoselective Diels−Alder reactions. The selectivity is attributed to the careful design of precursors, which afforded the desired products through a sterically favored reaction pathway. A detailed examination of the proposed synthetic route as well as the proposal of a more convenient route are illustrated in the end.

Table of Contents

List of Schemes

List of Figures

List of Tables

List of Abbreviations

Ac_2O	Acetic Anhydride
AcOH	Acetic Acid
CNB	Carbon Nanobelt
CNT	Carbon Nanotube
CPP	Cycloparaphenylene
d	Doublet
DBU	1,8-Diazabicyclo[5.4.0]undec-7-ene
DCM	Dichloromethane
DDQ	2,3-Dichloro-5,6-dicyano-1,4-benzoquinone
DFT	Density Functional Theory
DMF	Dimethylformamide
DMSO	Dimethylsulfoxide
DPT	3,6-Di(pyridin-2-yl)-1,2,4,5-tetrazine
EtOAc	Ethyl Acetate
ESI	Electrospray Ionization
GC	Gas Chromatography
HMDS	Hexamethyldisilazane

HOMO	Highest Occupied Molecular Orbital
HRMS	High Resolution Mass Spectrometry
Hz	Hertz
i-Pr	Isopropyl
IR	Infrared
LDA	Lithium Diisopropyl Amide
LDI	Laser Desorption Ionization
LRMS	Low Resolution Mass Spectrometry
LUMO	Lowest Unoccupied Molecular Orbital
M	Molar
MALDI	Matrix-assisted Laser Desorption Ionization
MeOH	Methanol
mL	Milliliters
mm	Millimeters
MP	Melting Point
MS	Mass Spectrometry
*n*BuLi	*n*-Butyl Lithium
nm	Nanometers

NMR	Nuclear Magentic Resonance
o-Tol	*ortho*-Tolyl
OFET	Organic Field-Effect Transistor
OLED	Organic Light-Emitting Diode
OPV	Organic Photovoltaic
OSC	Organic Solar Cell
ORTEP	Oak Ridge Thermal Ellipsoid Plot
OTf	Triflate
PAH	Polycyclic Aromatic Hydrocarbon
PEPPSI-IPR	Pyridine-Enhanced Precatalyst Preparation Stabilization and Initiation-Isopropyl
Ph	Phenyl
ppm	Parts Per Million
PTSA	*para*-Toluene Sulfonic Acid
p-Tol	*para*-Tolyl
Py	Pyridinyl
QTOF	Quadrupole Time-Of-Flight
SPR	Structure−Property Relationship

t-Bu	*tert*-Butyl
TASF	Tris(dimethylamino)sulfonium Difluorotrimethylsilicate
TBAF	Tetrabutylammonium Fluoride
TEA	Triethylamine
TFA	Trifluoroacetic acid
TFAA	Trifluoroacetic Anhydride
THF	Tetrahydrofuran
TIPS	Triisopropylsilyl
TLC	Thin Layer Chromatography
TMS	Tetramethysilane
TMSA	(Trimethylsilyl)acetylene
TMSCl	Chlorotrimethylsilane
Tol	Toluene
TPAP	Tetrapropylammonium Perruthenate
UV-Vis	Ultraviolet–visible spectroscopy

Chapter 1 Introduction to Polycyclic Aromatic Hydrocarbons

1.1 A Brief Overview of Polycyclic Aromatic Hydrocarbons History

Polycyclic aromatic hydrocarbons (PAHs) are a class of organic compounds composed of multiple fused aromatic rings. The delocalized π system of PAHs usually exceeds 10 electrons; thus, the structures of anthracene and phenanthrene represent the simplest members of the PAH family.[1] PAHs are naturally occurring and were initially discovered in the residue of fossil fuel combustion.[2] In the early days, however, only a few PAHs were known and characterized. Chemical studies such as purification and analysis of high molecular weight PAHs were hard to establish due to the lack of powerful separation and characterization techniques.

Pioneering studies of polycyclic aromatics were made by Scholl[3] and Clar[4] in the early 20th century. At the early stage of PAH synthesis, the reaction conditions that Scholl and Clar applied were generally harsh, which usually involves high temperature or strong oxidizing reagents. With the development of synthetic methods and highly effective collaborations, the studies of PAHs were greatly advanced in the 1930s. One of the most notable achievements at the time was the synthesis of pentacene **1.1** by Clar and John.[5] They isolated pentacene *via* dehydrogenation of a dihydropentacene isomer, which had been synthesized in 1911 when Phillipi first claimed a synthesis of pentacene.[5] Combining their efforts led to a simpler and more efficient approach to parent pentacene in the following two decades (**Scheme 1-1**).[6] This highly efficient synthesis started with the condensation between *o*-phthalaldehyde and cyclohexane-1,4-dione to generate quinone **1.2**, followed by reduction with Al powder to give pentacene in two steps. Later in 1939,

Clar suggested that the polycyclic aromatic compounds comprised of linearly fused benzenoid units to be called "acenes".[7] Since then, numerous functionalized acene derivatives have been prepared, allowing chemists to establish a relationship between the linearly conjugated structures and their properties as organic functional materials.

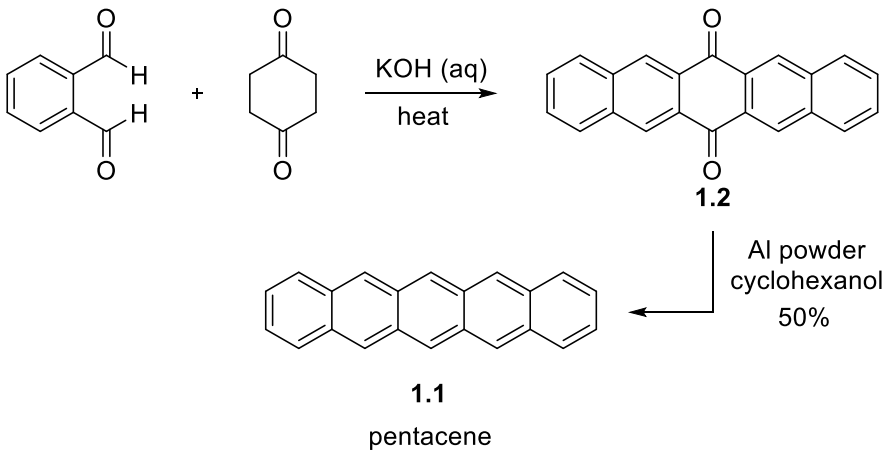

Scheme 1-1 Synthesis of pentacene.

While most acene studies were aiming at the extension of conjugation length or functional group derivatizations, Scholl explored a broader study into PAHs that involved a two-dimensional pattern. In fact, Scholl was the first to prepare two polyarene structures coronene **1.3** and bisanthene **1.4** in the 1930s, which was regarded as the foundation for future benzenoid PAHs (**Scheme 1-2**).[8] However, due to the limitation of synthetic methods, the investigation of polyarene chemistry was very difficult at that time. One specific challenge was that the 2-D polyarene structures possess high molecular weight and are usually insoluble and/or chemically unstable. Besides the difficulty in chemical synthesis, the structure analysis of such molecules relies on state-of-art instruments such as high-resolution mass spectroscopy and high-performance liquid chromatography

techniques, which were not available then. Nowadays, advanced analogs of this type of molecules are categorized as 2D graphene molecules or graphene nanoribbons (GNRs).[9]

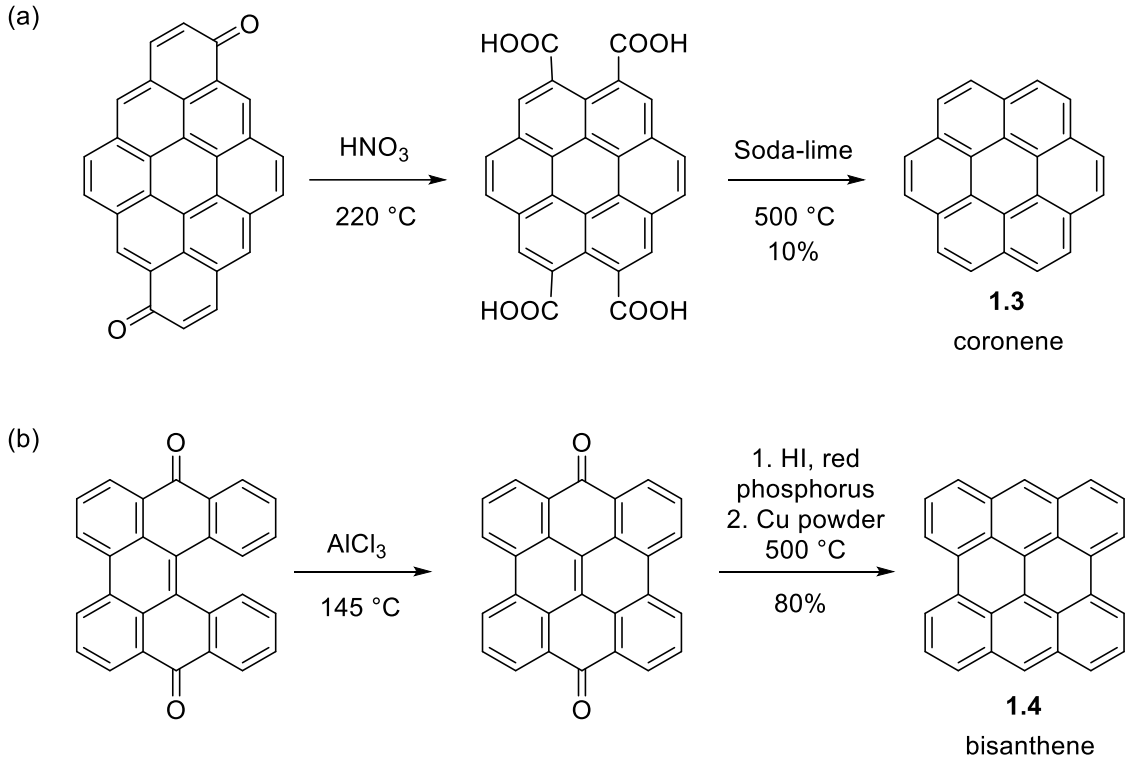

Scheme 1-2 Examples of early synthesis of 2-D polyarenes: (a) coronene and (b) bisanthene.

Following the evolution from acenes to GNRs, a logical next step would be expanding the scope towards three-dimensional space. This branch of PAH studies started from the synthesis of triptycene in the 1940s. The native triptycene molecule **1.5** was isolated by Bartlett and coworkers in 1942, which originated from their work related to bridgehead functionalization on bicyclic systems (**Scheme 1-3**).[10] However, one could easily imagine that the 3-D nature of an organic molecule does not necessarily come from C-sp^3 hybridization. In other words, an aromatic structure can be curved by strain or steric encumbrance. The most representative examples of this class are corannulene **1.6** and

buckminsterfullerene **1.7**. Corannulene was first prepared in 1966 and characterized as a bowl-shaped PAH. Two decades later, fullerene C_{60} was discovered in graphite vapor[11] and became available in macroscopic quantities in 1990[12]. The three-dimensional feature of such molecules is not only a novelty in chemical structures or unique chemical reactivity, but also finds application in organic electronics, host-guest chemistry and other smart materials.

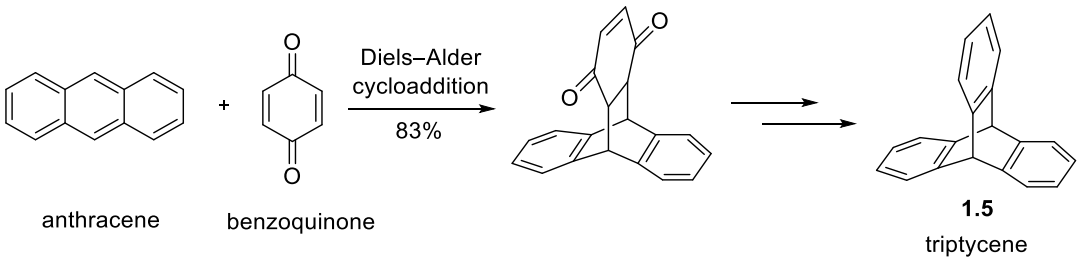

Scheme 1-3 Early synthesis of triptycene *via* Diels−Alder cycloaddition.

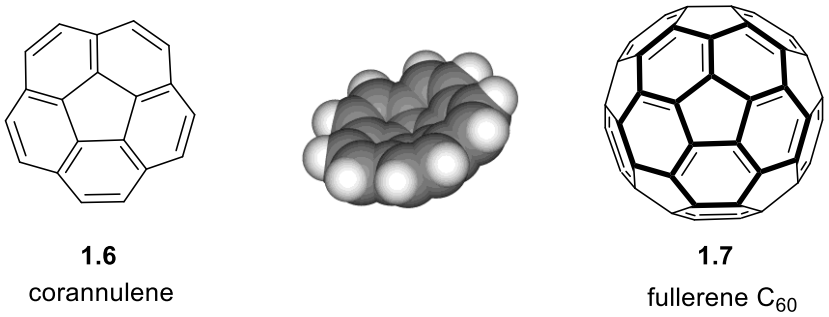

Scheme 1-4 Structure of corannulene and fullerene C_{60}. The curved nature of corannulene is shown in space-filling model (middle).

1.2 General Properties of PAHs and Their Application as Opto-electronic Materials

In recent years, the study of the physical properties of organic materials has gained increased significance.[13] In general, organic compounds have many inherent advantages over inorganic compounds, when used as materials. Firstly, organic compounds exist abundantly on earth and may be more environmentally benign than inorganic compounds. Secondly, the wide variety of organic compounds, as well as the ability to modify them *via* unlimited synthetic methods arouse higher prospects in creating innovative materials. Thirdly, organic compounds have superior processability than inorganic compounds due to their better solubility in common organic solvents, which enable their application in flexible and large-area devices.[14]

As PAHs contain multiple fused benzenoid rings, they are comprised of a linear series of overlapping p_z orbitals with sp^2 hybridization, thereby forming a conjugated domain of delocalized electrons. Similar to conducting metals which include a delocalized "sea of electrons", free-moving delocalized π electrons in conjugated organic molecules creates the possibility of electricity conduction. Thus, such a feature in their electronic structure qualifies PAHs as strong candidates for organic semiconductors.

Acene derivatives as a central component of PAHs are particularly characterized as semiconductive materials for two classes of electronic devices: organic field-effect transistors (OFETs) and organic light-emitting diodes (OLEDs) (**Figure 1-1**). The field-effect transistors reflect the charge transport properties of the organic material, in which the conductivity of the organic semiconductor changes due to the applied electric field

normal to its surface. The light-emitting diodes examine the electroluminescence property of the organic material, in which the organic layer becomes light emitting in response to an electric current.

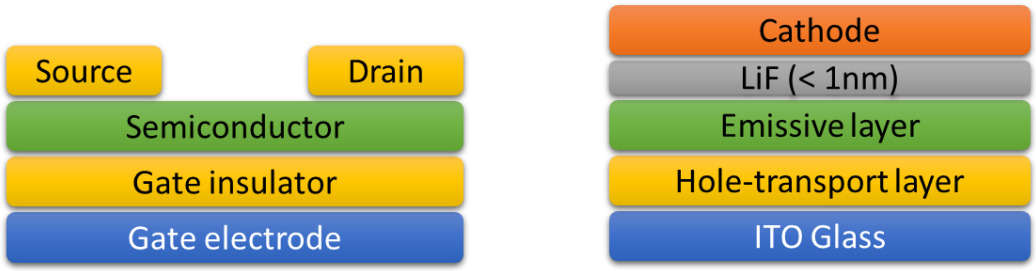

Figure 1-1 A typical device configuration of OFET (left, top contact configuration) and OLED (right).

Besides acene derivatives, other PAH analogs bearing unique structural features such as fullerenes have shown great promise in organic photovoltaics (OPVs), which absorb solar energy and produce electricity.[15] As compared to polymer solar cells, semiconducting small conjugated molecules are valuable because (a) they can be readily purified and (b) they are able to form well-defined, long range ordered structures that enable high charge carrier mobilities. Small molecules can also serve as model systems for fundamental studies of the charge-transport mechanisms and dynamics.

Therefore, echoing the early comparison between organic materials and inorganic materials, conjugated PAHs have several specific and intrinsic advantages that make them competitive candidates for the next-generation optoelectronic materials. Firstly, the small and tunable bandgap that based on varied conjugation length of PAHs allows easy charge injection of holes into HOMO and/or electrons into LUMO; Secondly, PAHs usually have a strong absorption coefficients. As a result, a thin layer of materials, which can be

conveniently fabricated through solution-based methods, will be enough to harvest light energy and produce desired electric energy. Thirdly, PAHs contain a rigid aromatic backbone that reduce the pathways for non-radiative energy loss, thus the overall efficiency of OPV and OLED can benefit from by the high quantum efficiency of photoluminescence.

1.3 Principles for the Rational Design of Organic Semiconductors

A core topic in current organic semiconductor research is to understand the relationship between the chemical structure and their performance in electronic devices, the so-called structure−property relationship (SPR).[16] However, it is extremely challenging to establish an explicit linkage between the two as the overall process can be affected by many complicated factors that are inherently related. Moreover, organic electronics is an interdisciplinary science that involve complementary knowledge inputs from many fields such as chemical synthesis, computational simulation, photophysics and material engineering. Regardless, the rational design and synthesis of semiconductive molecules serves as the foundation since the inherent properties of the organic layer sets the upper limit of the overall device performance. According to Marcus theory[17], the rate of charge transport in organic semiconductors is determined by transfer integral and reorganization energy. The transfer integral is used to describe the degree of molecular orbital overlap between neighboring molecules. This factor is affected by the molecular arrangements in the solid states, such as the distance of π−π stacking, the relative distance of packing displacement. The reorganization energy is the energy cost to reorganize the molecular structure to without electron transfer occurring. An ideal organic semiconductor should have large transfer integral and small reorganization energy, both of which are determined by the identity of the chemical structure as well as the packing arrangements in the solid

state. Through the extensive efforts in pursue of high-performance semiconductors, several principles for the rational design of organic molecules can be found in the literature. Although a systematic approach to a "dream molecule" still remains open-ended, the principles discussed in the following paragraphs are supported by the combination of physical theories and experimental observations. To illustrate the principles concisely, linear acenes are used as examples to discuss the relationship between the chemical structure and physical properties.

1.3.1 The Effect of Conjugation Length

In **Figure 1-2**, structures of several parent linear acenes were shown. From anthracene to hexacene, the conjugation length is extended in a linear fashion. As a result, their physical properties were affected as observed in the following two trends: 1) the HOMO−LUMO bandgap decreases as the conjugation length increases, as a result, the absorption and emission spectrum of longer acenes are red shifted; 2) the stability of acenes decrease with longer backbone.[18] This phenomenon cannot be rationalized by traditional Hückel's aromaticity theory.[19] However, the stability trend of acenes can be well explained by Clar's sextet rule[20], in which the diene character is gradually built up with the extension of the conjugation length. Thus, longer acenes readily decompose *via* photo-oxidation or Diels−Alder reactions to destroy the conjugated backbone. Theoretical calculations further associated the instability trend to the increase of open-shell singlet diradical contribution in longer acenes.[21] To date, the longest unsubstituted acene isolated and characterized is heptacene, which can be formed by thermally induced cycloreversion from diheptacenes and can persist for an extended period of time in the solid states[22]. Interestingly, the hole transport mobilities of parent acenes increase from anthracene to pentacene as measured in

single-crystal OFETs.[23] As mentioned earlier, the electronic properties of acenes strongly depend on their solid-state arrangements. Theoretical calculation of hole transport properties of anthracene, tetracene and pentacene based on their crystal structure data are in good agreement with the experimental data.[24] These results have demonstrated that extending the conjugation length in linear acenes is a viable approach to improve their charge transporting properties.

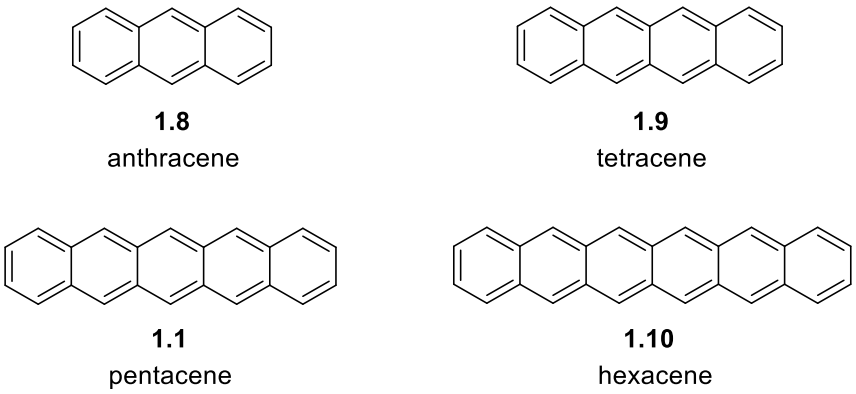

Figure 1-2 Chemical structures of linear acenes.

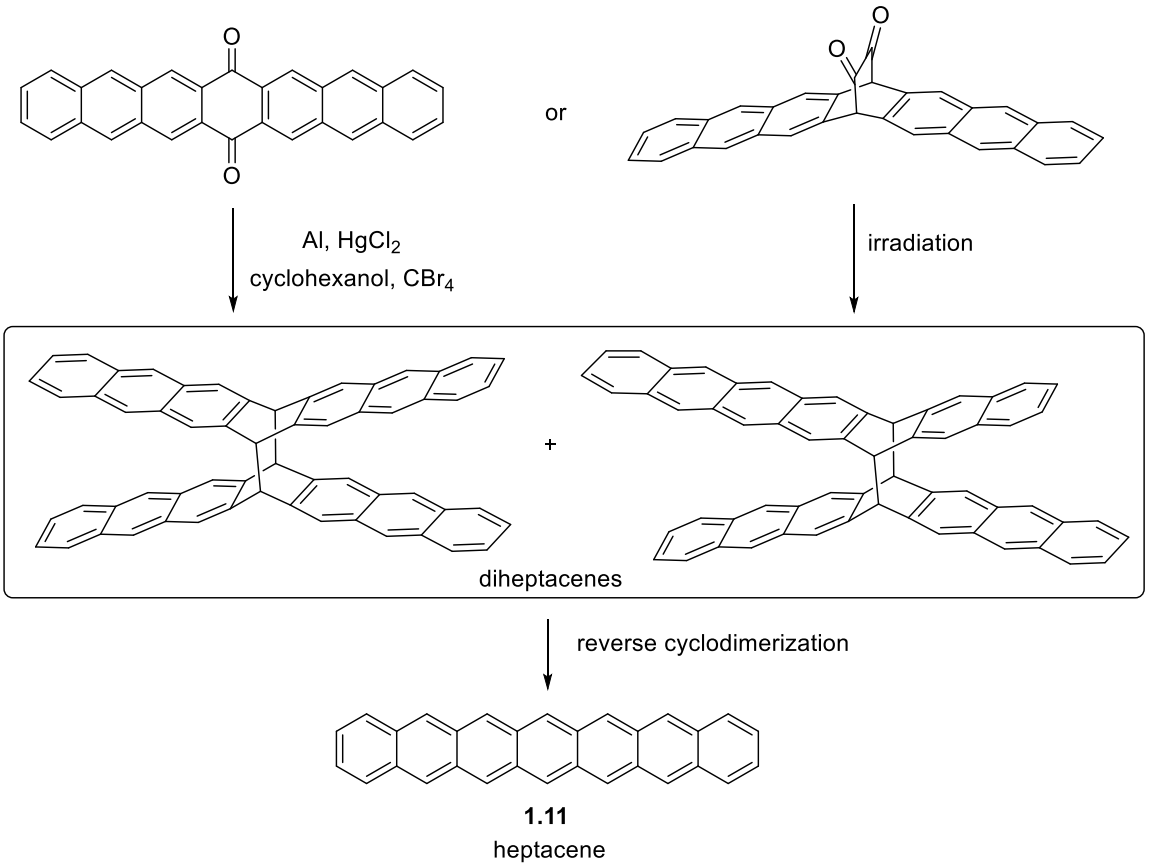

Scheme 1-5 Chemical synthesis of heptacene.

1.3.2 Crystal Engineering on the Solid-State Packing Motifs

Organic single crystals are considered the ideal form of materials when used as the active layer in electronic devices. Compared with an amorphous film or powder, a single crystalline solid contains highly ordered molecular arrangements that can minimize electronic disorder during charge transport. However, a highly ordered packing motif does not necessarily lead to high device performance as a strong electronic coupling must be manifested. In general, the solid-state packing motif of PAH molecules are affected by several intermolecular interactions including hydrogen bonding, edge-to-face interactions, π–π stacking and Van der Waals interactions. To maximize the electronic coupling of

neighboring molecules, efficient stacking of the conjugated backbone must be present in the crystal packing.

In this regard, two major packing motifs adopted by acene derivatives usually yield strong intermolecular overlap.[25] Taking functionalized pentacene derivatives as an example, comparison of the packing motifs between unsubstituted pentacene and 6,13-bis(triisopropylsilylethynyl)pentacene (TIPS-pentacene) reveals striking differences (**Figure 1-3**).[26] Specifically, the unsubstituted pentacene packs in a herringbone motif, which is dominated by the aromatic edge-to-face interactions. TIPS-pentacene, however, adopts a 2-D "brick-wall" packing motif. In the 2-D brick-wall packing, the pentacene backbone stacks in a coplanar arrangement with displacement along the long axis. The π–π stacking distance in TIPS-pentacene (3.47 Å) is greatly decreased than pentacene (6.27 Å), as a result, the intermolecular orbital overlap is greatly increased. The drastic difference between the two packing motifs can be explained by the steric effect of the added TIPS group, which disrupts the edge-to-face interaction and therefore facilitates π–π stacking as the driving force for the molecular assembly.

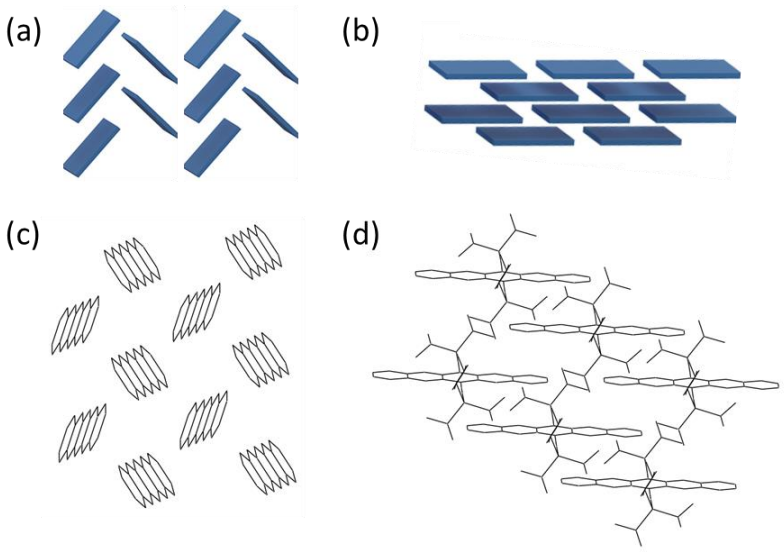

Figure 1-3 Examples of packing motifs in organic crystals: (a) herringbone packing, (b) 2-D brick wall packing, (c) crystal packing of pentacene and (d) crystal packing of TIPS-pentacene. Hydrogen atoms are omitted for clarity in (c) and (d).

Another example is the herringbone packing of rubrene ($C_{42}H_{28}$). The chemical structure of rubrene contains a tetracene backbone and tetra-phenyl substitution at the 5-, 6- ,11- ,12-positions (**Figure 1-4**). The crystal structure of rubrene is known to have different polymorphs. The one that is of great interest to material chemists is the orthorhombic rubrene crystal. In this form, rubrene molecules adopts the herringbone motif with a strong π-stacked arrangement. Computational studies have shown that the particular intermolecular arrangement of rubrene happens to be ideal for charge transport, as the displacement of the tetracene backbone results in a large transfer integral for both HOMO and LUMO.[27] Because of the optimized crystal packing, the transport property of rubrene and its derivatives has been intensively studied. The Douglas group has explored other strategies to tune the crystal packing of rubrene derivatives, such as the functional group

introduction on the phenyl groups, in order to discover more interesting packing motifs. A detailed discussion will be made in Chapter 2 of this dissertation.

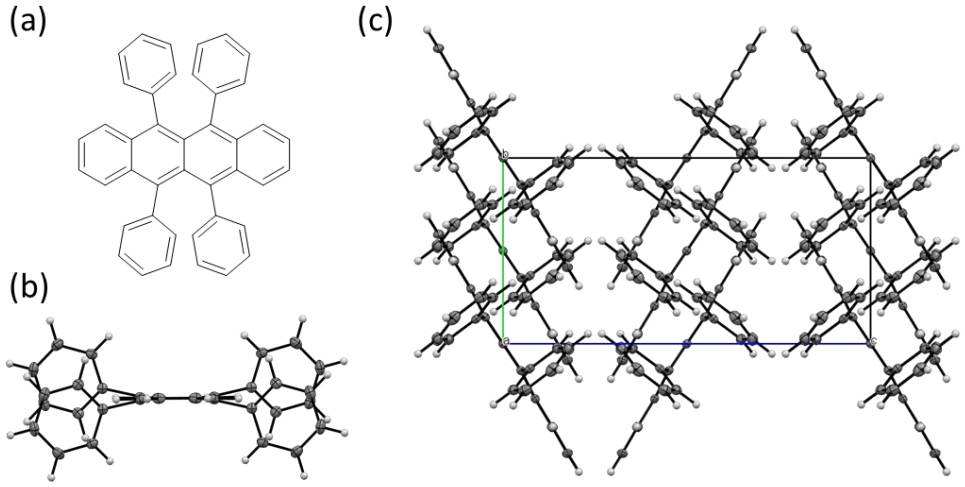

Figure 1-4 (a) Chemical structure of rubrene. (b) Crystal structure of rubrene revealing the planar tetracene backbone. (c) Herringbone packing of orthorhombic rubrene containing strong intermolecular overlap of the tetracene backbone.

1.3.3 Tuning the Electronic Properties *via* Core Modification

An efficient approach to tuning the opto-electronic properties of PAHs is introducing functional groups on the aromatic core. By attaching electron-donating group (EDG) or electron-withdrawing group (EWG) to the conjugated system, the electron density can be adjusted through inductive effect[28] or resonance effect[29], thus the optical or electronic property of the organic material can be impacted. One of the long-standing challenge in the organic electronics research has been the imbalance between the rapid advance in high-performance p-type semiconductor and the slow development of n-type or ambipolar semiconductor. One shortcut venue to convert a p-type semiconductor to n-type or

ambipolar semiconductor is to add EWGs to the conjugated core. Such a chemical modification generally leads to materials with low-lying LUMO levels, which is conducive to efficient electron injection and allows for operational stability in air.[30] Commonly used EWGs include halogen atoms, carbonyl-containing groups, nitro groups and cyano groups. Among these functionalities, fluorination is the most popular choice based on several advantages: a) fluorine has the largest electronegativity of all the elements so it significantly lowers the electron density of the conjugated system *via* inductive effect. b) the size of fluorine atom is not drastically different from hydrogen, which minimizes the steric change of the molecule upon substitution. This is a valuable feature compared with other EWGs in that it is possible to maintain the desired solid-state packing motif of the parent molecule by slightly altering the molecular size. c) addition of fluorine atoms would invoke intermolecular interactions *via* fluorine-based interaction, which provides an opportunity to form highly ordered packing motifs.

For example, perfluoropentacene **1.12** was synthesized by Suzuki and co-workers in five steps from tetrafluorophthalic anhydride **1.13** and hydroquinone **1.14** (**Scheme 1-6**).[31] In the solid states, perfluoropentacene packs in the herringbone motif similar to pentacene but with a larger edge-to-face angle (91.2° as compared with 51.9° in pentacene, **Figure 1-5**). In transistor devices, perfluoropentacene showed electron transport behavior with mobilities up to 0.22 $cm^2/(Vs)$. These results have demonstrated that fluorination is a viable approach in preparing n-type semiconductive materials from parent p-type material. In Chapter 2 of this thesis, the synthesis of a perfluorinated rubrene is illustrated. In this work, we will discuss our synthetic strategy towards fluorine introduction as well as the impact on crystal structures *via* fluorine-based interactions.

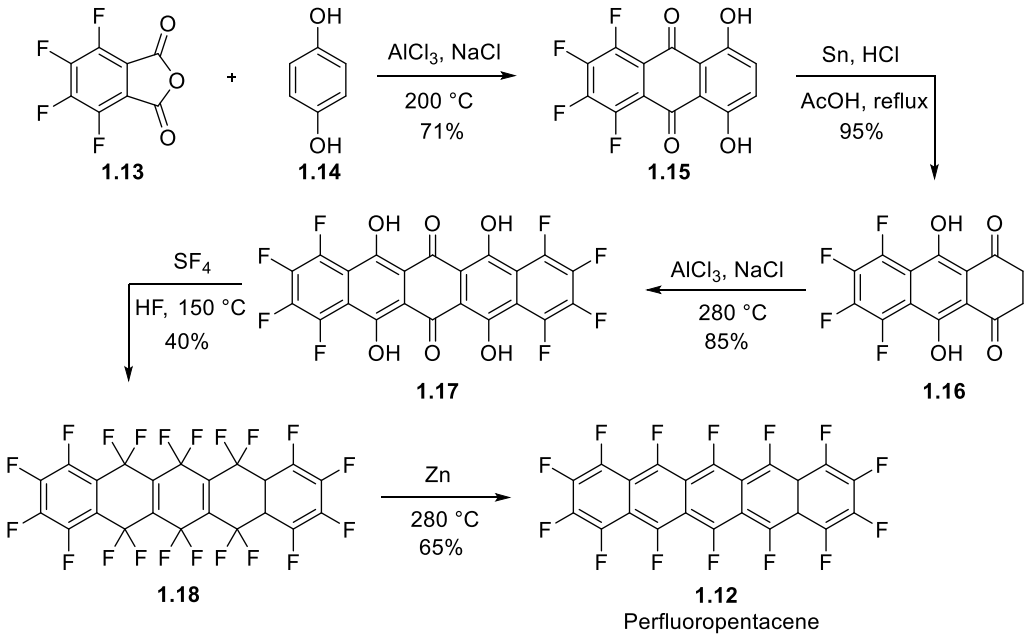

Scheme 1-6 Synthesis of perfluoropentacene.

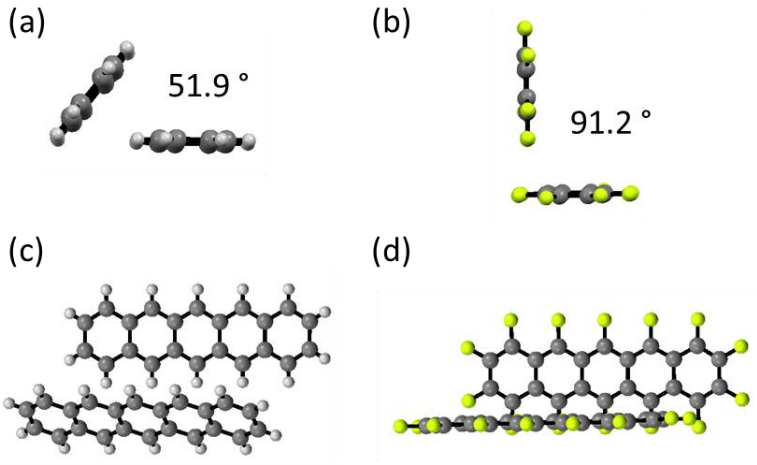

Figure 1-5 Comparison of the crystal structures of pentacene (a) side view, (c) top view and perfluoropentacene (b) side view, (d) top view.

Besides functional group introduction, partial heteroatom replacement of the aromatic core serves as another strategy for property tuning. In this case, sulfur and nitrogen are the most frequently used heteroatoms, not only due to the ease of chemical synthesis but also

their unique impact on the conjugated system. Specifically, the benzene unit in the acene backbone can be replaced with the thiophene unit to give oligothienoacenes. (**Scheme 1-7 (a)**)[32] The fused thiophene units maintain the aromaticity and rigidity of the backbone, while adding an electron-rich feature to the conjugated system. Thus, thiophene-fused acenes constitute an important family of p-type semiconductors; In contrast, replacing the CH units with electron-withdrawing sp^2-hybridized nitrogen atom in the conjugated backbone of acenes affords azaacenes (**Scheme 1-7 (b)**).[33] The properties of azaacenes can be tuned by altering the number, position and oxidative states of nitrogen. By nitrogen replacement, the azaacenes are electron-deficient, therefore their electron affinities are increased, which makes them suitable targets for n-type or ambipolar semiconductors.[34] It worth mentioning that the azaacenes can be reduced to *N,N'*-dihydroazaacenes (**Scheme 1-7 (b)**). Due to the breakup of the aromatic core, the degree of aromaticity is lower, but they are more stabilized. The reduced azaacenes are generally p-type materials as the N-H groups are strong electron donors and contribute to the electron-rich character of these analogs.[35] For example, the dihydrodiazapentacene **1.20** shows p-type, hole-transporting characteristics with a hole mobility up to 5×10^{-5} cm^2 V^{-1} S^{-1}; the tetraaza-version of TIPS-pentacene **1.21** shows a strong electron transporting mobility of 3.3 cm^2 V^{-1} S^{-1}.

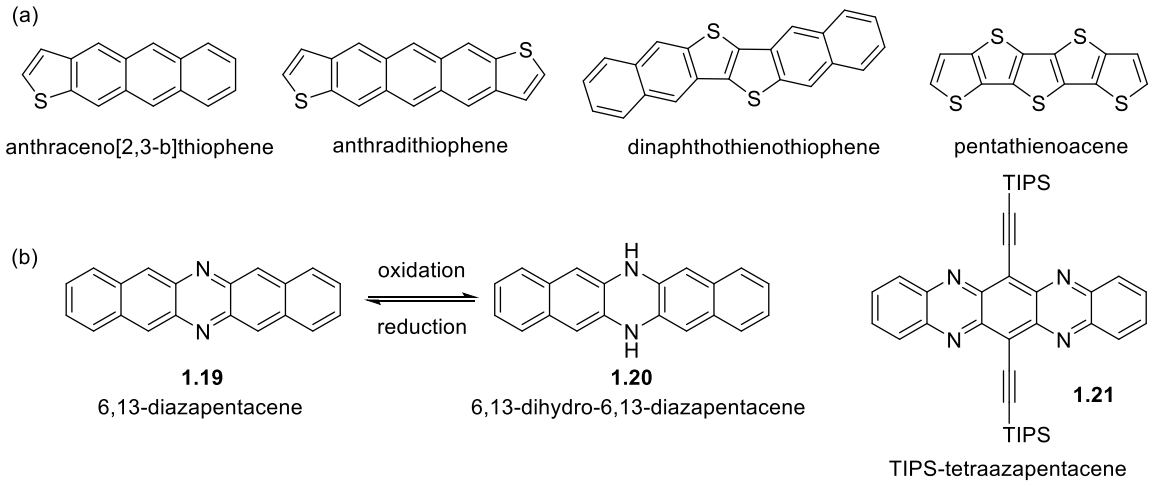

Scheme 1-7 Example structures of oligoheteroacenes: (a) oligothienoacenes and (b) azaacenes and reduced azaacenes.

1.4 Scope and Organization of This Dissertation

In this dissertation, we continue to pursue the studies toward the design, synthesis and characterizations of novel acene-based PAHs. In general, we are interested in acene derivatives that have potential applications as semiconductive materials. The design principles for the target molecules fit into three levels.

Level 1. Optimization of the electronic property of known molecular moieties through functional groups introduction (EDG, EWG, solubilizing group and/or steric group).

Level 2. Development of synthetic methods for innovative aromatic core units containing unique features: five-membered ring attachment, heteroatom introduction or different conjugated patterns.

Level 3. Design and synthesis of conjugated organic molecules with 3-D architectures that involve twisted/curved conjugation and serve as fragment structural units of fullerene or carbon-nanotubes.

Following these principles, Chapter 2 discussed the synthetic studies toward fluorinated rubrene derivatives. This synthesis work features a different approach in the construction of a perfluorinated tetracene core and a modified reaction sequence in attaching the peripheral perfluorinated phenyl substituents, as compared with literature reported methods. A systematic study towards the crystal structures of various fluorinated rubrene derivatives, including perfluorinated rubrene ($C_{42}F_{28}$) and partial fluorinated rubrenes (F_{10}-rubrene and F_{20}-rubrene), was performed to unravel the impact of fluorination on the intermolecular interaction and how it alternates the crystal packing motifs. This study provided an insightful link between fluorinated PAHs and their crystal packing motifs, which could guide future material design for high-performance n-type semiconductive materials.

Chapter 3 outlines the studies toward another PAH analog called rubicene. The structure of rubicene can be viewed as a planar form of fullerene C_{70} fragment, which consists of an anthracene core fused with two five-membered rings. In this project, a series of dibenzo[*g*,*s*]rubicene derivatives were synthesized *via* an unconventional approach, namely a one-pot cascade reaction combining Sonogashira cross-coupling and tetra-dehydro-Diels−Alder (TDDA) reaction. This methodology provides a rapid and convenient access to the highly fused polycyclic aromatic framework of dibenzo[*g*,*s*]rubicene, which is potentially useful for efficiently constructing other complicated aromatic structures. The dibenzo[*g*,*s*]rubicene structures constitute a new type of chromophores, which exhibit strong absorption property across the majority of visible-light region and are highly emissive upon photo-excitation. Electrochemical and computational studies reveal the

important role of five-membered rings in contributing to the anti-aromatic feature of the conjugated system, and the increase in electron affinity.

Chapter 4 summarizes the synthetic attempts to [n]cyclacene, the shortest possible benzenoid-ring-containing zig-zag carbon nanotube. As the cyclacene structure is highly strained, a specific synthetic route is proposed to strategically avoid the ring strain build up. Specifically, a series of stereoselective Diel−Alder cycloadditions and benzyne Diels−Alder cycloadditions are proposed to efficiently construct the macrocyclic framework; post-functionalization to the fully conjugated cyclacene structure would involve a thermally-driven cheletropic rearrangement. To date, an advanced intermediate prior to macrocyclization has been successfully prepared *via* a one-pot three-component Diels−Alder cycloaddition sequence, the structure of which consists of the desire *syn*-configuration of a bis-bridge structural unit.

Chapter 2 Studies of Fluorinated Rubrene: Synthesis and Crystal Structure Analysis

2.1A Brief Review of Rubrene: Molecular Structure, Solid-State properties and Single-Crystal OFET Device Performance

Rubrene is known since the 1920s as a red solid, the structure of which contains a tetracene core substituted with four phenyl groups at the 5, 6, 11, 12-positions. Due to steric repulsions, the side phenyl groups are twisted out of the tetracene backbone, which can still maintains its planarity. Rubrene has displayed a variety of unique chemical and photo-physical properties, including photooxidation [36], electroluminescence [37], chemiluminescence[38] and fluorescence[39]. As a result, rubrene has shown great promise as potential electronic materials for use in organic light emitting diodes (OLED)[40], organic photovoltaics (OPV)[41], and organic field-effect transistors (OFET).[42] For example, rubrene is currently the most intriguing target in OFET application due to its exemplary hole-transporting properties in p-type semiconductors. In fact, rubrene holds the record to date for the highest reproducible charge-carrier mobilities (up to 40 $cm^2 V^{-1} s^{-1}$) in single-crystal field-effect transistors.[42]

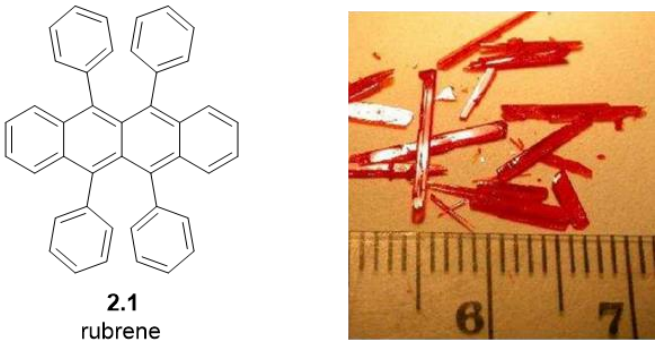

Figure 2-1 Chemical structure of rubrene (2.1, left) and image of rubrene single crystals (right).[43]

What makes rubrene outperform other small molecules from a material perspective? One major aspect in determining the charge-transport property of organic semiconductors is the degree of electronic coupling in the solid states. Single crystalline rubrene is known to adopt a variety of packing motifs, which are referred to as polymorphs. In **Table 2-1**, three distinctive polymorphs are listed, showing drastically different unit cell parameters. Among these crystal systems, orthorhombic Cmca rubrene performs the best in OFET devices. Before we elaborate on the intermolecular packing rearrangement, there are several notable unimolecular features in the orthorhombic rubrene crystals (**Figure 2-2**). First, the tetracene backbone adopts a planar conformation. This is a critical feature for unsubstituted rubrene. As we will see later in this chapter, there are many rubrene derivatives that adopt twisted tetracene backbones, which disrupts efficient π-stacked overlap. Second, due to steric repulsions, the planes of all four side phenyl groups are positioned nearly orthogonal (about 84˚) to the tetracene backbone. Thirdly, the side phenyl groups also distort away from the tetracene plane by about 11˚. Such a rubrene conformation allows the tightly packed herringbone motif, in which highly ordered π-π overlap between adjacent rubrenes is observed.

Table 2-1 Parameters for three different rubrene polymorphic crystals.[44]

	Monoclinic	Triclinic	Orthorhombic
Space group	$P2_1/c$	P-1	Cmca
Formula	$C_{42}H_{28}$	$C_{42}H_{28}$	$C_{42}H_{28}$
Temperature (K)	173	173	293
Unit Cell	a = 8.7397(17) Å b = 10.125(2) Å c = 15.635(3) Å α = 90˚ β = 90.98(3)˚ γ = 90˚	a = 7.0194(14) Å b = 8.5432(17) Å c = 11.948(2) Å α = 93.04(3)˚ β = 105.58(3)˚ γ = 96.28(3)˚	a = 26.860(10) Å b = 7.193(3) Å c = 14.433(5) Å α = 90˚ β = 90˚ γ = 90˚
Volume ($Å^3$)	1383.33	683.504	2788.51
Z	2	1	4
Density (g/cm^3)	1.28	1.29	1.27

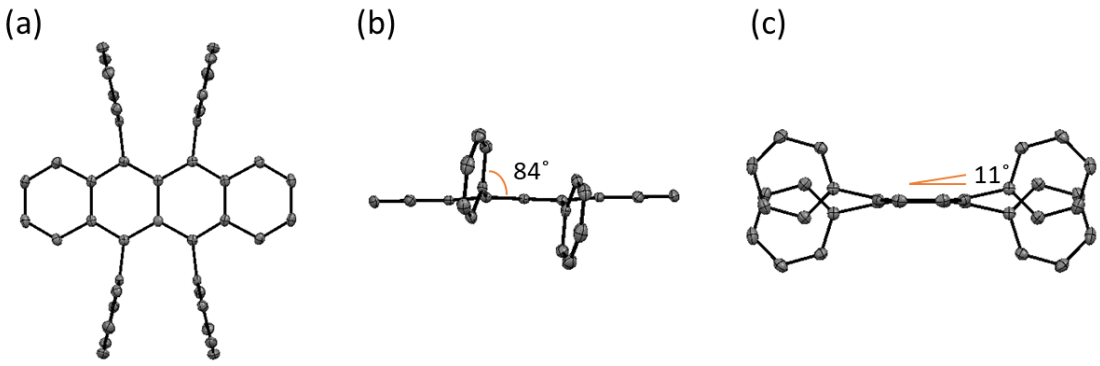

Figure 2-2 Rubrene crystal structure in the orthorhombic Cmca crystals: (a) top view, (b) side view along the short axis of tetracene backbone showing the dihedral angle between tetracene plane and phenyl plane is about 84 ˚and (c) side view along the long axis of tetracene backbone showing the out-of-plane torsion angle is about 11˚.

The herringbone packing along the b-axis in the orthorhombic rubrene crystal is shown in **Figure 2-3 (a)**. As indicated by the yellow arrow, the π-stack distance between a packing dimer is 3.74 Å. The green arrow shows the tetracene core slipped 6.13 Å to mitigate the steric interactions due to the side phenyl groups. Through calculation, Brédas et al have

found that such an orientation is optimal for efficient charge transport in that the extrema of transfer integrals for both HOMO and LUMO can be achieved at the same time.[27]

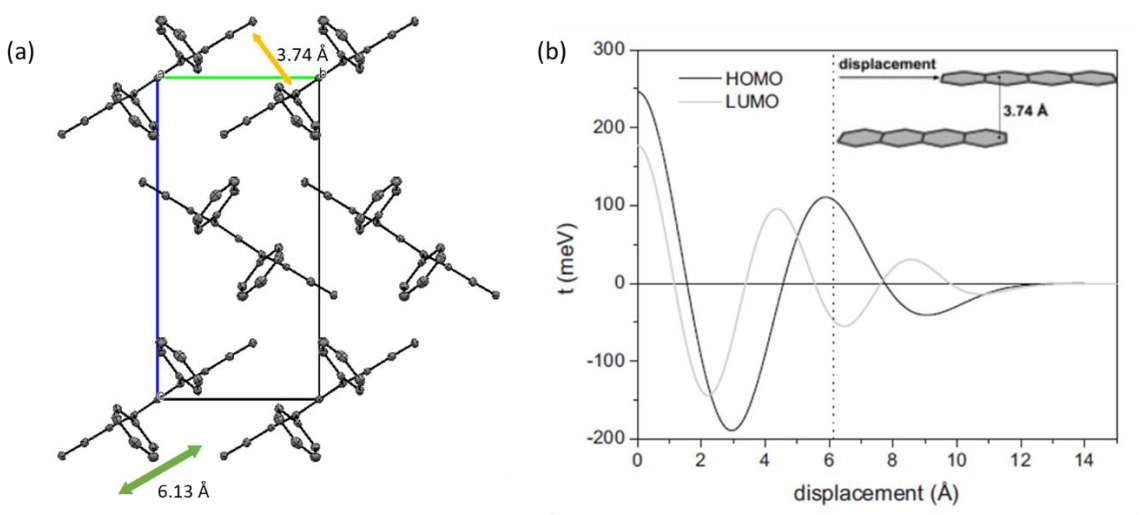

Figure 2-3 (a) Herringbone packing with highly ordered slipped π-stack of rubrene backbone. Yellow arrow indicates the π-π stacking distance of 3.74 Å and green arrow indicates parallel displacement distance of 6.13 Å. (b) Calculated of the HOMO and LUMO transfer integrals as a function of displacement, for a packed tetracene dimer at a fixed stacking distance of 3.74 Å. The vertical dotted line at 6.13 Å marks the displacement distance in the real crystal system, which closely corresponds to extrema in the oscillations of both the HOMO and LUMO transfer integrals. Figure (b) is adopted from the work of Brédas et al.[27]

While predicting the crystal packing from the chemical structure is rather challenging, there are several lessons we can learn by taking a closer look at the rubrene example. It is clear that the side phenyl groups are responsible for the transition of packing motifs from tetracene to rubrene. In this case, the particular intermolecular arrangement is more attributed to steric factors than electronic reasons. As the phenyl groups are positioned

orthogonal to the tetracene backbone, the distribution of molecular orbitals is very similar between unsubstituted tetracene and the tetracene moiety in rubrene. However, the side phenyl groups work as suitable space groups that minimize the edge-to-face interaction, which usually dominate in herringbone packing of acene crystals. As a result, the face-to-face π-stacking interaction becomes the main factor for the assembly of rubrene molecules. Additionally, the size of phenyl group is also critical as a different choice of space group will likely cause variations in the displacement distance and cause decreases in transfer integrals.

Therefore, the rubrene moiety serves as an excellent platform for the design and synthesis of high-performance organic semiconductors. Through rational modification of the chemical structure, one could a) systematically correlate between structural features and crystal packing characteristics b) create materials on-demand *via* fine-tuning of crystallographic/electronic properties and c) discover novel packing motifs.

2.2The Rubrene Family: Classical Synthesis, Modified Synthesis and Notable Derivatives

This section summarizes the synthetic routes to rubrene as well as a few notable derivatives that are made to probe the structure−property relationship.

2.2.1 Classical Synthesis of Rubrene and Studies of Isotope Effect *via* Deuteration and ^{13}C Substitution

The first synthesis of rubrene was reported in 1926 by Moureu and co-workers. Shown in **Scheme 2-1**, the synthesis started from the dehydrobromination of (*E*)-(2-bromovinyl)benzene to afford phenylacetylene, which was then deprotonated and added to

benzophenone. The resulting propargyl alcohol **2.2** was then treated with phosphorous trichloride to achieve the propargyl chloride **2.3**. From this point, rubrene can be made in one step by simply heating **2.3** neat[45]. The mechanism of this transformation was considered going through the formation of 1,3,3-triphenylchloroallene **2.4**, followed by [4+2] cycloaddition, electrocyclization and loss of two equivalents of HCl.

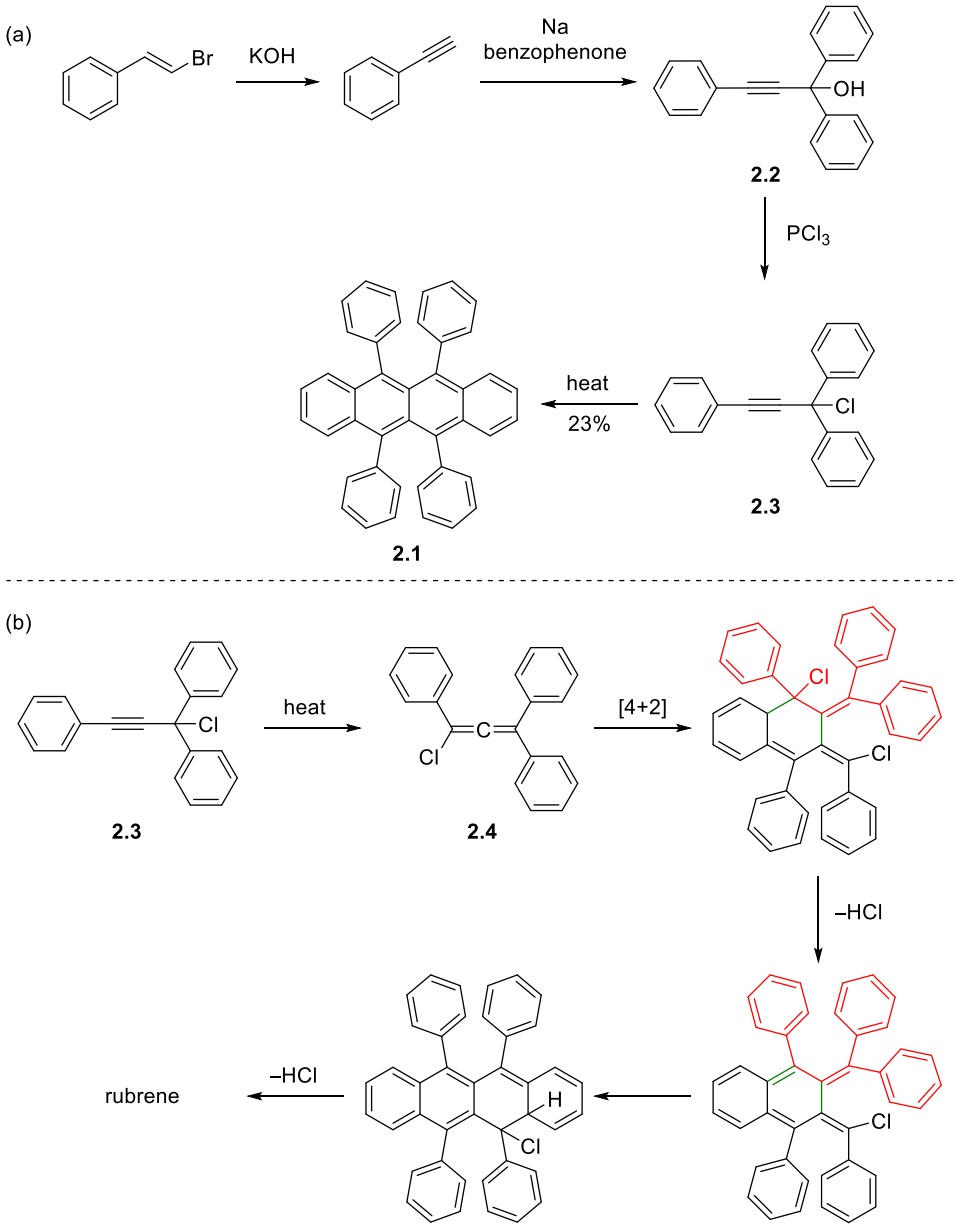

Scheme 2-1 Classic synthesis of rubrene *via* pericyclic mechanism.

Though this classical route is short in the number of steps, the final transformation to rubrene required tedious purification and resulted in a low yield (23%). Since then, others have studied modifications to this method for better efficiency or use for diverse rubrene synthesis. One notable modification was made by Braga et al. in 2011 (**Scheme 2-2**), in which they provided optimized conditions for the transformation from propargyl alcohol **2.2** to rubrene **2.1**. The combined two-step reaction gave increased yields to rubrene (60%).

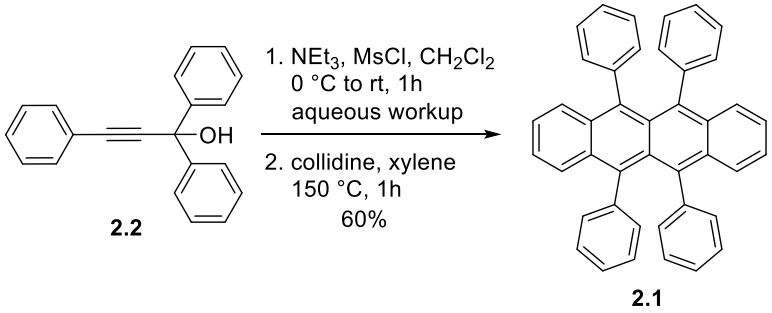

Scheme 2-2 Modified rubrene synthesis by Braga *et al.*

Following this classic route, isotopically substituted rubrenes were synthesized and studied in OFET devices. This category of study involved two congeners: perdeuterated rubrene (D_{28}-rubrene, $C_{42}D_{28}$) and ^{13}C-labeled rubrene ($^{13}C_{42}$-rubrene, $^{13}C_{42}H_{28}$). In 2013, Xie et al. reported the synthesis of D_{28}-rubrene and the transport properties in single crystal OFET devices.[46] Synthesis of D_{28}-rubrene was performed by McGarry (**Scheme 2-3**), an alumnus of the Douglas lab, using a modified synthetic route for native rubrene. As perdeuterated chemicals are expensive and hard to acquire, the global deuterium labelling was achieved by using perdeuterated bromobenzene (C_6D_5Br) **2.5** as the common starting materials for all the synthetic building blocks. OFET studies revealed that the vapor-grown D_{28}-rubrene maintained the remarkable transport behavior of native rubrene, in which a consistent high hole mobility (>10 $cm^2\ V^{-1}\ s^{-1}$, maximum mobility at 45 $cm^2\ V^{-1}\ s^{-1}$) could

be achieved in the vacuum-gap transistor architecture at room temperature. In order to further study the isotope effect on field-effect mobility, a fully isotope substitution of $^{13}C_{42}$-rubrene was later studied in 2017[47]. Similar to the synthesis of D_{28}-rubrene, the route to $^{13}C_{42}$-rubrene started from ^{13}C-labelled bromobenzene. It was found that the $^{13}C_{42}$-rubrene adopts the same crystal structure as native rubrene crystals grown *via* physical vapor transport. The characteristic transport nature of rubrene was also observed for $^{13}C_{42}$-rubrene. However, the field-effect mobility based on a large batch of rubrene devices (~ 74 devices) revealed that the ^{13}C isotopic substitution resulted in a 13% loss in the hole mobility of rubrene. The negative effect was attributed to the redshift of vibrational frequency, which was modeled *via* computer simulations.

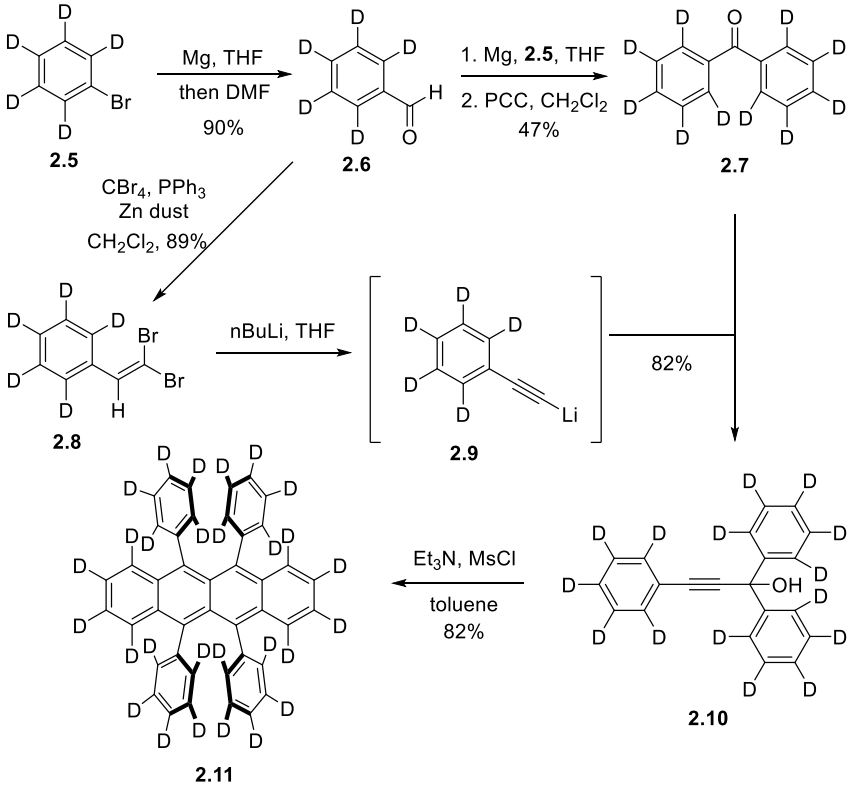

Scheme 2-3 McGarry's synthesis to D_{28}-rubrene.

2.2.2 Systematic Studies of Phenyl-Functionalized Rubrenes – Correlating Molecular Changes with Crystal Packing and Electronic Properties

The classical synthetic route to rubrene provided an efficient way to produce native rubrene in few steps. However, in an effort to achieve various functionalized rubrene congeners, the above methods are inefficient for rapid derivatization. To this end, an alternative approach needs to be developed which allows the introduction of diverse functional groups at a late-stage in the synthesis. Such a synthetic route would enable insightful studies of rubrene-based materials so that the knowledge gap between the chemical structures and material properties could be potentially be filled.

In 2013, McGarry and co-workers reported a systematic study of functionalized rubrene derivatives bearing alkyl and/or trifluoroalkyl substituents at the peripheral phenyl groups. There are two main design principles for the rubrene derivatives studied: 1) introduction of functional groups adjust the electronics of the side phenyl groups, which affects the conformation and electronic structure of the tetracene backbone 2) the substituents modify the steric characters of the side phenyl groups and thus potentially impact the crystal packing motifs and charge transport behaviors. In this work, the functionalized rubrenes were synthesized *via* step-wise introduction of substituted phenyl groups. Shown in **Scheme 2-4**, the synthesis commenced with Suzuki-Miyaura coupling between 6,11-dichloro-5,12-tetracenedione **2.12** and arylboronic acid. The former could be efficiently obtained from Friedel-Crafts acylation between 1,4-naphthalenediol and phthaloyl chloride, followed by subsequent chlorination using PCl_5[48]. The resulting 6,11-diaryltetracene-5,12-dione **2.13** was then subjected to nucleophilic addition of aryllithium

to install the second set of substituted phenyl groups. Finally, diol **2.14** was reduced and aromatized, regardless of the diastereomer ratio, to give rubrene derivatives **2.15**.

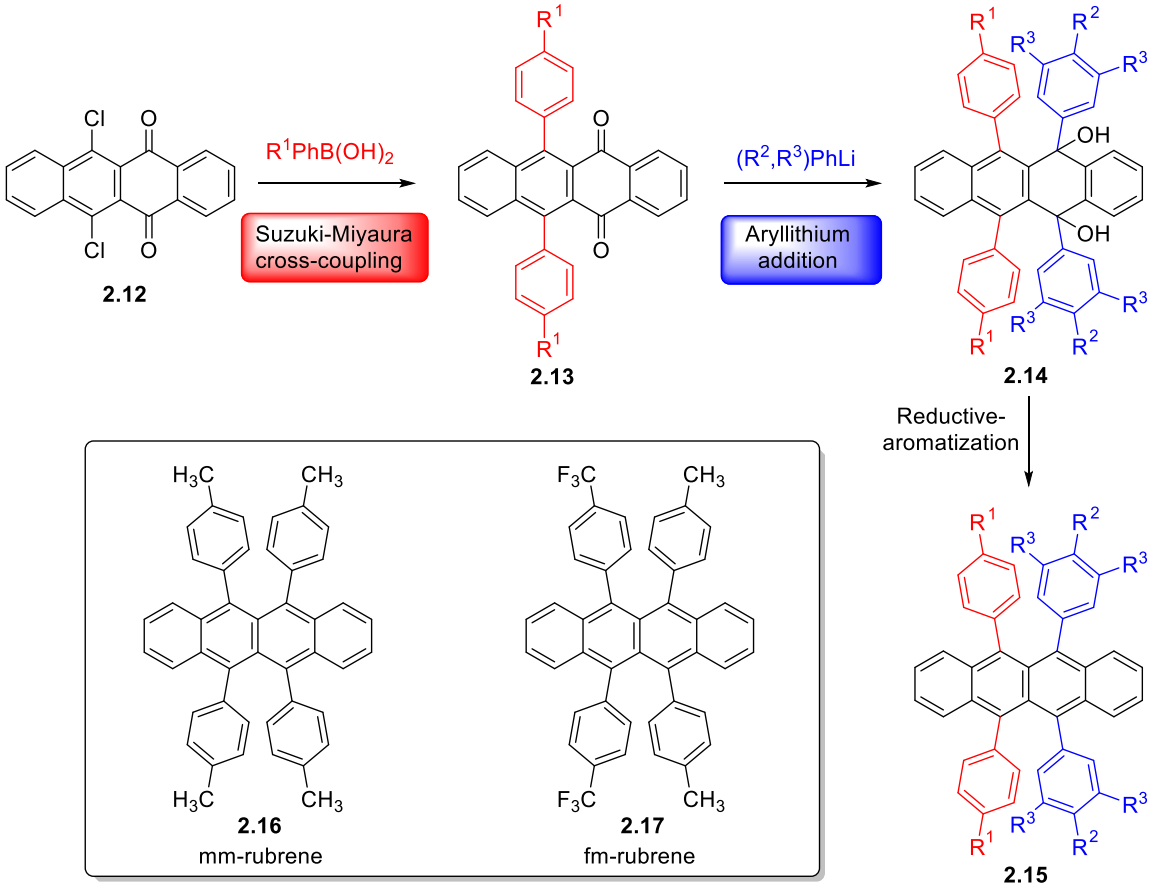

Scheme 2-4 Modified synthesis of phenyl-functionalized rubrenes by McGarry et al.[49]

Following this modified synthetic route, a variety of functionalized rubrenes were prepared. Characterization *via* single-crystal X-ray diffraction, cyclic voltammetry and OFET device performance revealed interesting features that are different from rubrene. For example, when functional groups were introduced onto the side phenyls, the conformation of the tetracene backbone could be affect. Specifically, for a typical tetra-alkyl substituted mm-rubrene **2.16**, the tetracene backbone was found in a non-planar conformation. As shown in **Figure 2-4**, the asymmetric unit of the crystal structure of mm-rubrene contains

two molecules, both of which adopt a twisted tetracene backbone with an end-to-end twist angle of 33.9° and 42.8°, respectively. Similar backbone twist was found in other phenyl-functionalized rubrenes with electron-donating alkyl substitutions at *para*- and/or *meta*-positions. Due to the backbone twist, mm-rubrene and other alkyl-substituted rubrene analogs no long persist the herringbone packing motif with highly ordered π-stacking. Instead, short contacts based on edge-to-face interaction between the tetracene cores of neighboring rubrene molecules become dominated in the packing arrangements.

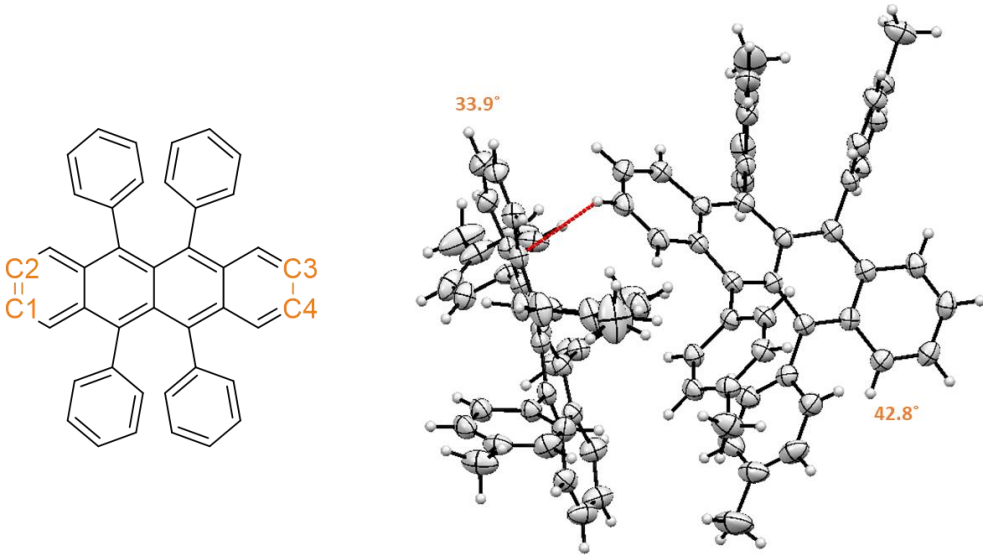

Figure 2-4 Left: the end-to-end twist angle of the tetracene backbone is defined by the torsion angle of the designated C1−C2 bond and C3−C4 bond. Right: the configuration of mm-rubrene molecules analyzed by single-crystal X-ray analysis. Red line shows the expanded short contact. Hydrogen atoms are omitted for clarity.

Interestingly, when replacing one set of electron-donating alkyl substituents with electron-withdrawing substituents, such as trifluoromethyl groups, the crystal structure changed drastically and the well-defined packing motif similar to rubrene was observed. Among the rubrene analogs studied by McGarry *et al.*, fm-rubrene **2.17** was found to be

the most attractive candidate that is comparable with native rubrene based on several aspects. In the crystal structure, fm-rubrene showed planar backbone cores and exhibited intermolecular π-stacking with a decreased π-π distance compared with rubrene (3.42 Å for fm-rubrene and 3.74 Å for rubrene, **Figure 2-5**). The herringbone motif was also observed with increased interlayer distance along the short axis of the tetracene core, which is attributed to the substituents acting as spacing groups. As the charge transport in rubrene is anisotropic: charge transport most efficiently along the π-stacks, increasing the interlayer spacing could potentially decrease the polarization of the surrounding "π-columns", and thus decrease the electronic disorder during charge transport[50]. Another interesting aspect of fm-rubrene is the well-tuned electronic properties and different OFET device performance. Though the side phenyl groups are not well conjugated with the tetracene backbone, McGarry et al. have found that the introduction of electron-withdrawing CF_3 groups could still affect the electronic properties of rubrene. Specifically, fm-rubrene shows larger electron affinity than native rubrene, which lower the electron injection barrier by about 0.3 eV. This results in the ambipolar transport behavior of fm-rubrene with maximum hole (electron) mobilities of 1.54 (0.28) $cm^2\ V^{-1}\ s^{-1}$. Such charge transport properties have rarely been found in the literature.

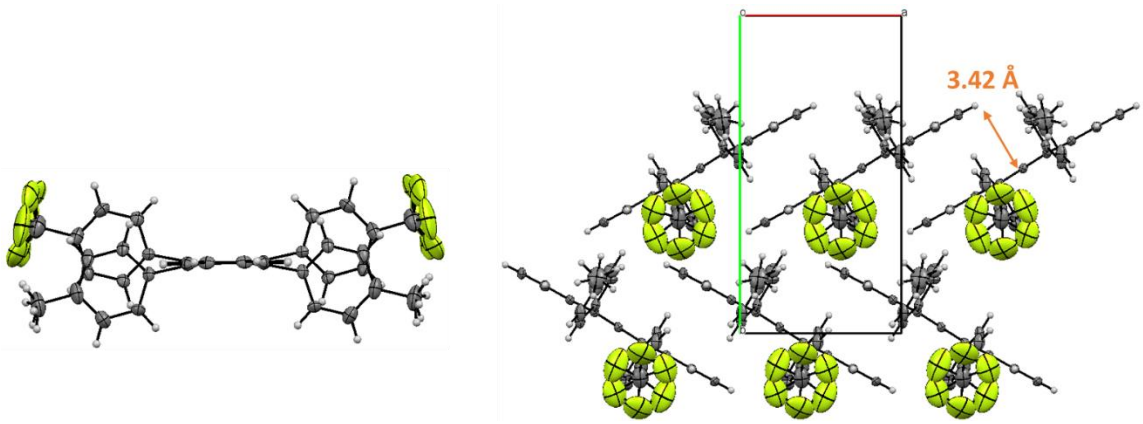

Figure 2-5 Crystal structure and π-stacked herringbone packing of fm-rubrene.

Collectively, these studies have demonstrated the utility of chemical modification in tuning material properties of rubrene. The electronic properties, solid-state packing arrangements and semiconductive properties can be effectively adjusted based on rational design of functionalized rubrene structures. The work mentioned above has just scratched the surface on the exploration of structure–property relationships. In the following section of this chapter, I will discuss another approach to functionalized rubrenes, which explicitly focus on the tetracene core modification and the effect of fluorine substitution.[51]

2.3 Studies into the Effect of Fluorination on Rubrene: Synthesis and Crystal Structures

As shown in the previous section, functionalized rubrenes have shown strong potential for optimized material properties. This section illustrates the continued research in exploring more structurally interesting rubrene derivatives. One major research topic in the current project is the effect of fluorination on rubrene. Based on the unique nature of fluorine atom as the functional group of choice, a couple of benefits could be anticipated. On the one hand, the fluorine atom is strongly electron-withdrawing. Through core or side-

phenyl fluorination, the electron affinity of rubrene can be increased, which would theoretically turn on or improve the electron transport abilities in OFET devices. Thus, fluorinated rubrenes are potential candidates for a new type of n-type or ambipolar semiconductors. On the other hand, the role of fluorine-based intermolecular interactions in solid-state organic crystals is not very clear to both organic chemists and material chemists.[52] Therefore, a systematic study of fluorinated rubrene would correlate the degree and position of fluorination to the impact on crystal packing and electronic properties. This will guide future crystal engineering of rubrene derivatives and, more broadly, the general material design for high-performance semiconductors.

2.3.1 Synthetic Studies Toward Partial and Full Fluorination of Rubrene: F_{10}-Rubrene, F_{20}-Rubrene and F_{28}-Rubrene

Based on previous work on side-phenyl-functionalized rubrenes, three new rubrene derivatives were proposed in this study: F_{10}-rubrene, F_{20}-rubrene and F_{28}-rubrene (perfluororubrene) (**Figure 2-6**). Our particular interest in fluorine substitution is due to its electronegative nature as well as the moderate size as compared with other electron-withdrawing groups. My coworkers and I envisioned that in F_{10}-rubrene and F_{20}-rubrene the electron density of the side phenyl groups could be decreased by incorporation of fluorine substituents. We believed these rubrene derivatives may tend to adopt planar backbone conformation, as evidenced in the early examples that fm-rubrene was planar while mm-rubrene was twisted (Chapter 2, Section 2.2.2). This idea was also supported by calculations performed by Brédas and co-workers in that the core structure of rubrene (and derivatives) twisted to reduce the unfavorable exchange−repulsion interaction between the side phenyl groups[53]. In F_{28}-rubrene, we were very interested in the change of electronic

character through core substitution as the HOMO/LUMO energy level can be more directly affected.

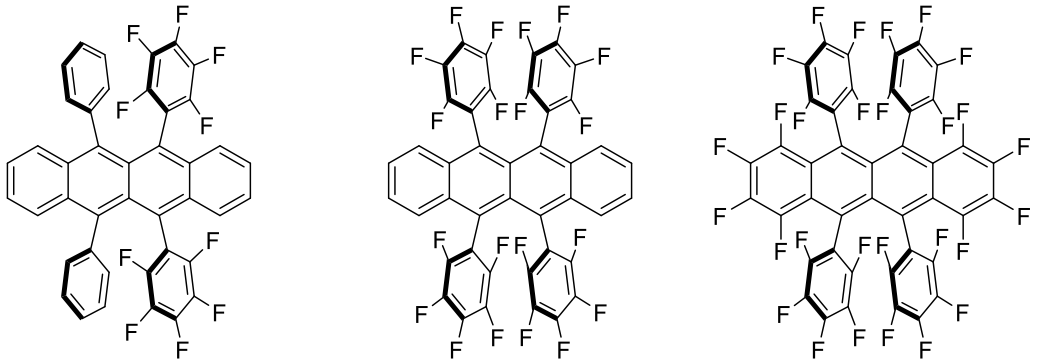

Figure 2-6 Structure of proposed fluorinated rubrene derivatives.

Synthesis of F_{10}-rubrene was first explored using the McGarry's route described previously in **Scheme 2-4**. As this modified route allows for late-stage diversification, desire rubrene derivatives can be made by using the appropriate arylboronic acid or aryllithium species. Starting from 6,11-dichloro-5,12-tetracenedione **2.12**, installation of the first set of side phenyl groups was achieved smoothly *via* Suzuki−Miyaura coupling with phenylboronic acid (88% yield). The diaryltetracenedione **2.21** was then subjected to the installation of the second set of aryl groups by addition of perfluorophenyl lithium to the ketone functionality. The resulting diol **2.23** was formed as a mixture of syn/anti diastereomers which was carried on directly into the reduction with stannous chloride/HCl to afford F_{10}-rubrene **2.18** in 60% yield over the two-step sequence. It is noteworthy that pentafluorophenyl lithium **2.24** is a challenging reagent to handle. Its nucleophilicity is lower than other common lithiated species due to its electron-deficient nature. Moreover, a possible side reaction pathway at play is the generation of the tetrafluorobenzyne **2.25**

through the loss of LiF above −20 °C, which readily decomposes without the presense of a proper trapping reagent.[54] Additionally, the choice of solvent also plays an important role for the efficient nucleophilic addition step. The use of diethyl ether, instead of THF, appeared to increase the solubility of the lithiated species. This fact was supported by the observation that, under same temperature and concentration, the diethyl ether solution was much clearer than the THF solution. Thus, diethyl ether was used as the solvent for a faster and more efficient transformation.

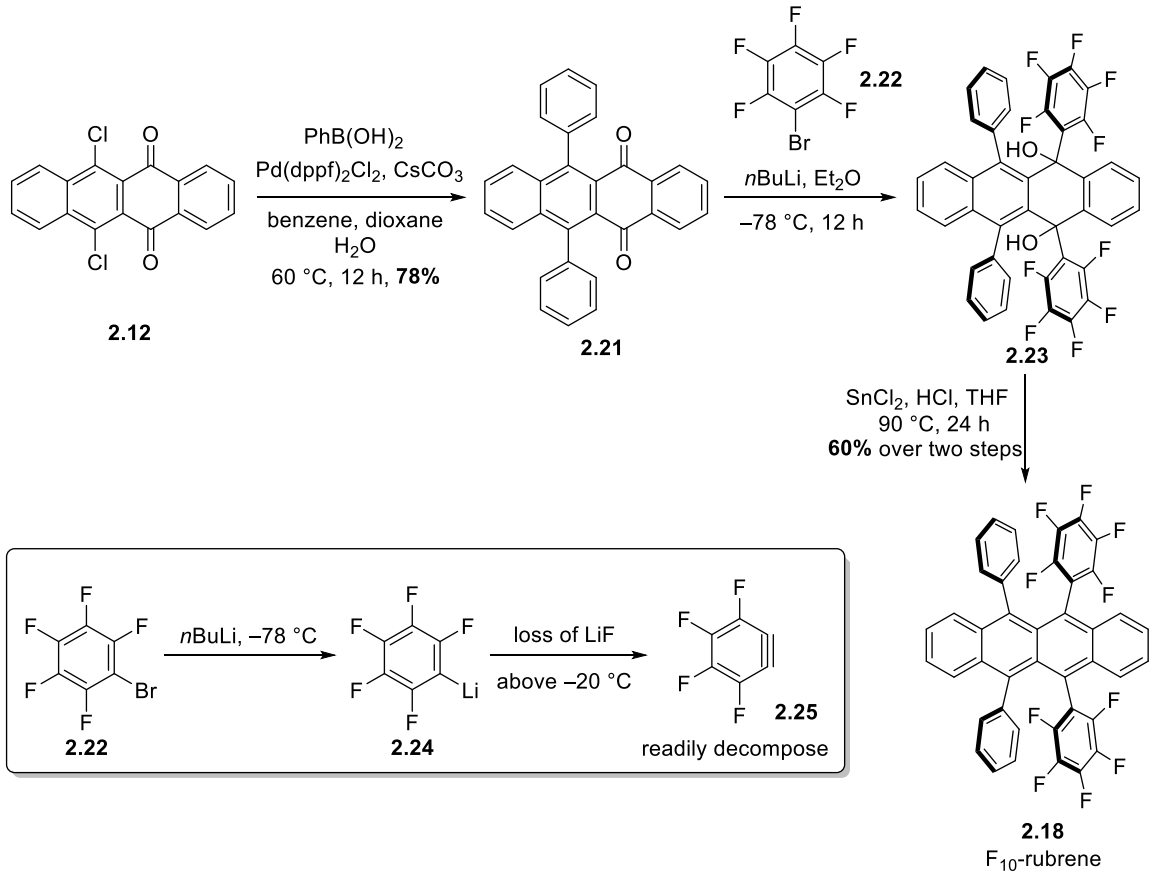

Scheme 2-5 Synthesis of F_{10}-rubrene.

After successful synthesis of F_{10}-rubrene, we set out to explore the synthesis towards F_{20}-rubrene. Keeping to the established route similar as in **Scheme 2-5**, We initially

attempted to install the first set of perfluorophenyl groups *via* Suzuki-Miyaura coupling between tetracenedione **2.12** and pentafluorophenylboronic acid **2.26**. However, this transformation was ineffective and gave only unreacted starting material (**Scheme 2-6a**). In fact, literature reports have shown that pentafluorophenylboronic acid **2.26** could decompose into pentafluorobenzene in the presence of base and heat[55] (**Scheme 2-6b**). Because of this hydrodeboration issue, an alternative route to install the perfluorophenyl groups need to be developed.

In light of the successful perfluorophenyl lithium addition used in the synthesis of F_{10}-rubrene, we sought to apply the same reaction conditions for F_{20}-rubrene (**Scheme 2-6**). Therefore, we started the sequence from 6,11-dimethoxytetracene-5,12-dione **2.29**, which can be easily made from methylation of 6,11-dihydroxytetracene-5,12-dione[48]. By careful control of the reaction temperature, nucleophilic addition of perfluorophenyl lithium to the quinone functionality afforded the desired diol adducts **2.30**. In order to remove the hydroxy groups and regain the tetracenedione moiety for subsequent nucleophilic addition, a Stork−Danheiser type rearrangement[56] under acidic conditions was attempted and afforded the desired diaryltetracenedione **2.27** in good yields (85%). Upon repeating the nucleophilic addition and reduction sequence, F_{20}-rubrene was smoothly obtained. Noted that trifluoroacetic acid (TFA) was required to accomplish the reduction step (**2.31** to **2.19**), as the protonation of hydroxyl groups was more challenging with strongly electron-efficient phenyl substituents[57].

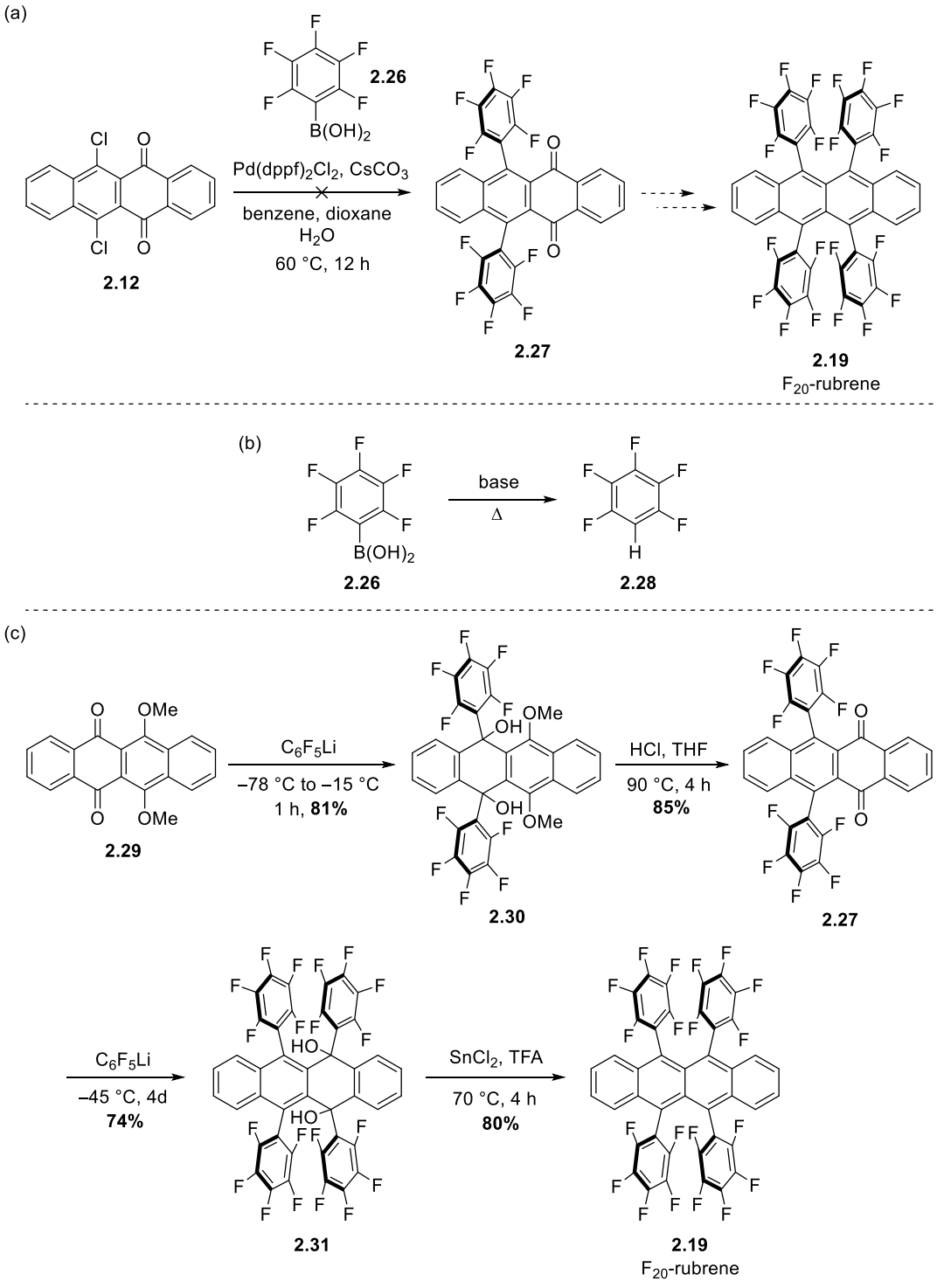

Scheme 2-6 Synthetic route to F_{20}-rubrene. (a) Attempted Suzuki-Miyaura coupling with pentafluorophenylboronic acid. (b) Decomposition of pentafluorophenylboronic acid. (c) Completed synthesis of F_{20}-rubrene.

After completing the synthesis of F_{20}-rubrene, we moved on to explore the synthesis towards perfluororubrene **2.20**. Since perfluororubrene contains multiple fluorine substitutions on the tetracene core, the tetracene dione moiety must be synthesized independently. While searching into literature for the synthesis of fluorinated acene skeleton, we noticed a few examples that provided valuable precedence. In the synthesis of perfluoropentacene by Suzuki and co-workers (**Scheme 1-6**), Friedel−Crafts acylation was used to build the corresponding perfluorinated pentacenedione moiety.[31a] A similar strategy was also used in building the perfluorinated tetracene core by Suzuki *et al.*[58] and Ono *et al.* [59] We recognized that 1,2,3,4,7,8,9,10-octafluoro-6,11-dihydroxy-5,12-naphthacenedione **2.34** is analogous to **2.29** in **Scheme 2-6c**, perfluororubrene could be presumably obtained by step-wise installation of the perfluorophenyl groups following the established sequence.

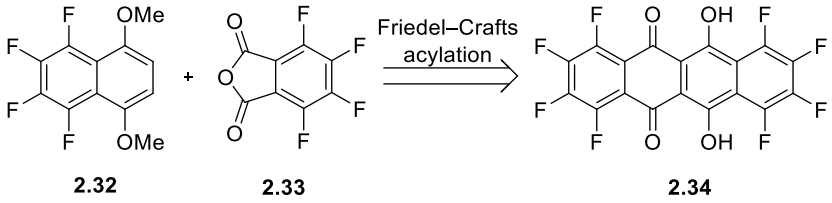

2.32 **2.33** **2.34**

Scheme 2-7 Synthesis of perfluorinated tetracene moiety by Ono *et al.* and Suzuki *et al.*

With this synthesis plan in mind, I set out to explore the synthesis of perfluororubrene. The first stage is to obtain the key precursor **2.32** for the Friedel−Crafts acylation step shown in **Scheme 2-7**. The synthesis started with electrophilic bromination of furan. Using *N*-bromosuccinimide (NBS) as the bromination reagent and dimethylformamide (DMF), 2-bromofuran was smoothly obtained by stirring the solution at room temperature.[60] Though this was a straight forward transformation, however, separation of bromofuran

from the solution mixture was indeed challenging. In this case, a steam distillation was proved to be the best method to efficiently separate 2-bromofuran **2.35** from the high-boiling solvent DMF. **Figure 2-7** shows the apparatus set up for the steam distillation, in which a constant jet of steam was generated from the two-neck round-bottom flask (positioned on the left) and directly injected into the reaction mixture *via* a vapor dispenser. The steam flow was finally condensed by cooling water and collected in the receiving flask. 2-Bromofuran was then transformed into 2-methoxyfuran **2.36** in the presence of copper(I) bromide and concentrated sodium methoxide solution (42.5 wt.%). Next, a benzyne Diels−Alder cycloaddition was performed between 2-methoxyfuran and tetrafluorobenzyne which was generated *in situ*. The cycloadduct **2.37** readily ring-opened upon acidic workup to afford the naphthalene moiety, which was subsequently methylated to give the desired **2.32**.

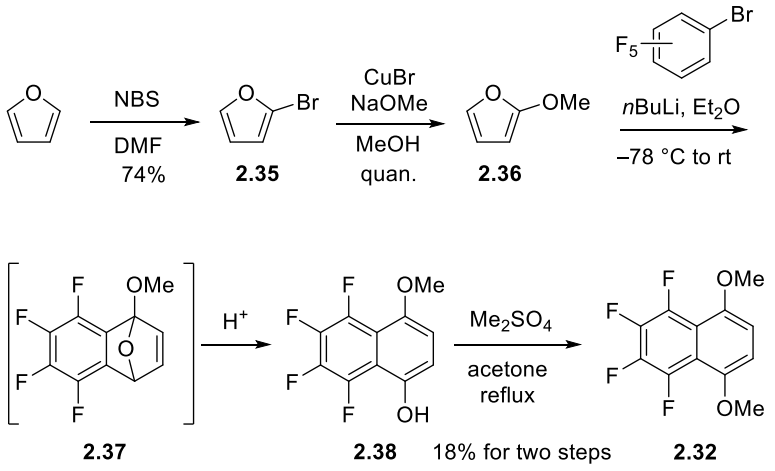

Scheme 2-8 Synthesis of 1,2,3,4-tetrafluoro-5,8-dimethoxy-naphthalene **2.32**.

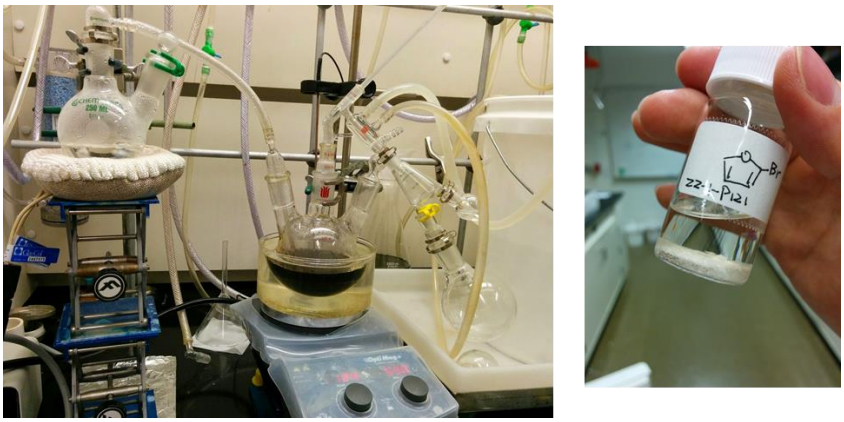

Figure 2-7 Left: steam distillation of 2-bromofuran. Right: purified 2-bromofuran stored over drying agent.

With 1,2,3,4-tetrafluoro-5,8-dimethoxy-naphthalene **2.32** in hand, I moved on to the Friedel−Crafts acylation for the synthesis of fluorinated tetracene core **2.34**. Adopting Ono and Suzuki's method, compound **2.34** was obtained by heating the mixture of compound **2.32** and **2.33** in the presence of aluminum trichloride and sodium chloride. The hydroxyl groups in **2.34** were protected using dimethylsulfate under basic conditions to give the corresponding dimethoxytetracenedione **2.35**. In general, acetone is the ideal solvent for this type of reactions as it is a polar solvent and easy to handle. However, in this case, elevated reaction temperature was required as the electron-deficient nature of the tetracene core retards the reaction. Fortunately, my coworker Ogden and I found that employing cyclohexanone as the reaction solvent allowed for higher reaction temperature and the reaction proceeded to give the desired methylated product **2.35** in moderate yield (57%). At this point, I attempted the step-wise installation of the side perfluorophenyl groups. Nucleophilic addition of perfluorophenyl lithium to the methyl-protected tetracenedione **2.35** formed an inconsequential mixture of diol diastereomers **2.36**, which was then converted into 6,11-diaryltetracene-5,12-dione **2.37** *via* an acid-promoted rearrangement.

The second set of perfluorophenyl groups was installed using the same method. However, the perfluorophenyllithium addition was less efficient this time, probably due to nucleophilic aromatic substitution between the *in situ* generated alkoxide and the nearby perfluorophenyl group, which could lead to decomposition. Finally, reductive aromatization of diol **2.38** using $SnCl_2$ in methanesulfonic acid solvent afforded perfluororubrene **2.20** in moderate yields. Using this route, perfluororubrene could be prepared in gram-scale quantities.

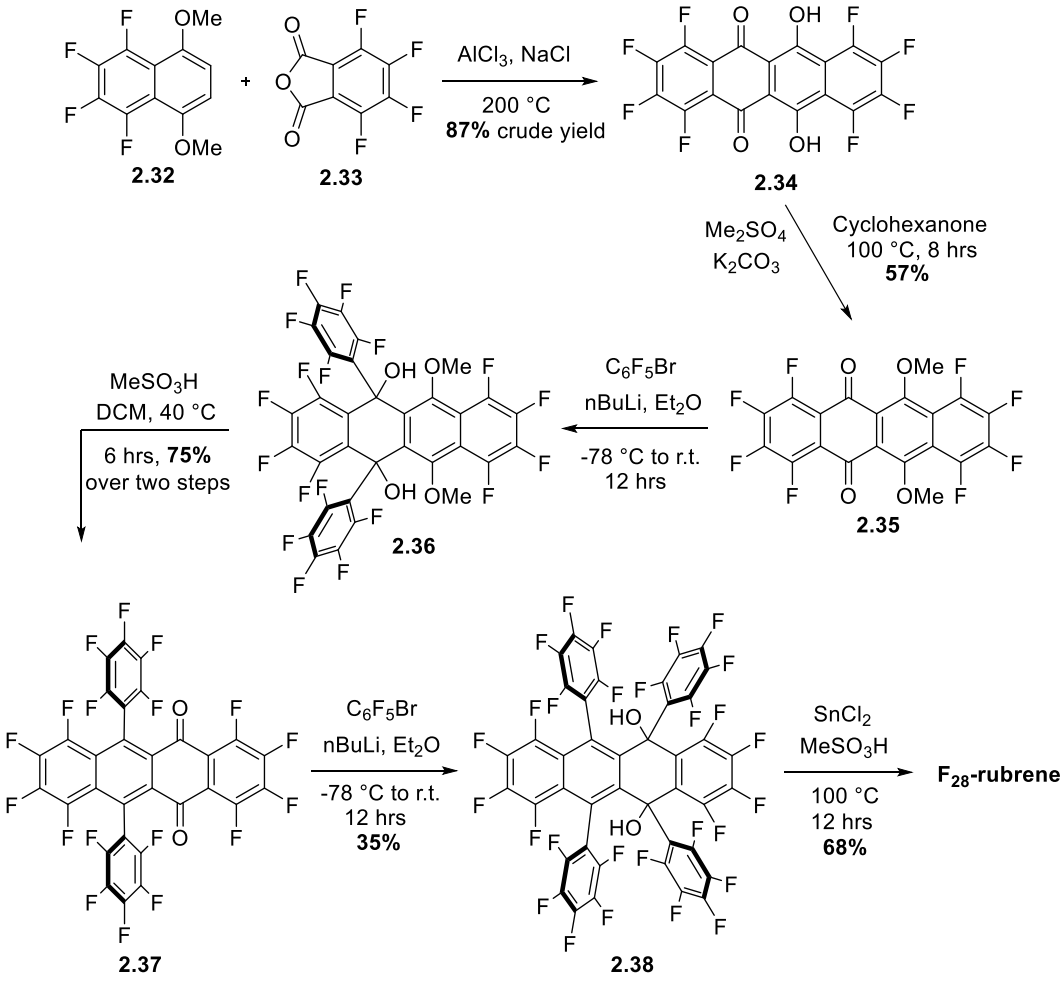

Scheme 2-9 Complete synthesis of perfluororubrene (F_{28}-rubrene).

2.3.2 Crystallography Studies of Fluorine-Substituted Rubrene: The Effect of Fluorine-Based Intermolecular Interaction

In this section, we will discuss the effect of fluorination on crystal packing. Analyses of the crystal structures mainly focus on the following aspects: 1) the planarity of the rubrene backbone; 2) the crystal packing motif; 3) identify the intermolecular interactions at play, which are responsible for, or help, stabilize the observed crystal packing. By focusing on these aspects, we hope to provide rational explanations for why certain rubrene molecules adopt unusual molecular conformation and/or solid-state arrangements. Moreover, the discovery of beneficial factors will provide future guidance for the crystal engineering of rubrene and/or other acene derivatives.

Crystals of fluorinated rubrene derivatives were grown from slow evaporation of solvents, small scale sublimation (**Figure 2-8a**) or physical vapor transport (**Figure 2-8b**). For all three fluorinated rubrenes, the sublimation method conveniently afforded high quality single crystals for X-ray diffraction experiments (**Table 2-2** & **Table 2-3**). Additionally, for F_{28}-rubrene, polymorphic crystal structures were also obtained from solution and physical vapor transport (**Table 2-3**).

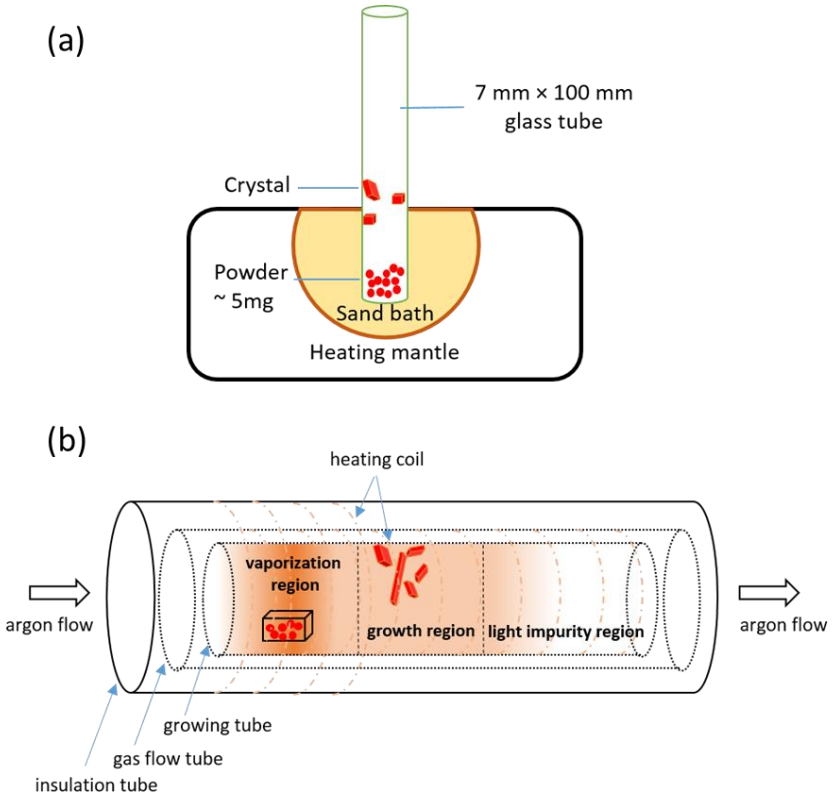

Figure 2-8 Schematic illustration of apparatus used for single-crystal growth experiments.

Table 2-2 Crystal parameters for F_{10}-rubrene and F_{20}-rubrene.

Crystal	F_{10}-Rubrene	F_{20}-Rubrene
Formula	$C_{42}H_{18}F_{10}$	$C_{42}H_8F_{20}$
Formula weight	712.59 g/mol	892.49 g/mol
Temperature	123 K	123 K
Crystal system	Triclinic	Triclinic
Space group	*P*-1	*P*-1
Unit cell dimensions	a = 7.3564(5) Å b = 14.7042(11) Å c = 15.7118(10) Å α = 65.973(4)˚ β = 88.823(4)˚ γ = 89.903(4)˚	a = 7.9792(3) Å b = 12.7930(5) Å c = 16.7743(6) Å α = 92.3130(18)˚ β = 95.3760(18)˚ γ = 105.3060(18)˚
Volume	1551.92(18) $Å^3$	1640.50(11) $Å^3$
Z	2	2
Crystal grown method	Sublimation	Sublimation

Table 2-3 Crystal parameters for three F_{28}-rubrene polymorphs.

Crystal	Polymorph A	Polymorph B	Polymorph C
Formula	$C_{42}F_{28}$·$CHCl_3$	$C_{42}F_{28}$	$C_{42}F_{28}$
Formula weight	1153.79	1036.42	1036.42
Temperature	123 K	123 K	123 K
Crystal system	Orthorhombic	Monoclinic	Triclinic
Space group	$P2_12_12_1$	$P2_1/n$	$P1$
Unit cell dimensions	a = 8.4500(4) Å b = 11.004(5) Å c = 42.680(2) Å α = 90˚ β = 90˚ γ = 90˚	a = 16.6651(6) Å b = 11.1489(5) Å c = 19.1918(7) Å α = 90˚ β = 90.213(3)˚ γ = 90˚	a = 12.5285 Å b = 17.8163 Å c = 24.7339 Å α = 90.202(4)˚ β = 101.264(3)˚ γ = 90.695(3)˚
Volume	3967.3(3) $Å^3$	3565.8(2) $Å^3$	5414.1(5) $Å^3$
Z	4	4	6
Crystal grown method	Solution	Sublimation	Physical vapor transport

Unlike rubrene or fm-rubrene, F_{10}-rubrene adopts a non-planar backbone conformation, with an end-to-end twist of 30.8˚ (**Figure 2-9a**). As seen previously, rubrene derivatives with significant backbone twist usually exhibit poor packing arrangements that are lack of sufficient π-π stacking between neighboring molecules. However, F_{10}-rubrene adopts a 2-D brickwall packing motif, which has not been observed in the past for other rubrene derivatives[49]. In the 2-D brickwall packing motif, significant π-π stacking of the tetracene cores are still observed even with twisted conformation. Interestingly, close contacts were found between the rubrene molecules that directly pack with each other. Specifically, C−F···H interactions can be found between the perfluorophenyl groups and the tetracene edge hydrogens (**Figure 2-9b**). These interactions may function as stabilizing factors for the observed slipped π stacks. Another interesting fact about F_{10}-rubrene crystal is the interlayer arrangements. The "interlayer" refers to rubrene molecules that locate in neighboring π-stacked columns instead of stacking with each other. As shown in **Figure**

2-9c, interlayer C−F···H interactions can only be found between phenyl and perfluorophenyl groups. No C−F···F or C−H···H interactions were found. We envision that such a "selective" interaction could potentially help orient the intralayer arrangement, thus contributing to the observed highly ordered packing motif. These observations also suggest that interlayer interactions between the side-phenyl groups on rubrene could also impact on intralayer packing arrangements. In this case, fluorine-based interactions are found in many circumstances that help stabilize or orient crystal packing.

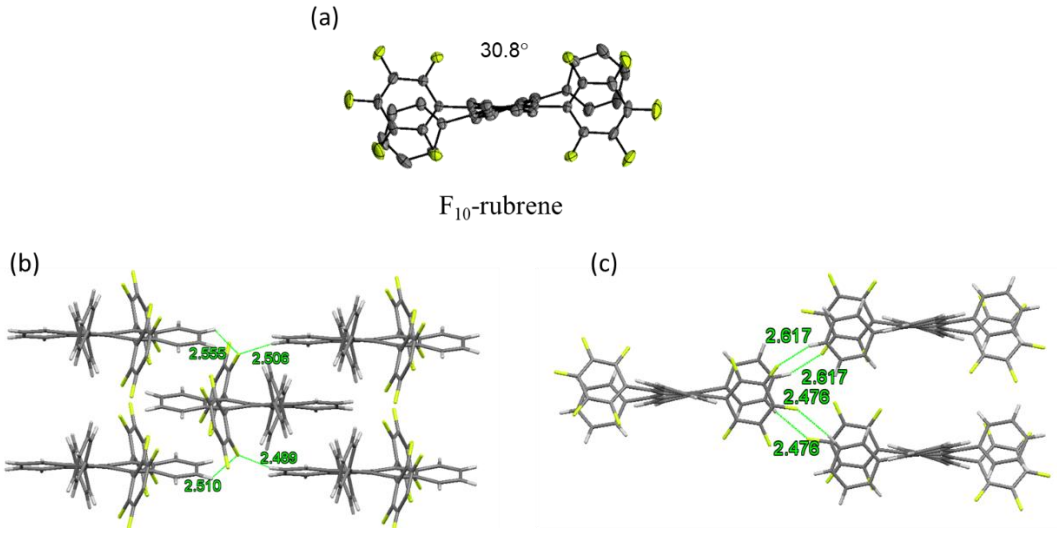

Figure 2-9 (a) Crystal structure of F_{10}-rubrene with twisted tetracene backbone. (b) 2-D brickwall packing motif in F_{10}-rubrene crystal. (c) Interlayer packing arrangements.

After examining the features in F_{10}-rubrene, we were curious to see how an additional set of perfluorophenyl groups would alter the crystal packing motif in F_{20}-rubrene. Interestingly, crystal structure of F_{20}-rubrene revealed a planar tetracene backbone similar to native rubrene (**Figure 2-10a**). However, when comparing the packing motif with native rubrene and F_{10}-rubrene, we noticed that F_{20}-rubrene did not adopt the 2-D brickwall motif as we expected, not did it pack in the classical herringbone motif. Instead, F_{20}-rubrene

showed a slipped herringbone motif, where the F_{20}-rubrene molecules are not perfectly aligned in the herringbone dimer as compared with rubrene (**Figure 2-10 b−d**). As a result, the F_{20}-rubrene crystal contained two sets of π-stack dimers, with one tightly packed (π-π distance at 3.63 Å, **Figure 2-10e**) and the other one loosely packed (π-π distance at 5.56 Å). By carefully examining the close contacts within the crystal structure, we identified several factors that may be responsible for the observed packing arrangements. Firstly, we looked at the cause for the herringbone dimer dislocation. As labelled in **Figure 2-10f**, a close contact at 3.48 Å was marked as a typical π-π_f interaction which occurred between the tetracene backbone and the perfluorophenyl group within the herringbone dimer. The formation of such π-π_f interaction can be attributed to the electron-deficient nature of the perfluorophenyl group, which competes with the edge-to-face (C−H···π) interaction in rubrene. Next, we continued to look for other close contacts. Surprisingly, we were able to find almost all kinds of fluorine-based interaction in the F_{20}-rubrene dimers, including C−F···F interaction (2.86 Å), C−F···H interaction (2.36 Å), C−F···π interaction (3.02 Å). These findings proved that fluorine-based interaction plays an important role in assembling and stabilizing the neighboring molecules in F_{20}-rubrene crystal.

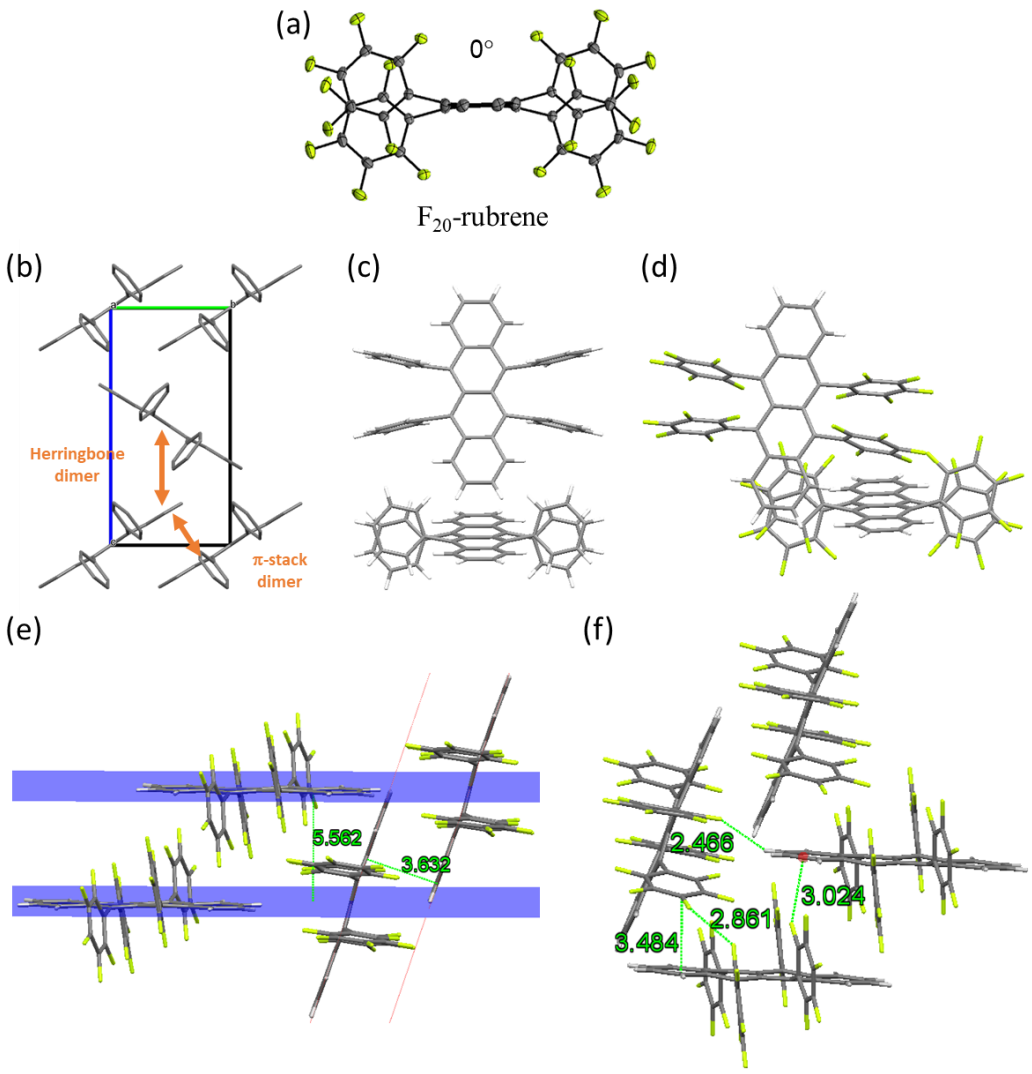

Figure 2-10 Crystal structure of F20-rubrene and comparison with native rubrene. (a) ORTEP drawing of F_{20}-rubrene showing the planar tetracene backbone. (b) Definition of different type of dimers in herringbone packing motif. (c) Herringbone dimer in native rubrene. (d) Herringbone dimer in F_{20}-rubrene showing displacement. (e) Two sets of π-stack dimer in F_{20}-rubrene crystals. (f) Multiple fluorine-based intermolecular interactions observed between packing dimers and herringbone dimers of F_{20}-rubrene crystals.

At last we examined the crystal structures of F_{28}-rubrene. Three different methods, including solvent evaporation, sublimation, and physical vapor transport (PVT) were

employed to grow single crystals of perfluororubrene. Interestingly, each method gave a unique crystal structure. The degree of twist in the tetracene backbone was different in each crystal. By slowly evaporating solvent from a chloroform solution, an orthorhombic crystal A (chloroform solvate) was obtained. In the crystal structure of polymorph A, the perfluororubrene molecule adopted a twisted backbone conformation with an end-to-end twist angle of 39.32° (**Figure 2-11a**). Since a solvent molecule was present, the solvate crystal possessed the longest *c* lattice dimension in the unit cell compared to the other two polymorphic crystal structures. As a result, the intermolecular packing was very loose. No face-to-face packing between tetracene backbones of nearby molecules was observed. Sublimation at 290 °C gave a monoclinic crystal B with the space group of $P2_1/n$, in which the tetracene backbones possessed a larger end-to-end twist angle of 45.37° (**Figure 2-11b**). Compared to the solvate crystal A, a tighter packing arrangement, including one-dimensional stack packing along the crystallographic *a*-axis was found (**Figure 2-12a**). A closer investigation of intermolecular interactions revealed that edge-to-face interactions between a side-perfluorophenyl group and the tetracene backbone of a nearby molecule exist in the spatial ordering. Although there are many examples of orthorhombic crystals for rubrene derivatives that are grown from vapor transport, in our experiment, the crystal structure C obtained from physical vapor transport (argon as the carrier gas, 220−230 °C) was found to be triclinic with the space group of *P*1. Crystal C featured an asymmetric unit containing three unique perfluororubrene molecules. The end-to-end twist angles for each molecule were different: 44.03°, 47.12° and 47.97°, respectively. In crystal C, a herringbone type packing motif was observed. Both the C−F···π interaction and π−π interaction may be responsible for the packing arrangement. A close π−π interaction was

found between the tetracene cores with a face-to-face distance of 3.38 Å (**Figure 2-12b**). we noted that even though the tetracene backbone was twisted, close intermolecular interactions still existed, which can be attributed to the inherent electron-deficiency of the perfluororubrene backbone.

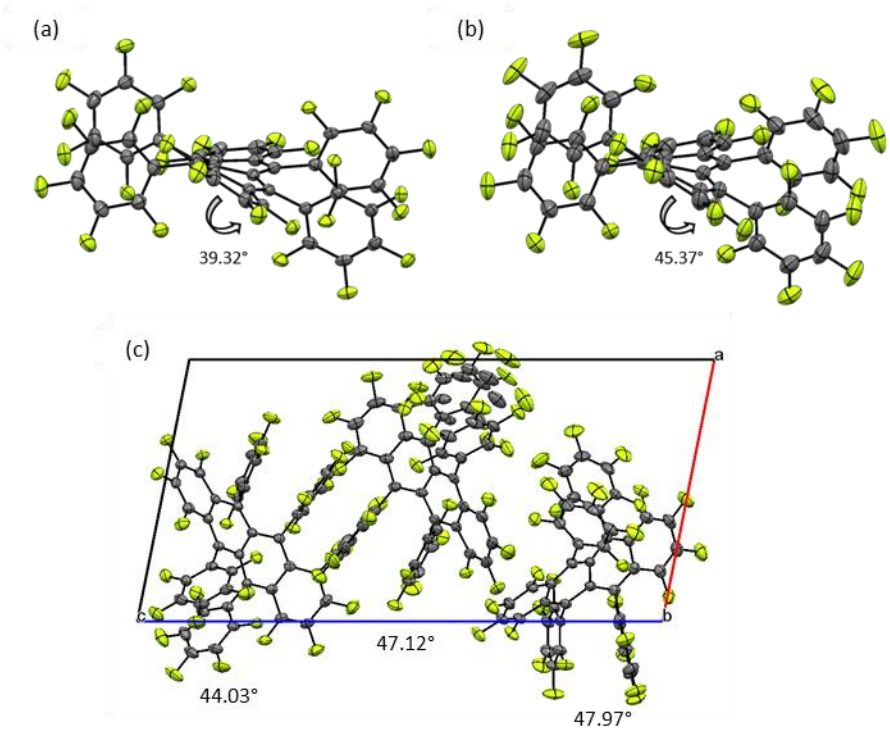

Figure 2-11 Crystal structure of F_{28}-rubrene: (a) polymorph A; (b) polymorph B; (c) polymorph C. Numbers indicate the end-to-end twist angle of the tetracene backbone.

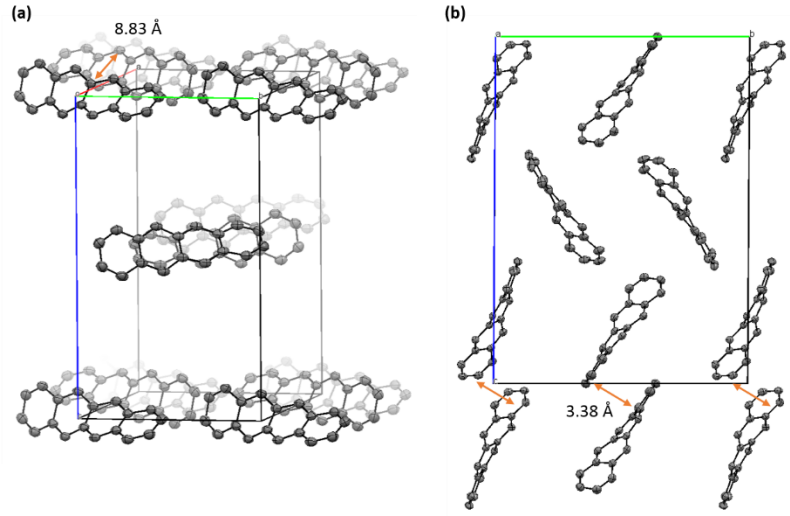

Figure 2-12 Packing arrangements for (a) crystal B and (b) crystal C, only the tetracene backbones were shown for clarity.

2.4 Conclusion

In conclusion, we have demonstrated a modified synthetic approach to rubrene derivatives containing side-perfluorophenyl groups (F_{10}-rubrene and F_{20}-rubrene). A complete total synthesis perfluorinated rubrene (F_{28}-rubrene) has also been established from simple and commercial available chemicals. For the new rubrenes obtained, single-crystal X-ray analysis provided insightful information on their molecular conformations as well as packing arrangements. In fluorinated rubrene derivatives, the tetracene backbone could exist in either planar or twisted conformations, depending on the pattern of fluorine substitution. Although the backbone twist usually serves as a disrupting factor for significant π–π overlap, in this case however, π–π or π–π_f interactions are still observed with twisted rubrenes due to the electron-deficient feature of fluorinated aromatic units. Other than affecting the electronic structure of rubrene, fluorine substitution also greatly impacts the solid-state packing motif *via* various fluorine-based interactions. These

interactions can potentially orient and stabilize the molecular ordering within the π-stacking layer, and help organize the packing arrangements through interlayer interactions.

In this study, we have demonstrated that when designing new rubrene derivatives, it is necessary to consider how new intermolecular interactions may occur. This work has identified unique intermolecular interactions that affect molecular packing in fluorinated rubrenes and has discovered new packing motifs for rubrene derivatives. Collectively, this work allows for the rational design and improved crystal engineering of new rubrene derivatives.

2.5 Experimental Details

Chemicals were used as received unless otherwise noted. All oxygen or moisture sensitive reactions were performed under nitrogen atmosphere following standard Schlenk techniques. Anhydrous diethyl ether was purchased from Sigma-Aldrich (ACS reagent, ⩾ 99.0%) and used without further purification. Dichloromethane was distilled from CaH_2 prior to use. Bromopentafluorobenzene (99%) was purchased from Synquest Labs, Inc. Methanesulfonic acid (⩾99.5%) was purchased from Sigma-Aldrich. Analytical thin layer chromatography (TLC) was performed using 0.25 mm silica plates from Silicycle. Flash chromatography was performed using 230–400 mesh (particle size 0.04–0.063 mm) silica gel purchased from Silicycle.

^{1}H NMR (400 or 500 MHz) and ^{13}C NMR (100 or 125 MHz) spectra were recorded on Bruker FT NMR instruments. ^{19}F NMR (282 MHz) were recorded on a Varian Inova NMR instrument. All NMR spectra were reported as δ values in ppm referenced to chloroform (7.26 ppm) or tetramethylsilane (TMS, 0.00 ppm) for 1H, chloroform (77.00 ppm) for ^{13}C,

and hexafluorobenzene (−163.00 ppm) for ^{19}F NMR. ^{13}C NMR spectra were obtained using a triple resonance probe with simultaneous ^{1}H and ^{19}F decoupling. In the cases where all fluorine nuclei could not be decoupled simultaneously (the spectral width between the most upfield and downfield resonances was greater than 20 ppm) two ^{13}C spectra were collected with the decoupling frequencies in the ^{19}F set at optimal values to maximize the number of fluorine resonances decoupled. High-resolution mass spectrometry (HRMS) using GC-MS was performed on an Agilent 7200-QTOF GC/MS, GC column RTX-5MS 30 m length, 0.255 mm ID, 0.25 μm df. Method: inlet temperature 250 ˚C, source temperature 280 ˚C. The initial column temperature was 120 ˚C and was held for 4 minutes after injection. Column temperature was ramped to 325 ˚C over 10 minutes and then held for 31 minutes. High-resolution mass spectrometry (HRMS) using ESI experiments were performed on a Bruker BioTOF II instrument or on a Waters GCT Premier, a high-resolution time-of-flight mass spectrometer using liquid injection field desorption ionization (LIFDI). The analyte was applied to the filament in dichloromethane and allowed solvent evaporation before ramping to a 12 K voltage field and ramping the filament current from zero to 50 mA. The sample ionized at 0−50 mA with peak ion counts ~35 mA. Chloropentafluorobenzene was used as an internal standard locking the peak at 201.9605 Da. Infrared (IR) spectra were obtained as films from CH_2Cl_2 or $CDCl_3$ on sodium chloride plates or as a KBr pellet on a Thermo Scientific FT-IR. Elemental analysis was performed by Atlantic Microlab, Inc., 6180 Atlantic Blvd, Suite M, Norcross, GA, 30071.

Crystallography: rubrene derivatives were examined by single-crystal XRD using a Bruker-AXS D8 VENTURE CMOS PHOTON 100 diffractometer with an Incoatec IμS CuKα microfocus source (λ = 1.54178 Å) at 123 K. Reflections were integrated using the

SAINT program. Absorption correction was performed using the SADABS program. Space group determination and data merge was performed using XPREP program. Structures were solved and refined with the APEX2 software. Hydrogen atoms were initially assigned automatically by the geometric placement and refined as riding atoms. Fluorine atoms were assigned *via* q-peaks. Fluorine conformational disorder was determined by examining residual q-peaks. Crystal structures were analyzed using the Mercury program. All C−H bond distances were normalized to 1.083 Å. Significant intermolecular interactions were defined as those within the van der Waals radii. Centroid distances reported herein represent geometrically averaged interaction distances for atoms shown to have multiple interaction to other atoms on a neighboring rubrene.

*Synthesis of 5,12-bis(perfluorophenyl)-6,11-diphenyl-5,12-dihydrotetracene-5,12-diol (**2.23**)*

In a flame dried round bottom flask under nitrogen, bromopentafluorobenzene (**2.22**, 7.3 mmol) in diethyl ether (12 mL) was cooled to –78 °C. *n*BuLi (2.5 M solution in hexanes, 2.8 mL, 7.0 mmol) was slowly added to the solution. The reaction was maintained at –78 °C for 2 h. The solution was then slowly transferred *via* cannula to a solution of quinone (**2.21**, 0.30 g, 0.7 mmol) in 12 mL diethyl ether at –78 °C. The reaction was allowed to warm to room temperature overnight. The reaction was quenched by pouring the resulting mixture into a saturated aqueous solution of ammonium chloride (20 mL). The organic layer was separated and the aqueous layer was extracted with diethyl ether (3 × 20 mL). The combined organic phase was washed with brine (30 mL), dried over Na_2SO_4, filtered through celite and concentrated *in vacuo*. The resulting crude product was purified *via*

column chromatography to give the tetracenediol **2.23** as a mixture of diastereomers. This procedure yielded tetracenediol **2.23** as a colorless solid (0.32g, 0.43 mmol, 58%).

^{1}H NMR (500 MHz, $CDCl_3$) δ 7.74 (dt, *J* = 7.6, 1.4, 2H), 7.61 (tdd, *J* = 7.6, 1.4, 0.6, 2H), 7.45 (tt, *J* = 7.5, 1.3, 2H), 7.30 (AA′BB′, *J* = 8.1, 6.9, 1.4, 0.0, 2H), 7.27-7.22 (m, 4H), 7.13 (td, *J* = 7.6, 1.2, 2H), 7.02 (AA′BB′, *J* = 8.7, 6.8, 1.3, 0.6, 2H), 6.45 (dt, *J* = 7.7, 1.3, 2H), 3.56 (s, 2H) **^{19}F NMR** (282 MHz, $CDCl_3$) δ -136.8, -143.3, -156.8 (t, *J* = 21.3), -163.2 (app. t, *J* = 19.1). **HRMS** (EI) calcd for $C_{42}H_{20}F_{10}O_2$ *m/z* 746.1289, found [M^+] 746.1305.

*Synthesis of 5,12-bis(perfluorophenyl)-6,11-diphenyltetracene (**2.18**)*

Tetracenediol **2.23** (0.40g, 0.563 mmol), $SnCl_2$ (2.00 g, 10.7 mmol), THF (14 mL) and concentrated HCl (5 mL) were added to a 20 mL scintillation vial. The vial was flushed and filled with argon, sealed, and heated at 90 °C for 24 h in the dark. The reaction was cooled to room temperature and poured onto 75 mL of H_2O at which point the product precipitated out of the solution. The solid product was collected via vacuum filtration and washed with water (10 mL) and methanol (10 mL) to give rubrene product **2.18** as a red solid (0.27 g, 0.38 mmol, 71%).

*Synthesis of 6,11-dimethoxy-5,12-bis(perfluorophenyl)-5,12-dihydrotetracene-5,12-diol (**2.30**)*

In a round bottom flask, diethyl ether (30 mL) and *n*-butyl lithium (6.0 mL of a 2.5 M solution in hexanes, 14.9 mmol) were cooled to –78 °C. Bromopentafluorobenzene (1.96 mL, 15.7 mmol) was added slowly and the resultant solution was allowed to stir for 1 hour at –78 °C. The solution was then transferred *via* cannula to a solution of 5,12-dimethoxy-6,13-tetracene quinone (**2.29**, 0.450 g, 1.4 mmol) in diethyl ether (30 mL) at –78 °C. The

reaction mixture was warmed to –15 °C for 15 minutes then cooled back down to –78 °C and quenched with ammonium chloride (30 mL). Upon warming the mixture to room temperature, the product was extracted with diethyl ether (3 × 20 mL), washed with brine (1 × 20 mL), dried ($MgSO_4$), and concentrated to give a light yellow solid. The product was purified by flash chromatography (1:1 CH_2Cl_2 : hexanes) to provide tetracenediol **2.30** as a colorless solid (753 mg, 1.15 mmol, 81%)

^{1}H NMR (500 MHz, $CDCl_3$) δ 8.03 (AA′BB′ *J* = 8.6, 6.7, 1.2, 0.6, 2H), 7.36 (AA′BB′, *J* = 8.1, 7.1, 1.3, 0.0, 2H), 58–7.53 (m, 4H), 4.40 (s, 2H), 3.80 (s, 6H). **^{19}F NMR** (282 MHz, $CDCl_3$) δ -142.5 (br, 4F), -157.3 (dd, *J* = 21.5, 1.8 Hz, 4F), -163.5 (m, 4F). **HRMS** (FD TOF) calcd for $C_{32}H_{16}O_4F_{10}$, *m/z* 654.0889, found [M^+] 654.0897.

*Synthesis of 6,11-bis(perfluorophenyl)tetracene-5,12-dione (**2.27**)*

In a 20 mL vial, 6,11-dimethoxy-5,12-bis(perfluorophenyl)-5,12-dihydrotetracene-5,12-diol (**2.30**) (0.715 g, 1.1 mmol) was dissolved in THF (11 mL) and treated with 1M HCl (9 mL, 9.0 mmol). The vial was sealed and heated to 90 °C for 4 hours. The reaction mixture was cooled to room temperature and poured into 200 mL of water at which point the product precipitated out of solution. The solid was filtered and washed with water (10 mL) and methanol (10 mL) to give the product as a yellow solid (0.550 g, 0.9 mmol, 85%).

^{1}H NMR (500 MHz, $CDCl_3$) δ 8.14 (AA′BB′, *J* = 7.8, 7.4, 1.3, 0.5 Hz, 2H), 7.80 (AA′BB′, *J* = 7.9, 7.3, 1.2, 0.5 Hz, 2H), 7.75 (AA′BB′, *J* = 8.6, 6.8, 1.2 Hz, 2H), 7.66 (AA′BB′, *J* = 8.8, 7.2, 1.0 Hz, 2H). **^{13}C NMR** (126 MHz, $CDCl_3$) δ 183.0, 143.8 (C–CF ^2J = 21.4 Hz), 141.2, 138.0, 134.6, 134.5, 134.0, 130.9, 129.3, 129.2, 127.3, 127.0, 113.4. **^{19}F NMR** (471 MHz, $CDCl_3$) δ -140.47 (dd, *J* = 22.9, 7.7 Hz, 4F), -154.08 (t, *J* = 20.8 Hz, 2F), -161.68

(td, J = 22.6, 7.5 Hz, 4F). **HRMS** (FD TOF) calcd for $C_{30}H_8O_2F_{10}$ *m/z* 590.0365, found [M^+] 590.0387. **IR** (KBr Pellet) 1685, 1525, 1498, 1263 cm^{-1}. **Melting point** 289−294 °C (phase change), 297−299 °C (melt).

*Synthesis of 5,6,11,12-tetrakis(perfluorophenyl)-5,12-dihydrotetracene-5,12-diol (**2.31**)*

In a 25 mL round bottom flask, diethyl ether (10 mL) and *n*-BuLi (2.5 M solution in hexanes, 3.2 mL, 8.0 mmol) were cooled to –78 °C. Bromopentafluorobenzene (1.06 mL, 8.5 mmol) was added slowly and the resultant solution was allowed to stir for 1 hour at –78 °C. 6,11-bis(perfluorophenyl)tetracene-5,12-dione (**2.27**) (0.500 g, 0.9 mmol) was added in one portion. The reaction mixture was placed in a –45 °C bath (maintained through use of a cryocooler) for 4 days. The reaction was then cooled back down to –78 °C and quenched with HCl (6 M, 4 mL). The aqueous phase was extracted with diethyl ether. The combined organic extracts were washed with brine, dried, and concentrated to give an off-white solid. The solid was suspended in heptane, filtered, and the residue was rinsed with dichloromethane. The filtrate was concentrated to provide pure product **2.31** as a colorless solid (0.580 g, 0.63 mmol, 74%).

^{1}H NMR (500 MHz, $CDCl_3$) δ 7.51 (AA′BB′, J = 8.7, 6.8, 1.1, 0.0, 2H), 7.41 (AA′BB′, J = 8.1, 7.2, 1.3, 0.0, 2H), 7.33 (AA′BB′, J = 8.2, 7.1, 1.3, 0.0, 2H), 7.20 (AA′BB′, J = 8.5, 6.7, 1.3, 0.7, 2H), 3.06 (s, 2H). **HRMS** (FD TOF) calcd for $C_{42}H_{10}O_2F_{20}$ *m/z* 926.0361, found [M^+] 926.0374.

*Synthesis of 5,6,11,12-tetrakis(perfluorophenyl)tetracene (**2.19**)*

5,6,11,12-tetrakis(perfluorophenyl)-5,12-dihydrotetracene-5,12-diol **2.31** (0.300 g, 0.32 mmol), TFA (10 mL), and $SnCl_2$ (0.569 g, 3 mmol) were added to a pressure vessel. The

vessel was sealed and the mixture was heated at 70 °C. Immediately the reaction turned a purple color. After 4 hours the reaction was allowed to cool to room temperature to give a brown-red mixture. The mixture was poured into 150 mL of water at which point the product precipitated out of solution. The resultant solid was filtered, washed with water (100 mL) and methanol (10 mL), and dried to yield an orange solid (0.227 g, 0.25 mmol, 80%).

^{1}H NMR (500 MHz, $CDCl_3$) δ 7.46 (AA′BB′, *J* = 9.3, 6.3, 1.1, 0.0, 4H), 7.31 (AA′BB′, *J* = 9.0, 6.7, 1.0, 0.6, 4H). **^{13}C NMR** (126 MHz, $CDCl_3$) δ 144.1, 141.2, 137.4, 131.4, 129.2, 128.5, 124.9, 121.7, 114.2. **^{19}F NMR** (471 MHz, $CDCl_3$) δ -135.51 (d, *J* = 22.6 Hz, 8 F), -151.77 (t, *J* = 20.5 Hz, 4 F), -161.19 (td, *J* = 7.9, 23.1 Hz, 8 F). **HRMS** (FD TOF) calcd for $C_{42}H_8F_{20}$ [M^+] *m/z* 892.0307, found 892.0290 [M^+]. **IR** (KBr Pellet) 1649, 1522, 1499, 1100, 995, 882 cm^{-1}. **Melting point** 325−330 °C (phase change), 340 °C (sublimation), 347−350 °C (melt).

*Synthesis of 1,2,3,4,7,8,9,10-octafluoro-6,11-dihydroxy-5,12-naphthacenedione (**2.34**)*

Aluminum trichloride (20.5 g, 154 mmol) and sodium chloride (3.60 g, 61.6 mmol) were mixed in a 250 mL round-bottom flask and heated to 200 °C until the formation of a molten salt. To the stirring molten salt was added the mixture of 1,2,3,4-tetrafluoro-5,8-dimethoxynaphthalene **2.32** (4.00 g, 15.4 mmol) and tetrafluorophthalic anhydride **2.33** (4.06 g, 18.4 mmol) in small portions. After complete addition of the starting materials, the round-bottom flask was loosely capped and heated with vigorous stirring at 200 °C for one hour. Upon cooling, the reaction mixture was carefully poured into 150 mL ice cold 1M HCl. The reaction flask was further rinsed with 50 mL of 1M HCl. All the acidic aqueous solutions were combined and heated to 100 °C for half an hour until the aqueous phase was

decolorized to light yellow and the formation of red solids. Crude product was collected through vacuum filtration and washed with water and methanol. The red solid (5.79 g, 87 %) was dried and used for the next step without further purification.

*Synthesis of 1,2,3,4,7,8,9,10-octafluoro-6,11-methoxy-5,12-naphthacenedione (**2.35**)*

To a 100 mL round-bottom flask was added **2.34** (5.048 g, 11.63 mmol), K_2CO_3 (16.04 g, 116.3 mmol) and cyclohexanone (100 mL) under nitrogen atmosphere. Dimethyl sulfate (14.67 g, 116.3 mmol) was then transferred to the solution *via* syringe. The resulting mixture was heated to 100 °C for 8 hours. After the reaction was complete, the mixture was cooled to room temperature and filtered through celite to remove potassium carbonate. The filtrate was concentrated *in vacuo* to remove cyclohexanone. The resulting mixture was then dissolved in 100 mL diethyl ether, followed by slow addition of 15 mL triethyl amine. After stirring at room temperature for 0.5 h, 40 mL 1M HCl was added. The organic layer was separated and washed with sat. aq. NH_4Cl (30 mL), brine (30 mL), dried over $MgSO_4$ and concentrated *in vacuo*. The product was then purified by column chromatography over silica gel (Hexane/EA = 10/1, v/v) to give **2.35** as a yellow solid: 2.68 g (38 %).

^{1}H NMR (500 MHz, $CDCl_3$) δ 4.12 (s, 3H). **^{13}C NMR** (125 MHz, $CDCl_3$) δ 177.7, 153.1, 146.0, 144.4, 144.2, 141.3, 123.5, 119.9, 119.5, 64.9. **^{19}F NMR** (470 MHz, $CDCl_3$) δ -139.94–-140.07 (m, 2F), -142.58–-142.68 (m, 2F), -145.73–-145.86 (m, 2F), -150.85–-150.95 (m, 2F). **HRMS (ESI)** calcd for $C_{20}H_6F_8O_4$ [M+Na^+] *m/z* 485.0031, found [M+Na^+] 485.0035. **IR** (neat) 2957, 1681, 1648, 1619, 1514 cm^{-1}. **Melting point**: 182−184 °C.

*Synthesis of 1,2,3,4,7,8,9,10-octafluoro-6,11-bis(perfluorophenyl)-tetracene-5,12-dione (**2.37**)*

To a flame-dried 250 mL round-bottom flask was added bromopentafluorobenzene (4.89 g, 19.8 mmol) and 30 mL diethyl ether under nitrogen atmosphere. While stirring, the solution was cooled to −78 °C in a dry ice/acetone cooling bath. *n*-Butyl lithium 2.5 M solution in hexane (7.8 mL, 19.5 mmol) was then transferred dropwise into the solution *via* syringe. The solution was allowed to stir at −78 °C for an hour before (**2.35**) was added as a solid. The resulting mixture was slowly warmed to room temperature in 5 hours and kept stirring at room temperature overnight. The reaction was performed under nitrogen atmosphere for the entire time. After the reaction was complete, the mixture was diluted with ethyl acetate (10 mL), quenched by adding sat. aq. NH_4Cl (20 mL). The organic layer was separated and washed with brine (20 mL × 2). After drying over $MgSO_4$, the solvent was removed *in vacuo* to give crude product as a light yellow solid, which was used for next step without further purification.

To a flame-dried, nitrogen protected 100 mL round-bottom flask containing crude product from the last step was added 20 mL dichloromethane. The flask was capped using a rubber septum with a needle connected to the nitrogen line. Methane sulfonic acid (3 mL) was then transferred into the flask dropwise *via* syringe. The reaction was allowed to stir at 40 °C for 3 hours. After the reaction was complete, the solution was washed with water (20 mL × 2), sat. aq. $NaHCO_3$ (20 mL × 2) and brine (10 mL). The organic layer was collected and dried over $MgSO_4$. Solvent was then removed *in vacuo* to give a brown solid mixture, which was purified by column chromatography over silica gel (hexanes/DCM = 5/1 to 2/1, v/v) to give **2.37** as a yellow solid: 1.75 g (75% over two steps).

^{13}C NMR (125 MHz, $CDCl_3$) δ 178.4, 146.3, 144.9, 144.8, 143.9, 142.0, 141.9, 137.8, 131.6, 125.0, 121.3, 118.9, 111.6. **^{19}F NMR** (470 MHz, $CDCl_3$) δ -138.13–-138.33 (m, 4F), -142.64–-142.73 (m, 4F), -143.14 – -143.27 (m, 2F), -147.02–-147.12 (m, 2F), -153.09 (t, $J_1 = J_2$ = 40.0 Hz), -162.63 – -162.82 (m, 4F). **LRMS (EI)** calcd for $C_{30}F_{18}O_2$ [M^+] *m/z* 734.0, found [M^+] 734.0. **IR** (neat) 1694, 1621, 1515, 1500, 1485 cm^{-1}. **Melting point**: 178−180 °C.

*Synthesis of 1,2,3,4,7,8,9,10-octafluoro-5,6,11,12-tetrakis(perfluorophenyl)-5,12-dihydrotetracene-5,12-diol (**2.38**)*

To a flame-dried 100 mL round-bottom flask was added bromopentafluorobenzene (200 mg, 0.27 mmol) and diethyl ether (anhydrous, 10 mL) under nitrogen atmosphere. The solution was cooled to −78 °C in a dry ice/acetone bath. *n*-Butyl lithium (1.66 mmol, 2.5 M in hexane solution) was then slowly transferred into the solution *via* syringe. The resulting mixture was kept at −78 °C for 0.5 h and was then added **2.37** as a solid. The reaction was then allowed to slowly warm to room temperature in 6.5 hours and stirred at room temperature for 12 hours. After the reaction was complete, the solution was diluted with diethylether (10 mL), followed by the addition of saturated NH_4Cl (10 mL). The organic layer was separated and washed with deionized water (10 mL) and brine (10 mL). The organic solution was then dried over magnesium sulfate and concentrated *in vacuo* to give a brown mixture as the crude product, which was then subjected to column chromatography (hexane/dichloromethane = 5/1 to 3/1, v/v) to give **2.38** as white solid: 114 mg (39%).

*Synthesis of perfluororubrene (**2.20**)*

To a 20 mL reaction vial was added **2.38** (205 mg, 0.19 mmol), $SnCl_2$ (363 mg, 1.9 mmol) and methanesulfonic acid (5 mL). The vial was then sealed and allowed to stir at 110 °C for 12 hours. After the reaction was complete, the mixture was cooled to room temperature and poured into 20 mL 1M HCl. Red solid was collected *via* vacuum filtration as crude product, which was further purified by column chromatography (hexane / dichloromethane = 2/1, v/v) to give perfluororubrene (**2.20**) as a red solid (133 mg, 68%).

^{13}C NMR (125 MHz, $CDCl_3$) δ 143.9, 142.2, 141.9, 140.1, 137.2, 130.6, 120.4, 118.9, 113.1. **^{19}F NMR** (470 MHz, $CDCl_3$) δ -137.36 – -137.47 (m, 8F), -142.58 – -142.63 (m, 4F), -149.95 – -150.00 (m, 4F), -150.34 (t, $J_{F\text{-}F}$ = 40.0 Hz, 4F), -161.69–-161.86 (m, 8F). **LRMS (EI)** calcd for $C_{42}F_{28}$ [M^+] *m/z* 1036.0, found [M^+] 1036.0. **Anal. Calcd** for $C_{42}F_{28}$: C, 48.67; F, 51.33. Found: C, 48.21. **IR** (neat) 1677, 1575, 1494, 1449, 1417 cm^{-1}. **Melting point**: 260−263 °C.

Chapter 3 A Synthetic Study Towards Five-Membered Ring Containing Dibenzo[*g*,*s*]rubicenes and Characterization of their Optoelectronic Properties

The development of novel organic opto-electronic materials relies on the invention of chemical structures and optimized device fabrication techniques [61]. Though the macroscopic device characteristics can be affected by many complicated factors, the intrinsic property of the organic molecules used as the active layer usually set the baseline to the level of overall device performance. For the material development of organic semiconductors, there is a long-standing challenge in progressing n-type semiconductor discovery as carbon-rich aromatic compounds, in general, possess appropriate frontier molecular orbital (FMO) energy levels for p-type semiconductors[62]. A common practice to create n-type semiconductive materials is the adjustment of FMO levels *via* core functionalization of the conjugated backbone. Our work illustrated in Chapter 2 has demonstrated the convenience and flexibility of this strategy. While core functionalization is a powerful approach towards rapid derivatization of promising molecular segments, the scope of research is rather limited to a certain molecular platform. In this sense, creation of innovative aromatic core structures can greatly extend the object of study. As most acene derivatives are based on benzenoid units, varying the ring size seems to be a convenient strategy to alter the conjugation pattern and impact the electronic property. Quite recently, much research has focused on incorporating five-membered rings into the aromatic systems, creating so-called cyclopenta-fused polycyclic aromatic hydrocarbons (CP-PAH)[63]. The embedded cyclopenta moiety could undergo a reduction to achieve Hückel's 4n+2

aromaticity. This unique feature makes CP-PAHs superior electron-acceptor materials compared to benzenoid PAHs.

3.1 Recent Advances in CP-PAH Studies: Design, Synthesis and Optoelectronic Properties

The synthesis of small molecule CP-PAHs has grown over several decades, from the early discovery of corannulene[64] to the recent report of fullerene derivatives[65]. Traditional CP-PAHs were made either to study aromaticity[66] or to provide access to study challenging structures[67]. With the recent development in both synthetic methodology and organic functional materials, the study of CP-PAH quickly emerges as a promising area for the discovery of high-performance optoelectronic materials. One of the merits in CP-PAH research is to replicate the material properties of fullerenes, which are the most widely used electron-acceptor materials in organic photovoltaics[68]. As the structure of fullerenes (C_{60}, C_{70}, etc.) contains both six-membered rings and five-membered rings, many small molecule CP-PAH can be viewed as structural fragments of fullerenes. As the small molecules are more synthetically accessible, study of the CP-PAH would help identify the core functionality of fullerenes and opens further opportunity in designing materials with superior performance.

As shown in **Figure 3-1**, several typical fullerene fragments are presented. These CP-PAH structures are attractive targets to both synthetic chemists and materials chemists because they contain unique conjugation patterns and are novel types of chromophores. For synthetic chemists, efficient routes need to be developed to access these structures. The

methods need to allow the rapid construction of the conjugated core, as well as convenient post-functionalization to tune the solubility or electronic properties as needed.

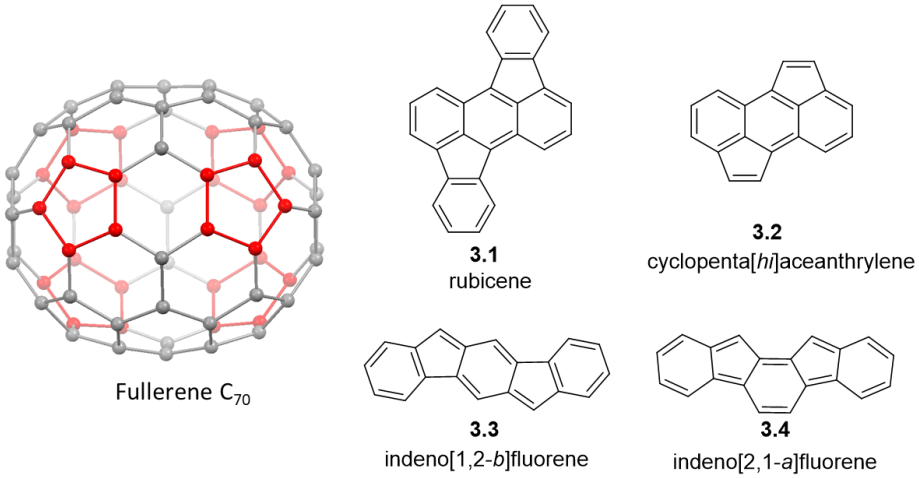

Figure 3-1 Structure of fullerene C_{70} and representative fragment structures containing five-membered rings.

Among the CP-PAHs presented in **Figure 3-1**, the indenofluorene (IF) derivatives have been intensively studied in the past two decades. The IF scaffold resembles the structure moiety of pentacene. The 6−5−6−5−6 fused system contains two less carbon atoms compared to pentacene, which features an anti-aromatic 20-electron π-system. Similar to the common approach to functionalized acenes, the synthesis of IF derivatives also rely on the corresponding polycyclic dione or halogenated precursors. In 1994, Swager *et al.* reported the synthesis of tetraiodoindenofluorene **3.6** *via* iodine-mediated intramolecular cyclization of a strained tetrayne precursor **3.5**[69]. Compound **3.6** was prone to air-oxidation to afford 5,11-diiodoindenofluorene-6,12-dione **3.7**. The halogenated indenofluorenedione serves as a versatile precursor for IF synthesis *via* reductive aromatization of ketone and cross-coupling arylation of aryl halide. In 2002, Wang *et al.* reported a three-step

Suzuki/Friedel−Crafts sequence to synthesize indenofluorene-6,12-dione **3.10**, which enabled a more convenient large-scale preparation of IF precursors[70].

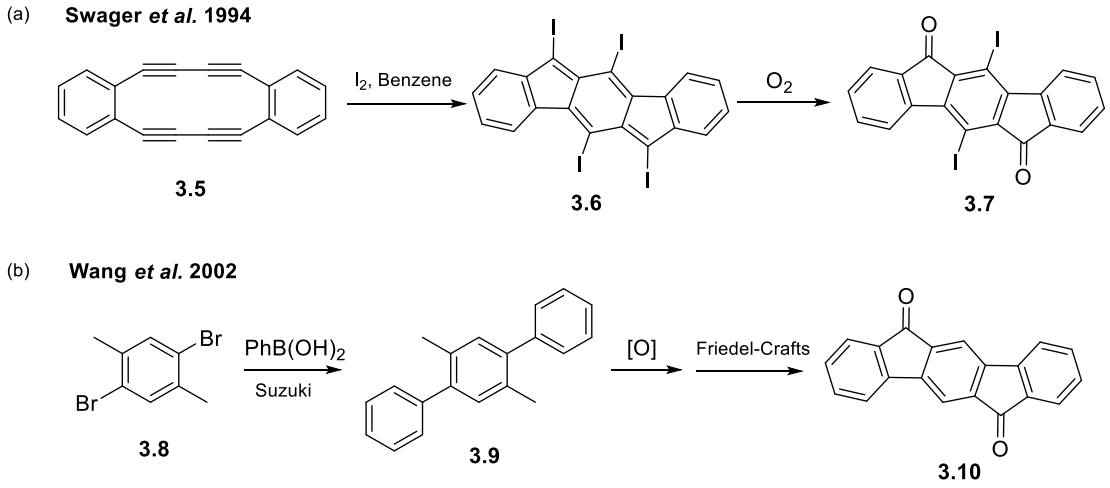

Scheme 3-1 Synthesis of indenofluorene-6,12-dione.

Based on the synthesis of indenofluorene-6,12-dione (**3.10**), Haley *et al.* have synthesized and characterized a series of functionalized indenofluorenes (**Scheme 3-2a**). One example is the study of 6,12-diarylindeno[1,2-*b*]fluorene[71]. By aryllithium addition and sequential reductive aromatization, the IF scaffold was obtained with electron-rich or electron-deficient phenyl substituents. By varying the electronic nature of the aryl substituents, the redox properties of the diaryl-IFs **3.12** can be greatly affected. In a similar study, Haley *et al.* also prepared core substituted dialkynyl-IFs **3.13**[72]. They found that variation of the substituents (such as halogen atoms, aryl groups) bound to the conjugated core only showed modest impact on the absorption profiles. For **3.12** and **3.13**, the cyclic voltammetry experiments revealed the two-electron oxidation and reduction features, in which the 20-electron conjugated system (4n electrons) readily gain or lose two electrons to reach a 22- or 18-electron system (4n+2 electrons) wherein Hückel's aromaticity can be

achieved. The low-lying LUMO levels of the functionalized IFs also suggested their intrinsic electron-accepting characteristics as compared to acenes with similar size of conjugation length. Utilizing the same synthetic strategy, syntheses of other IF regio-isomers such as flurenofluorenes, indacenethiophene were also reported, enriching the scope of CP-PAH[73] (**Scheme 3-2b**).

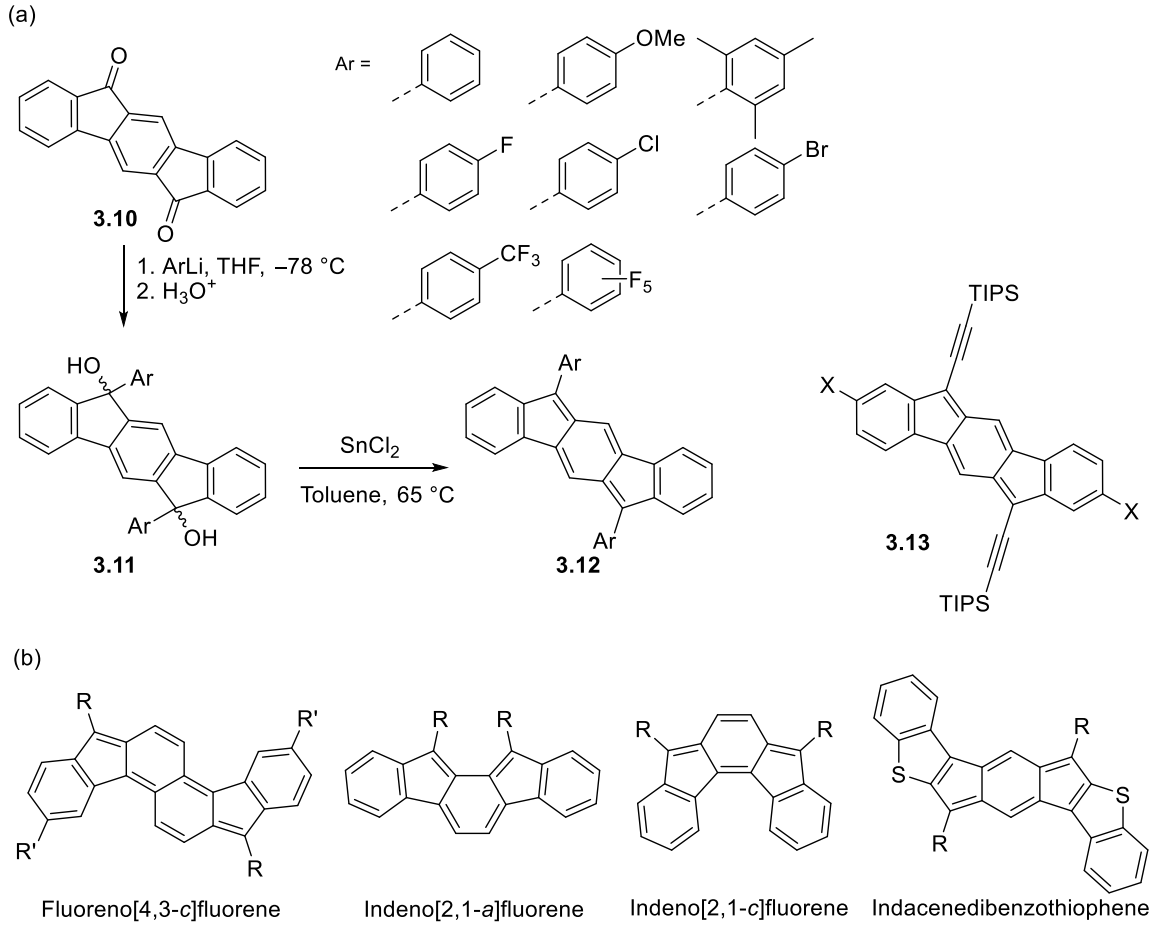

Scheme 3-2 (a) Synthesis of 6,12-diarylindeno[1,2-*b*]fluorene. (b) Examples of other IF analogs.

For CP-PAH synthesis, a core issue is to construct five-membered rings in an efficient chemical transformation. In the IF synthesis mentioned earlier, the cyclopenta moiety is

included in the precursor. Although the synthesis enabled convenient diversification, the conjugation pattern is only limited to the few indenofluorenedione precursors. Thus, it is necessary to design synthetic routes that would generate the cyclopenta moiety from broader and easily acquired substrates. In this sense, transition-metal-catalyzed cross-coupling reaction as a well applied C−C bond formation reaction in modern synthetic chemistry can be used as a powerful tool for five-membered ring formation, especially in a conjugated system. Interestingly, transition-metal-catalyzed cross-coupling reactions sometime give unexpected cyclized product *via* C−H functionalization. For example, in 2001, Garcia-Garibay *et al.* [74] first discovered the cyclopentenelation of aromatic compounds *via* copper-free Sonogashira cross-coupling[75] reactions (**Scheme 3-3a**). Later in 2012, Plunkett *et al.* utilized this method to obtain the cyclopenta[*h,i*]aceanthrylene **3.17** as an electron-acceptor unit[76]. Upon halogenation and cross-coupling reactions, the CP-PAH unit could be incorporated into donor−acceptor type of copolymers[77] (**Scheme 3-3a**). These polymers exhibited low bandgaps and served as potential candidates for n-type materials in organic electronic devices.

There are two established efforts for CP-PAH synthesis in the Douglas lab. In the first example shown in **Scheme 3-4a**, diarylindenotetracene **3.22** was synthesized utilizing a Kumada cross-coupling reaction on tetrachlorotetracene **3.21**, followed by *in situ* cyclopenta annulation *via* C−H activation[78]. The resulting diarylindenotetracene proved to be a novel donor material for organic photovoltaics. To further tune the electronic properties, a second method was developed to achieve asymmetrically substituted diarylindenotetracenes **3.26** *via* late-stage diversification[79]. In this route, a Scholl-type oxidation was applied to afford the cyclopenta moiety.

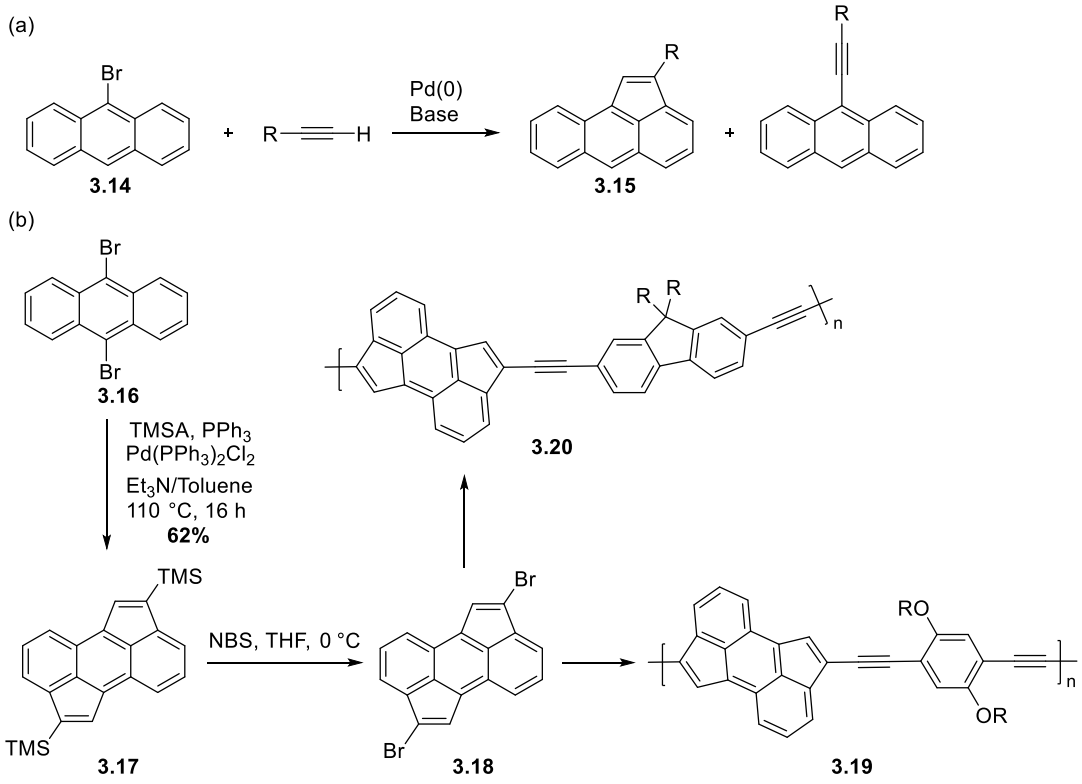

Scheme 3-3 (a) Garcia-Garibay's synthesis of aceanthrylenes. (b) Plunkett's synthesis CP-PAH based donor−acceptor copolymer.

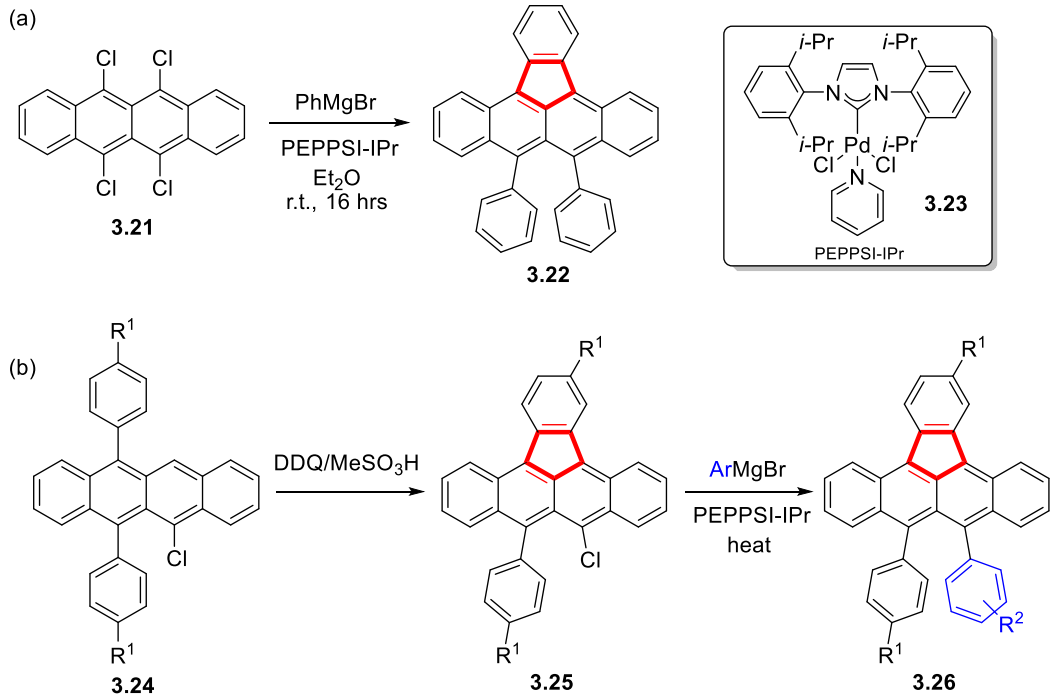

Scheme 3-4 (a) Kumada cross-coupling on tetrachlorotetracene **3.21** gives indenotetracene **3.22** instead of rubrene. (b) Synthesis of asymmetrically substituted indenotetracene derivatives *via* a Scholl-type oxidative annulation.

The synthetic methods mentioned so far are powerful in terms of five-membered ring formation. However, these methods are less efficient in producing a polycyclic conjugated system: only one ring-closure event is accomplished per reaction. Such a weakness will lead to prolonged synthesis when a complicated polycyclic system is targeted.

In the rest of this chapter, I will present a strategy to prepare a series of complicated CP-PAH through rapid construction of the conjugation system. The route was an indirect five-membered ring formation.

3.2 Synthesis of Dibenzo[*g,s*]rubicene *via* One-Pot Sonogashira Cross-Coupling and Tandem Tetradehydro Diels−Alder Cascade

3.2.1 Rubicene, Dibenzo[*g,s*]rubicene and Synthetic Design

The chemical structure of rubicene contains an anthracene core fused with two indene moieties. It can also be viewed as a planar fragment of fullerene C_{70}. As the fullerene family is widely used as electron-acceptor materials in organic photovoltaics, studying the core structure of fullerene would help us further understand structure−property relationships. However, the material properties rubicene has rarely been studied due to the lack of valuable structural candidates. The synthesis of native rubicene, along with several modified analogs is known in the literature[80]. Yet, core-extended rubicene derivatives, such as dibenzo[*g,s*]rubicene, are harder to make based on the reported methods. Given the fact

that dibenzo[*g*,*s*]rubicene is also a fragment structure of naturally occurring C_{70}, we are interested in developing a facile synthesis for this family of molecules.

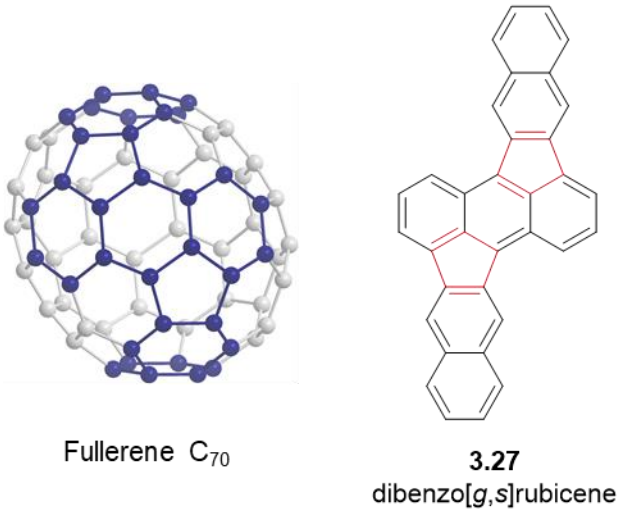

Figure 3-2 Structure of dibenzo[*g*,*s*]rubicene as a fragment of C_{70}.

The synthesis of rubicene is usually achieved *via* intramolecular Heck coupling reaction or Scholl-type oxidative cyclization (**Figure 3-3a**). However, these reactions usually involve harsh reaction conditions, such as high temperature (> 120 ˚C) or strongly acidic reagents (trifluoroacetic acid). To avoid these issues and, more importantly, increase the efficiency of cyclization, we were interested in designing ring formation reaction under mild conditions. In the past decade, dehydro-Diels−Alder (DDA) reaction has emerged as a powerful tool for the facile synthesis of cyclic compounds[81]. Specifically, tetra-dehydro-Diels−Alder (TDDA, **Figure 3-3b**) reaction produces a benzene ring from a pair of enyne and alkyne precursors. The reaction is usually performed under thermal conditions. Interestingly, with well-designed substrates, TDDA reaction can also be used to efficiently construct PAHs containing five-membered rings, where the cyclopenta moiety can be made indirectly. In **Figure 3-3c**, we proposed an unconventional pathway to achieve the fused

polycyclic moiety embedded in the structure of dibenzo[*g*,*s*]rubicene. We envisioned that the "enyne + alkyne" moiety in **3.29** would be easily obtained *via* Sonogashira cross-coupling reactions on aryl-halide **3.28**. As heat is usually required for the Sonogashira cross-coupling reaction, the intermediate **3.29** generated *in situ* would readily undergo TDDA reaction to afford the polycyclic framework depicted in compound **3.30**.

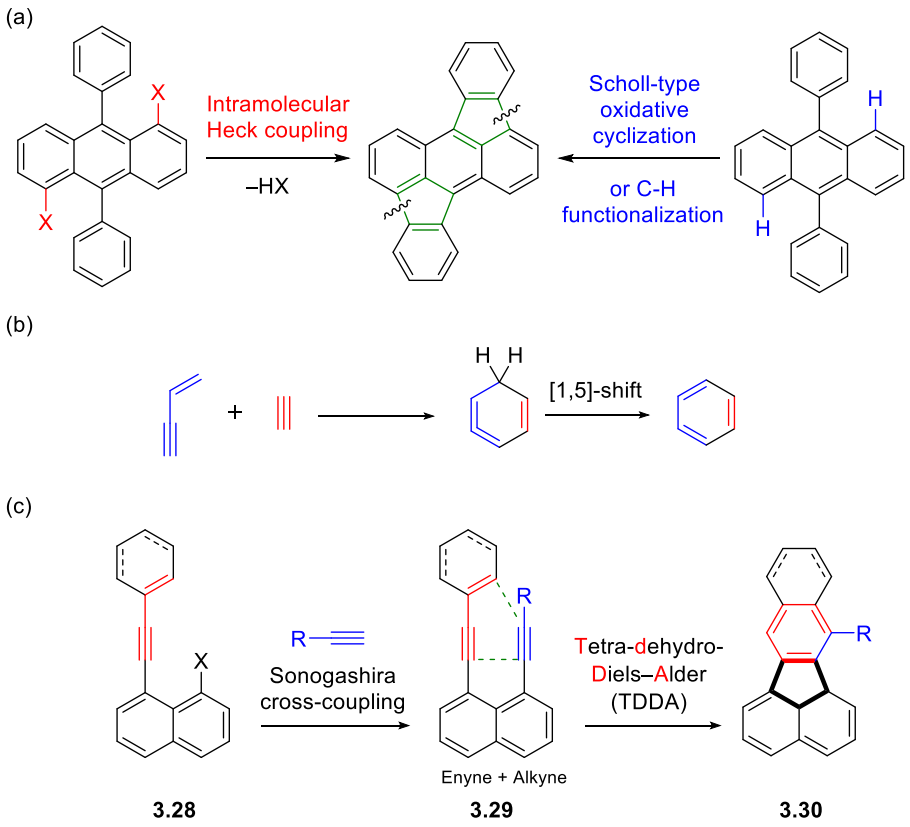

Figure 3-3 (a) General synthesis of rubicene. (b) Schematic illustration of tetra-dehydro-Diels−Alder reaction. (c) Proposed synthesis of one-pot Sonogashira and TDDA cascade.

3.2.2 Preliminary Examination on the Proposed One-Pot Sonogashira and Diels−Alder Cascade

To test the proposed one-pot transformation, we initially prepared 1,4-dibromo-9,10-bis(phenylethynyl)anthracene as a precursor. If a two-fold Sonogashira cross-coupling

reaction occurs, a tetrayne intermediate should be formed as the sole product. When subjecting the dibromide **3.31a** and phenylacetylene into the standard Sonogashira conditions, a dark red solid product was formed in a significant amount and readily precipitated out of solution due to poor solubility. Upon purification *via* recrystallization and column chromatography, the product was characterized by ^{1}H NMR for structural identification. However, the ^{1}H NMR spectrum of the product suggested highly asymmetric structure, which ruled out the assignment of the cross-coupling tetrayne product **3.32a**. Through single crystal X-ray analysis, the product was assigned as structure **3.33a**, which contains a five-membered ring based polycyclic framework. The formation of **3.33a** fit well with our hypothesized TDDA process based on the intermediate **3.32a**.

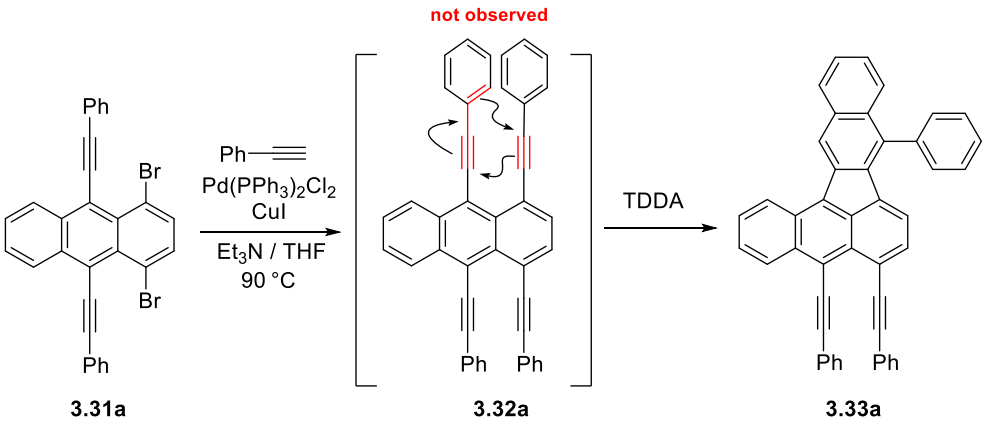

Scheme 3-5 Initial attempt on the proposed one-pot Sonogashira and TDDA cascade.

Encouraged by this finding, we then moved on to identify the optimized reaction conditions. By briefly screening the catalyst loading, temperature and reaction time, the optimal reaction condition was found as indicated in entry 5 of **Table 3-1**. It was found that the reaction was quite efficient and generally resulted in isolated yield over 80%.

Table 3-1 Optimization of Reaction in **Scheme 3-5** Initial attempt on the proposed one-pot Sonogashira and TDDA cascade.

Entry	Catalyst mol %	Temp ˚C	Solvent	Time	Yield [a]
1 [b]	10	90	THF/Et_3N	24	85%
2 [c]	5	90	THF/Et_3N	24	83%
3 [d]	2.5	90	THF/Et_3N	24	87%
4 [c]	5	150	Tol/ Et_3N	24	73%
5 [c]	**2.5**	**90**	**THF/Et_3N**	**2**	**87%**

[a] isolated yields after column chromatography. [b] 0.1 mmol of substrate. [c] 0.2 mmol of substrate. [d] 0.4 mmol of substrate.

Although this overall transformation worked fairly well, there are still several questions that need to be addressed. The first question is whether or not the reaction undergoes the tetrayne intermediate **3.32a**. If the answer is yes, is the palladium or copper catalyst also involved in the TDDA cyclization step? To answer this question, we sought to prepare the tetrayne intermediate **3.32a** from another approach in which heating is not involved. As the one-pot cascade reaction is based on the Sonogashira cross-coupling reaction, a reasonable approach is to seek modified Sonogashira conditions without heating. Since aryliodides are more reactive than arylbromides in Sonogashira cross-couplings, we hope that cross-coupling based on the iodo- analog of anthracenediyne **3.31a** should proceed under lower temperature, thus inhibiting the TDDA reaction.

Carrying this hypothesis into practice, we set out to prepare 1,4-diiodo-9,10-bis(phenylethynyl)anthracene **3.34**. Starting from the commercially available 1,4-diaminoanthraquinone **3.35**, the Sandmeyer reaction was attempted to directly synthesize the diiodoanthraquinone **3.37**. However, this transformation was not successful, even though this method worked well for the previous large-scale preparation of the

dibromoanthraquinone **3.36**. Fortunately, with **3.36** in hand, a copper-mediated aromatic Finkelstein reaction smoothly afforded the desired diiodide **3.37** in 61% yield[82]. Compound **3.37** was then transformed into **3.34** *via* a well-established two-step sequence.

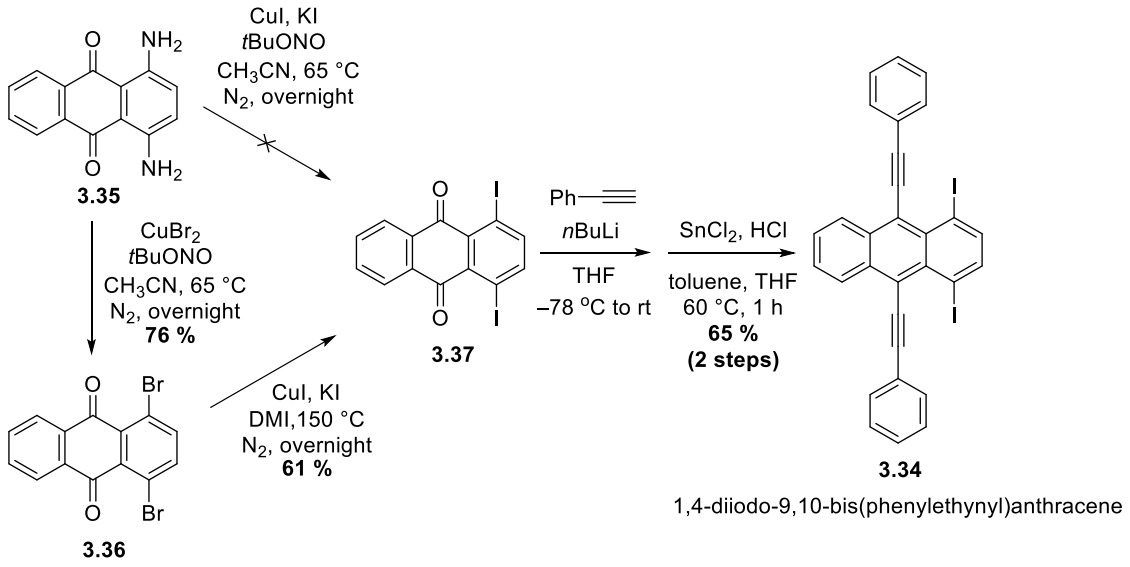

Scheme 3-6 Synthesis of 1,4-diiodo-9,10-bis(phenylethynyl)anthracene **3.34**.

With **3.34** prepared, Sonogashira cross-coupling was performed at room temperature to install the second set of phenylacetylene groups. As we expected, the reaction smoothly proceeded to the stage of tetrayne **3.32a** formation and no other transformation was observed thereafter. Upon purification, compound **3.32a** was then subjected to thermal conditions without any palladium or copper catalyst. Surprisingly, after heating for two hours, the cyclized product **3.33a** was formed in quantitative yield. Based on these results, we concluded that the overall one-pot cyclization was a two-step tandem reaction combining the Sonogashira cross-coupling and thermal TDDA cyclization. The TDDA step does not necessarily require transition-metal catalysts.

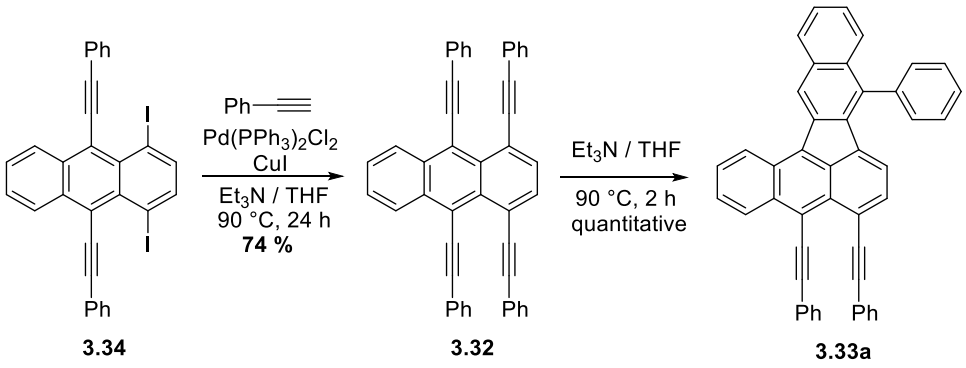

Scheme 3-7 Demonstration of thermally-driven TDDA reaction.

Although this one-pot transformation is quite efficient in polycyclic ring formation, however, it was noted that the TDDA reaction only occurred on one side of the enyne-diyne moieties. For the ease of discussion, compounds like **3.33a** is referred to as *mono-cyclized* product in the rest of this chapter. As illustrated in **Scheme 3-8**, there are two other potential products for this one-pot cascade reaction. One is the regioisomer of the mono-cyclized product **3.34**, in which the phenyl group is positioned on the opposite side of the formed polycyclic structure. In theory, **3.34** could be formed *via* TDDA reaction between the other pair of enyne−alkyne moiety (marked as red in **Scheme 3-8a**, **3.32a**). We envisioned that **3.34** could not be generated in this reaction due to the steric encumbrance between the side phenyl group and anthracene edge C−H bond. The second possible product is the *double-cyclized* product with a more symmetrical structure **3.38**. However, this product was also not observed in the reaction mixture. To explain this result, we took a closer look at the crystal structure of mono-cyclized product **3.33a**. We noticed that the unreacted diyne moiety adopted a wider bond angle than a typical sp^2 hybridized configuration (**Scheme 3-8b**). We believe that the electron repulsion between the phenylacetylene groups should have little effect on such a configuration as they could

rotate to mitigate such repulsions. We attributed the tilted angle to the increased ring strain upon the five-membered ring formation. This molecular geometry increased the spatial distance between the enyne−alkyne moieties, and as a result, further reaction was prohibited. This is an unfortunate result, however, it also inferred out reaction design towards dibenzo[*g*,*s*]rubicenes. As shown in **Scheme 3-8c**, mono-cyclized compound **3.39** would contain the "not yet reacted" enyne−alkyne moiety that is pushed into close proximity due to the strain effect of cyclopenta ring fusion. We hypothesized that a double-cyclized compound **3.40** should be readily obtained, which features a core-extended rubicene moiety.

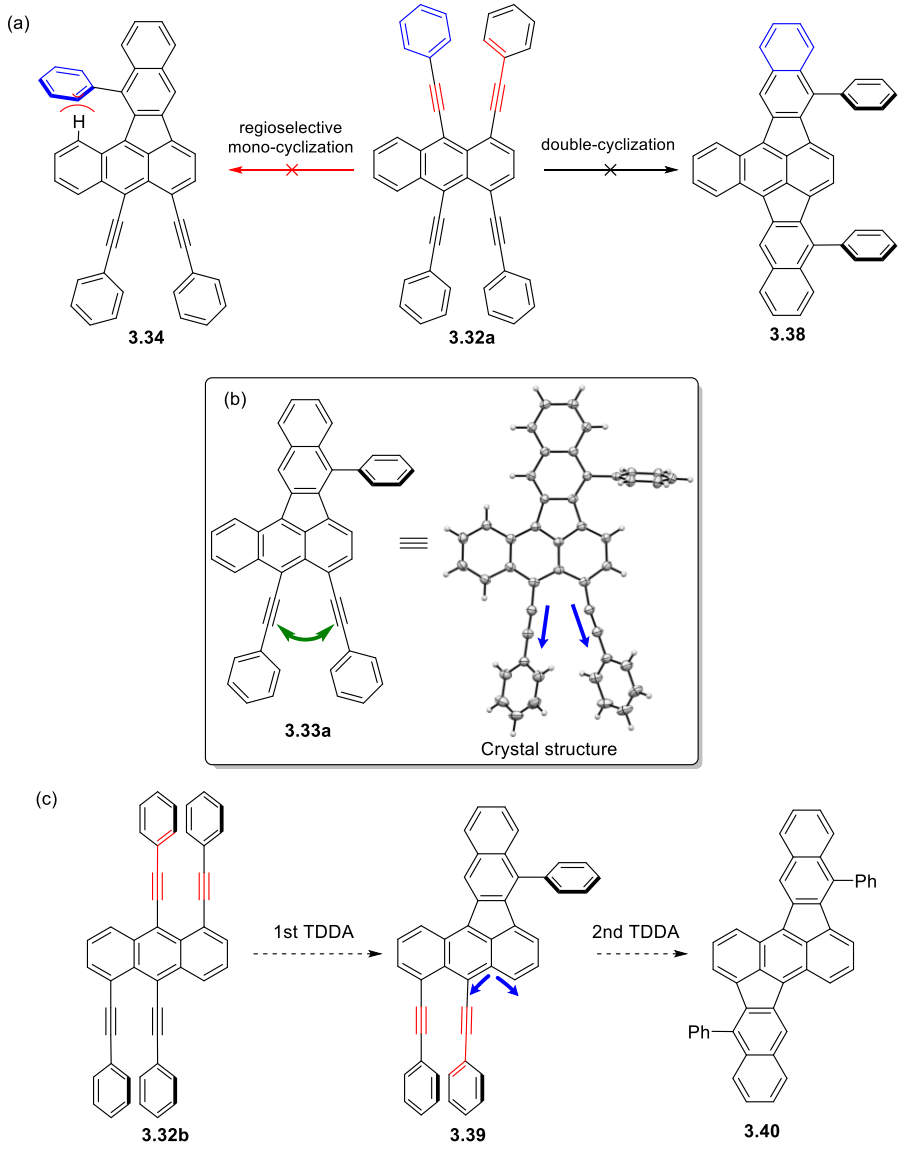

Scheme 3-8 (a) Two possible reaction pathways that were not observed experimentally. (b) Illustration of structure geometry *via* X-ray single-crystal structure of **3.33a**. (c) Proposed synthesis of dibenzo[*g*,*s*]rubicene derivative **3.40**.

3.2.3 Synthesis of Dibenzo[*g*,*s*]rubicene and Naphtho[2,3-*a*]aceanthrylene analogs

In order to test the idea illustrated in **Scheme 3-8c**, 1,5-dibromo-9,10-bis(phenylethynyl)anthracene **3.43a** needs to be prepared as cyclization precursor. Starting from 1,5-diaminoanthraquinone **3.41**, Sandmeyer reaction smoothly afforded the desired

1,5-dibromoanthraquinone **3.42**. It is worth noting that the reagent order of addition was crucial in this reaction. To achieve a better yield and simplify the separation process, **3.41** need to be added last, portion-wise, to control the slow generation of diazonium ion. A two-step addition-reduction sequence was applied again to afford **3.43a** as the cyclization precursor. When we attempted the one-pot cascade on **3.43a** using the previously optimized conditions, we found that the overall transformation gave a mixture containing the desired rubicene product **3.44a** and a significant amount of uncyclized intermediates. Both the tetrayne and partially cyclized intermediate was identified by ^{1}H NMR. It was noted that the NMR signal for **3.44a** showed very poor signal to noise ratio, which could either be due to the very poor solubility in chloroform solution or the inefficiency of the transformation. Though the yield for the rubicene product is very low as compared to the uncyclized intermediates, the formation of the double-cyclized product encouraged us to further optimized conditions to increase the conversion yield. As we still want to keep the transformation in a one-pot fashion, alternative Sonogashira conditions were considered. One common variation to Sonogashira cross-coupling reaction is the use of silver catalyst as the substitute of copper catalyst. Given that silver is a "softer" metal than copper, as well as a more π-Lewis acidic catalyst, the use of silver catalyst might assist the cycloaddition event by activating the alkyne functionality[83]. After attempting several silver salts, we were glad to find that silver(I) acetate (AgOAc) greatly facilitated the TDDA event and afforded the dibenzo[*g*,*s*]rubicene product **3.44a** in good yield (83%).

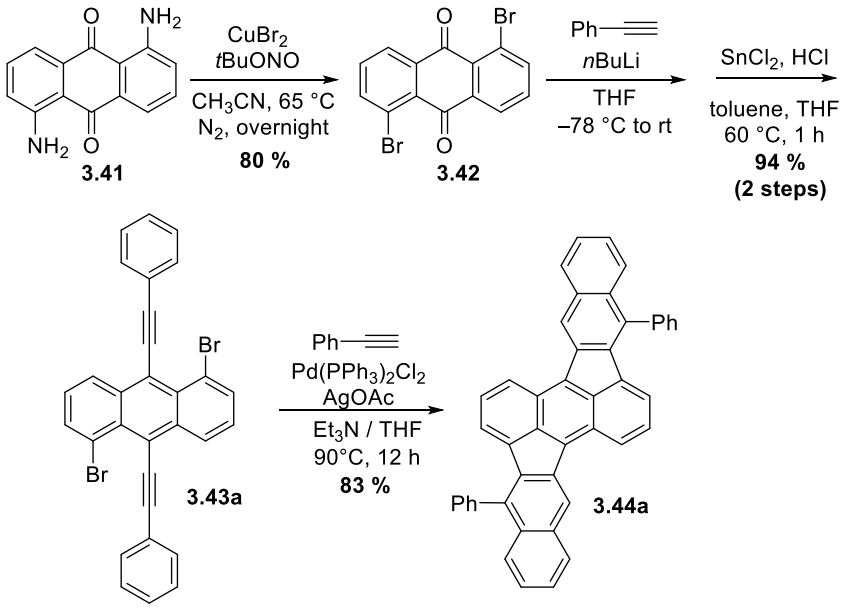

Scheme 3-9 Synthesis of dibenzo[*g*,*s*]rubicene moiety *via* modified one-pot cascade conditions.

Applying the modified one-pot cascade conditions, the utility of this reaction in generating naphtho[2,3-*a*]aceanthrylene **3.33b−m** and dibenzo[*g*,*s*]rubicene analogs **3.44b−l** was explored. The dibromo substrates **3.31b−m** and **3.43b−l** were first prepared using the previously established methods (**Table 3-2** and **Table 3-3**). The substrates are designed with variation of functionalized aryl groups attached to the 9,10-acetylene group. The variety of aryl groups contains phenyl groups substituted with steric/electronic groups at different positions, less-conjugated cyclohexenyl group, core-extended 1-naphthyl group, and thienyl groups. The choice of these functional groups would provide us with more detailed information on the reactivity, regio-selectivity and functional group tolerance of the one-pot cyclization.

The results of the one-pot cyclization reactions on 1,4- and 1,5-dibromo substrates are summarized in **Table 3-4** and **Table 3-5**. Herein we will briefly discuss about several

characteristics of this ring-closure methodology. Firstly, we examined substrates with the 1-cyclohexenylacetylene groups (**3.31j** and **3.43j**). Interestingly, both desired products were obtained in satisfying yields (**3.33j, 98%** and **3.44j, 83%**). These results demonstrated that the alkene portion of the enyne moiety need not originate from an aromatic ring. To further prove the TDDA reaction model, **3.33k** and **3.44i** were also obtained under the same conditions, in which the alkene moiety was embedded within a naphthyl group. We then examined substrates containing aryl groups with varied alkyl substitutions: **3.31b−f** and **3.43b−f**. It is worth noting that for ortho-methyl substituted substrates, only regio-isomers **3.33b** and **3.44b** were observed, indicating the TDDA occurs on the less substituted side. Substitutions at the para-position of the phenyl group had little influence on the reactivity. Next, we looked at the impact of inductive effects by introducing electron-donating alkoxy groups and electron-withdrawing CF_3 groups. The results strongly indicated that electron-withdrawing group deactivated the enyne by decreasing the electron density and led to lower yields. However, electron-donating groups tend to form the cyclized product more easily. Although this could not be directly inferred from the experiment data, yet in our early optimization stage we noticed that under regular (CuI) Sonogashira conditions, the electron-rich substrates gave the double-cyclized rubicene products in significantly higher yields than alkyl- or electron-withdrawing group substituted precursors. Lastly, to further extend the scope of this method, thiophene substituted alkyne precursors (**3.31l,m** and **3.43k,l**) were also tested. As thiophene is an electron-rich aromatic unit, cyclization reaction proceeded in good yields. However, for **3.31m** and **3.43l**, only one set of regio-isomers were observed. This can be explained by the difference in double-bond character between the b-bond and c-bond in the thiophene

ring. Specifically, the stronger double-bond character makes the b-bond more reactive in the TDDA reaction.

Table 3-2 Synthesis of 1,4-dibromoanthracene derivatives **3.31b–m**.

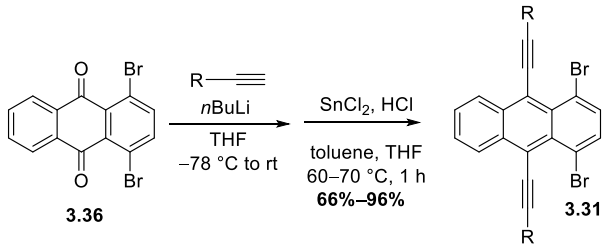

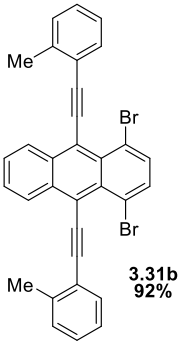 **3.31b** **92%**	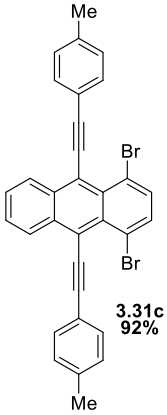 **3.31c** **92%**	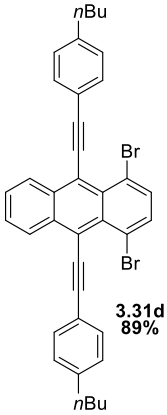 **3.31d** **89%**	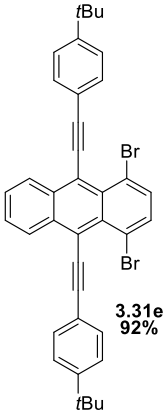 **3.31e** **92%**
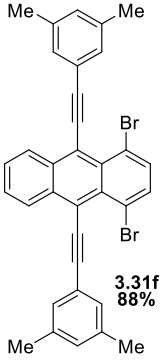 **3.31f** **88%**	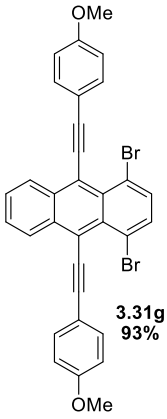 **3.31g** **93%**	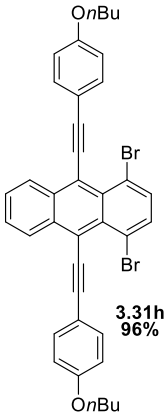 **3.31h** **96%**	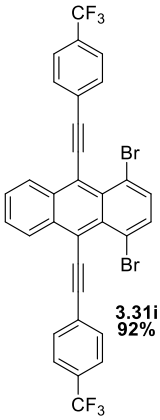 **3.31i** **92%**
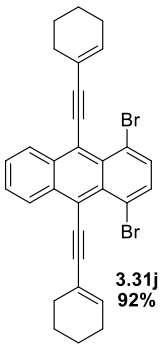 **3.31j** **92%**	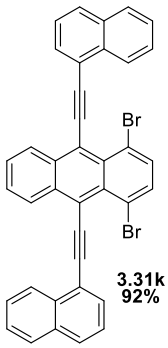 **3.31k** **92%**	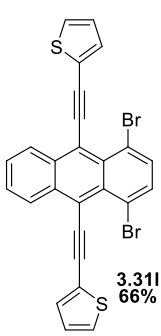 **3.31l** **66%**	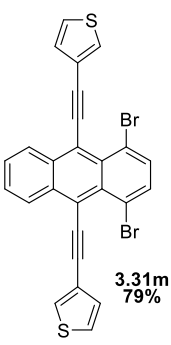 **3.31m** **79%**

Table 3-3 Synthesis of 1,5-dibromoanthracene derivatives **3.43b–l**.

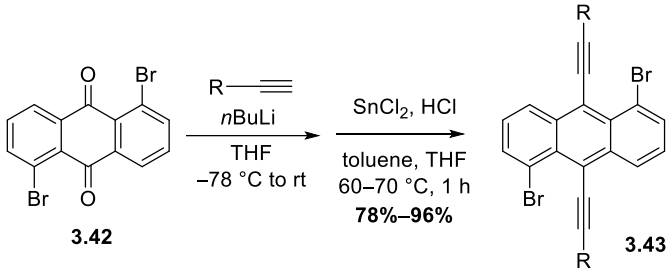

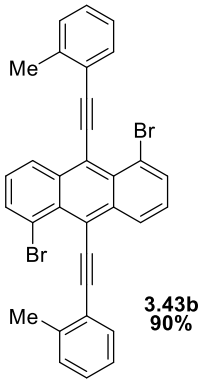 **3.43b** **90%**	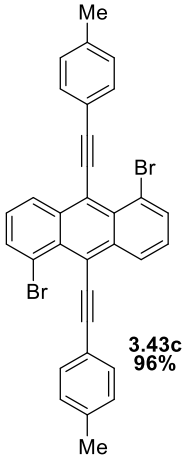 **3.43c** **96%**	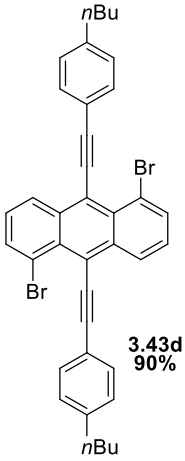 **3.43d** **90%**	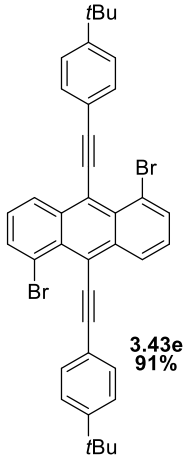 **3.43e** **91%**
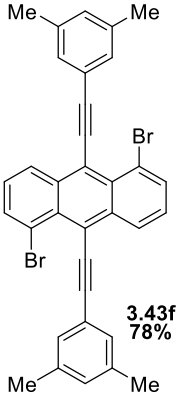 **3.43f** **78%**	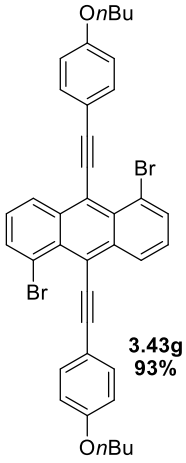 **3.43g** **93%**	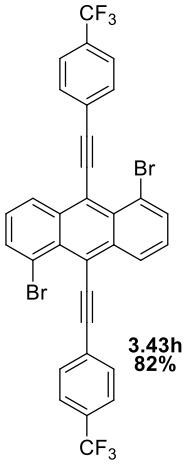 **3.43h** **82%**	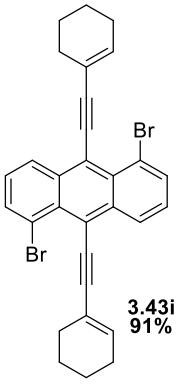 **3.43i** **91%**
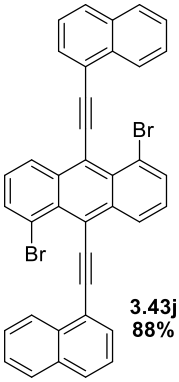 **3.43j** **88%**	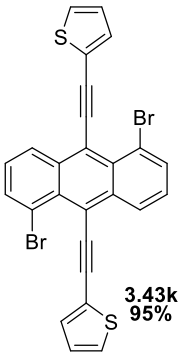 **3.43k** **95%**	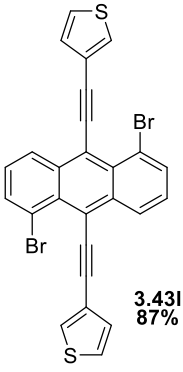 **3.43l** **87%**	

Table 3-4 Synthesis of naphtho[2,3-*a*]aceanthrylene derivatives **3.33b–m**.

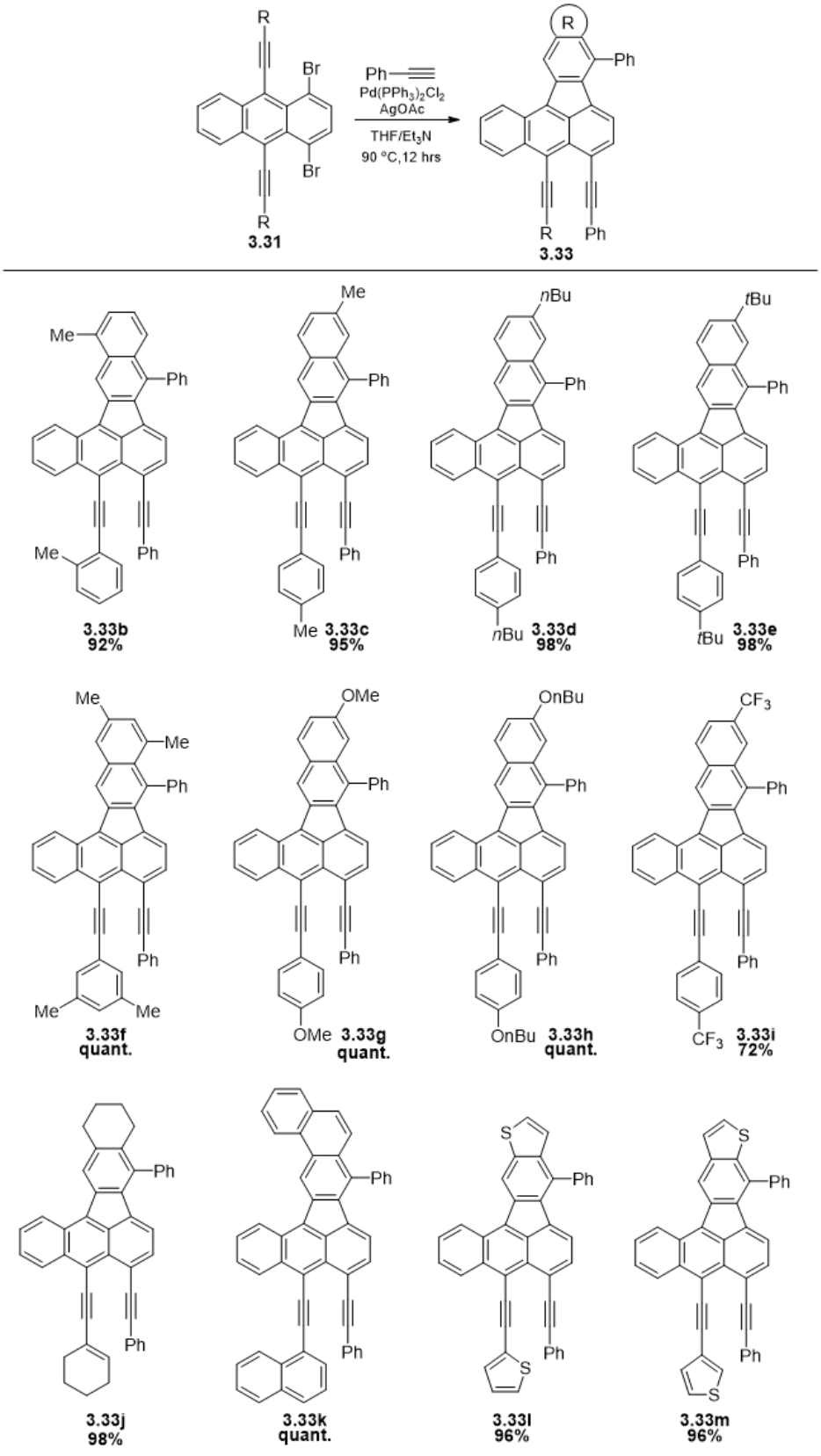

Table 3-5 Synthesis of dibenzo[*g*,*s*]rubicene derivatives **3.44b–l**.

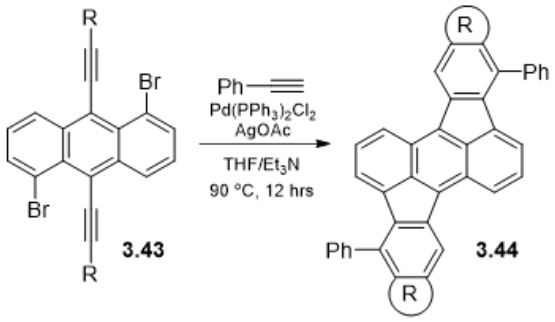

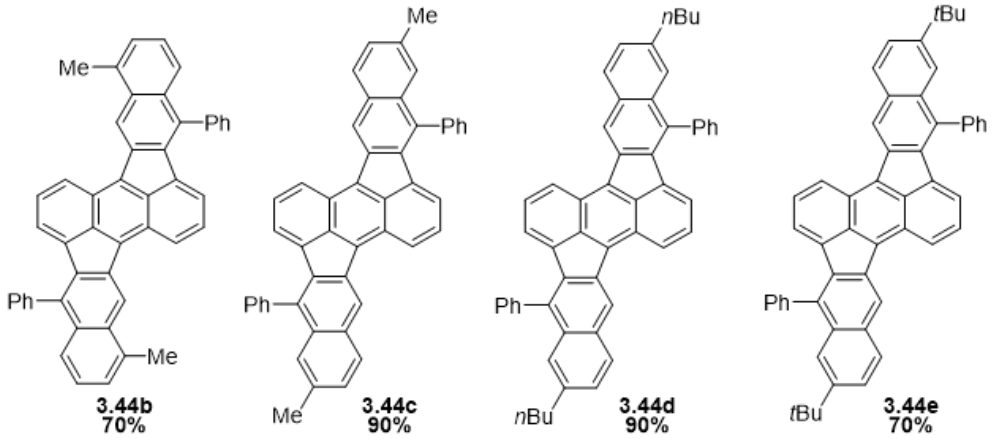

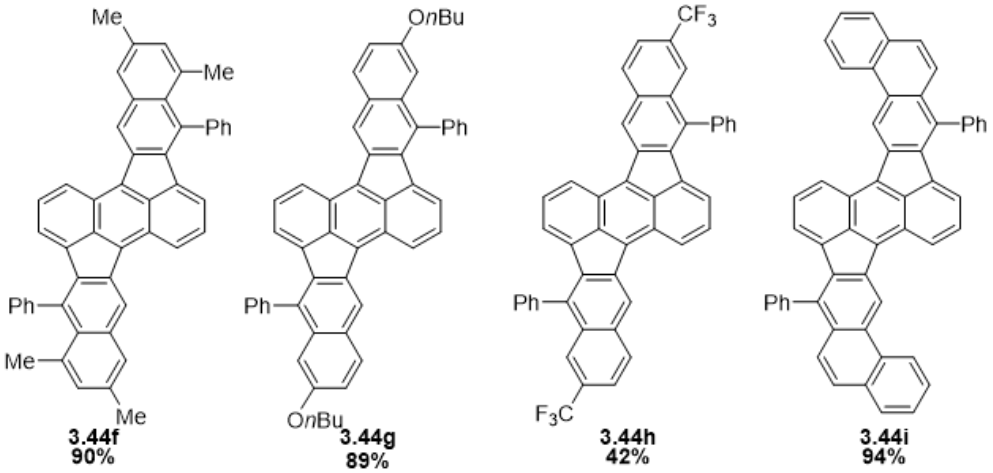

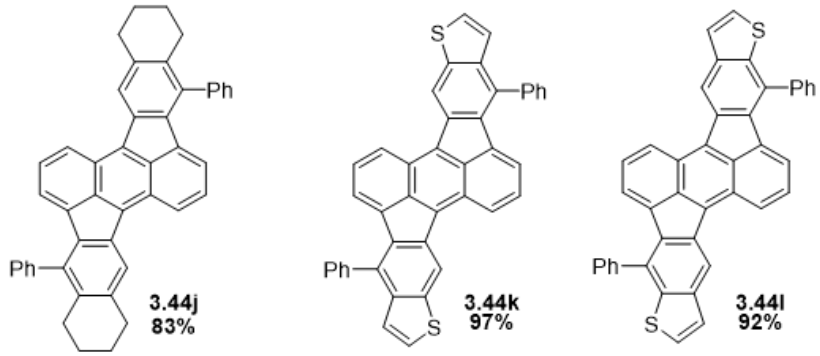

3.3 Optical and Electrochemical Characterization of Synthesized CP-PAHs

3.3.1 Absorption and Emission Properties

We initially characterized the optical properties of the obtained CP-PAHs with ultraviolet-visible (UV-Vis) spectroscopy. The absorption spectra were measured in THF solutions at the concentration of ~ 10^{-5} mol/L. The compounds measured display broad absorption over the visible light region. The absorption peaks with large intensities between 450 to 600 nm are characteristic of the acene family. In **Figure 3-4**, the influence of conjugation pattern was first compared between CP-PAHs containing different polycyclic systems. The uncyclized tetrayne intermediate **3.32b** had the lowest extinction coefficient among all the compounds. The dibenzo[*g*,*s*]rubicene derivatives exhibited more red-shifted spectra as compared with the mono-cyclized naphtho[2,3-*a*]aceanthrylene derivatives. This finding suggested that the bandgap of dibenzo[*g*,*s*]rubicene derivatives were decreased due to extended conjugation. Compound **3.33a** and **3.44i** displayed more pronounced vibrational structures which could be attributed to their more rigid π-scaffold. In **Figure 3-5**, absorption and emission patterns of compounds containing EDG, EWG and heteroatoms were compared. Compounds **3.44g–l** exhibited similar absorption patterns with absorption maximum range between 475 nm and 600 nm. The electron-rich compound **3.44g** showed a more red-shifted absorption maximum than the electron-deficient compound **3.44h**. Interestingly, even though compound **3.44k** and **3.44l** differs only at the position of the sulfur atom, yet the absorption spectra showed a noticeable shift of 12 nm.

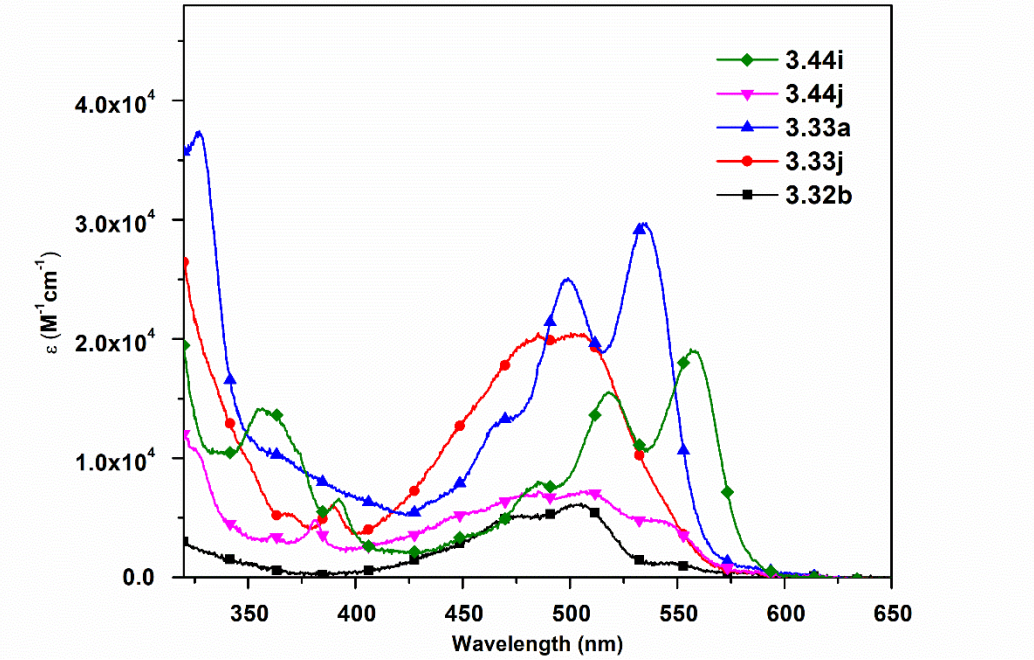

Figure 3-4 Absorption spectra of selective CP-PAHs containing different polycyclic structures.

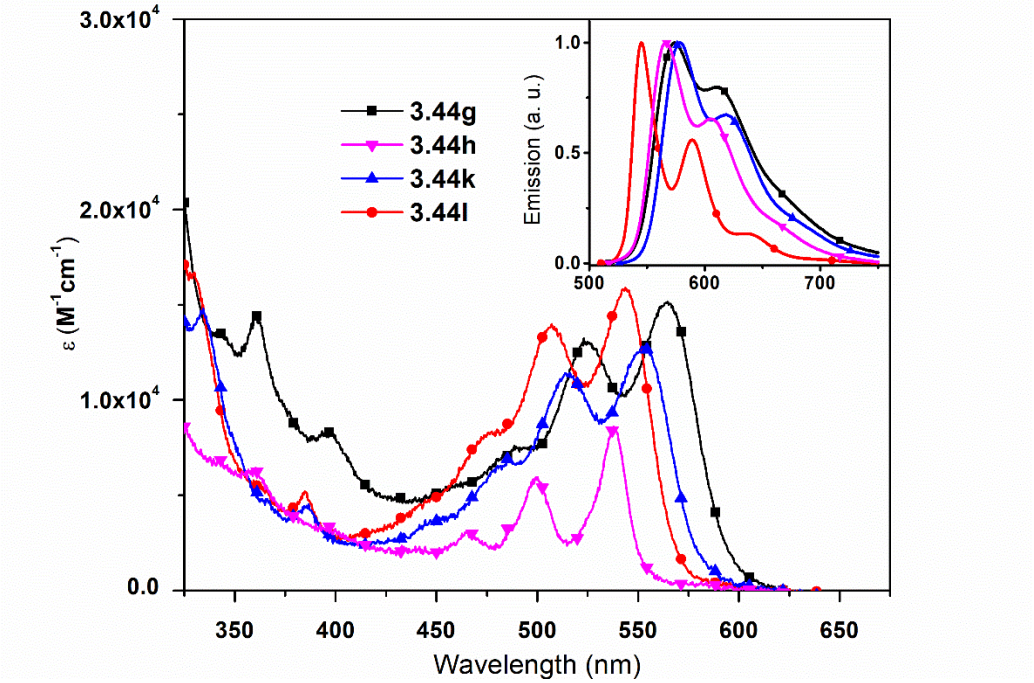

Figure 3-5 Absorption spectra of dibenzo[*g*,*s*]rubicene derivatives.

The emission properties of CP-PAHs were then characterized by fluorescence spectroscopy (**Figure 3-6** and **Figure 3-7**). When excited at ~ 475 nm, the emission spectra for all the cyclized products showed intense emission peaks between 500 nm and 750 nm. The CP-PAHs substituted with electron-donating groups **3.33g** and **3.44g** were found to exhibit the most red-shifted emission pattern among their analogs. Interestingly, both the dibenzo[*g*,*s*]rubicene and naphtho[2,3-*a*]aceanthylene derivatives were highly emissive due to the rigid conjugated backbone. The optical spectra data and fluorescence quantum yields were summarized in **Table 3-6**.

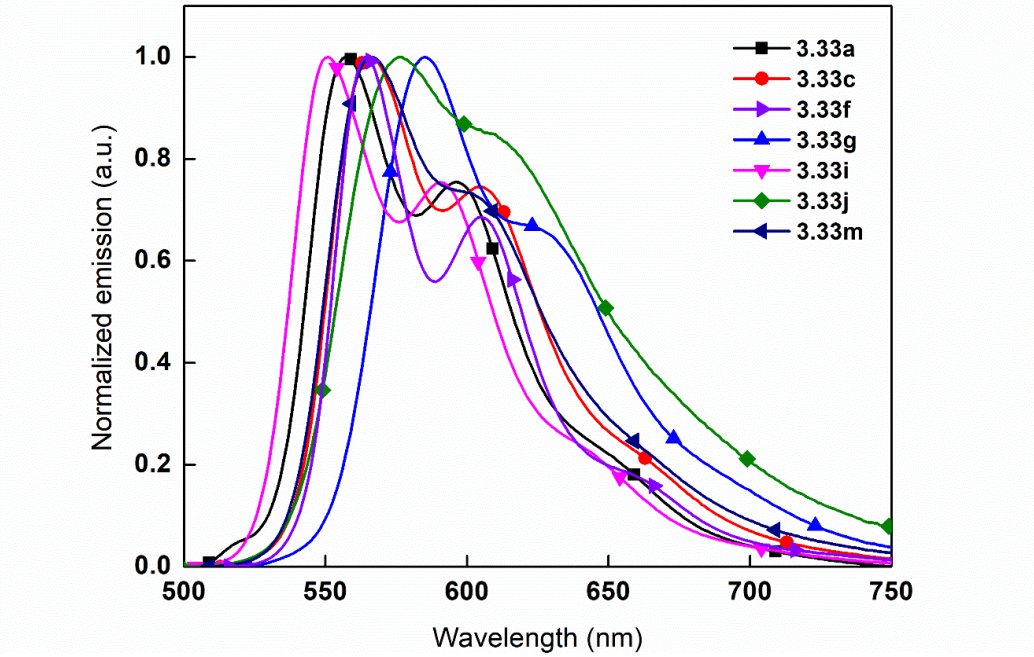

Figure 3-6 Emission spectra of selective naphtho[2,3-*a*]aceanthrylene derivatives.

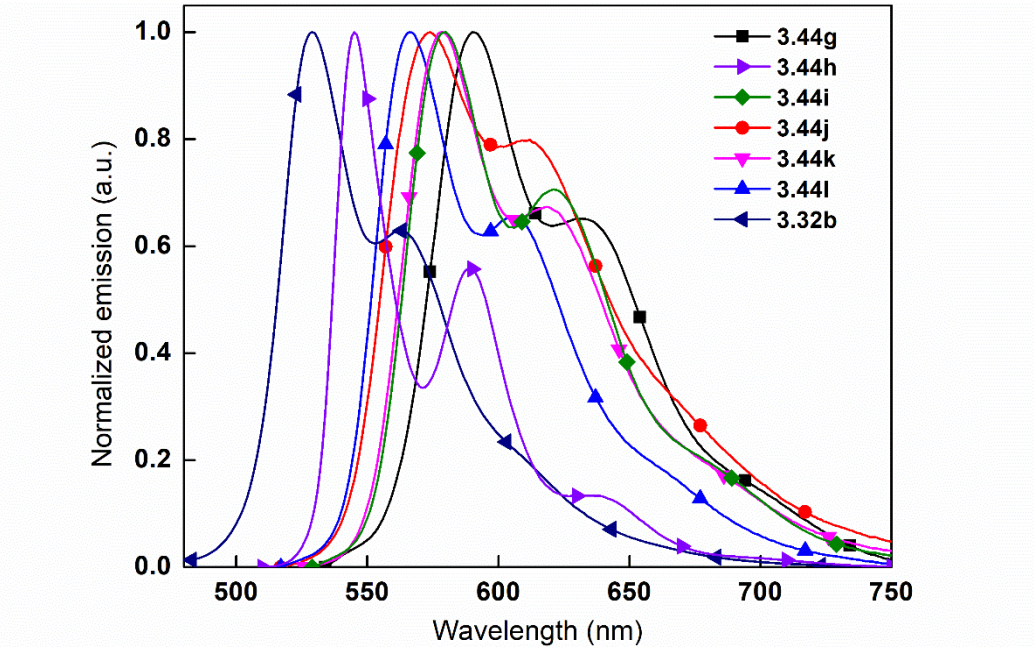

Figure 3-7 Emission spectra of selective dibenzo[*g*,*s*]rubicene derivatives **3.44g–l** and uncyclized tetrayne **3.32b**.

Table 3-6 Optical data and fluorescence yield for selective compounds.

Compound	Absorption λ_{max} (nm)	Emission λ_{max} (nm)	Optical bandgap (eV)	Quantum Yield
3.33a	499, 535	557, 597	2.19	51%
3.34g	523, 563	590, 633	2.07	66%
3.34h	500, 537	545, 589, 634	2.23	75%
3.34i	484, 517, 556	578, 621	2.12	79%
3.34j	477, 505, 535	573, 612	2.18	28%
3.34k	515, 554	578, 619	2.12	30%
3.34l	507, 542	566, 606	2.18	17%

3.3.2 Electrochemical Characterization *via* Cyclic Voltammetry

The dibenzo[*g*,*s*]rubicene derivatives showed two-electron reduction features as revealed by cyclic voltammetry. The measurements were taken in 1 mmol/L THF solutions.

Oxidation waves were not observed within the solvent window. The LUMO energies were calculated according to the potential of first reversible reduction waves. Among the measured molecules, compound **3.44g** showed the highest HOMO level due to the electron-donating O*n*Bu groups and compound **3.44h** showed the lowest LUMO level because of the electron-withdrawing CF_3 substitutions. Noticeably, the LUMO levels of dibenzo[*g*,*s*]rubicene derivatives ranged between −3.22 to −3.47 eV, which are significantly lower than common acene derivatives (anthracene −2.25 eV, tetracene −2.61 eV and perylene −2.55 eV). These results indicated that dibenzo[*g*,*s*]rubicene derivatives exhibit stronger electron affinity than normal acenes, even without the incorporation of electron-withdrawing groups.

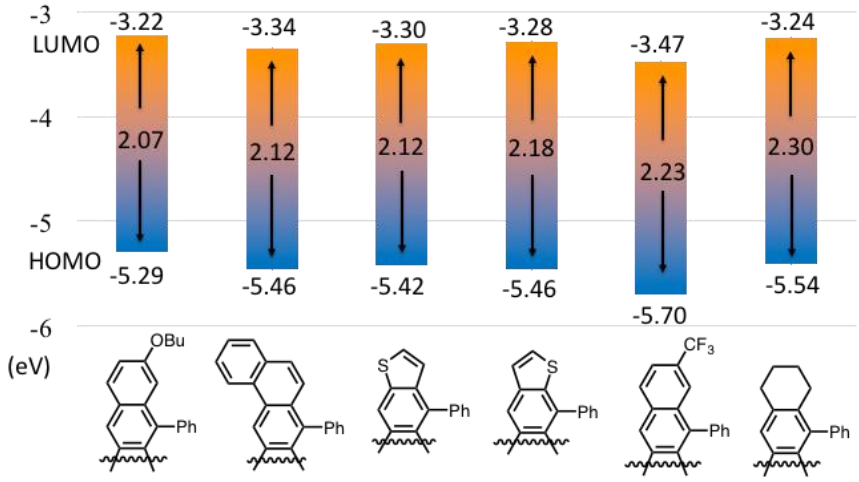

Figure 3-8 Energy level diagram of newly synthesized CP-PAHs.

3.3.3 Computational Studies: DFT and NICS Calculations

To further study the conjugation properties, computational studies were performed. The electronic structures of both mono-cyclized and double-cyclize products were calculated *via* density functional theory (DFT) calculation using B3LYP functional and 6-31+G(d)

basis set. The bandgap obtained from computational results matched well with the optical bandgap within 0.13 eV difference. As shown in **Figure 3-9**, the HOMO/LUMO plots of **3.44a** showed considerable orbital density across the entire conjugated core. In **3.33a**, the delocalized character was also observed and extended from the polycyclic segment to the phenylacetylene unit. This orbital model is consistent with the similar measured bandgap data between dibenzo[*g*,*s*]rubicenes and naphtho[2,3-*a*]aceanthrylenes.

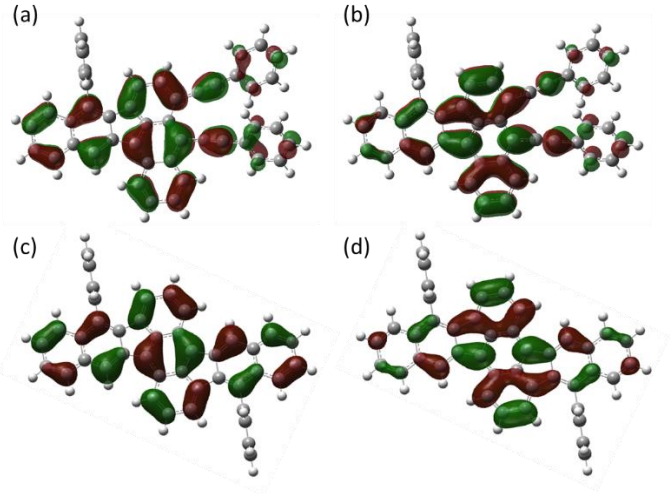

Figure 3-9 DFT calculated molecular orbitals: (a) HOMO of **3.33a**, (b) LUMO of **3.33a**, (c) HOMO of **3.44a**, (d) LUMO of **3.44a**.

In order to further understand the aromatic features of the CP-PAHs, nucleus-independent chemical shifts (NICS) calculations were performed on **3.44a** [84]. We specifically focused on the NICS (0) and NICS (1) values of the five-membered ring and its neighboring benzenoid rings. As shown in **Figure 3-10**, both NICS (0) and NICS (1) values were obtained as positive numbers at the center of the five-membered ring. It indicated that the cyclopenta moiety has antiaromatic contribution to the conjugated system. This is also consistent with the increased electron affinity as we previously observed *via*

cyclic voltammetry. Our observation is also consistent with other work on CP-PAH molecules, where the antiaromatic character was associated with increased electron affinity and decreased bandgap[85].

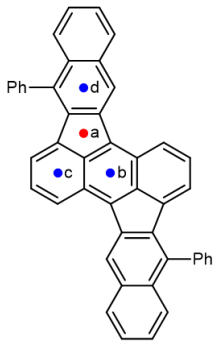

Position	NICS(0)	NICS(1)
a	5.59	1.13
b	−7.40	−9.10
c	−5.86	--
d	−5.34	--

Figure 3-10 NICS (0) and NICS (1) values for **3.44a**.

3.4 Conclusion and Future Work

In conclusion, we have developed a convenient method to construct five-membered ring containing polycyclic aromatic hydrocarbons. The synthesized dibenzo[*g*,*s*]rubicene analogs displayed narrow bandgap and unique optical characteristics. The embedded cyclopenta ring moiety and extended conjugation area resulted in low-lying LUMO levels as compared to benzenoid PAHs. NICS calculations have confirmed the antiaromatic contributions to the π system due to the cyclopenta moiety. Collectively, these results have demonstrated the potential of derivatives as novel semiconductive materials. In future studies, the OFET device of dibenzo[*g*,*s*]rubicene single crystals and thin films should be fabricated to further examine their electronic and semiconductive properties. The synthetic methodology studied in this work can be extended to other PAH substrates to generated more complicated and structurally interesting aromatic compounds.

3.5 Experimental Details

General Details: Unless otherwise noted, all reactions were carried out using oven-dried glassware under a nitrogen atmosphere. Dichloromethane (CH_2Cl_2), Acetonitrile (CH_3CN) and toluene were distilled from CaH_2 prior to use. Tetrahydrofuran (THF) was distilled from Na/benzophenone prior to use. Anhydrous diethyl ether (Et_2O) were purchased from Sigma-Aldrich and used without further purification. Unless otherwise noted, all chemicals were purchased from commercial sources and used as received. Palladium, copper and silver salts were purchased from Sigma-Aldrich or Strem and used as received. 1-Butyl-4-eth-1-ynylbenzene, 3-ethynylthiophene, 1-ethynyl-4-methoxybenezne, 4-(trifluoromethyl)phenylacetylene, 4-*tert*-butylphenylacetylene and 1-ethynylcyclohexene were purchased from commercial sources and used as received. The 2-ethynylthiophene, 1-ethynyl-4-methoxybenzene, 4-ethynyltoluene, 1-butoxy-4-ethynylbenezne, 1-ethynylnaphthalene, 2-ethynylnaphthalene, 1-ethynyl-3,5-dimethylbenzene and 2-ethynyltoluene were prepared *via* the desilylation of the Sonagashira cross-coupling products of the corresponding commercially available aryl bromides or iodides with trimethylsilylacetylene.

Analytical thin-layer chromatography (TLC) and preparative thin-layer chromatography were carried out using 250 μm and 1000 μm silica plates (SiliCycle), respectively. Eluted plates were visualized first with a UV lamp (254 nm) and then stained with potassium permanganate or *p*-anisaldehyde, followed by heating. Flash column chromatography was performed using 230−400 mesh (particle size 40−63 μm) silica gel purchased from SiliCycle.

^{1}H NMR (300, 400 and 500 MHz) and ^{13}C NMR (75, 100 and 125 MHz) spectra were obtained on Varian Inova and Bruker Avance instruments. ^{1}H NMR spectra data were reported as δ values in ppm relative to chloroform (δ 7.26) if collected in $CDCl_3$. ^{13}C NMR spectra data were reported as δ values in ppm relative to chloroform (δ 77.00) if collected in $CDCl_3$ or THF (δ 25.31, 67.21) if collected in THF-d_8. Note: Due to the extremely poor solubility, the ^{13}C NMR spectra of rubicene derivatives were not collected. ^{19}F NMR spectra data were reported as δ values in ppm relative to hexafluorobenzene (−164.9). ^{1}H NMR coupling constants were reported in Hz, and multiplicity was indicated as follows: s (singlet); d (doublet); t (triplet); q (quartet); quint (quintet); m (multiplet); dd (doublet of doublets); ddd (doublet of doublet of doublets); dddd (doublet of doublet of doublet of doublets); dt (doublet of triplets); td (triplet of doublets); ddt (doublet of doublet of triplets); dq (doublet of quartets); app (apparent); br (broad). IR spectra were obtained with an ATR source using a Nicolet iS5 FT-IR spectrometer. High-resolution mass spectra (HRMS) were performed using either electrospray ionization (ESI) or GC/MS. ESI methods were performed on a Bruker BioTOF II (Time-of-flight) instrument using PEG-300, PEG-400 or PPG-400 as an internal standard. GC/MS were collected on an Agilent 7200 GC/QTOF-MS instrument using a direct solid probe method in which the samples were heated to 325 °C. Note: Many of the new compounds reported in this dissertation lack HRMS data due to extremely poor solubility in polar solvents (methanol or acetonitrile), which make ionization of such hydrocarbons very challenging. For compounds that HRMS data were not acquired, LRMS data were collected using laser desorption ionization (LDI) on an AB-Sciex 5800 MALDI/TOF instrument.

UV-vis extinction spectra were obtained using a Mikropack DH-2000 UV-Vis-NIR spectrometer. Equipped with a K-Sphere "Petite" integrating sphere, PTI QuantaMaster™ 400 fluorescence spectrofluorometer was used to determine steady state fluorescence emission and quantum yield (QY). To be more specific, the integrating sphere used "direct excitation" method to measure the absolute QY, and the measurement for each sample was completed in four individual scans, namely the excitation scattering and the emission for both the solvent and the sample. The integral of each scan was calculated by the fluorometer software, PTI Felix GX, and so was the value of absolute QY, which can be expressed as follows:

$$\mathrm{QY}(\%) = \frac{I_{smpl\ em} - I_{sol\ em}}{I_{smpl\ ex} - I_{sol\ ex}} \times 100\%$$

Where $I_{smpl\ em}$ is the integral of the emission of the sample solution, $I_{sol\ em}$ and is the integral of the emission of the solvent; correspondingly, $I_{smpl\ ex}$ is the integral of the excitation scattering of the sample solution, $I_{sol\ ex}$ and is the integral of the excitation scattering of the solvent.

Cyclic voltammograms were recorded on a CHI600C potentiostat. A gold electrode was used as the working electrode, a platinum wire as the counter electrode, and an Ag wire in 10 mM $AgNO_3$/0.1M $TBAClO_4$ in acetonitrile as the reference electrode. The gold electrode was polished with aqueous dispersions of alumina (0.3 and 0.05 μm). Then, the electrode was cleaned in water and ethanol by ultrasonication and dried with nitrogen flow. The scan speed was 50 mV/s. The potential in THF solution was measured with tetrabutylammonium hexafluorophosphate ($TBAPF_6$, 0.1 M) employed as supporting electrolyte. The energy level of Fc/Fc^+ is assumed to be −4.8 eV below the vacuum level.

Cyclic voltammograms of newly synthesized CP-PAHs

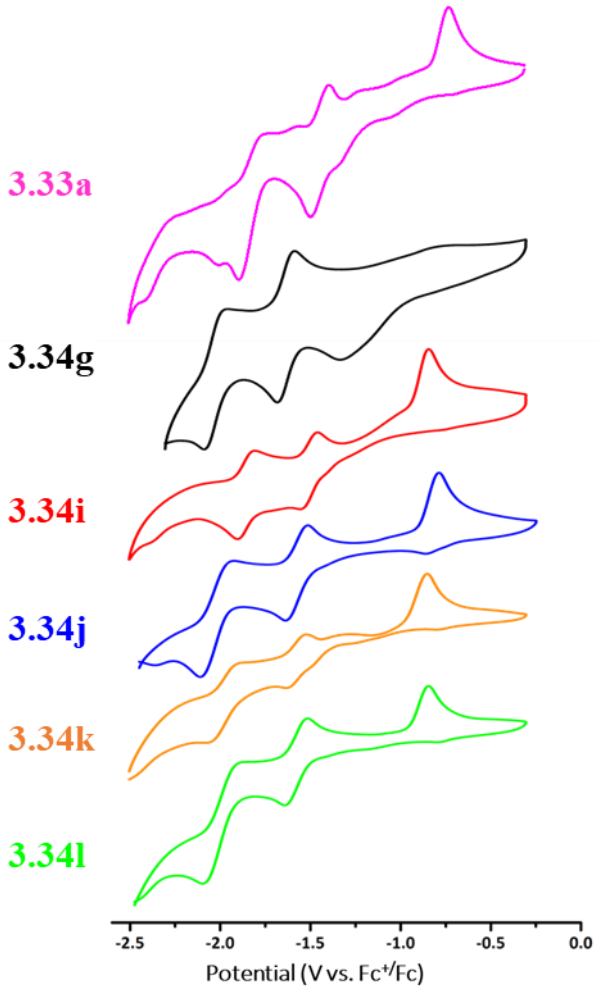

Synthesis of 1,4-dibromoanthracene-9,10-dione ***3.36***

To a 50 mL flame-dried round bottom flask were added 1,4-diaminoanthraquinone (2.22 g, 90% purity, 8.39 mmol), $CuBr_2$ (4.22 g, 18.9 mmol), *t*-butylnitrite (2.5 mL, 90% purity, 18.9 mmol) and dry acetonitrile (16 mL) under N_2. The mixture was stirred at 65 °C overnight under N_2 protection. After cooling to room temperature, the volatiles were removed *in vacuo* and the residue was partitioned between CH_2Cl_2 (100 mL) and 6M HCl (50 mL). The organic layer was separated and washed with 1M HCl (50 mL × 2) and brine (50 mL). The organic layer was dried over Na_2SO_4 and concentrated *in vacuo*. The residue

was purified by column chromatography on silica gel (40 mm × 250 mm, CH_2Cl_2/hexanes 1:3 to 1:2 to 1:1) to afford the product as a yellow solid (2.32 g, 76%).

^{1}H NMR ($CDCl_3$, 500 MHz) δ 8.21 (dd, *J* = 6.0, 3.5 Hz, 2H), 7.82 (s, 2H), 7.80 (dd, *J* = 6.0, 3.5 Hz, 2H). ^{13}C NMR ($CDCl_3$, 125 MHz) δ 181.6, 140.6, 134.2, 133.5, 133.4, 126.9, 122.0.

Synthesis of 1,5-dibromoanthracene-9,10-dione ***3.42***

To a 500 mL flame-dried three-neck round bottom flask were added $CuBr_2$ (48.8 g, 218 mmol), *t*-butylnitrite (33 mL, 90% purity, 250 mmol) and dry acetonitrile (200 mL) under N_2. The mixture was stirred at 65 °C and 1,5-diaminoanthraquinone (21.74 g, 92% purity, 84 mmol) was added in small portions over 30 minutes under N_2 protection. After nitrogen evolution the reaction mixture was cooled to room temperature and the volatiles were removed *in vacuo.* The residue was purified by column chromatography on silica gel (80 mm x 250 mm, CH_2Cl_2/hexanes 1:3 to 1:2 to 1:1 to 1:0) to afford the product as a yellow solid (24.56 g, 80%).

^{1}H NMR ($CDCl_3$, 500 MHz) δ 8.33 (dd, *J* = 8.0, 1.0 Hz, 2H), 8.03 (dd, *J* = 8.0, 1.0 Hz, 2H), 7.60 (t, *J* = 8.0 Hz, 2H). ^{13}C NMR ($CDCl_3$, 125 MHz) δ 140.8, 137.0, 134.1, 130.1, 127.7, 121.9. The carbonyl carbon signal was not observed due to poor solubility.

Procedure I*: Synthesis of 1,4-dibromo-9,10-bis(phenylethynyl)anthracene* ***3.31a***

To a 100 mL flame-dried round bottom flask were added phenylacetylene (0.70 mL, 6.4 mmol), and dry THF (16 mL) under N_2. The mixture was cooled to −78 °C and *n*BuLi (2.5 M in hexanes, 2.4 mL, 6.0 mmol) was added dropwise. The resulting mixture was stirred

at −78 °C for 1h before the addition of quinone (732 mg, 2.0 mmol) all at once. The mixture was allowed to warm up to room temperature and stirred overnight. To the mixture was added toluene (16 mL). A solution of $SnCl_2$ (2.28 g, 12 mmol) in 4M HCl (8 mL) was added to the above mixture. The resulting mixture was stirred at 60 °C for 1h before cooling to room temperature. The volatiles were removed *in vacuo*. The residue filtered and washed with H_2O (50 mL) and MeOH (50 mL). The crude product was purified by column chromatography on silica gel (20 mm x 250 mm, CH_2Cl_2/hexanes 1:20 to 1:10) to afford the product as an orangish red solid (988 mg, 92%)

^{1}H NMR ($CDCl_3$, 500 MHz) δ 8.88 (dd, *J* = 6.5, 3.5 Hz, 2H), 7.76-7.70 (m, 8H), 7.48-7.42 (m, 6H). ^{13}C NMR ($CDCl_3$, 125 MHz) δ 133.6, 133.5, 131.1, 130.9, 128.8, 128.5, 128.2, 127.3, 123.8, 120.9, 119.5, 109.7, 88.0. LRMS (LDI) cacld for $C_{30}H_{16}Br_2$ [M^+] *m*/*z* 536.0, found [M^+] 535.8. IR (neat, cm^{-1}) 3079, 2193, 1488, 1385.

Synthesis of 1,4-dibromo-9,10-bis((4-butylphenyl)ethynyl)anthracene ***3.31d***

Prepared from 4.0 mmol of quinone according to Procedure I; 89% yield; orangish red solid.

^{1}H NMR ($CDCl_3$, 500 MHz) δ 8.87 (dd, *J* = 7.0, 3.0 Hz, 2H), 7.70 (dd, *J* = 7.0, 3.0 Hz, 2H), 7.68 (s, 2H), 7.66 (d, *J* = 8.0 Hz, 4H), 7.26 (d, *J* = 8.0 Hz, 2H), 2.67 (t, *J* = 7.5 Hz, 4H), 1.66-1.62 (m, 4H), 1.42-1.36 (m, 4H), 0.95 (t, *J* = 7.5 Hz, 6H). ^{13}C NMR ($CDCl_3$, 125 MHz) δ 144.1, 133.5, 133.5, 131.0, 130.8, 128.7, 128.1, 127.4, 121.0, 120.9, 119.5, 110.1, 87.6, 35.7, 33.4, 22.3, 14.0. IR (neat, cm^{-1}) 3031, 2957, 2927, 2857, 2185, 1511, 1504, 1390. LRMS (LDI) cacld for $C_{38}H_{32}Br_2$ [M^+] *m*/*z* 648.1, found [M^+] 647.9.

Synthesis of 1,4-dibromo-9,10-bis((4-(tert-butyl)phenyl)ethynyl)anthracene ***3.31e***

Prepared from 2.0 mmol of quinone according to Procedure I; 92% yield; orangish yellow solid.

^{1}H NMR ($CDCl_3$, 500 MHz) δ 8.87 (dd, *J* = 6.5, 3.0 Hz, 2H), 7.71-7.67 (m, 8H), 7.48 (dd, *J* = 6.5, 2.0 Hz, 4H), 1.37 (s, 18H). ^{13}C NMR ($CDCl_3$, 125 MHz) δ 152.2, 133.5, 133.5, 131.0, 130.6, 128.1, 127.4, 125.6, 120.9, 120.8, 119.5, 110.0, 87.5, 34.9, 31.2. HRMS (ESI) cacld for $C_{38}H_{32}Br_2$ [M^+] *m*/*z* 648.0850, found [M^+] 648.0825. IR (neat, cm^{-1}) 3060, 2963, 2195, 1502, 1390.

Synthesis of 1,4-dibromo-9,10-bis((4-butoxyphenyl)ethynyl)anthracene ***3.31h***

Prepared from 2.0 mmol of quinone according to Procedure I; 96% yield; orangish red solid.

^{1}H NMR ($CDCl_3$, 500 MHz) δ 8.86 (dd, *J* = 7.0, 3.5 Hz, 2H), 7.69 (dd, *J* = 7.0, 3.5 Hz, 2H), 7.67 (dd, *J* = 7.0, 2.0 Hz, 2H), 7.67 (s, 2H), 6.96 (dd, *J* = 7.0, 2.0 Hz, 2H), 4.03 (t, *J* = 7.0 Hz, 2H), 1.83-1.78 (m, 4H), 1.55-1.49 (m, 4H), 1.00 (t, *J* = 7.5 Hz, 2H). ^{13}C NMR ($CDCl_3$, 125 MHz) δ 159.8, 133.4, 133.4, 132.4, 131.0, 128.00, 127.5, 120.9, 119.4, 115.8, 114.8, 110.1, 87.1, 67.8, 31.2, 19.2, 13.9. HRMS (ESI) cacld for $C_{38}H_{32}Br_2O_2$ [M^+] *m*/*z* 680.0749, found [M^+] 680.0748. IR (neat, cm^{-1}) 3069, 2956, 2928, 2868, 2183, 1601, 1508, 1463, 1249.

Synthesis of 1,4-dibromo-9,10-bis(p-tolylethynyl)anthracene ***3.31c***

Prepared from 3.0 mmol of quinone according to Procedure I; 92% yield; orangish red solid.

^{1}H NMR ($CDCl_3$, 500 MHz) δ 8.87 (dd, *J* = 6.5, 3.0 Hz, 2H), 7.70 (dd, *J* = 6.5, 3.0 Hz, 2H), 7.69 (s, 2H), 7.64 (d, *J* = 8.0 Hz, 2H), 7,26 (d, *J* = 8.0 Hz, 2H). ^{13}C NMR ($CDCl_3$, 125 MHz) δ 139.1, 133.5, 133.5, 131.0, 130.8, 129.3, 128.1, 127.4, 120.9, 120.8, 119.5, 110.0, 87.6, 21.7. IR (neat, cm^{-1}) 3071, 3026, 2186, 1507, 1393. HRMS (ESI) cacld for $C_{32}H_{20}Br_2$ [M^+] *m*/*z* 563.9911, found [M^+] 563.9894.

Synthesis of 1,4-dibromo-9,10-bis((3,5-dimethylphenyl)ethynyl)anthracene ***3.31f***

Prepared from 2.0 mmol of, 88% yield quinone according to Procedure I; orangish red solid.

^{1}H NMR ($CDCl_3$, 500 MHz) δ 8.86 (dd, *J* = 6.5, 3.0 Hz, 2H), 7.71 (dd, *J* = 6.5, 3.0 Hz, 2H), 7.69 (s, 2H), 7.37 (s, 4H), 7.06 (s, 2H), 2.39 (s, 12H). ^{13}C NMR ($CDCl_3$, 125 MHz) δ 138.1, 133.6, 133.5, 131.1, 130.8, 128.5, 128.1, 127.4, 123.5, 120.9, 119.5, 110.2, 87.4, 21.2. HRMS (ESI) cacld for $C_{34}H_{24}Br_2$ [M^+] *m*/*z* 595.0224, found [M^+] 592.0172. IR (neat, cm^{-1}) 2914, 2859, 2184, 1709, 1595, 1393, 1374.

Synthesis of 1,4-dibromo-9,10-bis(o-tolylethynyl)anthracene ***3.31b***

Prepared from 2.0 mmol of quinone according to Procedure I; 92% yield; orangish red solid.

^{1}H NMR ($CDCl_3$, 500 MHz) δ 8.91 (dd, *J* = 6.5, 3.0 Hz, 2H), 7.75 (d, *J* = 7.5 Hz, 2H), 7.70 (dd, *J* = 6.5, 3.0 Hz, 2H), 7.70 (s, 2H), 7.33-7.31 (m, 4H), 7.29-7.26 (m, 2H), 2.69 (s, 6H). ^{13}C NMR ($CDCl_3$, 125 MHz) δ 140.1, 133.7, 133.5, 131.42, 131.1, 129.8, 128.8, 128.1, 127.5, 125.8, 123.6, 120.8, 119.7, 109.2, 91.5, 21.3. HRMS (GC/MS solid probe) cacld for

$C_{32}H_{20}Br_2$ [M^+] *m/z* 563.9911, found [M^+] 563.9967. IR (neat, cm^{-1}) 3066, 2177, 1576, 1485, 1456, 1385, 1375.

Synthesis of 2,2'-((1,4-dibromoanthracene-9,10-diyl)bis(ethyne-2,1-diyl))dithiophene ***3.31l***

Prepared from 2.0 mmol of quinone according to Procedure I; 66% yield; dark red solid.

^1H NMR ($CDCl_3$, 500 MHz) δ 8.76 (dd, *J* = 6.5, 3.0 Hz, 2H), 7.70 (dd, *J* = 6.5, 3.0 Hz, 2H), 7.69 (s, 2H), 7.48 (d, *J* = 3.5 Hz, 2H), 7.43 (d, *J* = 5.0 Hz, 2H), 7.13 (dd, *J* = 5.0, 3.5 Hz, 2H). ^{13}C NMR ($CDCl_3$, 125 MHz) δ 133.7, 133.0, 131.6, 131.0, 128.3, 128.2, 127.4, 127.2, 123.8, 120.9, 119.1, 103.7, 92.2. IR (neat, cm^{-1}) 3106, 2171, 1578, 1520. LRMS (LDI) cacld for $C_{26}H_{12}Br_2S_2$ [M^+] *m/z* 547.9, found [M^+] 547.7.

Synthesis of 3,3'-((1,4-dibromoanthracene-9,10-diyl)bis(ethyne-2,1-diyl))dithiophene ***3.31m***

Prepared from 2.0 mmol of quinone according to Procedure I; 79% yield; orangish red solid.

^1H NMR ($CDCl_3$, 500 MHz) δ 8.82 (dd, *J* = 6.5, 3.0 Hz, 2H), 7.74 (dd, *J* = 2.5, 1.5 Hz, 2H), 7.70 (dd, *J* = 7.0, 3.5 Hz, 2H), 7.69 (s, 2H), 7.42-7.40 (m, 4H). ^{13}C NMR ($CDCl_3$, 125 MHz) δ 133.6, 133.4 131.1, 129.0, 128.6, 128.2, 127.3, 125.8, 123.0, 120.9, 119.3, 105.1, 87.5. IR (neat, cm^{-1}) 3107, 2916, 2849, 2191, 1579, 1361. LRMS (LDI) cacld for $C_{26}H_{12}Br_2S_2$ [M^+] *m/z* 547.9, found [M^+] 547.7.

Procedure II: *Synthesis of 1,4-dibromo-9,10-bis((4-(trifluoromethyl)phenyl)ethynyl)-anthracene* ***3.31i***

To a 250 mL flame-dried round bottom flask were added 4-(trifluoromethyl)phenylacetylene (2.18 g, 12.8 mmol), and dry THF (40 mL) under N_2. The mixture was cooled to −78 °C and *n*BuLi (2.5 M in hexanes, 4.8 mL, 12.0 mmol) was added dropwise. The resulting mixture was stirred at −78 °C for 1h before the addition of quinone (1.464 g, 4.0 mmol) all at once. The mixture was allowed to warm up to room temperature and stirred overnight. NH_4Cl (sat. aq. 10 mL) was added to the flask. A solution of $SnCl_2$ (7.6 g, 40 mmol) in 4M HCl (40 mL) was added to the above mixture. The resulting mixture was stirred at 60 °C for 1h before cooling to room temperature. The volatiles were removed *in vacuo*. The residue filtered and washed with H_2O (50 mL) and MeOH (50 mL). The crude product was purified by column chromatography on silica gel (20 mm × 250 mm, CH_2Cl_2/hexanes 1:5 to 1:2 to 1:1) to afford the product as an orangish red solid (2.47 g, 92%).

^{1}H NMR ($CDCl_3$, 500 MHz) δ 8.84 (dd, *J* = 6.5, 3.0 Hz, 2H), 7.84 (d, *J* = 7.5 Hz, 4H), 7.75 (dd, *J* = 6.5, 3.0 Hz, 2H), 7.74 (s, 2H) 7.71 (d, *J* = 7.5 Hz, 4H). ^{13}C NMR ($CDCl_3$, 126 MHz) δ 134.0, 133.6, 131.4, 131.1, 130.5 (q, *J* = 33 Hz), 128.6, 127.3, 127.2, 125.6 (q, *J* = 3.8 Hz), 123.9 (q, *J* = 274.7 Hz), 120.8, 119.3, 108.2, 90.0. HRMS (GC/MS solid probe) cacld for $C_{32}H_{14}Br_2F_6$ [M^+] *m*/*z* 671.9346, found [M^+] 671.9349. IR (neat, cm^{-1}) 2926, 1608, 1315.

Synthesis of 1,4-dibromo-9,10-bis((4-methoxyphenyl)ethynyl)anthracene ***3.31g***

Prepared from 4.0 mmol of quinone according to Procedure II; 93% yield; orangish red solid.

^{1}H NMR ($CDCl_3$, 500 MHz) δ 8.86 (dd, *J* = 6.5, 3.0 Hz, 2H), 7.71-7.76 (m, 8H), 6.98 (dd, *J* = 6.5, 1.5 Hz, 2H), 3.88 (s, 6H). ^{13}C NMR ($CDCl_3$, 125 MHz) δ 160.2, 133.4, 132.4, 131.0, 128.0, 127.5, 120.9, 119.4, 116.0, 114.3, 109.9, 87.1, 80.7, 55.4. HRMS (ESI) cacld for $C_{32}H_{20}Br_2O_2$ [M^+] *m/z* 595.9810, found [M^+] 595.9792. IR (neat, cm^{-1}) 3071, 3006, 2967, 2926, 2833, 2183,1601, 1505, 1454, 1435, 1287, 1249.

Synthesis of 1,4-dibromo-9,10-bis(naphthalen-1-ylethynyl)anthracene ***3.31k***

Prepared from 4.0 mmol of quinone according to Procedure II; 92% yield; orangish red solid.

^{1}H NMR ($CDCl_3$, 500 MHz) δ 9.05 (dd, *J* = 6.5, 3.0 Hz, 2H), 8.65 (d, *J* = 8.5 Hz, 2H), 8.00 (dd, *J* = 7.0, 1.0 Hz, 2H), 7.95-7.92 (m, 4H), 7.76 (dd, *J* = 6.5, 3.0 Hz, 2H), 7.75 (s, 2H), 7.67-7.63 (m, 2H), 7.61-7.55 (m, 4H). ^{13}C NMR ($CDCl_3$, 125 MHz) δ 133.9, 133.7, 133.4, 133.2, 131.3, 130.1, 129.3, 128.4, 128.4, 127.6, 127.1, 126.6, 126.5, 125.5, 121.5, 120.9, 119.8, 108.7, 92.4. IR (neat, cm^{-1}) 3043, 2189, 1581, 1504, 1408, 1333. LRMS (LDI) cacld for $C_{38}H_{20}Br_2$ [M^+] *m/z* 636.0, found [M^+] 635.8.

Synthesis of 1,4-dibromo-9,10-bis(cyclohex-1-en-1-ylethynyl)anthracene ***3.31j***

Prepared from 4.0 mmol of quinone according to Procedure II; 92% yield; orangish red solid.

^{1}H NMR ($CDCl_3$, 500 MHz) δ 8.70 (dd, *J* = 6.5, 3.0 Hz, 2H), 7.63 (dd, *J* = 6.5, 3.0 Hz, 2H), 7.61 (s, 2H), 6.46-6.43 (m, 2H), 2.45-2.40 (m, 4H), 2.27-2.22 (m, 4H), 1.79-1.74 (m, 4H), 1.72-1.66 (m, 4H). ^{13}C NMR ($CDCl_3$, 125 MHz) δ 135.6, 133.4, 133.2, 130.9, 127.8, 127.4, 121.8, 121.0, 119.5, 111.8, 85.7, 28.2, 26.0, 22.3, 21.6. HRMS (GC/MS solid probe)

cacld for $C_{30}H_{24}Br_2$ [M^+] *m*/*z* 544.0224, found [M^+] 544.0303. IR (neat, cm^{-1}) 3067, 2927, 2857, 2184, 1579, 1394.

Synthesis of 1,5-dibromo-9,10-bis((4-butylphenyl)ethynyl)anthracene ***3.43d***

Prepared from 2.0 mmol of quinone according to Procedure I; 90% yield; orangish red solid.

^{1}H NMR ($CDCl_3$, 500 MHz) δ 8.97 (dd, *J* = 8.5, 1.0 Hz, 2H), 7.98 (dd, *J* = 8.5, 1.0 Hz, 2H), 7.66 (dd, *J* = 6.5, 1.5 Hz, 4H), 7.40 (dd, *J* = 8.5, 6.5 Hz, 2H), 7.26 (d, *J* = 6.5 Hz, 4H), 2.67 (t, *J* = 7.5 Hz, 4H), 1.67-1.60 (m, 4H), 1.41-1.36 (m, 4H), 0.95 (t, *J* = 7.5 Hz, 6H). ^{13}C NMR ($CDCl_3$, 125 MHz) δ 144.2, 135.6, 135.0, 130.8, 129.5, 128.7, 128.2, 126.9, 120.9, 120.6, 119.3, 109.5, 88.0, 35.7, 33.4, 22.3, 14.0. IR (neat, cm^{-1}) 3086, 3037, 2955, 2928, 2858, 1505, 1393, 1376. LRMS (LDI) cacld for $C_{38}H_{32}Br_2$ [M^+] *m*/*z* 648.1, found [M^+] 647.9.

Synthesis of 1,5-dibromo-9,10-bis((4-(tert-butyl)phenyl)ethynyl)anthracene ***3.43e***

Prepared from 2.0 mmol of quinone according to Procedure I; 91% yield; orangish red solid.

^{1}H NMR ($CDCl_3$, 500 MHz) δ 8.97 (dd, *J* = 8.5, 1.0 Hz, 2H), 7.98 (dd, *J* = 7.5, 1.0 Hz, 2H), 7.68 (dd, *J* = 6.5, 2.0 Hz, 4H), 7.47 (dd, *J* = 6.5, 2.0 Hz, 4H), 7.40 (dd, *J* = 9.0, 7.5 Hz, 2H), 1.37 (s, 18H). ^{13}C NMR ($CDCl_3$, 125 MHz) δ 152.3, 135.6, 135.0, 130.7, 129.6, 128.2, 126.9, 125.6, 120.7, 120.7, 119.3, 109.4, 87.9, 34.9, 31.2. IR (neat, cm^{-1}) 3089, 2961, 2866, 2186, 1502, 1392, 1376, 1360, 1273. LRMS (LDI) cacld for $C_{38}H_{32}Br_2$ [M^+] *m*/*z* 648.1, found [M^+] 647.9.

*Synthesis of 1,5-dibromo-9,10-bis(p-tolylethynyl)anthracene **3.43c***

Prepared from 2.0 mmol of quinone according to Procedure I; 96% yield; orangish red solid.

^{1}H NMR ($CDCl_3$, 500 MHz) δ 8.97 (dd, *J* = 9.0, 1.5 Hz, 2H), 7.98 (dd, *J* = 7.5, 1.0 Hz, 2H), 7.64 (d, *J* = 8.5 Hz, 4H), 7.40 (dd, *J* = 9.0, 7.5 Hz, 2H), 7.26 (d, *J* = 8.5 Hz, 2H). ^{13}C NMR ($CDCl_3$, 125 MHz) δ 139.2, 135.6, 135.0, 130.8, 129.6, 129.4, 128.2, 126.9, 120.7, 120.6, 119.3, 109.4, 87.9, 21.7. HRMS (GC/MS solid probe) cacld for $C_{32}H_{20}Br_2$ [M^+] *m*/*z* 563.9911, found [M^+] 563.9864. IR (neat, cm^{-1}) 3039, 2914, 2190, 1606, 1506, 1392, 1376.

*Synthesis of 1,5-dibromo-9,10-bis((3,5-dimethylphenyl)ethynyl)anthracene **3.43f***

Prepared from 2.0 mmol of quinone according to Procedure I; 78% yield; orangish red solid.

^{1}H NMR ($CDCl_3$, 500 MHz) δ 9.01 (dd, *J* = 8.5, 1.5 Hz, 2H), 7.98 (dd, *J* = 7.0, 1.5 Hz, 2H), 7.42 (dd, *J* = 8.5, 7.0 Hz, 2H), 7.37 (s, 4H), 7.06 (s, 2H), 2.38 (s, 12H). ^{13}C NMR ($CDCl_3$, 125 MHz) δ 138.2, 135.7, 135.0, 130.9, 129.6, 128.5, 128.2, 126.9, 123.4, 120.7, 119.3, 109.6, 87.8, 21.2. HRMS (GC/MS solid probe) cacld for $C_{34}H_{24}Br_2$ [M^+] *m*/*z* 592.0224, found [M^+] 592.0202. IR (neat, cm^{-1}) 3033, 2913, 2858, 2187, 1607, 1596, 1471, 1395, 1383, 1294.

*Synthesis of 1,5-dibromo-9,10-bis(o-tolylethynyl)anthracene **3.43b***

Prepared from 2.0 mmol of quinone according to Procedure I; 90% yield; orangish red solid.

^{1}H NMR ($CDCl_3$, 500 MHz) δ 9.01 (dd, *J* = 9.0, 1.0 Hz, 2H), 7.98 (dd, *J* = 7.5, 1.0 Hz, 2H), 7.75 (d, *J* = 7.5 Hz, 2H), 7.40 (dd, *J* = 9.0, 7.5 Hz, 2H), 7.33-7.31 (m, 4H), 7.29-7.26 (m, 2H), 2.68 (s, 6H). ^{13}C NMR ($CDCl_3$, 125 MHz) δ 140.1, 135.8, 135.0, 131.4, 129.8, 129.6, 128.9, 128.1, 126.9, 125.8, 123.6, 120.6, 119.6, 108.7, 91.8, 21.3. HRMS (GC/MS solid probe) cacld for $C_{32}H_{20}Br_2$ [M^+] *m*/*z* 563.9911, found [M^+] 563.9905. IR (neat, cm^{-1}) 3068, 3018, 2972, 2920, 2181,1608, 1486, 1456, 1386, 1376.

Synthesis of 1,5-dibromo-9,10-bis(cyclohex-1-en-1-ylethynyl)anthracene ***3.43i***

Prepared from 2.0 mmol of quinone according to Procedure I; 91% yield; orangish red solid.

^{1}H NMR ($CDCl_3$, 500 MHz) δ 8.81 (dd, *J* = 8.5, 1.0 Hz, 2H), 7.91 (dd, *J* = 7.5, 1.0 Hz, 2H),7.33 (dd, *J* = 8.5, 7.5 Hz, 2H), 6.46−6.43 (m, 2H), 2.44−2.40 (m, 4H), 2.27−2.22 (m, 4H), 1.80−1.74 (m, 4H), 1.72−1.68 (m, 4H). ^{13}C NMR ($CDCl_3$, 125 MHz) δ 135.7, 135.7, 135.5, 134.7, 129.4, 128.1, 126.6, 121.7, 120.7, 119.3, 111.1, 86.1, 28.2, 26.0, 22.3, 21.6. HRMS (GC/MS solid probe) cacld for $C_{30}H_{24}Br_2$ [M^+] *m*/*z* 544.0224, found [M^+] 544.0222. IR (neat, cm^{-1}) 2925, 2857, 2825, 2181, 1605, 1444, 1432, 1395, 1346.

Synthesis of 2,2'-((1,5-dibromoanthracene-9,10-diyl)bis(ethyne-2,1-diyl))dithiophene ***3.43k***

Prepared from 2.0 mmol of quinone according to Procedure I; 95% yield; dark red solid.

^{1}H NMR ($CDCl_3$, 500 MHz) δ 8.89 (dd, *J* = 9.0, 1.0 Hz, 2H), 7.99 (dd, *J* = 7.5, 1.5 Hz, 2H), 7.94 (dd, *J* = 3.5, 1.0 Hz, 2H), 7.45-7.41 (m, 4H), 7.13 (dd, *J* = 5.0, 3.5 Hz, 2H). ^{13}C NMR ($CDCl_3$, 126 MHz) δ 135.3, 135.2, 131.7, 129.5, 128.3, 128.0, 127.4, 127.1, 123.7,

120.7, 119.0, 103.2, 92.6. IR (neat, cm^{-1}) 3090, 2170, 1604, 1505, 1434, 1378, 1333, 1219. LRMS (LDI) cacld for $C_{26}H_{12}Br_2S_2$ [M^+] *m/z* 547.9, found [M^+] 547.7.

Procedure III: *Synthesis of 3,3'-((1,5-dibromoanthracene-9,10-diyl)bis(ethyne-2,1-diyl))dithiophene* ***3.43l***

To a 100 mL flame-dried round bottom flask were added 3-ethynylthiophene (691 mg, 6.4 mmol), and dry THF (16 mL) under N_2. The mixture was cooled to -78 °C and *n*BuLi (2.5 M in hexanes, 2.4 mL, 6.0 mmol) was added dropwise. The resulting mixture was stirred at -78 °C for 1h before the addition of quinone (732 mg, 2.0 mmol) all at once. The mixture was allowed to warm up to room temperature and stirred overnight. To the mixture was added toluene (16 mL). A solution of $SnCl_2$ (2.28 g, 12 mmol) in 4M HCl (8 mL) was added to the above mixture. The resulting mixture was stirred at 60 °C for 1h before cooling to room temperature. The volatiles were removed *in vacuo*. The residue filtered and washed with H_2O (50 mL), MeOH (50 mL), CH_2Cl_2 (20 mL) and MeOH (20 mL) to afford the product as an orangish red solid (956 mg, 87%).

^{1}H NMR ($CDCl_3$, 500 MHz) δ 8.98 (dd, *J* = 9.0, 1.0 Hz, 2H), 7.99 (dd, *J* = 7.5, 1.0 Hz, 2H), 7.75 (t, *J* = 2.0 Hz, 2H), 7.43-7.39 (m, 6H). ^{13}C NMR ($CDCl_3$, 126 MHz) δ 135.1, 129.7, 129.1, 128.7, 128.2, 128.2, 127.5, 127.0, 125.8, 122.9, 120.6. Not all carbon signals were observed due to poor solubility. IR (neat, cm^{-1}) 3100, 3043, 2189, 1607, 1584, 1505, 1410, 1377, 1361, 1336, 1214. LRMS (LDI) cacld for $C_{26}H_{12}Br_2S_2$ [M^+] *m/z* 547.9, found [M^+] 547.7.

Synthesis of 1,5-dibromo-9,10-bis(phenylethynyl)anthracene ***3.43a***

Prepared from 2.0 mmol of quinone according to Procedure I; 94% yield; orangish red solid.

^{1}H NMR ($CDCl_3$, 500 MHz) δ 8.98 (dd, *J* = 9.0, 1.5 Hz, 2H), 8.00 (dd, *J* = 7.0, 1.0 Hz, 2H), 7.76-7.74 (m, 4H), 7.48-7.40 (m, 8H). ^{13}C NMR ($CDCl_3$, 125 MHz) δ 135.7, 135.1, 130.9, 129.7, 128.9, 128.6, 128.1, 127.0, 123.7, 120.6, 119.3, 109.2, 88.4. IR (neat, cm^{-1}) 3053, 2926, 2192, 1606, 1593, 1489, 1438, 1391, 1376. LRMS (LDI) cacld for $C_{30}H_{16}Br_2$ [M^+] *m*/*z* 536.0, found [M^+] 535.8.

Synthesis of 1,5-dibromo-9,10-bis(naphthalen-1-ylethynyl)anthracene ***3.43j***

Prepared from 2.0 mmol of quinone according to Procedure III; 88% yield; orangish red solid.

^{1}H NMR ($CDCl_3$, 500 MHz) δ 9.16 (d, *J* = 8.5 Hz, 2H), 8.64 (d, *J* = 8.5 Hz, 2H), 8.04 (d, *J* = 7.0 Hz, 2H), 8.00 (d, *J* = 6.5 Hz, 2H), 7.94-7.92 (m, 4H), 7.73-7.67 (m, 2H), 7.61-7.55 (m, 4H), 7.47 (dd, *J* = 9.0, 7.0 Hz, 2H). ^{13}C NMR ($CDCl_3$, 126 MHz) δ 136.0, 135.2, 133.4, 133.2, 130.2, 129.3, 128.5, 128.3, 127.2, 127.1, 126.6, 126.5, 125.5, 121.5, 120.8, 119.7, 108.2, 92.8. Not all carbon signals were found (one aromatic carbon signal missing). IR (neat, cm^{-1}) 3042, 2188, 1608, 1584, 1575, 1505, 1462, 1409, 1377, 1214. LRMS (LDI) cacld for $C_{38}H_{20}Br_2$ [M^+] *m*/*z* 636.0, found [M^+] 635.8.

Synthesis of 1,5-dibromo-9,10-bis((4-butoxyphenyl)ethynyl)anthracene ***3.43g***

Prepared from 2.0 mmol of quinone according to Procedure I; 93% yield; orangish red solid.

^{1}H NMR ($CDCl_3$, 500 MHz) δ 8.97 (dd, *J* = 9.0, 1.0 Hz, 2H), 7.97 (dd, *J* = 7.5, 1.0 Hz, 2H), 7.67 (dd, *J* = 7.5, 2.0 Hz, 4H), 7.40 (dd, *J* = 9.0, 7.5 Hz, 2H), 6.96 (dd, *J* = 7.0, 2.0 Hz, 4H), 4.03 (t, *J* = 6.5 Hz, 4H), 1.83-1.79 (m, 4H), 1.55-1.49 (m, 6H), 1.00 (t, *J* = 7.5 Hz, 6H). ^{13}C NMR ($CDCl_3$, 126 MHz) δ 159.8, 135.6, 134.9, 132.4, 129.5, 128.2, 126.8, 120.7, 119.3, 115.7, 114.8, 109.5, 87.5, 67.9, 31.3, 19.3, 13.9. IR (neat, cm^{-1}) 3091, 3063, 2953, 2868, 2189, 1601, 1507, 1448, 1395, 1375, 1288, 1246. LRMS (LDI) cacld for $C_{38}H_{32}Br_2O_2$ [M^+] *m*/*z* 680.1, found [M^+] 680.0.

Synthesis of 1,5-dibromo-9,10-bis((4-(trifluoromethyl)phenyl)ethynyl)anthracene ***3.43h***

Prepared from 2.0 mmol of quinone according to Procedure III; 82% yield; orangish red solid.

^{1}H NMR ($CDCl_3$, 500 MHz) δ 8.94 (dd, *J* = 9.0, 1.5 Hz, 2H), 8.03 (dd, *J* = 7.5, 1.0 Hz, 2H), 7.84 (d, *J* = 8.0 Hz, 4H), 7.71 (*J* = 8.0 Hz, 4H), 7.46 (dd, *J* = 9.0, 7.5 Hz, 2H). ^{13}C NMR is unobtainable due to bad solubility in $CDCl_3$. HRMS (GC/MS solid probe) cacld for $C_{32}H_{14}Br_2F_6$ [M^+] *m*/*z* 671.9346, found [M^+] 671.9349. IR (neat, cm^{-1}) 3095, 2925, 2191, 1608, 1568, 1405, 1393, 1318.

Synthesis of 9-phenyl-5,6-bis(phenylethynyl)naphtho[2,3-a]aceanthrylene ***3.33a***

A 100 mL flame-dried Schlenk flask was evacuated and backfilled with N_2 three times. Dibromide (2107 mg, 0.2 mmol), $Pd(PPh_3)_2Cl_2$ (3.5 mg, 0.005 mmol), CuI (1 mg, 0.005 mmol), phenylacetylene (53 µL, 0.48 mmol), dry THF (2 mL) and dry Et_3N (2 mL) were added under N_2. The flask was sealed and the mixture was stirred at 90 °C for 2h before cooling to room temperature. The volatiles were removed *in vacuo*. The residue was

purified by column chromatography on silica gel (25 mm x 200 mm, CH_2Cl_2/hexanes 1:6 to 1:5 to 1:2) to afford the product as a red solid (101 mg, 87%)

^{1}H NMR ($CDCl_3$, 500 MHz) δ 9.05 (d, *J* = 8.5 Hz, 1H), 8.99 (d, *J* = 8.5 Hz, 1H), 8.87 (s, 1H), 8.09 (d, *J* = 8.0 Hz, 1H), 7.82 (t, *J* = 7.5 Hz, 1H), 7.74-7.64 (m, 5H), 7.60-7.52 (m, 6H), 7.43 (t, *J* = 7.5 Hz, 1H), 7.35-7.32 (m, 2H), 7.28-7.22 (m, 2H), 7.21-7.17 (m, 2H), 7.15-7.11 (m, 2H), 6.55 (d, *J* = 7.0 Hz, 1H). ^{13}C NMR (THF-*d*8, 125 MHz) δ 139.5, 138.6, 138.4, 137.3, 137.1, 137.1, 135.0, 134.8, 134.4, 134.3, 133.5, 132.9, 132.5, 132.5, 132.5, 130.7, 130.2, 130.2, 129.5, 129.2, 129.2, 129.0, 128.8, 128.8, 128.4, 127.7, 127.5, 127.3, 127.2, 125.6, 124.8, 124.6, 124.4, 122.5, 121.0, 119.0, 106.1, 98.1, 91.0, 88.7. HRMS (EI) cacld for $C_{46}H_{26}$ [M^+] *m*/*z* 578.2035, found [M^+] 578.2061. IR (neat, cm^{-1}) 3052, 2197, 1595, 1440, 1428, 1405.

Synthesis of 1,4-diiodoanthracene-9,10-dione ***3.37***

To a 500 mL flame-dried round bottom flask were added dibromide (2.928 g, 8.0 mmol), CuI (15.24 g, 80 mmol), KI (39.84 g, 240 mmol) and dry 1,3-dimethyl-2-imidazolidinone (32 mL) under N_2. The mixture was stirred at 150 °C overnight under N_2 protection. After cooling to room temperature, CH_2Cl_2 (160 mL) and brine (80 mL) was added to the mixture. After filtration *via* a Buchner funnel, the organic layer was separated, dried over $MgSO_4$ and concentrated *in vacuo*. The residue was purified by column chromatography on silica gel (40 mm x 250 mm, CH_2Cl_2/hexanes 1:3 to 1:2 to 1:1 to 2:1). The resulting solid was

washed with hexanes to remove remaining DMI to afford the product as a yellow solid (2.23 g, 61%).

^{1}H NMR ($CDCl_3$, 500 MHz) δ 8.26 (dd, *J* = 6.0, 3.0 Hz, 2H), 7.99 (s, 2H), 7.80 (dd, *J* = 6.0, 3.0 Hz, 2H). ^{13}C NMR ($CDCl_3$, 125 MHz) δ 181.0, 147.9, 134.5, 134.3, 133.1, 127.1, 94.0.

Synthesis of 1,4-bis(phenylethynyl)anthracene-9,10-dione ***3.37'***

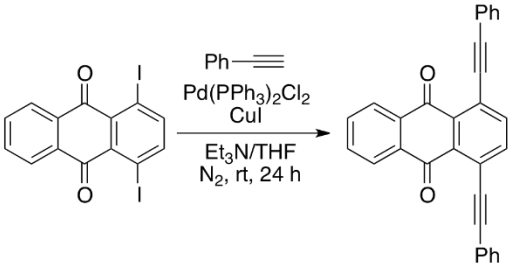

To a 250 mL flame-dried round bottom flask were added diiodide (2.30 g, 5.0 mmol), $Pd(PPh_3)_2Cl_2$ (176 mg, 0.25 mmol), CuI (48 mg, 0.25 mmol), dry THF (100 mL), dry Et_3N (25 mL) and phenylacetylene (1.32 mL, 12 mmol) under N_2. The mixture was stirred at room temperature for 24 h under N_2 protection. The volatiles were removed *in vacuo*. The residue was purified by column chromatography (1st column on silica gel, 40 mm × 250 mm, CH_2Cl_2/hexanes 1:2 to 1:1; 2nd column on neutral Al_2O_3, 40 mm × 150 mm, CH_2Cl_2/hexanes 1:1) to afford the product as a yellow solid (1.49 g, 73%).

^{1}H NMR ($CDCl_3$, 500 MHz) δ 8.33 (dd, *J* = 6.0, 3.0 Hz, 2H), 7.91 (s, 2H), 7.80 (dd, *J* = 6.0, 3.0 Hz, 2H), 7.74-7.72 (m, 4H), 7.44-7.40 (m, 6H). ^{13}C NMR ($CDCl_3$, 125 MHz) δ 181.9, 138.7, 134.4, 133.9, 133.3, 132.2, 129.0, 128.4, 127.1, 123.4, 123.1, 97.5, 89.5.

Synthesis of 1,4,9,10-tetrakis(phenylethynyl)anthracene ***3.32a***

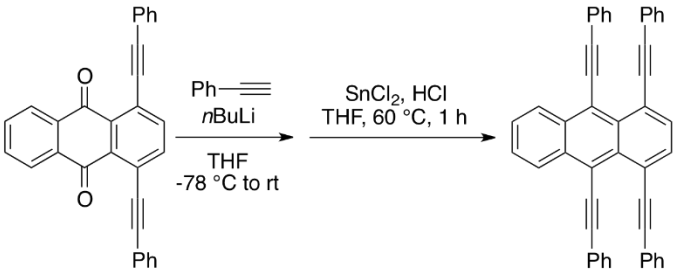

To a 50 mL flame-dried round bottom flask were added phenylacetylene (0.34 mL, 3.1 mmol), and dry THF (6 mL) under N_2. The mixture was cooled to -78 °C and *n*BuLi (2.5 M in hexanes, 1.2 mL, 3.0 mmol) was added dropwise. The resulting mixture was stirred at -78 °C for 1h before the addition of quinone (241 mg, 0.59 mmol) all at once. The mixture was allowed to warm up to room temperature and stirred overnight. NH_4Cl (sat. aq. 6 mL) was added to the mixture. The volatiles were removed *in vacuo*. The residue was partitioned between CH_2Cl_2 (12 mL) and H_2O (6 mL). The organic layer was separated, dried over $MgSO_4$ and concentrated *in vacuo*. The residue was purified by column chromatography on silica gel (20 mm x 250 mm, CH_2Cl_2/hexanes 1:1 to 2:1 to 4:1) to afford the diols (249 mg, 0.407 mmol) that were used in the next step.

To the 50 mL round bottom flask containing the purified diols (249 mg, 0.407 mmol) was added THF (5 mL). A solution of $SnCl_2$ (1.88 g, 3.3 mmol) in 6M HCl (5 mL) was added to the above mixture. The resulting mixture was stirred at 60 °C for 1h before cooling to room temperature. H_2O (66 mL) was added to the mixture. After filtration, the crude product was dissolved in CH_2Cl_2, dried over $MgSO_4$ and concentrated *in vacuo*. The residue was purified by column chromatography on silica gel (20 mm x 250 mm, CH_2Cl_2/hexanes 1:10 to 1:8 to 1:4) to afford the product as a dark red solid (188 mg, 55% over two steps)

^{1}H NMR ($CDCl_3$, 500 MHz) δ 8.86 (dd, *J* = 6.5, 3.0 Hz, 2H), 7.88 (s, 2H), 7.69 (dd, *J* = 6.5, 3.0 Hz, 2H), 7.54-7.52 (m, 4H), 7.38-7.36 (m, 4H), 7.28-7.13 (m, 12H). ^{13}C NMR ($CDCl_3$, 125 MHz) δ 134.4, 133.5, 131.6, 131.5, 130.9, 128.3, 128.1, 128.0, 127.9, 127.6, 127.4, 123.7, 123.6, 122.1, 119.1, 107.4, 99.9, 90.9, 88.2. IR (neat, cm^{-1}) 3052, 2927, 2190, 1595, 1441, 1399. LRMS (LDI) cacld for $C_{46}H_{26}$ [M^+] *m*/*z* 578.2, found [M^+] 578.1.

Procedure IV: General synthetic procedures for one-pot Sonogashira cross-coupling

The reactions were performed in a N_2-filled glovebox following the general procedure described below. To a 4-mL reaction vial was added dibromide substrate 0.1 mmol, $Pd(PPh_3)_2Cl_2$ (2.8 mg, 0.004 mmol), AgOAc (0.7 mg, 0.004 mmol), phenylacetylene (25 mg, 0.24 mmol), freshly distilled THF (2 mL) and Et_3N (1 mL). The vial was then sealed and heated to 90 °C for 12 hours before cooling to room temperature. The crude solution was mixed with 10 mL of methanol and was sonicated for 2 minutes. The resulting mixture was then proceeded to a vacuum filtration and washed with methanol (10 mL × 2) and diethyl ether (5 mL × 2). The product was collected as dark red solid with good purity. Further purification methods such as recrystallization and column chromatography were not applied unless otherwise noted.

Synthesis of 13-methyl-9-phenyl-6-(phenylethynyl)-5-(o-tolylethynyl)naphtho[2,3-a]aceanthrylene ***3.33b***

Prepared from 0.1 mmol of dibromide according to Procedure IV, the desired product was obtained as a red solid (92%).

^{13}C NMR ($CDCl_3$, 100 MHz) δ 140.3, 138.8, 137.6, 136.7, 136.5, 136.1, 135.2, 133.8, 133.8, 132.6, 132.3, 132.1, 131.5, 129.8, 129.4, 129.2, 129.1, 128.5, 128.4, 128.3, 128.1,

127.8, 127.8, 127.5, 126.6, 125.9, 125.4, 125.4, 124.4, 123.7, 123.7, 121.7, 120.3, 120.1, 119.2, 118.5, 104.1, 97.4, 91.4, 90.5, 21.1, 20.2. IR (neat, cm^{-1}) 3054, 2920, 1595, 1489, 1440. LRMS (LDI) cacld for $C_{48}H_{30}$ [M^+] *m*/*z* 606.2, found [M^+] 606.1.

Synthesis of 11-methyl-9-phenyl-6-(phenylethynyl)-5-(p-tolylethynyl)naphtho[2,3-a]aceanthrylene ***3.33c***

Prepared from 0.1 mmol of dibromide according to Procedure IV, the desired product was obtained as a red solid (95%).

^{1}H NMR ($CDCl_3$, 400 MHz) δ 8.98 (d, *J* = 9.2 Hz, 1H), 8.95 (d, *J* = 9.2 Hz, 1H), 8.76 (s, 1H), 7.94 (d, *J* = 8.4 Hz, 1H), 7.79−7.73 (m, 1H), 7.71−7.61 (m, 5H), 7.51 (dd, J_1 = 7.6 Hz, J_2 = 1.2 Hz, 2H), 7.41 (d, *J* = 8.0 Hz, 2H), 7.39−7.30 (m, 4H), 7.20 (d, *J* = 7.6 Hz, 1H), 7.19−7.11 (m, 2H), 7.00 (d, *J* = 8.0 Hz, 2H), 6.47 (d, *J* = 7.2 Hz, 1H), 2.44 (s, 3H), 2.34 (s, 3H). ^{13}C NMR ($CDCl_3$, 100 MHz) δ 138.6, 138.4, 137.7, 137.0, 136.5, 136.3, 136.1, 135.48, 134.3, 133.6, 132.6, 131.8, 131.8, 131.7, 131.7, 129.9, 129.3, 129.0, 128.9, 128.8, 128.5, 128.2, 128.0, 127.9, 127.7, 127.6, 127.6, 126.5, 125.9, 124.5, 123.9, 122.9, 121.6, 120.6, 119.9, 118.1, 105.3, 97.0, 90.5, 87.5, 22.0, 21.5. IR (neat, cm^{-1}) 3048, 2916, 1596, 1509, 1491, 1441, 1403, 1364. LRMS (LDI) cacld for $C_{48}H_{30}$ [M^+] *m*/*z* 606.2, found [M^+] 606.1.

Synthesis of 11-butyl-5-((4-butylphenyl)ethynyl)-9-phenyl-6-(phenylethynyl)naphtho[2,3-a]aceanthrylene ***3.33d***

Prepared from 0.1 mmol of dibromide according to Procedure IV, the desired product was obtained as a red solid (98%).

^{1}H NMR ($CDCl_3$, 400 MHz) δ 9.02 (d, *J* = 8.8 Hz, 1H), 8.97 (d, *J* = 8.4 Hz, 1H), 8.81 (s, 1H), 7.99 (d, *J* = 8.4 Hz, 1H), 7.79 (dd, J_1 = 8.0 Hz, J_2 = 6.8 Hz, 1H), 7.73−7.61 (m, 4H),

7.53 (dd, J_1 = 8.0 Hz, J_2 = 1.2 Hz, 2H), 7.49−7.30 (m, 7H), 7.23−7.17 (m, 1H), 7.15−7.10 (m, 1H), 7.00 (d, J = 8.0 Hz, 2H), 6.49 (d, J = 8.0H Hz, 1H), 2.69 (t, J_1 = J_2 = 8.0 Hz, 2H), 2.59 (t, J_1 = J_2 = 8.0 Hz, 2H), 1.69−1.48 (m, 4H), 1.36 (sext, J = 7.2 Hz, 4H), 0.96 (t, J_1 = J_2 = 7.6 Hz, 3H), 0.91 (t, J_1 = J_2 = 7.6 Hz, 3H). ^{13}C NMR ($CDCl_3$, 100 MHz) δ 143.4, 141.3, 138.6, 137.8, 137.0, 136.5, 136.1, 135.7, 135.3, 135.1, 134.3, 133.6, 132.6, 132.1, 131.9, 131.7, 131.7, 129.9, 129.3, 129.1, 128.9, 128.2, 128.0, 127.9, 127.8, 127.6, 127.6, 126.5, 125.4, 124.5, 123.9, 122.9, 121.6, 120.8, 119.9, 97.0, 96.3, 90.4, 87.5, 36.0, 35.6, 33.6, 33.5, 22.4, 22.3, 14.0, 13.9. IR (neat, cm^{-1}) 3050, 2955, 2925, 2854, 1440. LRMS (LDI) cacld for $C_{54}H_{42}$ [M^+] *m*/*z* 690.3, found [M^+] 690.2.

Synthesis of 11-(tert-butyl)-5-((4-(tert-butyl)phenyl)ethynyl)-9-phenyl-6-(phenylethynyl)naphtho[2,3-a]aceanthrylene ***3.33e***

Prepared from 0.1 mmol of dibromide according to Procedure IV, the desired product was obtained as a red solid (98%).

1H NMR ($CDCl_3$, 400 MHz) δ 9.04 (d, J = 8.6 Hz, 1H), 8.97 (d, J = 8.9 Hz, 1H), 8.82 (s, 1H), 8.02 (d, J = 8.6 Hz, 1H), 7.82 (d, J = 1.3 Hz, 1H), 7.72 – 7.60 (m, 7H), 7.56 – 7.51 (m, 2H), 7.49 – 7.45 (m, 2H), 7.32 – 7.28 (m, 2H), 7.23 – 7.15 (m, 3H), 7.11 – 7.06 (m, 2H), 6.54 (d, J = 7.3 Hz, 1H), 1.31 (s, 18H). ^{13}C NMR ($CDCl_3$, 100 MHz) δ 156.5, 151.5, 149.2, 138.5, 137.8, 137.3, 136.5, 136.2, 136.1, 134.2, 133.6, 132.4, 131.9, 131.8, 131.7, 131.5, 129.8, 129.2, 129.0, 128.8, 128.2, 128.0, 127.8, 127.7, 127.6, 126.5, 125.1, 125.1, 124.6, 123.9, 122.7, 122.1, 121.6, 120.7, 119.9, 119.7, 118.2, 105.2, 97.0, 90.4, 35.0, 34.8, 31.2, 31.1. IR (neat, cm^{-1}) 3055, 2959, 2865, 1491, 1361. LRMS (LDI) cacld for $C_{54}H_{42}$ [M^+] *m*/*z* 690.3, found [M^+] 690.2.

Synthesis of 5-((3,5-dimethylphenyl)ethynyl)-10,12-dimethyl-9-phenyl-6-(phenylethynyl)-naphtho[2,3-a]aceanthrylene ***3.33f***

^{1}H NMR ($CDCl_3$, 400 MHz) δ 9.03–8.95 (m, 2H), 8.76 (s, 1H), 7.82–7.67 (m, 3H), 7.58 (m, 6H), 7.39 (dd, *J* = 8.2, 1.3 Hz, 2H), 7.24−7.22 (m, 1H), 7.19–7.13 (m, 4H), 7.07 (s, 1H), 6.89 (s, 1H), 6.01 (d, *J* = 7.4 Hz, 1H), 2.51 (s, 3H), 2.13 (s, 6H), 2.07 (s, 3H). ^{13}C NMR ($CDCl_3$, 100 MHz) δ 142.6, 138.4, 137.6, 136.9, 136.8, 136.7, 136.5, 136.0, 135.7, 135.4, 135.1, 133.7, 132.9, 131.7, 131.3, 130.2, 129.9, 129.5, 128.8, 128.8, 128.6, 128.4, 128.2, 128.1, 127.9, 127.8, 127.5, 127.5, 126.4, 124.5, 124.0, 123.9, 123.2, 121.8, 119.6, 118.1, 105.6, 96.9, 90.5, 87.5, 25.2, 21.2, 21.0. IR (neat, cm^{-1}) 3024, 2914, 2863, 1596, 1442. LRMS (LDI) cacld for $C_{50}H_{34}$ [M^+] *m*/*z* 634.3, found [M^+] 634.1.

Synthesis of 11-methoxy-5-((4-methoxyphenyl)ethynyl)-9-phenyl-6-(phenylethynyl)naphtho[2,3-a]aceanthrylene ***3.33g***

Prepared from 0.1 mmol of dibromide according to Procedure IV, the desired product was obtained as a dark red solid (quantitative yield).

^{1}H NMR ($CDCl_3$, 400 MHz) δ 8.96 (d, *J* = 8.0 Hz, 1H), 8.94 (d, *J* = 8.0 Hz, 1H), 8.74 (s, 1H), 7.95 (d, *J* = 8.8 Hz, 1H), 7.76 (dd, J_1 = 7.6 Hz, J_2 = 7.2 Hz, 1H), 7.70−7.58 (m, 5H), 7.45 (d, *J* = 8.8 Hz), 7.36 (dd, J_1 = 7.2 Hz, J_2 = 1.2 Hz, 2H), 7.24−7.13 (m, 4H), 3.80 (s, 3H), 3.74 (s, 3H). ^{13}C NMR ($CDCl_3$, 100 MHz) δ 159.6, 158.2, 138.5, 137.7, 136.4, 135.8, 135.0, 134.7, 133.7, 133.3, 133.2, 131.8, 131.7, 130.6, 129.8, 129.4, 128.9, 128.9, 128.1, 123.0, 128.0, 127.8, 127.6, 127.5, 126.4, 124.5, 123.9, 122.9, 121.7, 120.0, 118.0, 117.9, 113.7, 106.2, 105.1, 97.0, 90.5, 87.0, 55.3, 55.1. IR (neat, cm^{-1}) 3058, 2950, 2926, 2830,

1614, 1604, 1507, 1462, 1430. LRMS (LDI) cacld for $C_{48}H_{30}O_2$ [M^+] *m*/*z* 638.2, found [M^+] 638.1.

Synthesis of 11-butoxy-5-((4-butoxyphenyl)ethynyl)-9-phenyl-6-(phenylethynyl)-naphtho[2,3-a]aceanthrylene ***3.33h***

Prepared from 0.1 mmol of dibromide according to Procedure IV, the desired product was obtained as a red solid (quantitative yield).

^{1}H NMR ($CDCl_3$, 400 MHz) δ 8.91 (d, *J* = 8.8 Hz, 1H), 8.91 (d, *J* = 8.4 Hz, 1H), 8.67 (s, 1H), 7.91 (d, *J* = 8.8 Hz, 1H), 7.72 (dd, J_1 = 8.4 Hz, J_2 = 6.8 Hz, 1H), 7.69−7.58 (m, 5H), 7.50 (dd, J_1 = 7.2 Hz, J_2 = 1.2 Hz, 2H), 7.43 (d, *J* = 8.8 Hz, 2H), 7.37 (dd, J_1 = 7.2 Hz, J_2 = 1.2 Hz, 2H), 7.22 (d, *J* = 7.2 Hz, 1H), 7.20−7.12 (m, 3H), 6.85 (d, *J* = 2.0 Hz, 1H), 6.69 (d, *J* = 8.8 Hz, 2H), 6.46 (d, *J* = 7.2 Hz, 1H), 3.94 (t, J_1 = J_2 = 6.4 Hz, 2H), 3.88 (t, J_1 = J_2 = 6.4 Hz, 2H), 1.84−1.68 (m, 4H), 1.57−1.40 (m, 4H), 1.00 (t, J_1 = J_2 = 7.2 Hz, 3H), 0.96 (t, J_1 = J_2 = 7.2 Hz, 3H). ^{13}C NMR ($CDCl_3$, 100 MHz) δ 159.3, 157.7, 138.6, 137.7, 136.4, 136.1, 135.7, 134.9, 134.7, 133.8, 133.3, 133.2, 131.8, 131.7, 130.6, 129.8, 129.4, 128.9, 128.8, 128.1, 128.1, 128.0, 127.8, 127.5, 127.4, 126.4, 124.5, 124.0, 122.9, 121.6, 120.0, 118.2, 118.0, 115.7, 114.3, 107.1, 105.2, 97.0, 90.6, 86.9, 67.8, 67.6, 31.3, 31.2, 19.3, 19.2, 13.9, 13.9. IR (neat, cm^{-1}) 3056, 2953, 2927, 2871, 2189, 1603, 1491, 1440, 1244, 1218.

Synthesis of 9-phenyl-6-(phenylethynyl)-11-(trifluoromethyl)-5-((4-(trifluoromethyl)-phenyl)ethynyl)naphtho-[2,3-a]aceanthrylene ***3.33i***

Prepared from 0.1 mmol of dibromide according to Procedure IV, the desired product was obtained as a red solid (72%).

^{1}H NMR ($CDCl_3$, 500 MHz) δ 8.99 (d, J = 8.6 Hz, 1H), 8.91 (d, J = 8.7 Hz, 1H), 8.86 (s, 1H), 8.16 (d, J = 8.5 Hz, 1H), 7.88 (s, 1H), 7.83 (t, J = 7.1 Hz, 1H), 7.75 – 7.69 (m, 6H), 7.58 (d, J = 8.1 Hz, 2H), 7.53 (dd, J = 7.2, 2.1 Hz, 2H), 7.40 (d, J = 8.2 Hz, 2H), 7.33 – 7.30 (m, 2H), 7.25 (t, J = 7.5 Hz, 1H), 7.15 (t, J = 7.6 Hz, 2H), 6.56 (d, J = 7.3 Hz, 1H). LRMS (LDI) cacld for $C_{48}H_{24}F_6$ [M^+] *m/z* 714.2, found [M^+] 714.1.

Synthesis of 9-phenyl-6-(phenylethynyl)-5-(thiophen-2-ylethynyl)benzo[5,6]-fluoranthe no[8,9-b]thiophene ***3.33l***

Prepared from 0.1 mmol of dibromide according to Procedure IV, the desired product was obtained as a red solid (96%).

^{1}H NMR ($CDCl_3$, 500 MHz) δ 8.91−8.87 (m, 3H), 7.79–7.75 (m, 1H), 7.70 – 7.66 (m, 2H), 7.64–7.57 (m, 5H), 7.43–7.39 (m, 3H), 7.25–7.18 (m, 4H), 7.11 (dd, J = 3.6, 1.0 Hz, 1H), 7.07 (d, J = 5.4 Hz, 1H), 6.88 (dd, J = 5.4, 3.6 Hz, 1H), 6.80 (d, J = 7.3 Hz, 1H). LRMS (LDI) cacld for $C_{42}H_{22}S_2$ [M^+] *m/z* 590.1, found [M^+] 590.0.

Synthesis of 5-(cyclohex-1-en-1-ylethynyl)-9-phenyl-6-(phenylethynyl)-10,11,12,13-tetrahydronaphtho[2,3-a]aceanthrylene ***3.33j***

Prepared from 0.1 mmol of dibromide according to Procedure IV, the desired product was obtained as a red solid (98%).

^{1}H NMR ($CDCl_3$, 400 MHz) δ 8.80 (dd, J = 8.6, 4.5 Hz, 2H), 8.10 (s, 1H), 7.69 (ddd, J = 8.5, 6.6, 1.3 Hz, 1H), 7.63 – 7.54 (m, 6H), 7.54 – 7.49 (m, 1H), 7.39 – 7.29 (m, 5H), 6.31 (d, J = 7.2 Hz, 1H), 6.19 (tt, J = 4.1, 1.8 Hz, 1H), 3.05 (t, J = 6.3 Hz, 2H), 2.50 (t, J = 6.3 Hz, 2H), 2.25 – 2.16 (m, 2H), 2.00–1.93 (m, 2H), 1.91–1.83 (m, 2H), 1.83 – 1.73 (m, 2H), 1.53 – 1.44 (m, 4H). ^{13}C NMR ($CDCl_3$, 101 MHz) δ 139.8, 138.6, 137.9, 137.6, 137.4,

136.0, 135.9, 135.8, 134.5, 134.3, 131.8, 131.5, 130.8, 129.1, 129.0, 128.9, 128.6, 128.0, 127.9, 127.5, 127.5, 127.3, 126.1, 124.4, 124.3, 124.3, 122.0, 121.3, 120.0, 118.9, 107.1, 96.6, 90.5, 85.4, 31.0, 29.1, 27.9, 25.7, 23.4, 23.1, 22.2, 21.4.

LRMS (LDI) cacld for $C_{46}H_{34}$ [M^+] *m*/*z* 586.3, found [M^+] 586.2.

Synthesis of 9-phenyl-6-(phenylethynyl)-5-(thiophen-3-ylethynyl)benzo[1,2]fluoranthe no[8,9-b]thiophene ***3.33m***

Prepared from 0.1 mmol of dibromide according to Procedure IV, the desired product was obtained as a red solid (96%).

^{1}H NMR ($CDCl_3$, 400 MHz) δ 8.96−8.84 (m, 2H), 8.76 (s, 1H), 7.79−7.58 (m, 8H), 7.54 (d, *J* = 4.8 Hz, 1H), 7.48 (d, *J* = 4.8 Hz, 1H), 7.43−7.32 (m, 4H), 7.25−7.12 (m, 4H), 6.84 (d, *J* = 7.2 Hz, 1H). ^{13}C NMR ($CDCl_3$, 100 MHz) δ 140.92, 139.50, 138.03, 137.17, 136.18, 131.57, 130.03, 129.37, 129.02, 129.00, 128.86, 128.73, 128.34, 128.05, 127.96, 127.67, 126.47, 126.45, 125.17, 124.38, 123.80, 122.84, 121.73, 120.09, 118.30, 105.08, 100.16, 90.35, 87.44. Not all the carbon signals were observed due to low solubility. IR (neat, cm^{-1}) 3053, 1490, 1442, 1364. LRMS (LDI) cacld for $C_{42}H_{22}S_2$ [M^+] *m*/*z* 590.1, found [M^+] 590.0.

Synthesis of 5-(naphthalen-1-ylethynyl)-9-phenyl-6-(phenylethynyl)phenanthro[3,2-a]aceanthrylene ***3.33k***

Prepared from 0.1 mmol of dibromide according to Procedure IV, the desired product was obtained as a red solid (quantitative yield).

^{1}H NMR ($CDCl_3$, 400 MHz) δ 9.72 (s, 1H), 9.13 (d, *J* = 8.8 Hz, 1H), 9.09 (d, *J* = 8.8 Hz, 1H), 8.97 (d, 8.4 Hz, 1H), 8.66 (d, *J* = 8.8 Hz, 1H), 7.91 (d, *J* = 8.8 Hz, 1H), 7.89−7.74 (m, 5H), 7.73−7.62 (m, 7H), 7.58−7.44 (m, 5H), 7.27 (dd, J_1 = 8.0 Hz, J_2 = 7.6 Hz, 1H), 7.06 (d, *J* = 8.0 Hz, 2H), 7.00 (dd, $J_1 = J_2$ = 7.6 Hz, 1H), 6.84 (dd, J_1 = 8.0 Hz, J_2 = 7.6 Hz, 2H), 6.56 (d, *J* = 7.2 Hz, 1H). ^{13}C NMR ($CDCl_3$, 100 MHz) δ 138.8, 138.2, 137.4, 136.6, 136.5, 136.3, 134.9, 133.3, 133.2, 133.0, 132.2, 132.1, 131.3, 130.8, 130.8, 130.5, 130.1, 129.9, 129.3, 129.1, 128.8, 128.7, 128.6, 128.1, 128.1, 128.0, 127.7, 127.6, 127.5, 127.0, 126.9, 126.8, 126.7, 126.3, 125.1, 125.0, 124.5, 123.5, 122.9, 122.3, 121.4, 120.5, 118.6, 117.7, 103.4, 97.5, 92.5, 90.3. Not all the carbon signals were resolved. IR (neat, cm^{-1}) 3058, 1597, 1413. LRMS (LDI) cacld for $C_{54}H_{30}$ [M^+] *m*/*z* 678.2, found [M^+] 678.1.

Synthesis of 8,17-dimethyl-4,13-diphenyldibenzo[g,s]rubicene ***3.44b***

Prepared from 0.1 mmol of dibromide according to Procedure IV, the desired product was obtained as a red solid (70%).

^{1}H NMR ($CDCl_3$, 400 MHz) δ 8.97 (s, 2H), 8.71 (d, *J* = 8.8 Hz, 2H), 7.75−7.64 (m, 6H), 7.61−7.54 (m, 6H), 7.48 (d, *J* = 8.4 Hz, 2H), 7.41 (d, *J* =7.2 Hz, 2H), 7.36−7.28 (m, 2H), 6.69 (d, *J* = 7.2 Hz, 2H), 2.97 (s, 6H). IR (neat, cm^{-1}) 3034, 2920, 2850, 1441, 1373, 1329. LRMS (LDI) cacld for $C_{48}H_{30}$ [M^+] *m*/*z* 606.2, found [M^+] 606.1.

Synthesis of 6,15-dimethyl-4,13-diphenyldibenzo[g,s]rubicene ***3.44c***

Prepared from 0.1 mmol of dibromide according to Procedure IV, the desired product was obtained as a red solid (89%).

^{1}H NMR ($CDCl_3$, 400 MHz) δ 8.75 (s, 2H), 8.72 (d, *J* = 8.4 Hz, 2H), 7.95 (d, *J* = 8.4 Hz, 2H), 7.74−7.62 (m, 6H), 7.59−7.53 (m, 6H), 7.39−7.32 (m, 4H), 6.64 (d, *J* = 7.2 Hz, 2H). IR (neat, cm^{-1}) 3055, 3038, 2972, 2945, 2859, 1612, 1600, 1448, 1361, 1325, 1286. LRMS (LDI) cacld for $C_{48}H_{30}$ [M^+] *m*/*z* 606.2, found [M^+] 606.1.

Synthesis of 6,15-dibutyl-4,13-diphenyldibenzo[g,s]rubicene ***3.44d***

Prepared from 0.1 mmol of dibromide according to Procedure IV, the desired product was obtained as a purple solid (90%).

^{1}H NMR ($CDCl_3$, 400 MHz) δ 8.74 (s, 2H), 8.71 (d, *J* = 8.4 Hz, 2H), 7.96 (d, *J* = 8.4 Hz, 2H), 7.74−7.63 (m, 6H), 7.60−7.49 (m, 6H), 7.39 (dd, J_1 = 8.4 Hz, J_2 = 1.2 Hz, 2H), 7.33 (s, 2H), 6.64 (d, *J* = 7.2 Hz, 2H), 2.68 (t, *J* = 8.0 Hz, 4H), 1.66−1.56 (m, 4H), 1.36 (sext, *J* = 7.6 Hz, 4H), 0.91 (t, *J* = 7.2 Hz, 6H). IR (neat, cm^{-1}) 3052, 2954, 2923, 2869, 2855, 1614, 1450, 1359, 1328. LRMS (LDI) cacld for $C_{54}H_{42}$ [M^+] *m*/*z* 690.3, found [M^+] 690.1.

Synthesis of 6,15-di-tert-butyl-4,13-diphenyldibenzo[g,s]rubicene ***3.44e***

Prepared from 0.1 mmol of dibromide according to Procedure IV, the desired product was obtained as a red solid (86%).

^{1}H NMR ($CDCl_3$, 400 MHz) δ 8.74 (s, 2H), 8.72 (d, *J* = 8.4 Hz, 2H), 7.99 (d, *J* = 8.8 Hz, 2H), 7.72−7.51 (m, 16H), 6.69 (d, *J* = 6.8 Hz, 2H), 1.31 (s, 18H). IR (neat, cm^{-1}) 3048, 2961, 2867, 1611, 1463, 1367, 1325, 1288, 1251. LRMS (LDI) cacld for $C_{54}H_{42}$ [M^+] *m*/*z* 690.3, found [M^+] 690.1.

Synthesis of 5,7,14,16-tetramethyl-4,13-diphenyldibenzo[g,s]rubicene ***3.44f***

Prepared from 0.1 mmol of dibromide according to Procedure IV, the desired product was obtained as a red solid (89%).

^{1}H NMR ($CDCl_3$, 400 MHz) δ 8.68 (s, 2H), 8.64 (d, *J* = 8.8 Hz , 2H), 7.72 (s, 2H), 7.64−7.56 (m, 10H), 7.44 (dd, J_1 = 8.4 Hz, J_2 = 7.2 Hz, 2H), 7.05 (s, 2H), 6.16 (d, *J* = 6.8 Hz, 2H), 2.49 (s, 6H), 2.07 (s, 6H).

IR (neat, cm^{-1}) 3025, 2966, 2923, 2862, 1620, 1607, 1573, 1435, 1337, 1293. LRMS (LDI) cacld for $C_{50}H_{34}$ [M^+] *m*/*z* 634.3, found [M^+] 634.1.

Synthesis of 6,15-dibutoxy-4,13-diphenyldibenzo[g,s]rubicene ***3.44g***

Prepared from 0.1 mmol of dibromide according to Procedure IV, the desired product was obtained as a red solid (89%).

^{1}H NMR ($CDCl_3$, 400 MHz) δ 8.70 (s, 2H), 8.69 (d, J = 8.8 Hz, 3H), 7.94 (d, J = 8.8 Hz, 2H), 7.72 – 7.61 (m, 6H), 7.56 (dd, J = 8.2, 1.8 Hz, 4H), 7.53 – 7.48 (m, 2H), 7.19 (dd, J = 8.8, 2.5 Hz, 2H), 6.89 (d, J = 2.5 Hz, 2H), 6.65 (d, J = 6.9 Hz, 2H), 3.90 (t, J = 6.4 Hz, 4H), 1.78 – 1.70 (m, 4H), 1.51 – 1.41 (m, 4H), 0.95 (t, J = 7.4 Hz, 6H). HRMS (ESI) cacld for $C_{54}H_{42}O_2$ [M^+] *m*/*z* 722.3185, found [M^+] 722.3186.

Synthesis of 4,13-diphenyl-6,15-bis(trifluoromethyl)dibenzo[g,s]rubicene ***3.44h***

Prepared from 0.1 mmol of dibromide according to Procedure IV, the crude product was purified *via* column chromatography (3:1 Hexanes/CH_2Cl_2) to afford the desired product as a red solid (42%).

^{1}H NMR ($CDCl_3$, 400 MHz) δ 8.82 (s, 2H), 8.74 (d, *J* = 8.8 Hz, 2H), 8.14 (d, *J* = 8.4 Hz, 2H), 7.87 (s, 2H), 7.76−7.67 (m, 8H), 7.60 (dd, J_1 = 8.4 Hz, J_2 = 7.2 Hz, 2H), 7.59−7.53

(m, 4H), 6.74 (d, *J* = 6.8 Hz, 2H). ^{19}F NMR ($CDCl_3$, 471 MHz) δ -65.27. HRMS (GC/MS solid probe) cacld for $C_{48}H_{24}F_6$ [M^+] *m/z* 714.1782, found [M^+] 714.1747. IR (neat, cm^{-1}) 3064, 1625, 1585, 1437, 1424, 1382, 1333, 1311, 1271.

Synthesis of 4,12-diphenylrubiceno[6,5-b:13,12-b']dithiophene ***3.44k***

Prepared from 0.1 mmol of dibromide according to Procedure IV, the desired product was obtained as a dark red solid (97%).

^{1}H NMR ($CDCl_3$, 400 MHz) δ 8.81 (s, 2H), 8.61 (d, J = 8.4 Hz, 2H), 7.68 – 7.57 (m, 10H), 7.52 (dd, J = 8.4, 6.9 Hz, 2H), 7.39 (d, J = 5.5 Hz, 2H), 7.07 (d, J = 5.4 Hz, 2H), 6.93 (d, J = 6.9 Hz, 2H). LRMS (LDI) cacld for $C_{42}H_{22}S_2$ [M^+] *m/z* 590.1, found [M^+] 590.0.

Synthesis of 4,13-diphenyl-5,6,7,8,14,15,16,17-octahydrodibenzo[g,s]rubicene ***3.44j***

Prepared from 0.1 mmol of dibromide according to Procedure IV, the desired product was obtained as a red solid (83%).

^{1}H NMR ($CDCl_3$, 400 MHz) δ 8.50 (d, J = 8.5 Hz, 2H), 8.06 (s, 2H), 7.65 – 7.49 (m, 8H), 7.47 – 7.32 (m, 8H), 6.44 (d, J = 6.8 Hz, 2H), 3.04 (t, J = 6.2 Hz, 4H), 2.50 (t, J = 6.3 Hz, 4H), 1.91 – 1.75 (m, 8H). ^{13}C NMR ($CDCl_3$, 101 MHz) δ 140.1, 138.6, 138.4, 137.6, 137.1, 135.0, 134.2, 133.5, 132.6, 129.1, 129.0, 128.7, 127.4, 125.1, 123.9, 123.6, 122.4, 30.9, 28.0, 23.5, 23.1. LRMS (LDI) cacld for $C_{46}H_{34}$ [M^+] *m/z* 586.3, found [M^+] 586.1.

Chapter 4 Studies into the Synthesis of [12]Cyclacene

The Study of theoretically interesting molecules (TIM) and their unpredictable properties has been a long and meaningful pursuit for chemists over the past century. One unique family of TIM is the carbon-rich molecules that consist of spherical or tube-shaped 3D structures. The discovery of fullerene C_{60} and carbon nanotubes (CNT), as well as their application in electronic devices, have demonstrated that aromatic stabilization can overcome the destabilizing factors that arise from the curved molecular surface. As the structure segments of fullerenes and CNTs, molecular hoops and belts have also received extensive attention. The unconventional curved structures make them attractive targets for organic synthesis. More importantly, success in synthesis will enable property studies and potential applications in materials science.

4.1 Cyclacene: Chemical Structure, Computational Studies and Potential Material Properties

The chemical structure of cyclacene was first proposed by Heilbronner in 1954[86]. [n]Cyclacene is consist of n laterally fused benzenoid rings. Such a highly strained macrocycle has not been synthetically achieved to date. However, the intriguing conjugated framework has stimulated many theoretical studies on its aromaticity and electronic structure.

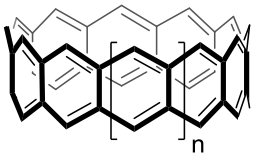

Figure 4-1 Chemical structure of [n]Cyclacene.

Although cyclacene shares the same structural unit (benzene) with acenes, however, their electronic structures are intrinsically different. As shown in **Figure 4-2**, the acene p orbitals align in a perpendicular relationship as to the molecular plane, while for cyclacene and other molecular belts in general, the orientation of the p orbitals is parallel to the molecular plane. This specific electron density distribution, plus the rigid, size-specific cavity feature, makes cyclacene a potential host molecule for host-guest chemistry.

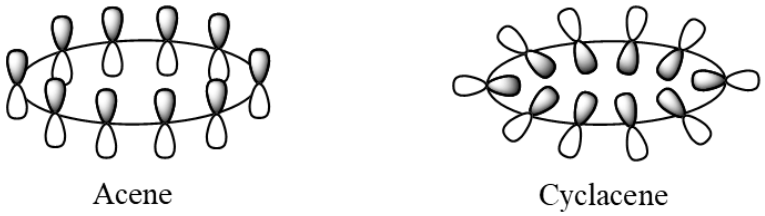

Figure 4-2 Different p-orbital alignments in acene and cyclacene.

The strain energy is an important issue when studying the synthesis of [n]cyclacenes. To quantify this synthetic challenge, Itami and co-workers have established a systematic calculation to the strain energy of carbon nanorings and carbon nanobelts[87]. By definition, carbon nanorings are macrocyclic structures that require cleavage of one bond to open the cyclic structure; while for carbon nanobelts, two or more bonds need to be cleaved to open the cycle. It was noted that [n]cyclacene is the most strained among the "monolayer" hoop-like structures. The less strained congeners, cyclophenacene isomer and cycloparaphenylene, have been synthesized in the past decade. In section **4.2**, the synthetic strategies applied in the successful synthesis of these carbon nanohoops will be discussed in detail.

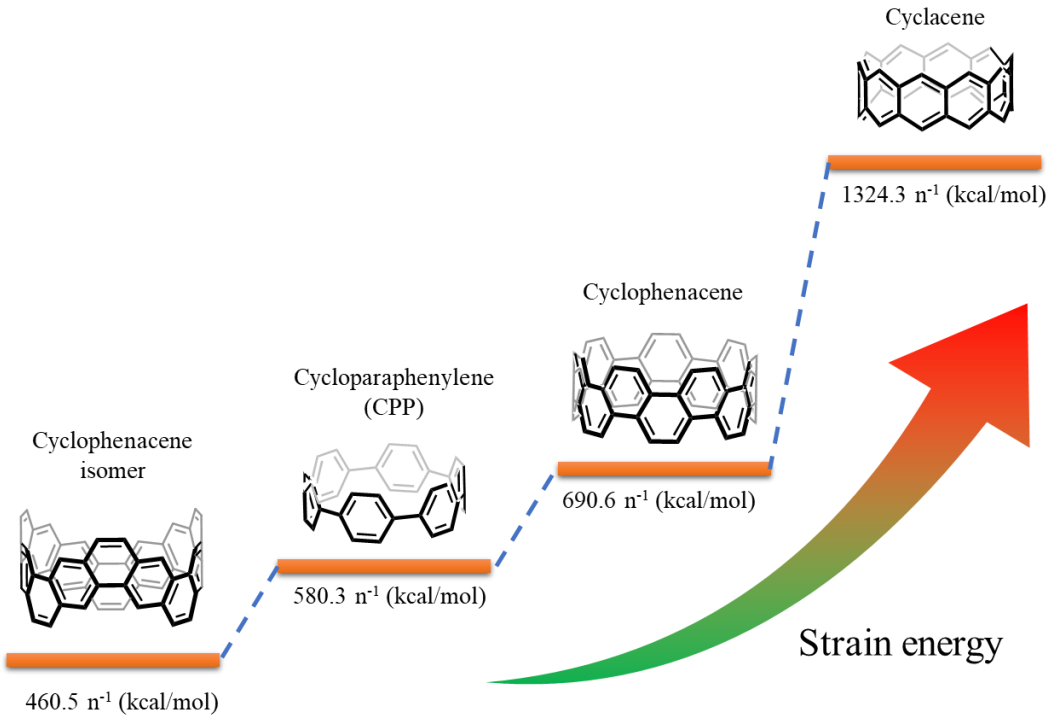

Figure 4-3 The strain diagram of carbon nanobelts and carbon nanorings.

Besides the strain energy, computational chemists have also attempted to predict the stability of cyclacene. Houk and coworkers have applied an unrestricted, broken spin-symmetry (UBS) wavefunction for DFT and ab inito calculations to probe the lowest energy ground state. The results predict that for cyclacenes with size equal or larger than six benzenoid rings ($n \geq 6$), the lowest energy ground state configuration will be an open-shell singlet[88]. This means that cyclacene would exhibit diradical character, which is susceptible to photo-oxidation and other decomposition pathways. The unstable diradical character could potentially explain why cyclacene synthesis is so challenging, as this is the same issue facing longer linear acenes. This is also a reminder that when designing a synthetic route to cyclacenes, suitable protecting groups will be necessary to stabilize the highly reactive ground state.

Although cyclacene and other molecular hoops are not naturally occurring, insights into their potential properties and applications were gained upon the discovery of CNTs in the 1990s[89]. The extraordinary optoelectronic properties of CNTs, along with their potential applications in nanoelectronics and photonics have been well established[90]. **Figure 4-4** showed two common types of carbon nanotubes, the armchair CNT and the zigzag CNT. Most hoop-shaped molecules can be found as monolayer units of their parent carbon nanotubes. For example, cycloparaphenylene (CPP) and cyclophenacene can be found in armchair CNTs, whereas cyclacene serves as the monolayer structure on the zigzag CNT. Interestingly, the property of CNTs vary drastically on the chirality. The armchair CNT show metallic properties whereas the zigzag CNT are semiconductive[91]. Along with chirality, the size and diameter of the CNT can also affect the properties. However, to specifically isolate or synthesize CNTs with well-defined diameter and chirality is very challenging. Therefore, the detailed study of the CNT structure–property relationship is difficult. To this end, developing the chemical synthesis of size-specific molecular hoops becomes a worthy objective in that the monolayer structures could serve as models for further material discovery and systematic property studies.

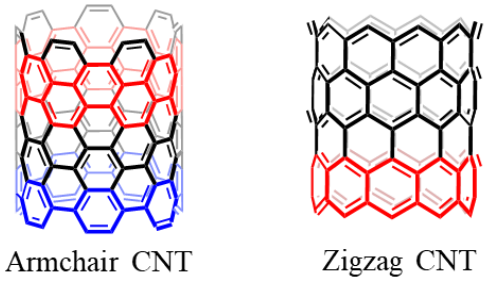

Figure 4-4 Armchair CNT and zigzag CNT.

4.2 Literature Precedence for Carbon Nanohoop Synthesis and Notable Synthetic Attempts toward [n]Cyclacenes

4.2.1 General Synthetic Approach and Examples of Successful Synthesis

Although the molecular belts are structurally simple, the high-level strain energy due to the bending of benzenoid rings in the conjugated system renders the synthesis rather challenging. The key step in the general synthesis is the construction of macrocycle, which usually contains a high level of ring strain. Such a macrocyclic structure normally requires the assembly of synthons that are not strained, possess suitable built-in curvature or both. The fashion of macrocycle formation can be one-pot, if the chemical transformation involved is highly efficient and stereo-selective, or step-wise where the advanced intermediates need to be isolated for identification of absolute molecular shape. Upon achieving the macrocycle, late-stage functionalization is usually applied to afford the fully conjugated or aromatized framework.

In 2008, Jasti and Bertozzi reported the first successful synthesis of carbon nanorings – [n]cycloparaphenylenes. The key intermediate used in this synthetic approach was 1,4-*syn*-dimethoxy-2,5-cyclohexadienes. The cyclohexadiene moiety was applied as masked benzene rings, which could be aromatized upon reduction. The *syn* configuration was appropriate for curvature build-up during the one-pot Suzuki−Miyuara cross-coupling/macrocyclization. As a result, macrocycles of varied size were obtained in the one-pot transformation, which can be isolated and separated from each other. In the final step, lithium naphthalenide was applied to reveal the fully conjugated molecular carbon

nanorings. Following this strategy, CPPs with ring size of 5−12 benzenes have been prepared[92].

In 2009, a similar approach to a size-specific [12]CPP was reported by the Itami group[93]. They utilized 1,4-*syn*-diarylcyclohexane as the curved synthon for the macrocycle synthesis. Different with Jasti and Bertozzi's synthon, the cyclohexane moiety is the reduced version of benzene. Upon achieving the macrocycle *via* Suzuki−Miyaura cross-coupling reactions, the cyclohexane containing macrocycle was aromatized to afford [12]CPP in good yields.

Another interesting synthesis was developed by the Yamago group later in 2009. In the synthetic efforts to [8]CPP, Yamago and co-workers adopted a template-assisted approach, in which a square-shaped tetranuclear platinum complex was used as the CPP precursor. Unlike Jasti/Bertozzi's and Itami's method, this route did not involve an aromatization process as the metal-complex macrocycle underwent reductive elimination to give the desired [8]CPP. This method has been used to access [6]CPP and [8]−[13]CPP in few steps and high yields[94].

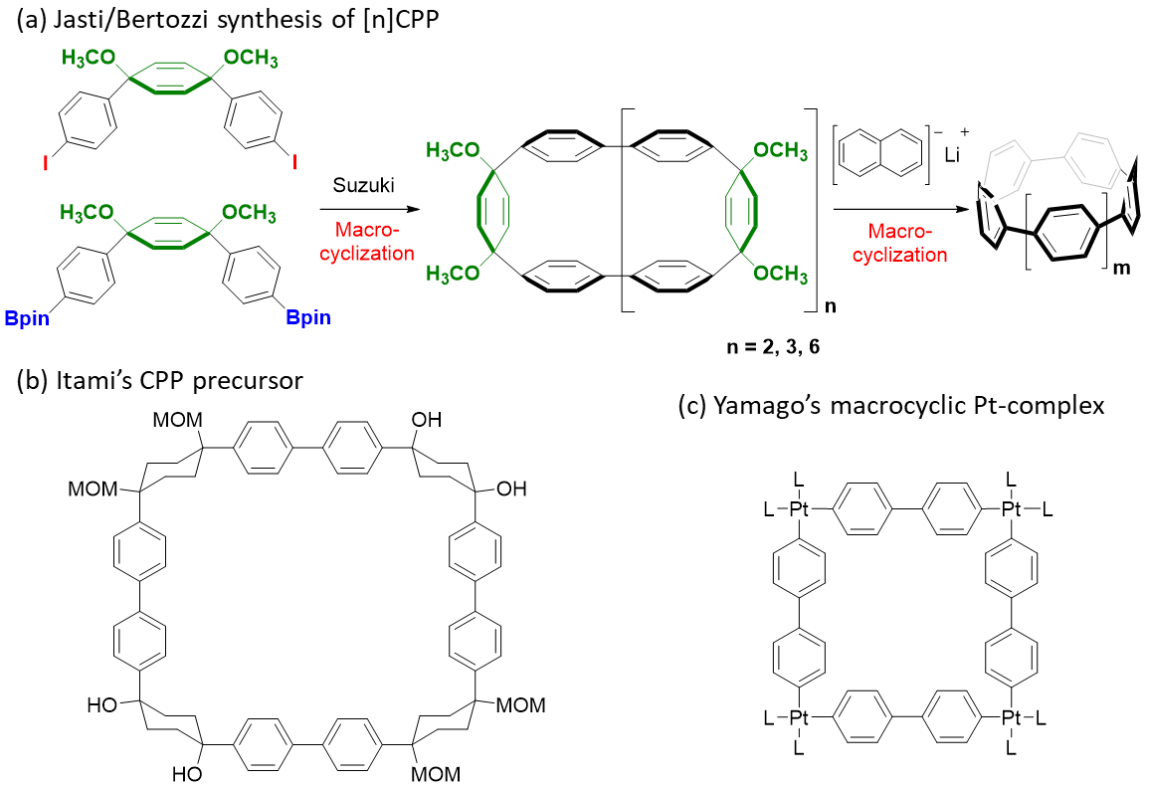

Figure 4-5 Synthetic efforts toward [n]CPPs.

Since the initial synthesis of carbon nanorings in 2008, the chemical synthesis and material studies of cycloparaphenylenes have emerged rapidly in the past decade. However, very few reports were found to advance the study towards the structurally more strained carbon nanobelts. Until 2017, the first and only report of nanobelt synthesis was published by the Itami group, in which a bottom-up synthesis and isolation of a cyclophenacene isomer was achieved (**Figure 4-6**). In this work, the precursor for macrocyclization featured a bifunctional Wittig moiety, which was turned into a macrocycle through cyclodimerization. The macrocycle contained six 1,4-dibromobenzene units and vinyl groups in between every two adjacent phenyl groups. In the final step, a six-fold aryl-aryl coupling reaction afforded the nanobelt structure in one-pot in 1% isolated yield. This is another example where post-macrocycle-aromatization was not involved.

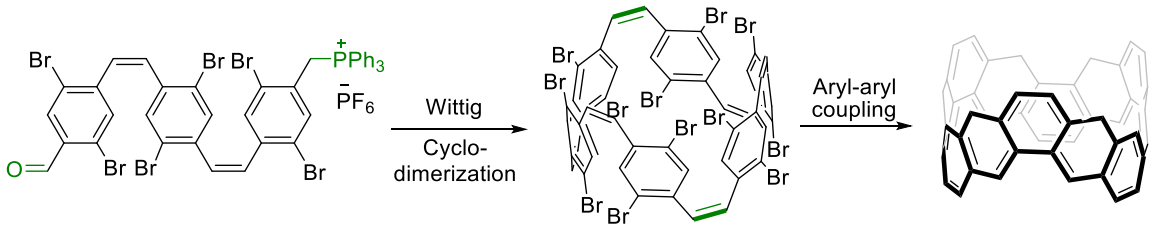

Figure 4-6 Itami's synthesis of a cyclophenacene isomer.

4.2.2 Summary of Previous Synthetic Attempts to Cyclacene

In late 1980s, Stoddart *et al.* attempted the synthesis towards [12]cyclacene. Although the synthesis was not successful in the end, significant progress was made during the study, which provided valuable guidance for future studies. Specifically, their strategy focused on utilizing the stereoselective Diels−Alder cycloaddition to construct fused benzenoid structures in a stepwise manner; curvature was also induced gradually by stepwise installation of curved units; an incredible size-specific macrocycle was achieved, however, late-stage functionalization proved to be difficult in that the extra hydrogen and oxygen-containing groups could not be removed to afford the fully conjugated structure. Detailed in **Scheme 4-1**, a suitable pair of bisdienophile **4.1** and bisdiene **4.2** was first identified and utilized. Under thermal conditions, bisdienophile **4.1** and bisdiene **4.2** could undergo a stereoselective Diels−Alder cycloaddtion to yield the mono-cycloadduct **4.3**. It was noted that the rate of monoadduct formation is significantly faster than double-adduct, which allowed the isolation of **4.3**. In theory, the bifunctionalized intermediate **4.3** could proceed to form the macrocycle **4.5** in either a cyclodimerization manner or a stepwise pathway. Yet in reality, intermediate **4.3** was noted to readily polymerize and only give the macrocycle in 3.5% yield. To circumvent this issue, intermediate **4.3** was first turned into the bisdiene **4.4**, followed by the macrocyclization with bisdienophile **4.1**. Under high

pressure conditions, a 12-membered macrocyclic framework **4.5** was achieved. However, further efforts to advance the macrocycle **4.5** to [12]cyclacene were not successful. Deoxygenation and oxidation proved to be extremely challenging.

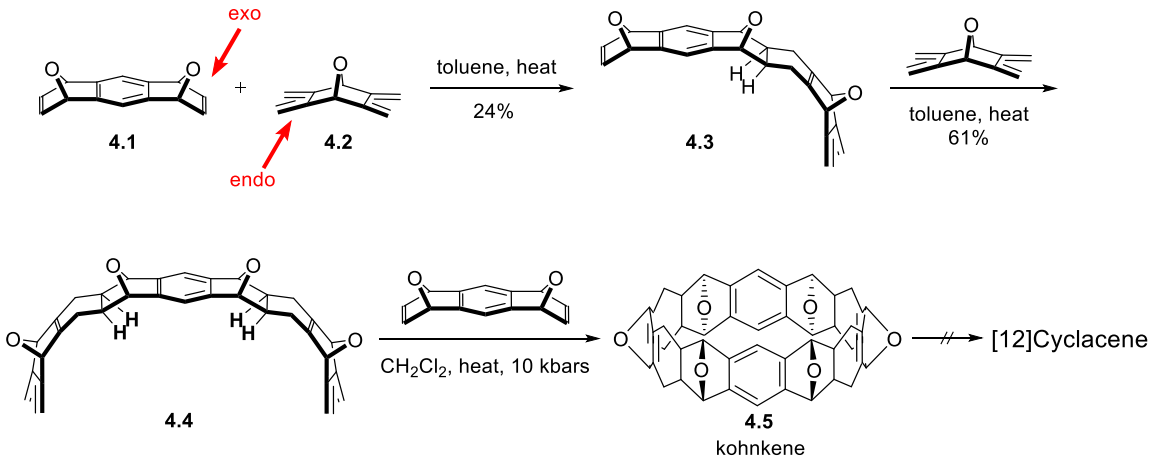

Scheme 4-1 Stoddart's attempt to [12]cyclacene.

Another interesting attempt was carried out by Cory *et al.* a few years later. This route aimed at the synthesis of an [8]cyclacene derivatives. Similar to Stoddart's approach, Cory also utilized Diels−Alder reaction as the macrocycle formation method. Instead of using curved precursors, Cory attempted a two-fold cycloaddition between the structurally flexible bisdiene **4.6** and anthracene-1,4,5,8-tetraone **4.7** as the dienophile. The quinone functionalities were included in hope that they can be removed *via* reductive aromatization or reduction-dehydration methods, as Stoddart's approach have demonstrated the challenge in oxidative aromatization. In practice, the proposed macrocycle was smoothly obtained in good yields. Attempts to proceed in this route included oxidation to reveal the anthracene moiety marked as bold in macrocycle **4.8**. However, varied products such as partially oxidized product and anthracene-9,10-dione formation were observed unexpectedly. No subsequent reports were seen beyond this point.

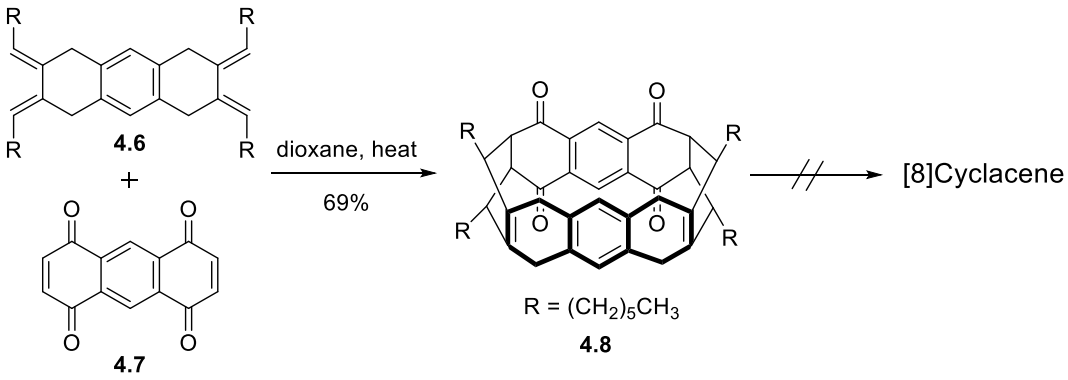

Scheme 4-2 Cory's attempt towards [8]cyclacene.

4.3 Proposed Synthesis of a [12]Cyclacene Derivative

Based on the previous examples of molecular belt synthesis, guiding principles for the design and synthesis of cyclacene can be summarized as follows:

1. To avoid the strain build-up during the synthesis, a three-stage route is usually applied: unstrained/curved synthon, stereoselective macrocyclization, late-stage functionalization.
2. Among the methodologies explored, Diels-Alder cycloaddition is proved to be a powerful method to efficiently construct benzenoid moiety and achieve stereoselectivity. However, the normal diene-dienophile [4+2] Diels−Alder cycloaddition usually results in cyclohexene unit, which requires further oxidation or dehydration steps to match the oxidative states with benzene. Such modifications have proved difficult on polycyclic systems, especially when the strained, macrocyclic frameworks are associated.
3. To this end, novel late-stage functionalization methods need to be developed to avoid red/ox process. As the fully conjugated macrocycle is highly strained and is

likely to dearomatize upon protonation or nucleophilic addition. Thus, ideal chemical transformation would be irreversible thermal or photochemical process, which could reduce the decomposition pathways for the ease of product isolation and purification.

Herein we present our proposed synthesis towards a [12]cyclacene derivative. There are two major principles to the molecular design and synthesis plan. The first consideration is made on the choice of late-stage functionalization methods. Informed by previous failed attempts, we intend to avoid direct oxidation/reduction after the macrocycle is built. In light of recent synthesis progress on longer linear acenes ($n \geq 6$), we envisioned that a cheletropic rearrangement would serve the purpose of installing the full conjugation. As precedented in the synthesis towards air-sensitive hexacene, Chow and co-workers have successfully applied the cheletropic extrusion of carbon monoxide under heating or irradiation.[95] We imagined that this irreversible process would be an efficient and clean pathway to produce cyclacene as a game-ending step. Specifically, a macrocyclic structure bearing multiple CO bridges could serve as an ideal precursor.

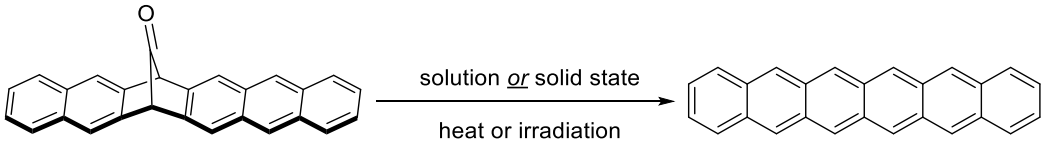

Figure 4-7 Synthesis of air-sensitive hexacene *via* cheletropic rearrangement.

Another consideration is made to the strategy of the macrocycle formation. We decided to stick with Diels−Alder cycloaddition as the primary macrocyclization transformation. However, variations need to be made in order to reduce the total number of steps and facilitate aromatization. In particular, the benzyne Diels−Alder reaction sequence outlined

in **Figure 4−8a** is a suitable model reaction for our goals. Nuckolls *et al.* have utilized this method to construct complex structures featuring densely substituted pentacene moieties (**Figure 4-8b**).[96] We believe this reaction is a convenient "connecting" methodology that couples two pieces of aromatic units together *via* a "benzene joint". Taking a closer look at the reaction sequence, one should note that multiple Diels−Alder reactions are involved in this overall transformation. The reaction first starts with initiation of a frequently used benzyne precursor **4.9**, 2-(trimethylsilyl)phenyl trifluoromethanesulfonate, to generate a reactive benzyne intermediate **4.10** under fluoride conditions. Subsequently, the benzyne could engage a [4+2] Diels−Alder cycloaddition event with 2,5-diphenyl-6H-1,3,4-oxadiazin-6-one **4.11** to afford a bridge intermediate **4.12**. Compound **4.12** readily undergoes an irreversible retro-Diels−Alder reaction at a loss of nitrogen gas to form a new diene **4.13**, which will further experience a second DA and retro-DA sequence to generate the final aromatic product **4.14**.

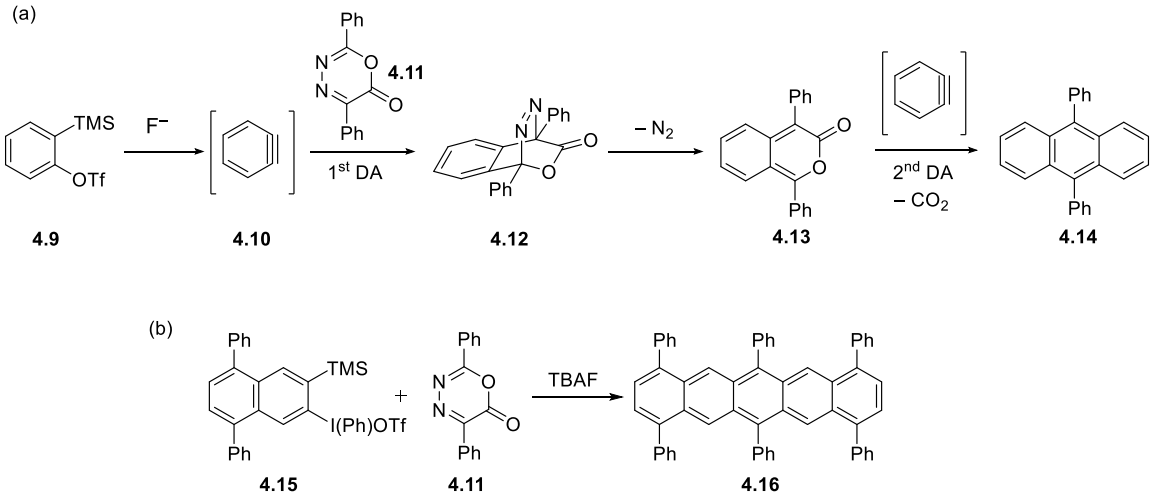

Figure 4-8 A benzyne Diels−Alder cycloaddition sequence applied for the construction of complex aromatic compounds.

Combining the two factors mentioned above, we outline our synthetic route in **Figure 4-9.** The proposed synthetic route contains three stages: i) preparation of macrocyclization precursor; ii) exploration of macrocyclization *via* benzyne Diels−Alder reaction and iii) late-stage aromatization. The first advanced intermediate is compound **4.17**, it is designed to be a 1/4 cycle subunit that contains multiple important functionalities: (a) the [2.2.1]-bridge moiety serves as the origin of curvature; (b) the trimethylsilyl (TMS) and trifluoromethanesulfonate (TfO) groups are designed as benzyne precursors in order to accomplish the benzyne Diels−Alder macrocyclization; (c) the quinone moiety allows for sequential transformations to extend **4.17** into further intermediates. (d) The R group is a temporary mask of ketone, which will be removed *via* oxidation to reveal the bridged C=O group. The method to construct **4.17** will be applied again to synthesize **4.18**, which serves as the half cycle and the macrocyclization precursor. However, synthesis of **4.18** is non-trivial. In order to form macrocyclized product, the configuration of the two bridge moieties on **4.18** must be *syn*. If *anti* configuration is achieved, polymerization or oligomerization instead of macrocyclization will dominate as the benzyne-Diels−Alder cycloadducts. Thus, how to selectively produce the *syn*-**4.18** over the *anti*-**4.18** is a challenge for us to solve. It is worth emphasizing that even a small percentage of the *anti*-isomer as the impurity could also lead to an imbalance of the reactive species and cause the formation of oligomers and polymers. In later sections, I will elaborate on how the stereoselectivity is achieved based on the steric effect of the R groups.

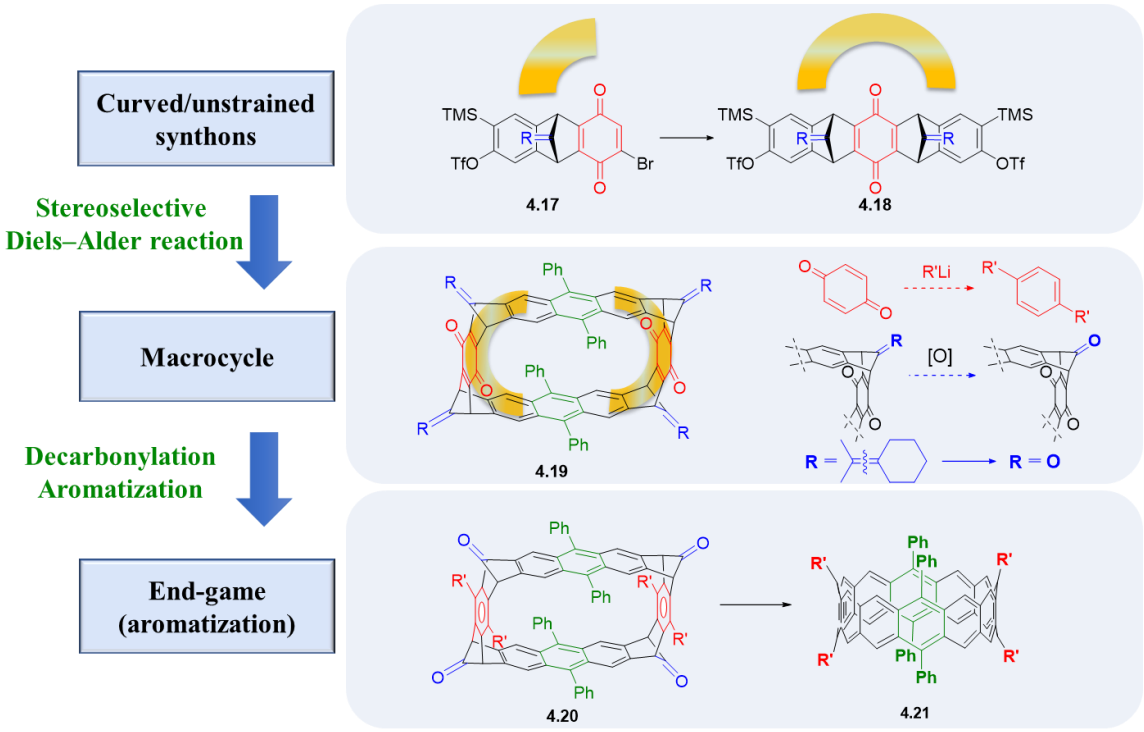

Figure 4-9 Proposed key intermediates for the synthesis of cyclacene **4.21**.

Upon successful synthesis of precursor **4.18**, the macrocyclization step will then be examined. As mentioned earlier, we envision that a two-fold benzyne-Diels−Alder reaction between the Kobayashi benzyne[97] and diazapyrone **4.11** should afford macrocycle **4.19**. Further modifications involve the quinone aromatization and oxidative cleavage of exocyclic double bond at the bridge head to reveal the ketone functionality. We keep in mind that direct manipulation of the macrocyclic framework can be risky, as evidenced in previous attempts. However, we feel confident in these proposed reactions in that a) the quinone reductive aromatization only forms benzene rings that are not in conjugation with the anthracene segments, this change is less likely to bring significant structural change to the macrocycle and add extra ring strain; b) for the same reason mentioned above, the reactivity of the exocyclic double bond should not be affected by the cyclic framework. If

compound **4.20** can be smoothly made according to plan, the global decarbonylation will be attempted as the end-game reaction for the synthesis of a [12]cyclacene derivative. The R' groups will be installed to help stabilized the possible ground state diradical form of cyclacene. Alkynes substituted with bulky silyl group would be an ideal candidate for such a purpose.

4.4 Synthesis of an Advanced Macrocyclization Precursor

As illustrated in **Scheme 4-3a**, the synthesis started from commercially available material hydroquinone **4.22**. In five steps, **4.22** was converted to the bis-benzyne precursor (BBP) **4.23**. In a separate effort, pentamethylenefulvene **4.25** was prepared *via* condensation between cyclohexanone **4.26** and cyclopentadiene **4.27**. With the BBP **4.23** and fulvene **4.25** in hand, we then explored the benzyne-Diels−Alder reaction in producing the mono-adduct **4.28**. It was found that the benzyne formation can be controlled by the equivalence of cesium fluoride and fulvene **4.25** and the reaction temperature.[98] Specifically, when the BBP was treated with 1.2 equivalence of cesium fluoride at room temperature, mono-activation of the silyl triflate functional group occurred to give the corresponding benzyne intermediate **4.24**, which was subsequently trapped with the diene functional group within the fulvene moiety. However, when treating BBP with extra cesium fluoride and diene at 80 ˚C, the two-fold benzyne-Diels−Alder cycloaddition was observed and resulted in the formation of double-bridge compound **4.29**. The resulting product contained an about 1:1 mixture of *syn*- and *anti*-isomer that were not separable by column. These experiments showed that **4.23** was a useful benzyne precursor and the reactivity of the bis-benzyne moiety can be controlled by temperature and equivalence of

fluoride. It was also noted that the silyl triflate functionalities in mono-cycloadduct **4.28** can be further activated to generate the benzyne intermediate under harsher conditions.

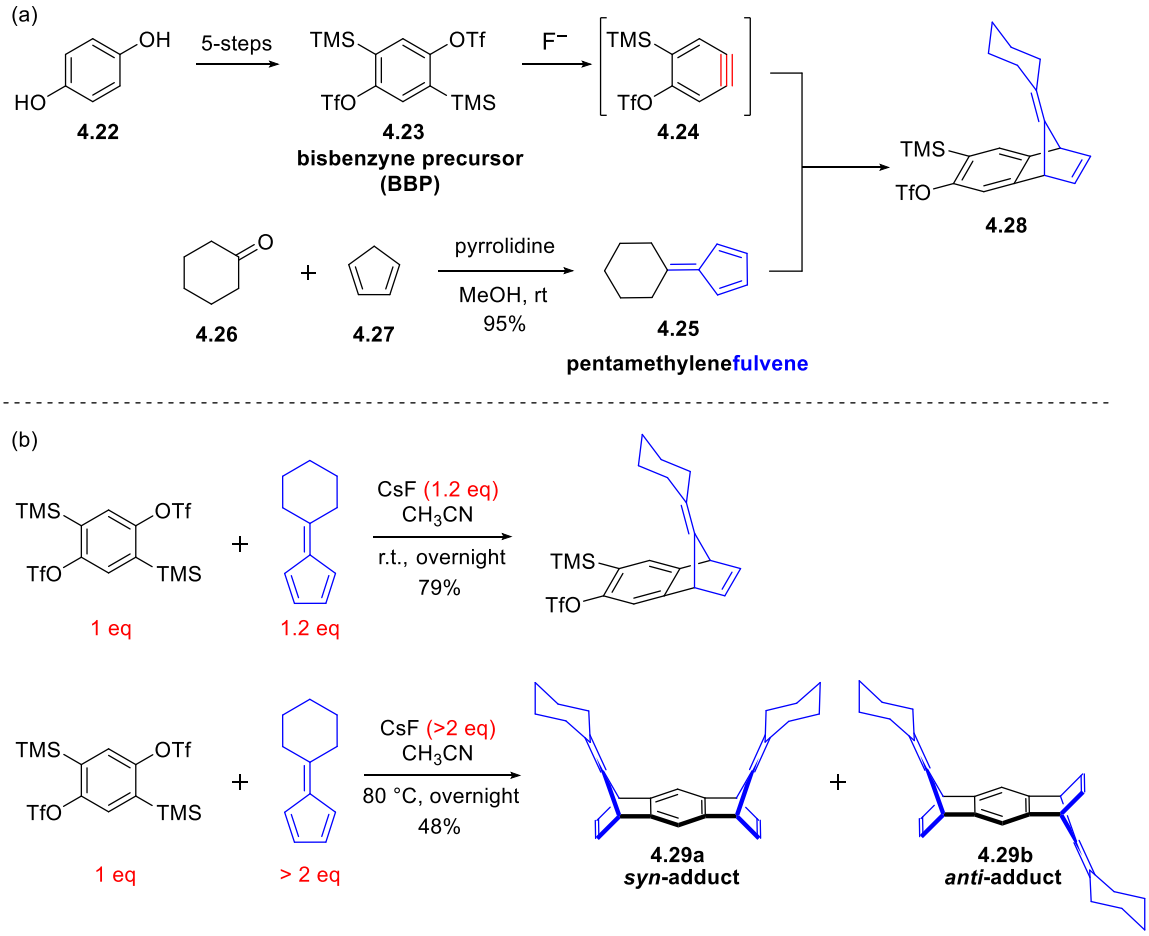

Scheme 4-3 Synthesis of bifunctional cycloadduct **4.28**.

We next focused on converting mono-cycloadduct **4.28** into the proposed 1/4 cycle **4.17**. The key reaction applied in the following study featured a one-pot three-component Diels−Alder cascade.[99] This overall transformation contains a series of Diels−Alder and retro-Diels−Alder events that occurred in a certain order. As proposed in **Scheme 4-4**, the reaction started with the cycloaddition between the mono-cycloadduct **4.28** and 3,6-dipyridinyl-tetrazine (DPT) **4.29**. Although the third component, dibromo-benzoquinone

4.34 is also present in the same reaction pot as an alternative dienophile, the reaction between **4.28** and **4.29** is favored because the electron-rich dienophile and electron-poor diene fit well into the model of an inverse electron demand Diels−Alder reaction. The resulting cycloadduct **4.30** readily proceeds to the diazine intermediate **4.31** by loss of N_2 gas, which could further undergo a retro-Diels−Alder reaction to form isobenzofulvene **4.33** at the loss of dipyridinyl-pyridazine unit **4.32**. The *in situ* generated fulvene moiety serves as a reactive and electron-rich diene that could be quickly trapped by dibromoquinone **4.34** *via* a normal demand Diels−Alder reaction. In the end, dehydrobromination of the corresponding Diels−Alder adduct would lead to the formation of the bis-bridge structure **4.18**.

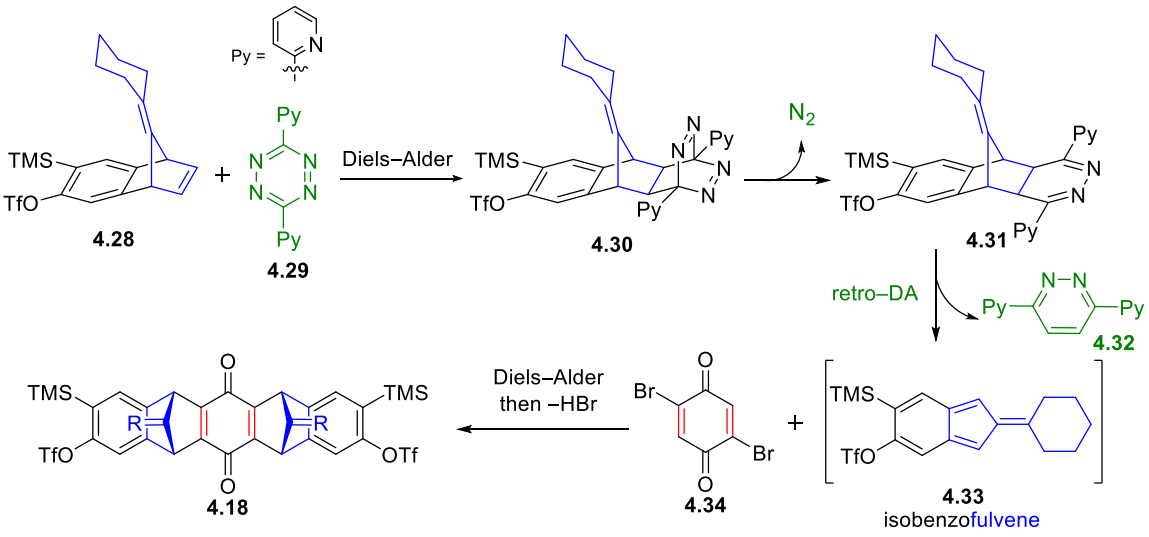

Scheme 4-4 Proposed three−component Diels−Alder cascade for the synthesis of half cycle **4.18**.

Putting this proposal into practice, my initial effort focused on the two-fold cascade reaction to synthesize the bis-bridge species **4.18** through a double-cycloadduct **4.35**. However, I found out that the mono-cycloadduct **4.36** was obtained as the sole product

even though excess amount of isobenzofulvene **4.33** was provided. This observation indicated that the second Diels−Alder reaction did not happen. Examining the 3D model structure of **4.36** (**Scheme 4-5b**), it was easily noted that both faces of the dione moiety were blocked by either the cyclohexylidene group or the bromine group. As the isobenzofulvene also contained the bulky cyclohexylidene group, the geometry of **4.36** could not allow the second [4+2] event because of steric encumbrance. Additionally, I also realized that the proposed bis-bridge intermediate **4.35** was highly congested and should not form due to steric reasons. Thus, alternative routes need to be developed for the synthesis of **4.18**.

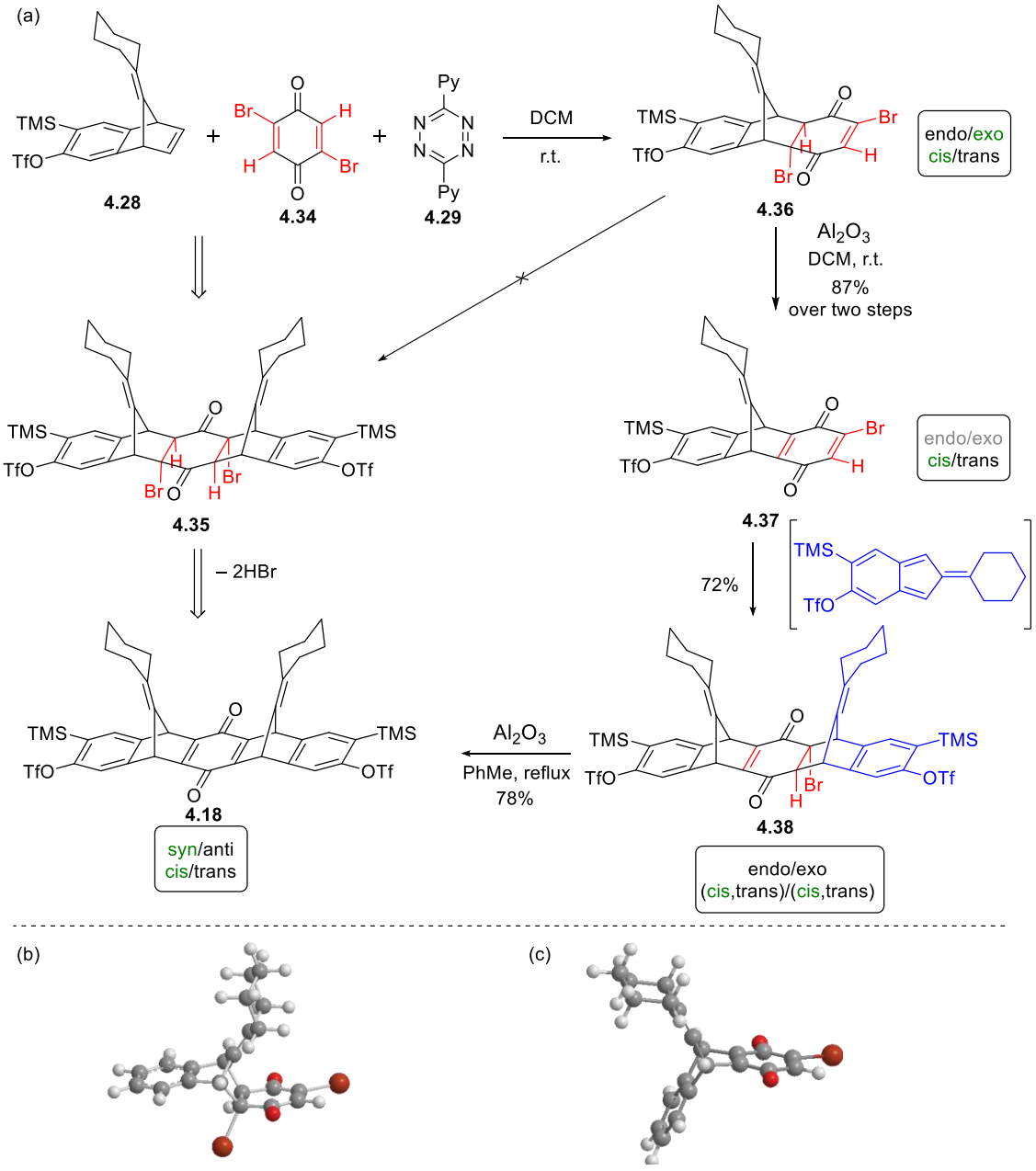

Scheme 4-5 Failed one-pot attempt on the synthesis of **4.35** and step-wise synthesis of **4.18**. (b) and (c) shows the molecular model of **4.36** and **4.37**, the silyl and triflate groups are omitted for clarity.

To circumvent the steric issue, the synthesis was attempted in a step-wise manner. Dehydrobromination of **4.36** using basic alumina smoothly afforded the desire product **4.37**.

Upon regaining the benzoquinone moiety, the dienophile became more sterically accessible, which allowed the second Diels−Alder reaction to occur. As a result, cycloadduct **4.38** was formed smoothly in 72% yield, which was subsequently converted to the desired **4.18** *via* HBr elimination. Comparing with the previous HBr elimination step, the second HBr elimination required higher temperature and longer reaction time. Specifically, the first HBr elimination readily occurred while eluting the corresponding DCM solution through a short plug of basic alumina. However, with the bis-bridge structure **4.38**, the elimination required refluxing with basic alumina in toluene for two hours.

So far, we have not considered the stereochemistry involved in this revised route. Indeed, all of the intermediates mentioned above were mixtures of related isomers. In the following discussion, I will elaborate on the analysis of stereoisomer formation and the interpretation from experimental results. Furthermore, I will also demonstrate that the above synthesis is useful in producing the desired *syn*-isomer of **4.18**.

In **Scheme 4-5**, compounds that contain possible stereoisomers were labelled with exo/endo, cis/trans and *syn*/*anti* terminologies. For example, the first three-component cascade reaction afforded **4.36** with a total of four possible isomers, including endo/exo products and cis/trans isomers with respect to the endo/exo configuration. The endo/exo products were generated from the stereoselectivity of Diels−Alder cycloaddition. The cis/trans isomers were generated due to the asymmetric nature of isobenzofulvene. Upon HBr elimination, **4.37** was obtained as a pair of cis/trans isomers with approximately 1:1 ratio. Since the cis/trans isomers do not affect the stereoselectivity or the reactivity of the following reactions, separation of the cis and trans regio-isomer was not attempted.

However, applying the 1:1 mixture of **4.37** could potentially double the number of stereoisomers produced in the next step.

Theoretically, the reaction between **4.37** (1:1 cis/trans mixture) and isobenzofulvene **4.33** could afford sixteen stereoisomers. Given the 3D chemical structure of **4.37**, four possible reaction pathways were available regarding the [4+2] cycloaddition. Of each particular reaction pathway, four possible regioisomers could be formed due to two sets of cis/trans divergence. The reaction pathways were depicted in **Figure 4-10** and defined explicitly in two "endo/exo" terms. Specifically, the first EXO/ENDO term (denoted in upper case) describes the face selectivity on how the diene **4.33** approach to the dienophile **4.37**; whereas the second exo/endo term (denoted in lower case), reflects the inherent endo/exo selectivity in Diels−Alder cycloaddition. For example, in the highlighted reaction pathway shown in **Figure 4-10**, the isobenzofulvene approaches to the EXO face of quinone alkene in an exo Diels−Alder manner. Comparing with the other three possible situations, the EXO-exo pathway experienced the least steric encumbrance between the cyclohexylidene groups. The EXO-endo pathway contained an increased steric interaction between the cyclohexylidene group and the bulky silyl and triflate groups. For the two ENDO pathways, the diene need to approach from the concave face of **4.37**. Due to the bulky groups attached to both sides of the diene moiety, these pathways were less likely to occur.

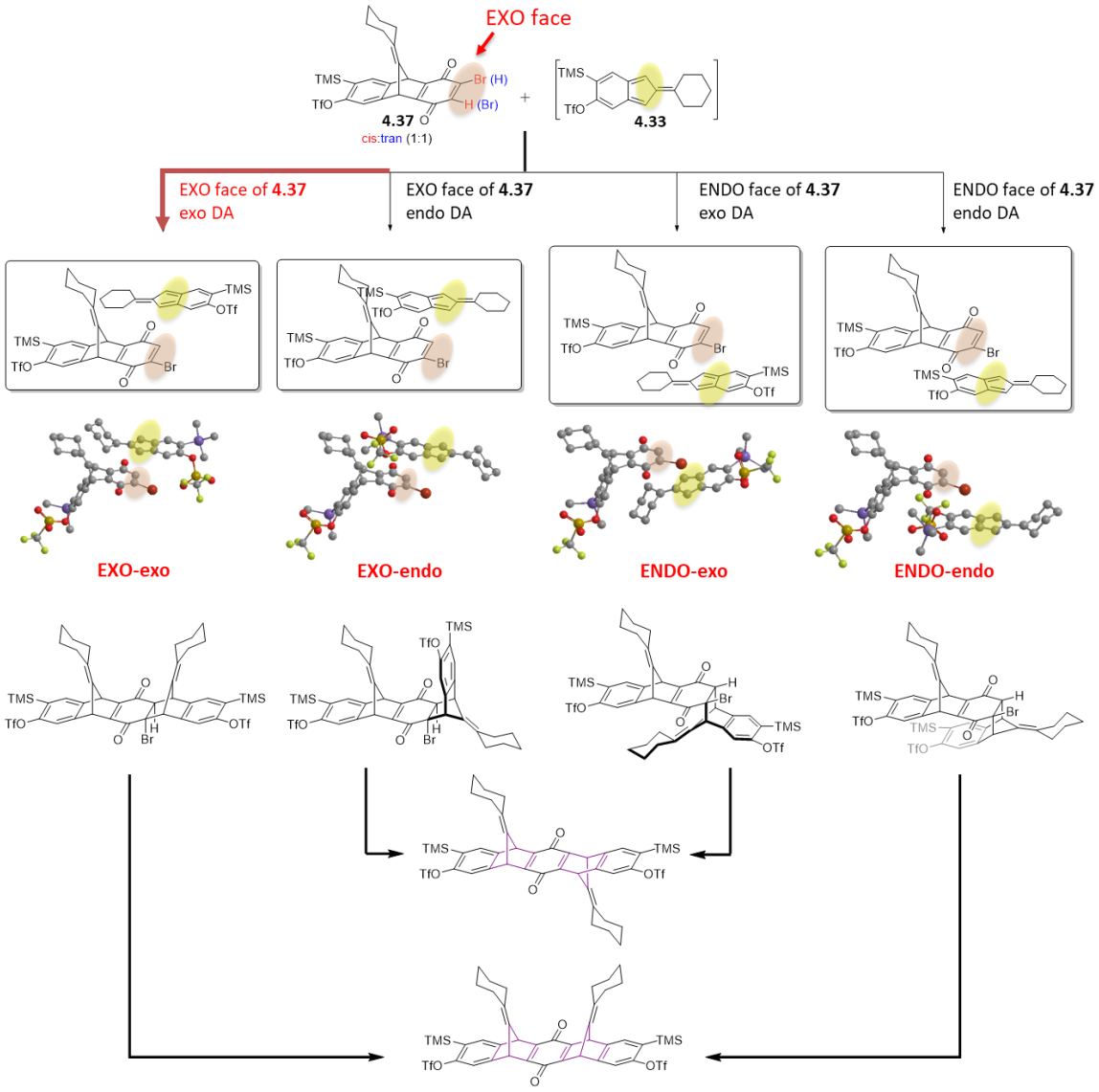

Figure 4-10 Steric analysis of Diels−Alder cycloaddition between **4.33** and **4.37**.

Examining the possible products generated from each reaction pathway, it was found that the EXO-exo and ENDO-endo could produce the desired *syn*-isomer upon dehydrobromination, whereas the EXO-endo and ENDO-exo pathways would lead to the formation of the undesired *anti*-isomer. Based on this steric analysis, we envisioned that stereoselectivity could likely be achieved from the difference in steric interactions during the Diels−Alder event. It is important to point out that the choice of pentamethylenefulvene

4.25 and silyl-triflate groups are crucial to this potential stereoselectivity. To be more specific, if the groups less bulky than cyclohexylidene was used, the ENDO-exo approach would become more plausible to produce the *anti*-isomer of **4.18**; if smaller benzyne precursor moiety was used (e.g. halogen substituents), EXO-endo would also become more likely due to diminished steric interactions. Collectively, the above steric analysis predicted that the reaction between **4.33** and **4.37** should favor the formation of *syn*-isomer of **4.18** after dehydrobromination.

To test this hypothesis, the ^{1}H NMR of the resulting **4.38** mixture was examined in detail. The structure of **4.38** in **Figure 4-11** only shows the EXO-exo product. The signals at 3−5 ppm clearly indicated the formation of the second bridge unit. The assignments of bridge-head protons were made according to the typical chemical shifts and splitting patterns. Interestingly, the endo/exo selectivity can be directly observed from this ^{1}H NMR spectrum. In the model study performed by Dr. Sarah Wegwerth (**Figure 4-12**), in the mono-bridge system, the endo-H appeared as a singlet at around 3.1 ppm, whereas the exo-H showed a doublet peak at around 4.0 ppm. The difference in chemical shift can be attributed to the shielding effect of the nearby benzene ring. Based on the molecular model calculated by MM2 method, the endo-H locates in the shielding region of the benzene ring, while the exo-H does not. Additionally, the difference in splitting pattern can be explained by the Karplus relationship, which describes the correlation between ^{3}J-coupling constants and dihedral torsion angles. By calculating the dihedral angles, it was found that the angle for endo-H and exo-H was 81˚ and 46˚, respectively. Therefore, the coupling constant for the endo-H peak should be smaller than the exo-H peak. After knowing the typical chemical shifts for the bridge-head protons, the key information of the Diels−Alder

selectivity can be deduced from the NMR spectrum shown in **Figure 4-11**. The intense peak appeared at 2.93 ppm clearly indicated that the major product contained endo-H, which was formed by exo Diels−Alder reaction pathways. The multiplicity of that peak also indicated that isomers with slightly different chemical environment were also present. Based on the steric analysis and a detailed chemical structure mapping in **Figure 4-10**. We believe that the major products were cis/trans isomers with the same framework. On the other hand, it was noted that minor products showed signals at around 3.05 ppm. Signals with similar intensity also showed up along with other peaks at around 4.2 ppm and 5.0 ppm. We hypothesized that these minor products were likely the exo Diels−Alder products containing a different carbon framework, which also consisted of cis/trans isomers.

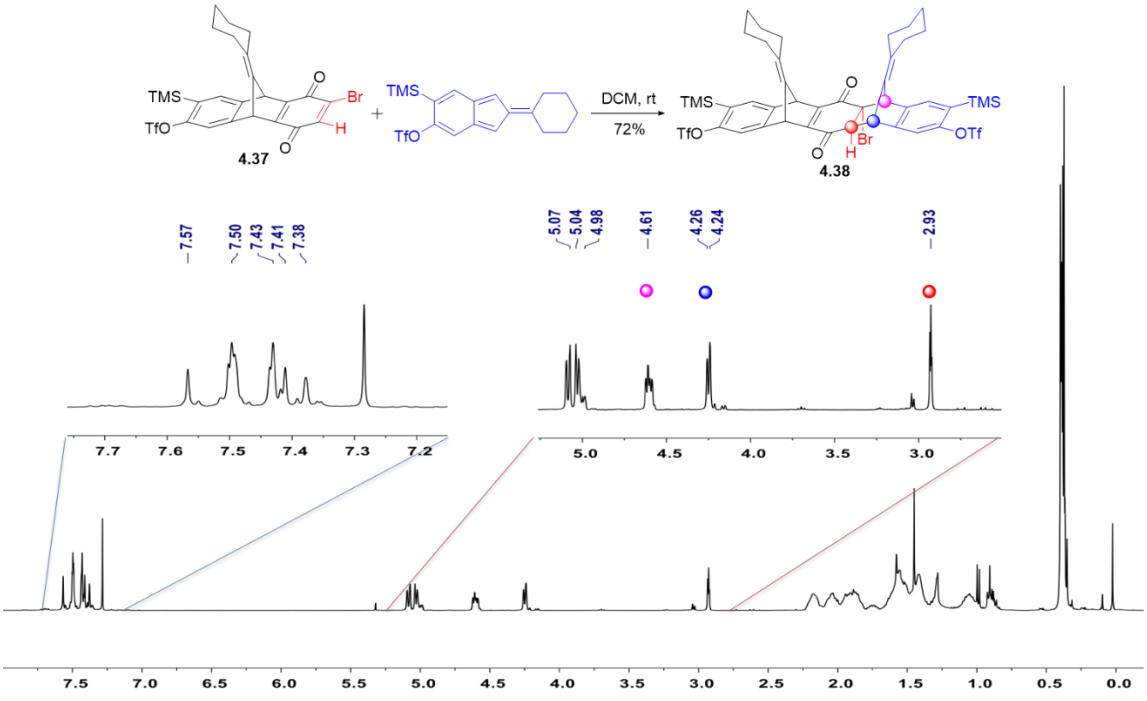

Figure 4-11 ^{1}H NMR spectra of **4.38** mixtures.

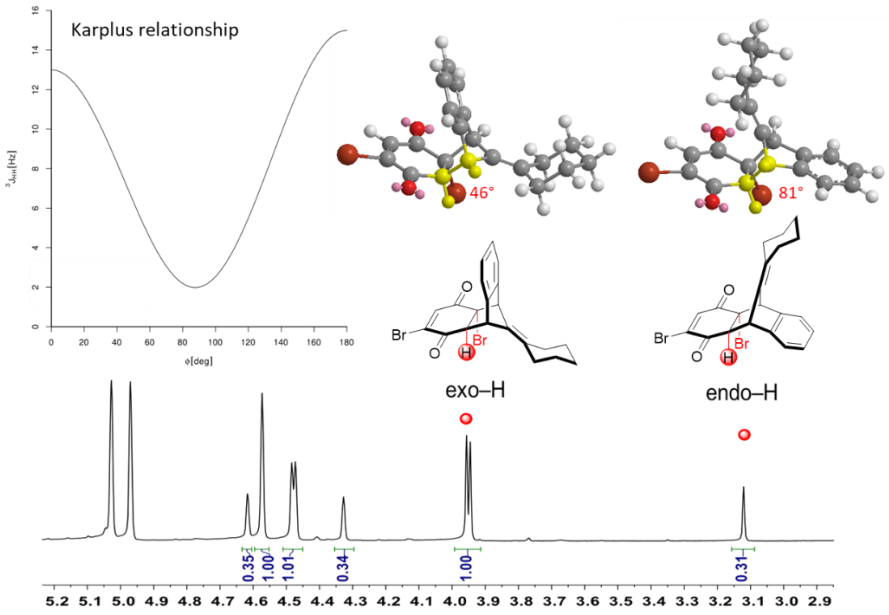

Figure 4-12 ^{1}H NMR spectrum of mono-bridge isomers in a model study. The Karplus relation graph is adopted directly from Wikipedia under "Karplus equation". The dihedral angles are measured from the highlighted H−C−C−H units. Molecular models are calculated from Chem3D software using MM2 method.

Up to this point, the ^{1}H NMR results have matched well with our proposed steric analysis. In the next move, the dehydrobromination products were examined by ^{1}H NMR and ^{19}F NMR spectroscopy. In the ^{1}H NMR spectrum, the disappearance of bridge-head peaks proved the success of HBr elimination. As a result, the products contained a higher degree of symmetry, in which the pattern in aromatic region was greatly simplified. Interestingly, as the proposed **4.18** structure should contain two aromatic singlets regardless of stereo- or regio-isomerism. The peaks in the aromatic region clearly indicated a major product and a minor product, which indicated that the stereoselectivity was achieved!

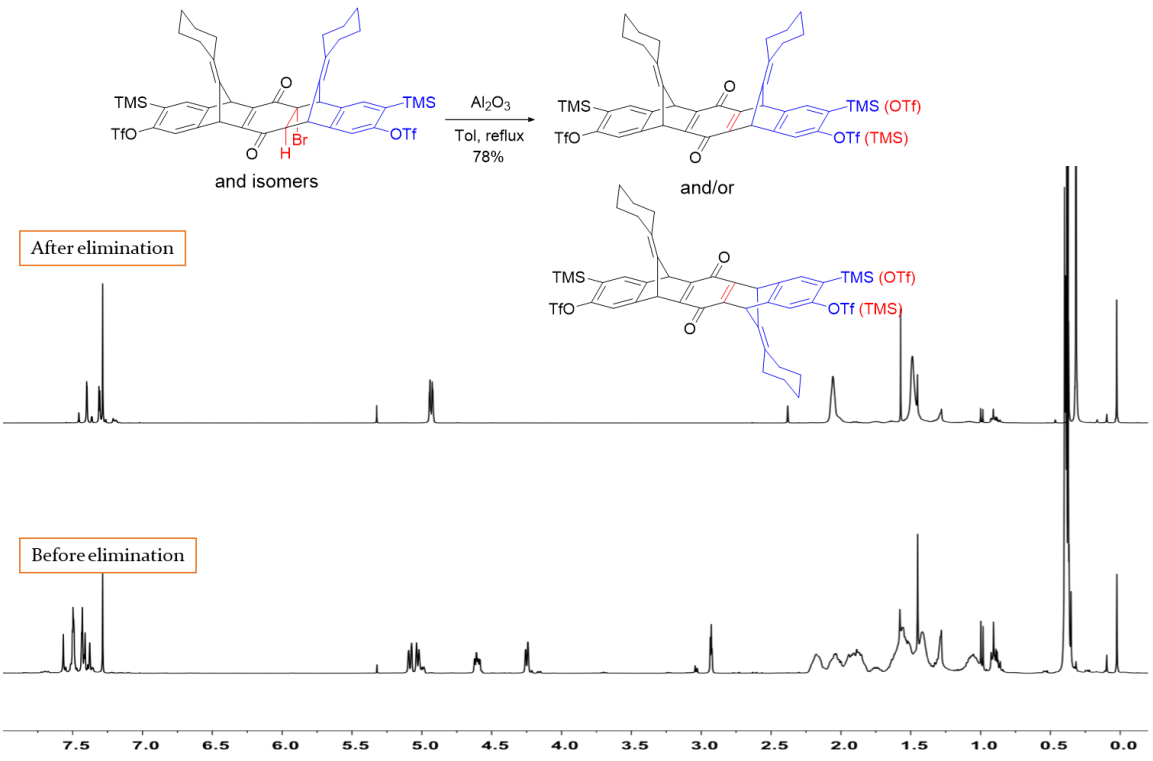

Figure 4-13 Comparison of ^{1}H NMR spectra before and after HBr elimination.

The ^{19}F NMR spectrum revealed more detailed information on the number of isomers. It was noted that, regardless of isomerism, the triflate group should appear as a singlet signal in ^{19}F NMR spectrum. Therefore, the four singlets observed in the final product mixtures clearly indicated that the mixture contained four isomers. Interestingly, the four singlets also "paired up" by their intensities. A 5:1 ratio was measured by integration between the major pair and minor pair, and a 1:1 ratio was measured within each pair. We envisioned that face selectivity on isobenzofulvene **4.33** should not be induced in the Diels−Alder events because the chemical and steric environments above and below the fulvene plane are rather similar. Thus, the 1:1 ratio should represent cis/trans isomers, while the 5:1 ratio indicated the stereoselectivity between *syn*- and *anti*- isomers. However, the identity of the major product cannot be confirmed by NMR spectroscopy. To find out

the exact configuration of the major product, the mixture was recrystallized to obtain a pure sample of the major isomer. Single crystal sample was then obtained by solvent evaporation methods.

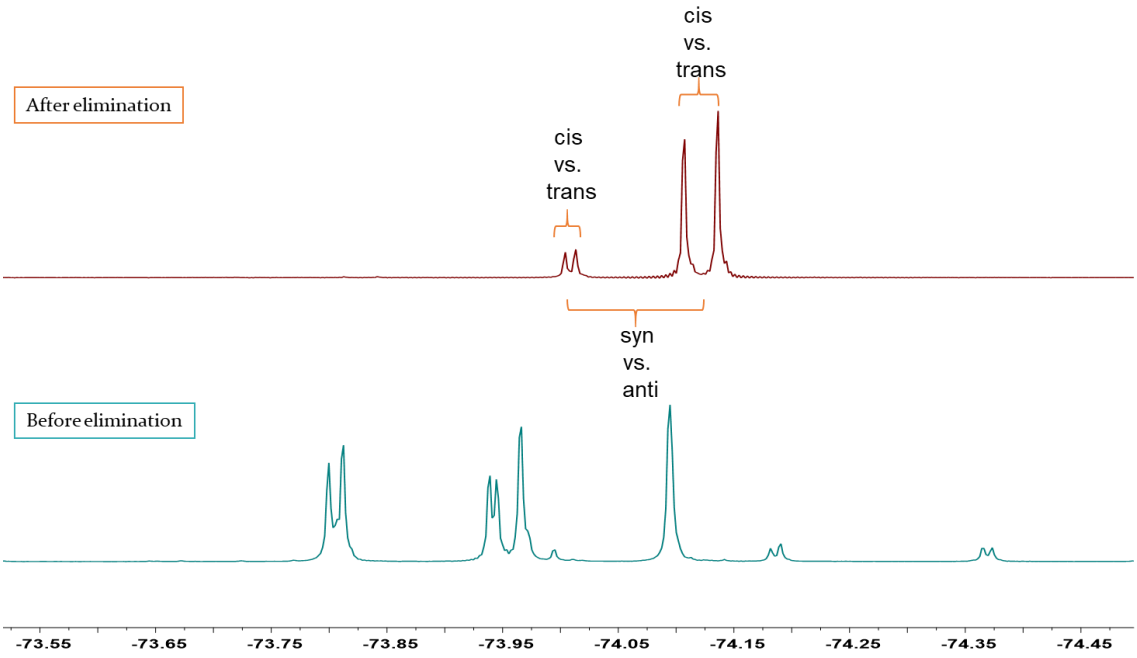

Figure 4-14 Comparison of ^{19}F NMR spectra before and after HBr elimination.

To our delight, the single-crystal X-ray analysis confirmed that the major product was indeed the *syn*-isomer of **4.18**. This result demonstrated the utility of this route to selectively synthesize the half cycle structure.

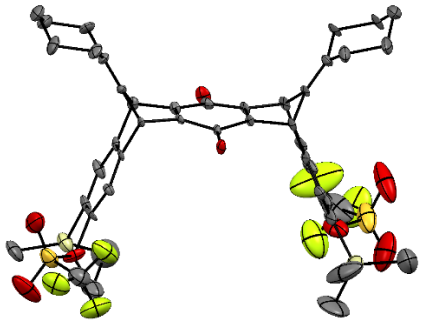

Figure 4-15 X-ray crystal structure of the major product showing the *syn*-configuration of the bridge units.

4.5 Progress Towards Macrocyclization and Future Work

Even though the *syn*-isomer of **4.18** was obtained, the success of macrocyclization still depended on stereoselective Diels−Alder reactions. We envisioned that the macrocyclization could potentially be conducted in a stepwise manner. As depicted in **Scheme 4-6**, dimerization of the half-cycle should lead to the macrocyclization precursor **4.39** upon careful control of mono-benzyne activation. In the second ring closing event, we believed that it was an easier process since the reaction sites have been placed in close proximity and no side reaction such as oligomerization should occur.

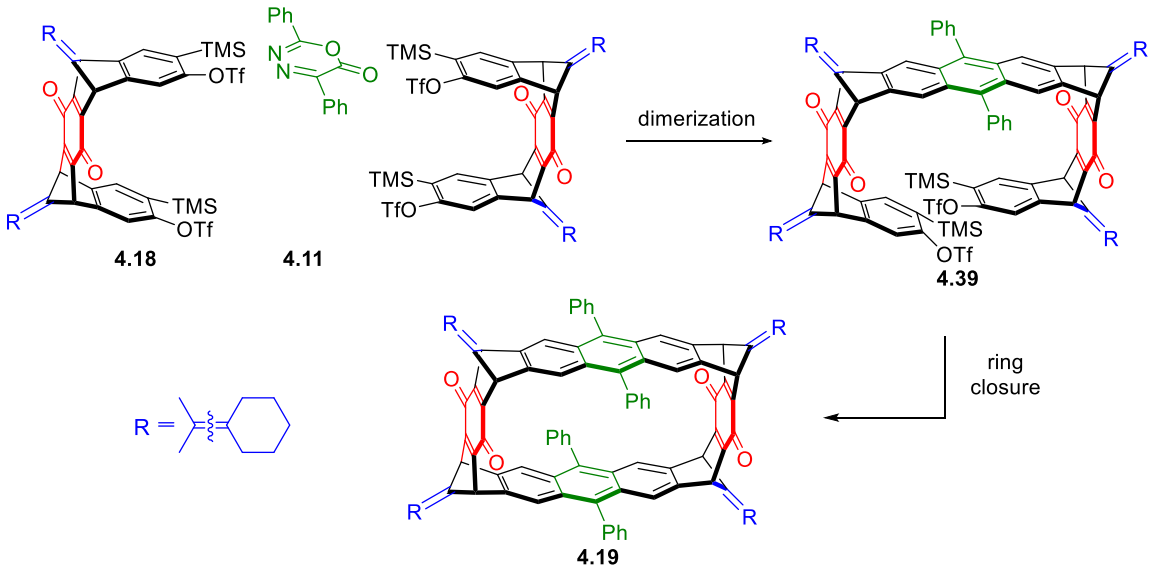

Scheme 4-6 Proposed synthesis of a 12-membered macrocycle **4.19**.

Steric analysis of the dimerization step was performed to support the hypothesis of stereoselective benzyne-Diels−Alder reaction. Upon slow addition fluoride addition, the benzyne intermediate **4.40** could presumably be formed and react with diazapyrone to afford the pyrone intermediate **4.41**. The two plausible reaction pathways of the benzyne-Diels−Alder reaction between the **4.40** and **4.41** were depicted in **Figure 4-15**. It is worth mentioning that in both cases, the benzyne approaches to the pyrone diene moiety from the *convex* face, which has less steric encumbrance. In contrast, the other two pathways (not shown in **Figure 4-16**) where benzyne would approach from the *concave* face were excluded due to steric effects. Of the two pathways shown, the one on the left contained strong steric interactions between the bulky silyl/triflate groups and the cyclohexylidene group, which the resulting *anti*-dimer was less likely to be generated. Consequently, the formation of the desired *syn*-dimer was more likely to occur *via* a less sterically congested reaction pathway shown on the right.

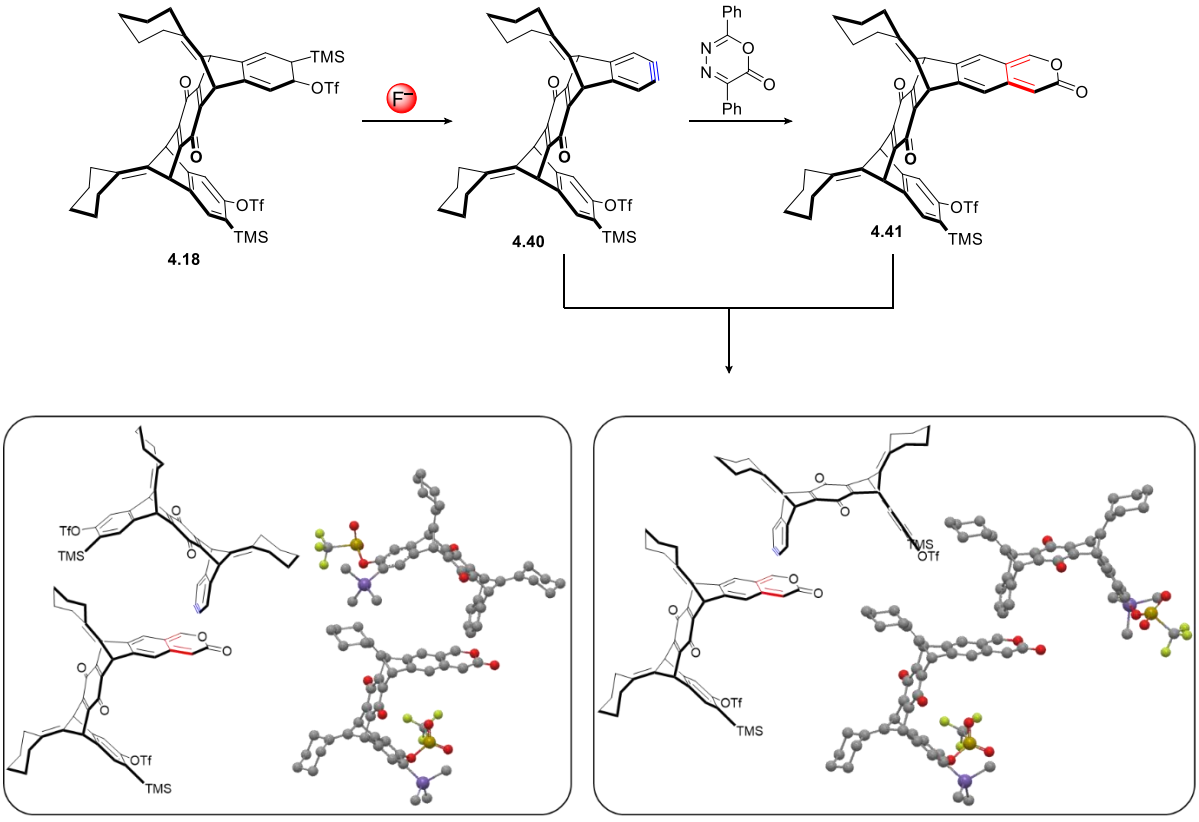

Figure 4-16 Steric analysis of benzyne-Diels−Alder reaction to synthesize dimer.

In practice, we attempted the dimerization using CsF as the fluoride source to generate the benzyne. However, no Diels−Alder product was identified. We envisioned that CsF might not be a good choice for this reaction due to the poor solubility of CsF solid in organic solvents. As the CsF can only be added as solid, slow addition of fluoride could not be achieved, thus both silyl/triflate units on **4.18** could be initiated to form oligomer side products. In order to control the rate of benzyne formation, tris(dimethylamino)sulfonium difluorotrimethylsilicate (TASF), a soluable organic fluoride source was used to remove the TMS group. By varying the equivalence of **4.18** and diazapyrone **4.11**, it was found that the benzyne precursor was efficiently consumed by the fluoride, however, the diazapyrone was mostly recovered. This indicated that the

benzyne Diels−Alder reaction did not occur and the benzyne species generated *in situ* were decomposed under unknown pathways. This result implied that the benzyne was either not stable or non-reactive.

In order to test the utility of this benzyne intermediate, I performed a series of benzyne transformations based on **4.18** and simple benzyne precursors **4.42**. As shown in **Scheme 4-7**, under similar conditions, benzyne precursor **4.42** was smoothly converted to the corresponding triazole **4.44** *via* click reaction with azide **4.43**. However, bis-triazole **4.45** was not observed in the reaction between **4.18** and **4.43** with complete consumption of the benzyne precursor. Moreover, using anthracene as a diene also proved the poor reactivity of the quinone-containing benzyne precursor **4.37**. These results strongly demonstrated that the quinone functionality resulted in negative influence on the reactivity of benzyne.

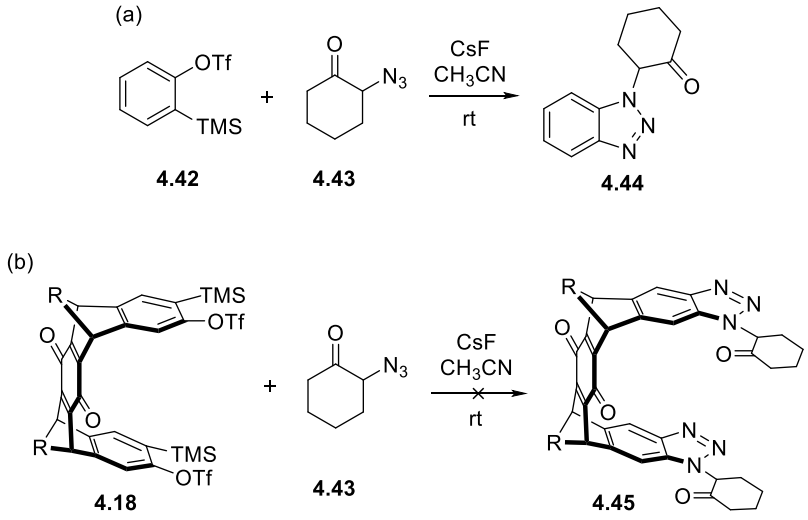

Scheme 4-7 Test of benzyne reactivity *via* click reaction.

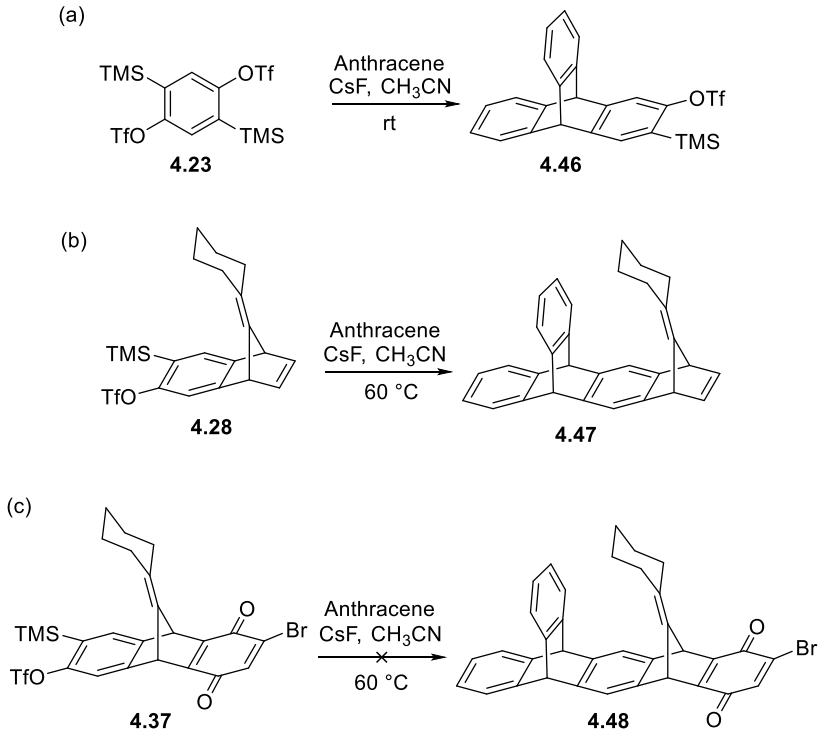

Scheme 4-8 Test of benzyne reactivity *via* Diels−Alder reactions with anthracene.

At this stage of the synthesis, we were not able to construct the macrocycle from the bis-bridge benzyne precursor **4.18**. In future work, the quinone functionality needs to be removed in order to further advance this route. Meanwhile, inspired by the successful experiments in the stereoselective three-component Diels−Alder reactions, an alternative route was proposed which could potentially simply the synthesis. As shown in **Scheme 4-9**, the order of reaction sequence is adjusted as compared with the previous route. It has been proved that the benzyne-Diels−Alder reaction between **4.28** and **4.11** can be successfully carried out to generate **4.49** as 1:1 *syn/anti*-mixtures. We envisioned that the mono-quinone intermediate **4.50** could potentially undergo a dimerization-cyclization process to form the 12-membered macrocycle **4.19** in one-pot. The highlight of this route is that it does not involve any identification and purification of stereoisomers. Specifically,

when treated with DPT **4.29**, the norbornene unit will be planarized by isobenzofulvene formation and add onto the bromo-quinone moiety in a stereoselective manner. As proved earlier, this stereoselective addition should favor the formation of *syn*-isomer. Finally, the intramolecular ring-closing event should afford the macrocycle **4.39**.

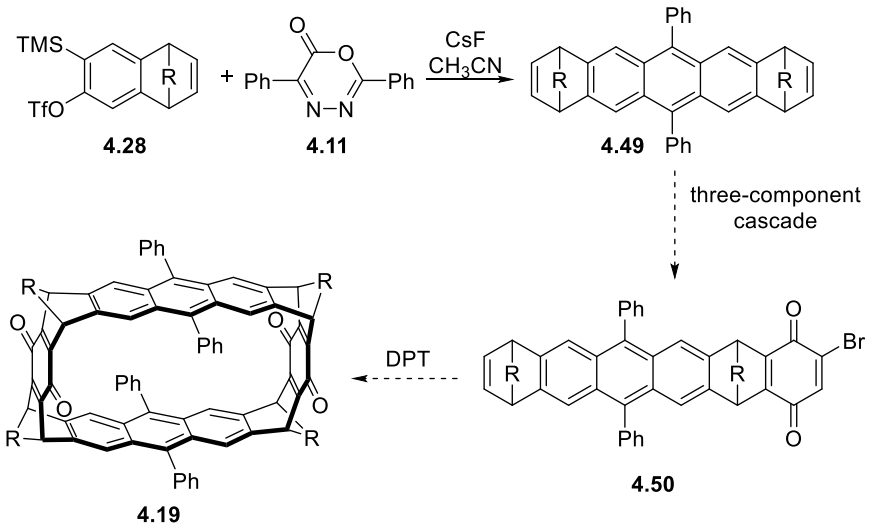

Scheme 4-9 Alternative synthetic route to macrocycle **4.19**.

4.6 Conclusion

In summary, a novel synthetic route to [12]cyclacene was proposed. This route featured a cheletropic rearrangement strategy to install the fully conjugated backbone. Efforts toward synthesizing a functionalized 12-membered macrocyclic framework has been made. An advanced intermediate, the half-cycle segment, has been successfully prepared. Diels−Alder cycloaddition has been applied as the key transformation to construct the bridge units embedded within the polycyclic framework of multiple intermediates. Stereoselectivity was controlled by the careful choice of steric functional groups on the precursors of Diels−Alder reactions. The observed selectivity was explained by steric

analysis based on the calculated molecular models. Future efforts should focus on the experimental practice to construct the macrocycle, as well as post-functionalization to achieve the fully conjugated [12]cyclacene target.

4.7 Experimental Details

All reactions were carried out using flame-dried glassware under nitrogen atmosphere unless aqueous solutions were employed as reagents. Tetrahydrofuran (THF) was dried by distillation from benzophenone/sodium under nitrogen. Dichloromethane (DCM) was dried by distillation from CaH_2 under nitrogen. All other chemicals were used as received unless otherwise noted.

Analytical thin layer chromatography (TLC) was carried out using 0.25 mm silica plates from Silicycle. Eluted plates were visualized first with UV light then they were stained using $KMnO_4$. Flash chromatography was performed using 230–400 mesh (particle size 0.04–0.063 mm) silica gel purchased from Silicycle. ^{1}H NMR (500, 400 MHz), ^{13}C NMR (126, 100 MHz), ^{19}F NMR (471, 376 MHz) spectra were obtained on a Bruker FT NMR instruments. NMR spectra were reported as δ values in ppm relative to TMS for ^{1}H (0.00 ppm), and chloroform for ^{13}C (77.00 ppm). ^{1}H NMR coupling constants are reported in Hz; multiplicity is indicated as follows; s (singlet); d (doublet); t (triplet); q (quartet); m (multiplet); dd (doublet of doublets); br (broad). Infrared (IR) spectra were obtained as films from DCM or $CDCl_3$ on sodium chloride plates or as KBr pellets on a Thermo Scientific FT-IR. High-resolution mass spectra (HRMS) for electrospray (ESI) experiments were performed on a Bruker BioTOF II.

2,5-bis(trimethylsilyl)-1,4-phenylene bis(trifluoromethanesulfonate) ***4.23***

2,5-Bis(trimethylsilyl)benzene-1,4-diol (2.70 g, 10.6 mmol) was dissolved in freshly distilled pyridine (30 mL). The solution was cooled in an ice bath then, triflic anhydride (7.48 g, 26.5 mmol) was added dropwise. Once the addition was complete, the ice water bath was removed, and the reaction was slowly warmed to room temperature and then heated with stirring at 50 °C for 2 hours. The resulting reaction mixture was cooled to room temperature and then concentrated to give a black sludge. This residue was extracted with hexanes (5 × 20 mL). The combined hexane fractions were then concentrated to give a light yellow solid. The crude product was recrystallized from hexanes to give bisbenzyne precursor **4.23** as a colorless solid (5.00 g, 91%).

^{1}H NMR (500 MHz, $CDCl_3$) δ 7.44 (s, 2H), 0.38 (s, 18H). ^{13}C NMR (126 MHz, $CDCl_3$) δ 153.1, 137.4, 126.9, 118.5 (q, J = 320 Hz), -1.3. ^{19}F NMR (471 MHz, Chloroform-*d*) δ -73.78. IR (solid film) 2961, 2904, 1421, 1339, 1218, 1141, 1080, 909, 844, 734 cm^{-1}. Mp 107–108 °C.

(1R,4S)-9-cyclohexylidene-7-(trimethylsilyl)-1,4-dihydro-1,4-methanonaphthalen-6-yl trifluoromethanesulfonate ***4.28***

In a round bottom flask, the bisbenzyne precursor **4.23** (2.27 g, 4.38 mmol), fulvene **4.25** (737 mg, 5.04 mmol), and CsF (798 mg, 5.25 mmol) were stirred vigorously in acetonitrile (20 mL) at room temperature overnight. The reaction mixture was then diluted with DCM (5 mL) and filtered through a plug of silica gel, which was rinsed with DCM (4 × 5 mL). The organic solution was concentrated to give a thick brown oil. Purification *via* column chromatography provided the desired product as a colorless oil (1.53 g, 79%).

^{1}H NMR (500 MHz, $CDCl_3$) δ 7.27 (s, 1H), 7.19 (s, 1H), 6.91–6.89 (m, 2H), 4.41–4.39 (m, 2H), 2.12–2.02 (m, 2H), 2.01–1.92 (m, 2H), 1.52–1.39 (m, 6H), 0.33 (s, 9H). ^{13}C NMR (126 MHz, $CDCl_3$) δ 158.6, 155.1, 152.3, 149.9, 143.4, 142.9, 127.1, 126.7, 113.1, 111.9, 50.6, 49.7, 29.7, 27.4, 27.4, 26.7, – 0.5. ^{19}F NMR (471 MHz, $CDCl_3$) δ -74.19. HRMS (QTOF) calcd for $C_{21}H_{25}F_3O_3SSi$ [M^+] *m/z* 442.1240, found [M^+] 442.1239.

*Synthesis of mono-cycloadduct **4.37**.*

To a 5 mL DCM solution containing **4.28** (70 mg, 0.16 mmol) and dibromoquinone **4.34** (20 mg, 0.08 mmol) was added dropwise the 5 mL DCM solution containing tetrazine **4.29** (39 mg, 0.17 mmol). The solution was added in the course of 15 min *via* a syringe pump. The resulting mixture was allowed to stir at room temperature for 2 hours. The reaction was then quenched by 5 mL 1 M HCl. The organic layer was then washed with water (5 mL × 2) and brine (10 mL × 1) and dried over Na_2SO_4. The combined organic layer was concentrated and dissolved in 10 mL DCM. The DCM solution was then filtered through a short plug of basic alumina (~ 200 mg). The crude product was collected *in vacuo* and purified *via* column chromatography. The final product was obtained as orange solid (34 mg, 75%).

^{1}H NMR (400 MHz, $CDCl_3$) δ 7.44−7.41 (m, 1H), 7.36−7.32 (m, 1H), 7.09 (d, *J* = 1.3 Hz, 1H), 5.02 (d, *J* = 7.0 Hz, 1H), 4.96 (d, *J* = 6.8 Hz, 1H), 2.13−1.96 (m, 4H), 1.53−1.38 (m, 6H), 0.33 (s, 9H). Note: the ^{1}H NMR contains the inseparable mixture of the cis/trans isomers. Thus, the aromatic peaks were labelled as multiplets.

*Synthesis of half-cycle **4.18**.*

To a degassed 100 mL round-bottom flask was added mono-cycloadduct **4.37** (290 mg, 0.48 mmol) and **4.28** (256 mg, 0.58 mmol). The mixture was dissolved with 10 mL methylene chloride. Tetrazine **4.29** (137 mg, 0.58 mmol) dissolved in 10 mL methylene chloride was then added dropwise to the above mixture *via* syringe. After the addition, the mixture was allowed to stir at room temperature for 2 hours. The solution was then concentrated *in vacuo* to afford an orange solid mixture, which was then dissolved in 6 mL toluene and transferred to a 20 mL reaction vial. Upon charging the toluene solution with basic alumina (100 mg), the vial was sealed and heat to 110 ˚C for 4 hours. After cooling, the resulting mixture was filtered to remove basic alumina. The crude product was collected *in vacuo* and obtained as a 5:1 *syn/anti* mixture (253 mg, 78%). Recrystallization to separate the *syn*-isomer was performed on a 50 mg scale using the crude mixture obtained above. In a 20 mL scintillation vial, 2 mL DCM was initially added to fully dissolve the mixture. Methanol (4 mL) was then added dropwise to afford a homogeneous mixture. The vial was left open to air overnight until all the DCM solvent is evaporated. Yellow solid was found to precipitate from the solution, which was collected by vacuum filtration (27 mg, 54 %).

^{1}H NMR (400 MHz, $CDCl_3$) δ 7.37 (s, 2H), 7.28 (s, 2H), 4.94−4.88 (m, 4H), 2.09−1.98 (m, 8H), 1.53−1.38 (m, 12H), 0.29 (s, 18H). ^{19}F NMR (376 MHz, $CDCl_3$) δ 74.10, 74.13. (The ^{1}H NMR and ^{19}F NMR sample contain a 1:1 mixture of cis/trans isomers for **4.18**

Bibliography

1 Feng, X.; Pisula, W.; Müllen, K. Large polycyclic aromatic hydrocarbons: synthesis and discotic organization. *Pure Appl. Chem.* **2009**, *81*(12), 2203−2224.

2 Haley, M. M.; Tykwinski, R. R. *Carbon-rich compounds: from molecules to materials*. John Wiley & Sons. **2006**.

3 (a) Scholl, R.; Seer, C.; Weitzenbock, R. Perylen, ein hoch kondensierter aromatischer Kohlenwasserstoff $C_{20}H_{12}$. *Eur. J. Inorg. Chem.* **1910**, *43***,** 2202–2209. (b) Scholl, R.; Seer, C.; Abspaltung aromatisch gebundenen Wasserstoffes unter Verknupfung aromatischer Kerne durch Aluminiumchlorid, 6. Mitteilung: Versuche mit Phenol-athern und mit Diphenyl-methan. *Ber. dtsch. Chem. Ges. A/B* **2006**, *55***,** 330–341.

4 (a) Clar, E.; Stewart, D. G. Aromatic Hydrocarbons. LXV. Triangulene Derivatives. *J. Am. Chem. Soc.* **1953**, *75*, 2667–2672. (b) Clar, E.; Schmidt, W. Localised vs delocalised molecular orbitals in aromatic hydrocarbons. *Tetrahedron* **1979**, *35***,** 2673–2680.

5 Clar, E.; and John, F. Über eine neue Klasse tiefgefärbter radikalischer Kohlenwasserstoffe und über das vermeintliche Pentacen von E. Philippi; gleichzeitig Erwiderung auf Bemerkungen von Roland Scholl und Oskar Boettger. (Zur Kenntnis mehrkerniger aromatischer Kohlenwasserstoffe und ihrer Abkömmlinge, VII. Mitteil.). *Berichte der deutschen chemischen Gesellschaft (A and B Series)*, **1930**, *63*(11), 2967−2977.

6 Ried, W.; and Anthöfer, F. Einfache Synthese für Pentacen-6,13-chinon. *Angew. Chem.* **1953**, *65*, 601.

7 Clar, E. Vorschläge zur nomenklatur kondensierter ringsysteme (aromatische kohlenwasserstoffe, XXVI. Mitteil.). *Berichte der deutschen chemischen Gesellschaft (A and B Series)* **1939**, *72*(12), 2137−2139.

8 Clar, E. *Polycyclic Hydrocarbons, Vol. I–II*, Academic Press, London, **1964**.

9 Wu, J.; Pisula, W.; Müllen, K. Graphenes as potential material for electronics. *Chem. Rev.* **2007**, *107*(3), 718−747.

10 Bartlett, P. D.; Ryan, M. J.; Cohen, S. G. Triptycene (9, 10-o-benzenoanthracene). *J. Am. Chem. Soc.* **1942**, *64*, 2649−2653.

11 Kroto, H. W.; Heath, J. R.; O'Brien, S. C.; Curl, R. F.; Smalley, R. E. *Nature* **1985**, *318*, 162−163.

12 Krätschmer, W.; Lamb, L. D.; Fostiropoulos, K.; & Huffman, D. R. Solid C_{60}: a new form of carbon. *Nature* **1990**, *347*, 354−358.

13 (a) Kuehne, A. J.; Gather, M. C. Organic lasers: recent developments on materials, device geometries, and fabrication techniques. *Chem. Rev.* **2016**, *116*, 12823−12864. (b) Beaujuge, P. M.; Reynolds, J. R. Color control in π-conjugated organic polymers for use in electrochromic devices. *Chem. Rev.* **2010**, *110*, 268−320.

14 Dimitrakopoulos, C. D.; Malenfant, P. R. Organic thin film transistors for large area electronics. *Adv.* Mater. **2002**, *14*, 99−117.

15 Ostroverkhova, O. Organic optoelectronic materials: mechanisms and applications. *Chem. Rev.* **2016**, *116*, 13279-13412.

16 Scherf, U.; List, E. J. Semiconducting polyfluorenes—towards reliable structure–property relationships. *Adv. Mater.* 2002, 14(7), 477−487.

17 (a) Marcus, R. A. Chemical and Electronchemical Electron-Transfer Theory. *Annu. Rev. Phys. Chem.* **1964**, *15*, 155−196. (b) Wang, L.; Nan, G.; Yang, X.; Peng, Q.; Li, Q.; Shuai, Z. Computational methods for design of organic materials with high charge mobility. *Chem. Soc. Rev.* **2010**, *39*, 423−434. (c) Coropceanu, V.; Cornil, J.; da Silva, D. A.; Olivier, Y.; Silbey, R.; Bredas, J. L. Charge transport in organic semiconductors. *Chem. Rev.* **2007**, *107*, 926−952.

18 Shi, X.; Chi, C. Different Strategies for the Stabilization of Acenes and Acene Analogues. *Chem. Rec.* **2016**, *16*, 1690−1700.

19 Hückel, E. Quantentheoretische beiträge zum benzolproblem. *Zeitschrift für Physik*, **1931**, *70*, 204−286.

20 E. Clar, *The Aromatic Sextet*, John Wiley & Sons, Ltd., London, **1972**.

21 (a) Bendikov, M.; Duong, H. M.; Starkey, K.; Houk, K. N.; Carter, E. A.; Wudl, F. Oligoacenes: theoretical prediction of open-shell singlet diradical ground states. *J. Am. Chem. Soc.* **2004**, *126*, 7416−7417; b) Tönshoff, C.; Bettinger, H. F. Photogeneration of octacene and nonacene. *Angew. Chem. Int. Ed.* **2010**, *49*, 4125−4128.

22 Einholz, R.; Fang, T.; Berger, R.; Grüninger, P.; Früh, A.; Chassé, A.; Fink, R. F.; and Bettinger, H. F. Heptacene: characterization in solution, in the solid state, and in films. *J. Am. Chem. Soc.* **2017**, *139*, 4435−4442.

23 (a) Aleshin, A. N.; Lee, J. Y.; Chu, S. W.; Kim, J. S.; Park, Y. W. Mobility studies of field-effect transistor structures basedon anthracene single crystals. *Appl. Phys. Lett.* **2004**, *84*, 5383−5385. (b) Boer, R. W. I. d.; Klapwijk, T. M.; Morpurgo, A. F. Field-effect transistors on tetracene single crystals. *Appl. Phys. Lett.* **2003**, *83*, 4345−4347. (c) Takeyama, Y.; Ono, S.; Matsumoto, Y. Organic single crystal transistor characteristics of single-crystal phase pentacene grown by ionic liquid-assisted vacuum deposition. *Appl. Phys. Lett.* **2012**, *101*, 083303.

24 Watanabe, M.; Chang, Y. J.; Liu, S.-W.; Chao, T.-H.; Goto, K.; IslamMd, M.; Yuan, C.-H.; Tao, Y.-T.; Shinmyozu, T.; Chow, T. J. The synthesis, crystal structure and charge-transport properties of hexacene. *Nat. Chem.* **2012**, *4*, 574−578.

25 Anthony, J. E. Functionalized Acenes and Heteroacenes for Organic Electronics. *Chem. Rev.* **2006**, *106*, 5028−5048.

26 (a) Anthony, J. E.; Brooks, J. S.; Eaton, D. L.; and Parkin, S. R. Functionalized pentacene: improved electronic properties from control of solid-state order. *J. Am. Chem. Soc.* **2001**, *123*, 9482−9483. (b) Anthony, J. E.; Eaton, D. L.; and Parkin, S. R. A road map to stable, soluble, easily crystallized pentacene derivatives. *Org. lett.* **2002**, *4*, 15−18. (c) Sheraw, C. D.; Jackson, T. N.; Eaton, D. L.; and Anthony, J. E. Functionalized pentacene active layer organic thin-film transistors. *Adv. Mater.* **2003**, *15*, 2009−2011.

27 da Silva Filho, D. A.; Kim, E. G.; Brédas, J. L. Transport properties in the rubrene crystal: electronic coupling and vibrational reorganization energy. *Adv. Mater.* **2005**, *17*, 1072−1076.

28 Stock, L. M. The origin of the inductive effect. *J. Chem. Educ.* **1972**, *49*, 400−404.

29 Pauling, L. "The Concept of Resonance". *The Nature of the Chemical Bond – An Introduction to Modern Structural Chemistry* (3rd ed.). Cornell University Press. **1960**, pp. 10−13.

30 (a) Jones, B. A.; Facchetti, A.; Wasielewski, M. R.; Marks, T. J. Tuning orbital energetics in arylene diimide semiconductors. Materials design for ambient stability of n-type charge transport. *J. Am. Chem. Soc*. **2007**, *129*, 15259−15278. (b) Newman, C. R.; Frisbie, C. D.; da Silva Filho, D. A.; Brédas, J. L.; Ewbank, P. C.; Mann, K. R. Introduction to organic thin film transistors and design of n-channel organic semiconductors. *Chem*. *Mater*. **2004**, *16*, 4436−4451.

31 (a) Sakamoto, Y.; Suzuki, T.; Kobayashi, M.; Gao, Y.; Fukai, Y.; Inoue, Y.; Sato, F.; Tokito, S. Perfluoropentacene: High-performance p−n junctions and complementary circuits with pentacene. J. *Am. Chem. Soc.* **2004**, *126*, 8138−8140. (b) Inoue, Y.; Sakamoto, Y.; Suzuki, T.; Kobayashi, M.; Gao, Y.; Tokito, S. Organic thin-film transistors with high electron mobility based on perfluoropentacene. *Jpn. J. Appl. Phys.* **2005**, *44*, 3663−3668.

32 (a) Cinar, M. E.; and Ozturk, T. Thienothioiphenes, dithienothiophenes, and thienoacenes: syntheses, oligomers, polymers, and properties. *Chem. Rev.* **2015**, *115*, 3036–3140. (b) Niimi, K.; Shinamura, S.; Osaka, I.; Miyazaki, E.; Takimiya, K. Dianthra[2,3-b:2',3'-f]thieno[3,2-b]thiophene (DATT): synthesis, characterization, and FET characteristics of new π-extended heteroarene with eight fused aromatic rings *J. Am. Chem. Soc.* **2011**, *133*, 8732–8739. (c) Laquindanum, J. G.; Katz, H. E.; Lovinger, A. J. Synthesis, morphology, and field-effect mobility of anthradithiophenes. *J. Am. Chem. Soc.* **1998**, *120*, 664–672. (d) Ebata, H.; Izawa, T.; Miyazaki, E.; Takimiya, K.; Ikeda, M.; Kuwabara, H.; and Yui, T. Highly soluble [1]benzothieno [3, 2-*b*] benzothiophene (BTBT) derivatives for high-performance, solution-processed organic field-effect transistors. **2007**, *129*, 15732–15733.

33 (a) Miao, Q. Ten years of N-heteropentacenes as semiconductors for organic thin-film transistors. *Adv. Mater.* **2014**, *26*, 5541–5549. (b) Bunz, U. H. F. The larger linear N-heteroacenes. *Acc. Chem. Res.* **2015**, *48*, 1676–1686. (c) Bunz, U. H. F.; Engelhart, J. U.; Lindner, B. D.; and Schaffroth, M. *Angew. Chem. Int. Ed.* **2013**, *52*, 3810–3821. (d) Tang, X.-D.; Liao, Y.; Geng, H.; and Shuai, Z.-G. Fascinating effect of dehydrogenation on the transport properties of *N*-heteropentacenes: transformation from p- to n-type semiconductor. *J. Mater. Chem.*, **2012**, *22*, 18181–18191.

34 (a) Wang, C.; Zhang, J.; Long, G.; Aratani, N.; Yamada, H.; Zhao, Y.; Zhang, Q. Synthesis, Structure, and Air-stable n-type field-effect transistor behaviors of functionalized octaazanonacene-8, 19-dione. *Angew. Chem. Int. Ed.* **2015**, *54*, 6292−6296. (b) Li, J.; and Zhang, Q. Linearly Fused Azaacenes: Novel Approaches and New Applications Beyond Field-Effect Transistors (FETs). *ACS Appl. Mater. Interfaces*, **2015**, *7*, 28049−28062. (c)

35 Miao, Q.; Nguyen, T. Q.; Someya, T.; Blanchet, G. B.; Nuckolls, C. Synthesis, Assembly, and Thin Film Transistors of Dihydrodiazapentacene: An Isostructural Motif for Pentacene. *J. Am. Chem. Soc.* **2003**, *125*, 10284−10287.

36 (a) Kytka, M.; Gerlach, A.; Schreiber, F.; Kováč, Real-time observation of oxidation and photo-oxidation of rubrene thin films by spectroscopic ellipsometry. J. *Appl. Phys. Lett.* **2007**, *90*, 131911. (b) Fumagalli, E.; Raimondo, L.; Silvestri, L.; Moret, M.; Sassella, A.; Campione, M. Oxidation dynamics of epitaxial rubrene ultrathin films. *Chem. Mater.* **2011**, *23*, 3246–3253. (c) Uttiya, S.; Raimondo, L.; Campione, M.; Miozzo, L.; Yassar, A.; Moret, M.; Fumagalli, E.; Borghesi, A.; Sassella, A. Stability to photo-oxidation of rubrene and fluorine-substituted rubrene. *Synth. Met.* **2012**, *161*, 2603–2606.

37 (a) Hercules, D. M. Chemiluminescence resulting from electrochemically generated species. *Science* **1964**, *145*, 808–809. (b) Vinyard, D. J.; Su, S.; Richter, M. M. Electrogenerated chemiluminescence of 9, 10-diphenylanthracene, rubrene, and anthracene in fluorinated aromatic solvents. *J. Phys. Chem. A* **2008**, *112*, 8529–8533. (c) Omer, K. M.; Bard, A. J. Electrogenerated chemiluminescence of aromatic hydrocarbon nanoparticles in an aqueous solution. *J. Phys. Chem. C* **2009**, *113*, 11575–11578. (d) Rodríguez-López, J.; Shen, M.; Nepomnyashchii, A. B.; Bard, A. J. Scanning Electrochemical Microscopy Study of Ion Annihilation Electrogenerated Chemiluminescence of Rubrene and $[Ru(bpy)_3]^{2+}$ *J. Am. Chem. Soc.* **2012**, *134*, 9240–9250.

38 (a) Rauhut, M. M.; Roberts, B. G.; Semsel, A. M. A Study of Chemiluminescence from Reactions of Oxalyl Chloride, Hydrogen Peroxide, and Fluorescent Compounds. *J. Am. Chem. Soc.* **1966**, *88*, 3604−3617. (b) Adam, W.; Cueto, O.; Yany, F. On the mechanism of the rubrene-enhanced chemiluminescence of *α*-peroxylactones. *J. Am. Chem. Soc.* **1978**, *100*, 2587−2589. (c) Larena, A.; Martinez-Urreaga, J. The rubrene character in chemiluminescent reactions studied by V-UV absorption spectroscopy. *Spectrosc. Lett.* **1985**, *18*, 463−472.

39 (a) Wilson, T. Fluorescence of rubrene excited by energy transfer from singlet oxygen. Temperature dependence and competition with oxidation. *J. Am. Chem. Soc.* **1969**, *91*, 2387–2388. (b) Yee, W. A.; Kuzmin, V. A.; Kliger, D. S.; Hammond, G. S.; Twarowski, A. J. Quenching of the fluorescent state of rubrene directly to the ground state. *J. Am. Chem. Soc.* **1979**, *101*, 5104–5106.

40 (a) Zhi-lin, Z.; Xue-yin, J.; Shao-hong, X.; Nagatomo, T.; Omoto, O. The effect of rubrene as a dopant on the efficiency and stability of organic thin film electroluminescent devices. *J. Phys. D: Appl. Phys.* **1998**, *31*, 32−35. (b) Sakamoto, G.; Adachi, C.; Koyama, T.; Taniguchi, Y.; Merritt, C. D.; Murata, H.; Kafafi, Z. H. Significant improvement of device durability in organic light-emitting diodes by doping both hole transport and emitter layers with rubrene molecules. *Appl. Phys. Lett.* **1999**, *75*, 766–768. (c) Xue, Q.; Xie, G.; Chen, P.; Lu, J.; Zhang, D.; Tang, Y.; Zhao, Y.; Hou, J.; Liu, S. White organic light-emitting devices with a bipolar transport layer between blue fluorescent and yellow phosphor-sensitized-fluorescent emitting layers. *Synth. Met.* **2010**, *160*, 829–831.

41 (a) Taima, T.; Sakai, J.; Yamanari, T.; Saito, K. Doping effects for organic photovoltaic cells based on small-molecular-weight semiconductors. *Sol. Energy Mater. Sol. Cells* **2009**, *93*, 742–745. (b) Perez, M. D.; Borek, C.; Forrest, S. R.; Thompson, M. E. Molecular and morphological influences on the open circuit voltages of organic photovoltaic devices. *J. Am. Chem. Soc.* **2009**, *131*, 9281–9286.

42 Podzorov, V.; Menard, E.; Borissov, A.; Kiryukhin, V.; Rogers, J. A.; and Gershenson, M. E. Intrinsic charge transport on the surface of organic semiconductors. *Phys. Rev. Lett.* **2004**, *93*, 086602.

43 De Boer, R. W. I.; Gershenson, M. E.; Morpurgo, A. F.; Podzorov, V. Organic single-crystal field-effect transistors. *Phys Status Solidi* **2004**, *201*, 1302–1331.

44 (a) Jurchescu, O. D.; Meetsma, A.; Palstra, T. T. M. Low-temperature structure of rubrene single crystals grown by vapor transport. *Acta Crystallogr. Sect. B* **2006**, *62*, 330–334. (b) Huang, L.; Liao, Q.; Shi, Q.; Fu, H.; Ma, J.; Yao, J. Rubrene micro-crystals from solution routes: their crystallography, morphology and optical properties. *J. Mater. Chem.* **2009**, *20*, 159–166. (c) El Helou, M.; Medenbach, O.; Witte, G. Rubrene microcrystals: a route to investigate surface morphology and bulk anisotropies of organic semiconductors. *Cryst. Growth Des.* **2010**, *10*, 3496–3501.

45 Moureu, C.; Dufraisse, C.; Dean, P. M. An organic peroxide separable from the rubrene peroxide. *Comptes Rendus Hebd. Seances Acad. Sci.* **1926**, *182*, 1440–1443.

46 Xie, W.; McGarry, K. A.; Liu, F.; Wu, Y.; Ruden, P. P.; Douglas, C. J.; and Frisbie, C. D. High-mobility transistors based on single crystals of isotopically substituted rubrene-d_{28}. *J. Phys. Chem. C*, **2013**, *117*, 11522−11529.

47 Ren, X.; Bruzek, M. J.; Hanfi, D. A.; Schulzetenberg, A.; Wu, Y.; Kim, C.-H.; Zhang, Z.; Johns, J. E.; Salleo, A.; Fratini, S.; Troisi, A.; Douglas, C. J.; and Frisbie, C. D. *Adv. Electron. Mater.* **2017**, *3*, 1700018.

48 Yagodkin, E.; McGarry, K. A.; Douglas, C. J. Preparation of 6, 11-Dihydroxy-5, 12-tetracenedione. *Org. Prep. Proced. Int.* **2011**, *43*, 360−363.

49 McGarry, K. A.; Xie, W.; Sutton, C.; Risko, C.; Wu, Y.; Young, V. G., Jr.; Brédas, J.-L.; Frisbie, C. D.; Douglas, C. J. Rubrene-based single-crystal organic semiconductors: synthesis, electronic structure, and charge-transport properties. *Chem. Mater.* **2013**, *25*, 2254−2263.

50 Minder, N. A.; Ono, S.; Chen, Z.; Facchetti, A.; Morpurgo, A. F. Band-like electron transport in organic transistors and implication of the molecular structure for performance optimization. *Adv. Mater.* **2012**, *24*, 503–508.

51 Sakamoto, Y.; Suzuki, T. Perfluorinated and half-fluorinated rubrenes: synthesis and crystal packing arrangements. *J. Org. Chem.* **2017**, *82*, 8111−8116.

52 (a) Taylor, R. It Isn't, It Is: The C–H···X (X = O, N, F, Cl) interaction really is significant in crystal packing. *Cryst. Growth Des.* **2016**, *16*, 4165−4168. (b) Taylor, R. Which intermolecular interactions have a significant influence on crystal packing? *CrystEngComm* **2014**, *16*, 6852−6865.

53 Sutton, C.; Marshall, M. S.; Sherrill, C. D.; Risko, C.; Brédas, J.-L. Rubrene: The interplay between intramolecular and intermolecular interactions determines the planarization of its tetracene core in the solid state. *J. Am. Chem. Soc*. **2015**, *137*, 8775−8782.

54 Lin, S.; Miller, J. M. Decomposition and byproducts from reactions involving pentafluorophenyl-Grignard and lithium reagents. a GC/MS study *J. Fluorine Chem.* **1977**, *9*, 161−169.

55 Frohn, H. -J.; Adonin, N. Y.; Bardin, V. V.; Starichenko, V. F. Base-catalysed hydrodeboration of polyfluorophenyl(dihydroxy)boranes *Z. Anorg. Allg. Chem.* **2002**, *628*, 2834−2838.

56 Stork, G.; Danheiser, R. L.; Ganem, B. Spiroannelation of enol ethers of cyclic 1,3-diketones. A simple stereospecific synthesis of *β*-vetivone. *J. Am. Chem. Soc*. **1973**, *95*, 3414−3415.

57 (a) Shimizu, A.; and Tobe, Y. Indeno[2,1-*a*]fluorene: an air-stable ortho-quinodimethane derivative. *Angew. Chem., Int. Ed.* **2011**, *50*, 6906−6910. (b) Chase, D. T.; Fix, A. G.; Kang, S. J.; Rose, B. D.; Weber, C. D.; Zhong, Y.; Zakharov, L. N.; Lonergan, M. C.; Nuckolls, C.; and Haley, M. M. 6,12-Diarylindeno[1, 2-*b*]fluorenes: syntheses, photophysics, and ambipolar OFETs. *J. Am. Chem. Soc*. **2012**, *134*, 10349−10352.

58 Sakamoto, Y; Suzuki, T.; Kobayashi, M.; Gao, Y.; Inoue, Y.; Tokito, S. Perfluoropentacene and perfluorotetracene: Syntheses, crystal structures, and FET characteristics. *Mol. Cryst. Liq. Cryst.* **2006**, *444*, 225−232.

59 Ono, K.; Hashizume, J.; Yamaguchi, H.; Tomura, M.; Nishida, J.-I.; and Yamashita, Y. Synthesis, crystal structure, and electron-accepting property of the BF_2 complex of a dihydroxydione with a perfluorotetracene skeleton. *Org. Lett.* **2009**, *11*, 4326−4329.

60 Raheem, M. A.; Nagireddy, J. R.; Durham, R.; Tam, W. Efficient procedure for the preparation of 2-bromofuran and its application in the synthesis of 2-arylfurans. *Synth. Commun.* **2010**, *40*, 2138−2146.

61 Mei, J.; Diao, Y.; Appleton, A. L.; Fang, L.; and Bao, Z. Integrated materials design of organic semiconductors for field-effect transistors. *J. Am. Chem. Soc.* **2013**, *135*, 6724−6746.

62 Lakshminarayana, A. N.; Ong, A.; and Chi, C. Modification of acenes for n-channel OFET materials. *J. Mater. Chem. C.* **2018**, *6*, 3551−3563.

63 (a) Plunkett, K. N.; What about the five-membered ring? cyclopenta-fused polycyclic aromatic hydrocarbons as a building block for functional materials. *Synlett* **2013**, *24*, 898−902. (b) Xia, H.; Liu, D.; Xu, X.; and Miao, Q. Ambipolar organic semiconductors from electron-accepting cyclopenta-fused anthracene. *Chem. Commun.* **2013**, *49*, 4301−4304. (c) Koper, C.; Sarobe, M.; Jenneskens, L. W. Redox properties of non-alternant cyclopenta-fused polycyclic aromatic hydrocarbons: The effect of peripheral pentagon annelation. *Phys. Chem. Chem. Phys.* **2004**, *6*, 319−327. (d) Modelli, A.; Mussoni, L.; and Fabbri, D.; Electron affinities of polycyclic aromatic hydrocarbons by means of B3LYP/6-31+G* calculations *J. Phys. Chem. A* **2006**, *110*, 6482−6486. (e) Wombacher, T.; Gassmann, A.; Foro, S.; von Seggern, H.; and Schneider, J. J.; Structural polymorphism and thin film transistor behavior in the fullerene framework molecule 5,6;11,12-di-*o*-phenylenetetracene. *Angew. Chem. Int. Ed.* **2016**, *55*, 6041−6046; *Angew. Chem.* **2016**, *128*, 6145−6150.

64 Barth, W. E.; Lawton, R. G. Dibenzo[ghi,mno]fluoranthene. *J. Am. Chem. Soc.* **1966**, *88*, 380−381.

65 (a) Clar, E.; *Polycyclic Hydrocarbons*; Academic Press: New York, **1964**. (b) Diederich, F.; Rubin, Y. Synthetic approaches toward molecular and polymeric carbon allotropes. *Angew. Chem., Int. Ed. Engl.* **1992**, *31*, 1101−1123.

66 (a) Trost, B. M.; Bright, G. M. Pyracylene: A pentalenoid system? *J. Am. Chem. Soc.* **1967**, *89*, 4244−4245. (b) Trost, B. M.; Bright, G. M.; Frihart, C.; Brittelli, D. Perturbed [12]annulenes: Synthesis of pyracylenes. *J. Am. Chem. Soc.* **1971**, *93*, 737−745.

67 *Fragments of Fullerenes and Carbon Nanotubes*; Petrukhina, M. A.; Scott, L. T., Eds.; John Wiley and Sons: Hoboken, **2012**.

68 Thompson, B. C.; Fréchet, J. M. J. Polymer−fullerene composite solar cells. *Angew. Chem. Int. Ed.* **2008**, *47*, 58−77.

69 Zhou, Q.; Carroll, P. J.; and Swager, T. M. Synthesis of diacetylene macrocycles derived from 1,2-diethynyl benzene derivatives: Structure and reactivity of the strained cyclic dimer. *J. Org. Chem.* **1994**, *59***,** 1294–1301.

70 Merlet, S.; Birau, M.; and Wang, Z. Y. Synthesis and characterization of highly fluorescent indenofluorenes. *Org. Lett.* **2002**, *4***,** 2157–2159.

71 Chase, D. T.; Fix, A. G.; Kang, S. J.; Rose, B. D.; Weber, C. D.; Zhong, Y.; Zakharov, L. N.; Lonergan, M. C.; Nuckolls, C.; and Haley, M. M. 6,12-Diarylindeno[1,2–*b*]fluorenes: Syntheses, photophysics, and ambipolar OFETs. *J. Am. Chem. Soc.* **2012**, *134***,** 10349–10352.

72 Chase, D. T.; Fix, A. G.; Rose, B. D.; Weber, C. D.; Nobusue, S.; Stockwell, C. E.; Zakharov, L. N.; Lonergan, M. C.; and Haley, M. M. Electron-accepting 6,12-diethynylindeno[1, 2-b]fluorenes: Synthesis, crystal structures, and photophysical properties. *Angew. Chem. Int. Ed.* **2011**, *50*, 11103−11106.

73 (a) Chase, D. T.; Rose, B. D.; McClintock, S. P.; Zakharov, L. N. and Haley, M. M. Indeno[1,2-b]fluorenes: Fully conjugated antiaromatic analogues of acenes. *Angew. Chem. Int. Ed. Engl.* **2010**, *50*, 1127–1130. (b) Rose, B. D.; Chase, D. T.; Weber, C. D.; Zakharov, L. N.; Lonergan, M. C.; and Haley, M. M. Synthesis, crystal structures, and photophysical properties of electron-accepting diethynylindenofluorenediones. *Org. Lett.* **2011**, *13*, 2106–2109. (c) Rose, B. D.; Vonnegut, C. L.; Zakharov, L. N.; and Haley, M. M. Fluoreno[4,3-*c*]fluorene: A closed-shell, fully conjugated hydrocarbon. *Org. Lett.* **2012**, *14*, 2426–2429. (d) Fix, A. G.; Deal, P. E.; Vonnegut, C. L.; Rose, B. D.; Zakharov, L. N.; and Haley, M. M. Indeno[2,1-*c*]fluorene: A new electron-accepting scaffold for organic electronics. *Org. Lett.* **2013**, *15*, 1362–1365. (e) Young, B. S.; Chase, D. T.; Marshall, J. L.; Vonnegut, C. L.; Zakharov, L. N.; and Haley, M. M. Synthesis and properties of fully-conjugated indacenedithiophenes. *Chem. Sci.* **2014**, *5*, 1008−1014. (f) Rose, B. D.; Sumner, N. J.; Filatov, A. S.; Peters, S. J.; Zakharov, L. N.; Petrukhina, M. A.; and Haley, M. M. Experimental and computational studies of the neutral and reduced states of indeno[1,2-*b*]fluorene. *J. Am. Chem. Soc.* **2014**, *136*, 9181–9189. (g) Shimizu, A.; and Tobe, Y. Indeno[2,1-*a*]fluorene: An air-stable ortho-quinodimethane derivative. *Angew. Chem. Int. Ed.* **2011**, *50*, 6906–6910.

74 (a) Dang, H.; Garcia-Garibay, M. A.; Palladium-catalyzed formation of aceanthrylenes: A simple method for peri-cyclopentenelation of aromatic compounds. *J. Am. Chem. Soc.* **2001**, *123*, 355−356. (b) Dang, H.; Levitus, M.; and Garcia-Garibay, M. A. One step Pd(0)-catalyzed synthesis, X-ray analysis, and photophysical properties of cyclopent[hi]aceanthrylene: Fullerene-like properties in a nonalternant cyclopentafused aromatic hydrocarbon. *J. Am. Chem. Soc.* **2002**, *124*, 136−143.

75 (a) Pugh, C.; Percec, V. J. Phase transfer Pd(0) catalyzed polymerization reactions. I. Synthesis of 1, 2-(4, 4′-dialkoxyaryl)acetylene monomers and 1,4-bis[2-(4′,4″-dialkoxyphenyl)ethynyl]benzene derivatives by phase transfer Pd(0) / Cu(I) catalyzed coupling reactions. *Polym. Sci. A Polym. Chem.* **1990**, *28*, 1101−1126. (b) Sonogashira, K.; Yatake, T.; Tohda, Y.; Takahashi, S.; Nagihara, N. *J. Chem. Soc., Chem. Commun.* **1977**, 291−292.

76 (a) Wood, J. D.; Jellison, J. L.; Finke, A. D.; Wang, L.; Plunkett, K. N. Electron acceptors based on functionalizable cyclopenta[*hi*]aceanthrylenes and dicyclopenta[*de*, *mn*]tetracenes. *J. Am. Chem. Soc.* **2012**, *134*, 15783–15789. (b) Lee, C.-H. and Plunkett, K. N. Orthogonal functionalization of cyclopenta[*hi*]aceanthrylenes. *Org. Lett.* **2013**, *15*, 1202–1205.

77 Jellison, J. L.; Lee, C.-H.; Zhu, X.; Wood, J. D.; and Plunkett, K. N. Electron acceptors based on an all-carbon donor–acceptor copolymer. *Angew. Chem. Int. Ed.* **2012**, *51***,** 12321–12324.

78 Gu, X.; Luhman, W. A.; Yagodkin, E.; Holmes, R. J.; and Douglas, C. J. Diarylindenotetracenes via a selective cross-coupling/C–H functionalization: Electron donors for organic photovoltaic cells. *Org. Lett.* **2012**, *14*, 1390–1393.

79 Purvis, L. J.; Gu, X.; Ghosh, S.; Zhang, Z.; Cramer, C.; Douglas, C. J. Synthesis and Characterization of Electron-Deficient Asymmetrically Substituted Diarylindenotetracenes. *J. Org. Chem.* **2018**, *83*, 1828−1841.

80 (a) Mohebbi, A. R.; and Wudl, F. Electron-accepting dithiarubicene (emeraldicene) and derivatives prepared by unprecedented nucleophilic hydrogen substitution by alkyllithium reagents. *Chem. Eur. J.* **2011**, *17*, 2642−2646. (b) Smet, M.; Van Dijk, J.; and Dahaen, W. An improved synthesis of substituted rubicenes providing access to heterocyclic rubicene analogues. *Synlett* **1999**, *1999*, 495-497. (c) Hseuh, H.-H.; Hsu, M. -Y.; Wu, T.-L.; and Liu, R.-S. Efficient synthesis and characterization of dibenzo[*a*,*m*]rubicenes and tetrabenzo[*a*,*f*,*r*,*m*]rubicenes. *J. Org. Chem.* **2009**, *74*, 8448−8451. (d) Smet, M.; Shukla, R.; Fülöp, L.; and Dehaen, W. A general synthesis of disubstituted rubicenes. *Eur. J. Org. Chem.* **1998**, 2769−2773.

81 (a) Wessig, P.; and Müller, G. The dehydro-Diels−Alder reaction. *Chem. Rev.* **2008**, *108*, 2051−2063. (b) Hoye, T. R.; Baire, B.; Niu, D.; Willoughby, P. H.; and Woods, B. P. The hexadehydro-Diels–Alder reaction. *Nature* **2012**, *490*, 208.

82 Fujisawa, R.; and Sugita, S. Method for producing iodinated aromatic compound. PCT/JP2011/051078.

83 Karmakar, R.; Lee, D. Reactions of arynes promoted by silver ions. *Chem. Soc. Rev.* **2016**, *45*, 4459−4470.

84 (a) von Ragué Schleyer, P.; Maerker, C.; Dranfeld, A.; Jiao, H.; and van Eikema Hommes, N. J. R. Nucleus-independent chemical shifts: A simple and efficient aromaticity probe. *J. Am. Chem. Soc.* **1996**, *118*, 6317. (b) Chen, Z.; Wannere, C. S.; Corminboeuf, C.; Puchta, R.; and von Ragué Schleyer, P. Nucleus-independent chemical shifts (NICS) as an aromaticity criterion. *Chem. Rev.* **2005**, *105*, 3842−3888.

85 (a) Frederickson, C. K.; Rose, B. D.; and Haley, M. M. Explorations of the indenofluorenes and expanded quinoidal analogues. *Acc. Chem. Res.* **2017**, *50*, 977−987. (b) Frederickson, C. K.; Zakharov, L. N.; and Haley, M. M. Modulating paratropicity strength in diareno-fused antiaromatics. *J. Am. Chem. Soc.* **2016**, *138*, 16827−16838.

86 Heilbronner, E. Molecular Orbitals in homologen Reihen mehrkerniger aromatischer Kohlenwasserstoffe: I. Die Eigenwerte yon, LCAO-MO's in homologen Reihen. *Helv. Chim. Acta* **1954**, *37*, 921–935.

87 Segawa, Y.; Yagi, A.; Ito, H.; Itami, K. A theoretical study on the strain energy of carbon nanobelts. *Org. Lett.* **2016**, *18*, 1430–1433.

88 (a) Chen, Z.; Jiang, D. E.; Lu, X.; Bettinger, H. F.; Dia, S.; Schleyer, P. V.; Houk, K. N. Open-shell singlet character of cyclacenes and short zigzag nanotubes. *Org. Lett.* **2007**, *9*, 5449–5452. (b) Bendikov, M.; Duong, H. M.; Starkey, K.; Houk, K. N.; Carter, E. A.; Wudl, F. Oligoacenes: theoretical prediction of open-shell singlet diradical ground states *J. Am. Chem. Soc.* **2004**, *126*, 7416–7417.

89 Iijima, S. Helical microtubules of graphitic carbon. *Nature* **1991**, *354*, 56–58.

90 Sgobba, V.; Guldi, D. M. Carbon nanotubes—electronic/electrochemical properties and application for nanoelectronics and photonics. *Chem. Soc. Rev.* **2009**, *38*, 165–184.

91 Dresselhaus, M. S.; Dresselhaus, G.; Saito, R. Physics of carbon nanotubes. *Carbon* **1995**, *33*, 883–891.

92 (a) Jasti, R.; Bhattacharjee, J.; Neaton J. B.; and Bertozzi, C. R. Synthesis, characterization, and theory of [9]-, [12]-, and [18]cycloparaphenylene: carbon nanohoop structures. *J. Am. Chem. Soc.* **2008**, *130*, 17646−17647. (b) Sisto, T. J.; Golder, M. R.; Hirst, E. S.; R. Jasti, R. Selective synthesis of strained [7] cycloparaphenylene: an orange-emitting fluorophore. *J. Am. Chem. Soc.* **2011**, *133*, 15800−15802. (c) Xia, J.; and Jasti, R. Synthesis, characterization, and crystal structure of [6] cycloparaphenylene. *Angew. Chem., Int. Ed.* **2012**, *51*, 2474–2476. (d) Xia, J.; Bacon, J. W.; and Jasti, R. Gram-scale synthesis and crystal structures of [8]- and [10]CPP, and the solid-state structure of C_{60}@[10] CPP. *Chem. Sci.* **2012**, *3*, 3018–3021. (e) Darzi, E. R.; Sisto, T. J.; and Jasti, R. Selective syntheses of [7]–[12]cycloparaphenylenes using orthogonal Suzuki–Miyaura cross-coupling reactions. *J. Org. Chem.* **2012**, *77*, 6624−6628. (f) Evans, P. J.; Darzi, E. R.; and Jasti, R. Efficient room-temperature synthesis of a highly strained carbon nanohoop fragment of buckminsterfullerene. *Nat. Chem.* **2014**, *6*, 404−408.

93 Takaba, H.; Omachi, H.; Yamamoto, Y.; Bouffard, J.; and Itami, K. Selective synthesis of [12]cycloparaphenylene. *Angew. Chem., Int. Ed.* **2009**, *48*, 6112−6116.

94 (a) Yamago, S.; Watanabe Y.; and Iwamoto, T. Synthesis of [8] cycloparaphenylene from a square-shaped tetranuclear platinum complex. *Angew. Chem., Int. Ed.* **2010**, *49*, 757−759. (b) Iwamoto, T.; Watanabe, Y.; Sakamoto, Y.; Suzuki, T.; and Yamago, S. Selective and random syntheses of [n] cycloparaphenylenes (n = 8–13) and size dependence of their electronic properties. *J. Am. Chem. Soc.* **2011**, *133*, 8354−8361. (c) Kayahara, E.; Sakamoto, Y.; Suzuki, T.; and Yamago, S. Selective synthesis and crystal structure of [10]cycloparaphenylene. *Org. Lett.* **2012**, *14*, 3284−3287. (d) Kayahara, E.; Iwamoto, T.; Suzuki, T.; and Yamago, S. Selective synthesis of [6]-, [8]-, and [10]cycloparaphenylenes. *Chem. Lett.* **2013**, *42*, 621−623. (e) Kayahara, E.; Patel, V. K.; and Yamago, S. Synthesis and characterization of [5]cycloparaphenylene. *J. Am. Chem. Soc.* **2014**, *136*, 2284−2287.

95 Watanabe, M.; Chang, Y. J.; Liu, S. W.; Chao, T. H.; Goto, K.; Islam, M. M.; Yuan, C. H.; Tao, Y. T.; Shinmyozu, T.; Chow, T. J. The synthesis, crystal structure and charge-transport properties of hexacene. *Nat. Chem.* **2012**, *4*, 574–578.

96 Miao, Q.; Chi, X.; Xiao, S.; Zeis, R.; Lefenfeld, M.; Siegrist, T.; Steigerwald, M. L.; Nuckolls, C. Organization of acenes with a cruciform assembly motif. *J. Am. Chem. Soc.* **2006**, *128*, 1340–1345.

97 Himeshima, Y.; Kobayashi, H.; and Sonoda, T. A first example of generating aryl cations in the solvolysis of aryl triflates in trifluoroethanol. *J. Am. Chem. Soc.* **1985**, *107*, 5286−5288.

98 Bhojgude, S. S.; Kaicharia, T.; Bhunia, A.; Biju, A. T. A Practical and General Diels–Alder Reaction of Pentafulvenes with Arynes. *Org. Lett.* **2012**, *14*, 4098–4101.

99 Watson, P. L.; Warrener, R. N. Isobenzofulvenes. I. The in situ preparation of 8,8-cimethyl-and 8,8-diphenylbenzo[b]fulveues and their pericyclic reactions with 2π-cycloaddends. *Aust. J. Chem.* **1973**, *26*, 1725–1750.